Modulating Protein Stability and Dynamics by Osmolytes and Electrolytes

Thesis submitted
By

Sandeep Kumar
(Regd. No. 901209003)

In fulfillment of the requirement for the degree of
Doctor of Philosophy

Under the supervision of
Dr. Rajesh Kumar
Associate Professor

School of Chemistry and Biochemistry
Thapar University
Patiala-147004
Punjab (India)

Acknowledgement

First and foremost, I praise God, the almighty, merciful and passionate, who provides me courage to do this work and helped me in completing this interesting research.

At the very outset, I would like to express my deep and sincere gratitude to my supervisor Dr. Rajesh Kumar (Associate Professor, School of Chemistry and Biochemistry, Thapar University, Patiala), whose positive attitude, patience, motivation, and immense knowledge and encouragement were played a crucial role towards the completion of this thesis. I could not have imagined having a better supervisor for my Ph.D study. He gave me the freedom to explore on my own and at the same time the guidance to improve when my steps faltered. I will never forget the time that he cared me like a guardian.

I would like to express my gratitude to Head, School of Chemistry and Biochemistry, Thapar University, Patiala and other faculty members of the School for providing all the necessary research facilities.

I would like to express my special appreciation to doctoral committee members, Dr. Manmohan Chhibber (School of Chemistry and Biochemistry), Dr. Bonamali Pal (School of Chemistry and Biochemistry) and Dr. Sanjai Saxena (Department of Biotechnology) for providing comments, advices and suggestions in the progress of research work.

Also I want to thank to Dr. Deepak Sharma (Institute of Microbial Technology, Chandigarh) and Dr. Abani K Bhuyan (School of Chemistry, University of Hyderabad, Hyderabad) for providing suggestions and consistent help throughout my Ph.D research work.

I must thank the Dr. B.N. Chudasama (School of Physics and Materials Science), Dr. Amjad Ali (School of Chemistry and Biochemistry) and Dr. H. Bhunia (Department of Chemical Engineering) for their kind support throughout my tenure at Thapar University. I acknowledge Chander Singh Thakur who always willing to help whenever required.

I appreciate my laboratory members Rajesh Kumar, Dr. Rishu Jain and Mukesh Chand Agarwal for valuable discussions and encouragement. I also appreciate of Navinder Kumar and Arpit Gupta for their help and support in Dr. Deepak's lab at IMTECH, Chandigarh. I would like to thank my friend Sumit Joshi, we did a lot together. We shared our foods, rooms, etc. but most of all we shared our loneliness.

I greatly acknowledge Council of Scientific and Industrial research (Govt. of India) for providing me financial support in the form of Senior Research Fellowship-direct (File No. 09/677(0024)/2015 EMR-I). A special thanks to Department of Science and Technology, University Grants Commissions and Indian Council of Medical Research (Govt. of India) for providing the financial assistance to carry out the research work.

At last none of this would have been possible without the love and support of my family. My parents, has been a constant source of love, concern, support and strength for all these years. Their love provided me inspiration and was my driving force. I would like to express my heart-felt gratitude to my father Shri Ompraksh and mother Smt. Saroj. I want to express my deepest love and thanks to my best friend, soul-mate and wife, Deepika. She has been a true and great

supporter and has unconditional love me during the tough and trying periods of research work. I thank my little son, Aarush for making me so happy with his cute smile. A special thanks to my younger sister Komal and brother in law Sandeep Kumar for their love and affection. My heartfelt regards goes to my father in law Shri Dharamveer, mother in law Smt. Roshni, sister in law Tripti and brother in law Parteek for their love and moral support.

Place: Patiala Sandeep Kumar
Date:

Candidate's Declaration

I hereby declare that the work presented in the thesis entitled "***Modulating Protein Stability and Dynamics by Osmolytes and Electrolytes***" being submitted in fulfillment of the requirements for the award of the degree of ***Doctor of Philosophy*** in the School of Chemistry and Biochemistry, Thapar University, Patiala. The matter embodied in this thesis has not been submitted in part or full to any other university or institute for the award of any degree of this or any other university.

Sandeep Kumar

Place: Patiala
Date: 20-10-2016

This is to certify that the above statement by the student concerned is correct and true to the best of my knowledge.

Supervisor
Dr. Rajesh Kumar

Head
School of Chemistry and Biochemistry
Thapar Univeristy

Dean of research and
Sponsored Projects

List of Abbreviations

methylurea	MU
N,N'-dimethylurea	DMU
ethylurea	EU
tetramethylurea	TMU
horse heart cytochrome *c*	Cyt *c*
horse heart myoglobin	Mb
ferrocytochrome *c*	Ferrocyt *c*
ferricytochrome *c*	Ferricyt *c*
myoglobin–CO complex	MbCO
molten globule	MG
Transferrin	Tf
ovotransferrin	oTf
serum transferrin	sTf
milk lactoferrin	Lf
C-lobe of Tf	Fe_CTf
N-lobe of Tf	Fe_NTf
N-lobe of sTf	FesTf
N-lobe of oTf	FeoTf
differric-Tf	Fe_2Tf
diferric-sTf	Fe_2sTf
differic-Lf	Fe_2Lf
diferric-oTf	Fe_2oTf
hen egg white Lysozyme	Lyz
protein data bank	PDB
egg white apo-ovotransferrin	apo-oTf
bovine serum apo-transferrin	apo-sTf
bathophenanthroline disulfonate	BPS
8-anilino-1-naphthalene sulfonate	ANS

4-(2-Hydroxyethyl)-1-piperazineethanesulfonate	HEPES
2-(*N*-mopholino) ethanesulfonate	MES
3-[Cyclohexylamino]-1-propanesulfonic acid	CAPS
circular dichroism	CD
guanidine hydrochloride	GdnHCl
ethylenediaminetetraacetic acid	EDTA
exchange NMR spectroscopy	EXSY
Wyman-Tanford equation	WT equation
linear extrapolation model	LEM
acid-denatured protein	U_A-state
NaCl-induced MG-state of acid denatured protein	A-state
base-denatured Cyt *c*	U_B-state
NaCl-induced MG-state of base denatured Cyt *c*	B-state
tryptophan	Trp
glycerol-induced MG-state of base denatured Cyt *c*	G_B-state
trehalose-induced MG-state of base denatured Cyt *c*	T_B-state
mean residue ellipticity	MRE
glycerol-induced MG-state of acid denatured Ferricyt *c*	G_A-state
thermal denaturation midpoint	T_m
enthalpy of denaturation	ΔH_m
heat capacity change	ΔC_p
free energy of denaturation	ΔG_D
surface area exposed by solvent	m_g
midpoint denaturant concentration	C_m
lysine	Lys
kinetically significant anion binding	KISAB
arginine	Arg
transferrin receptor	TFR
divalent metal transporter	DMT1
activation enthalpy	$\Delta H^{\ddagger}$

activation entropy	$\Delta S^{\ddagger}$
activation free energy	$\Delta G^{\ddagger}$
entropy change	$-T\Delta S^{\ddagger}$
adenosine triphosphate	ATP
histidine	His
electron paramagnetic resonance	EPR
pyrophosphate	pp_i
aspartic acid	ASP
tyrosine	TYR
histidine	HIS
cysteine	Cys
asparagines	ASN
alanine	ALA
glycine	GLY
methionine	MET or M
glutamic acid	GLU
histidine	HSE
leucine	LEU

Contents

Abstract

In chapter 3, the effects of urea and alkylureas were investigated on thermodynamic stability and internal dynamics of heme proteins (Cyt *c* and Mb). To determine the effects of urea and alkylureas on the internal dynamics of heme proteins, the kinetic and thermodynamic parameters for CO-association reaction of Ferrocyt *c* and CO-replacement reaction of MbCO by hexacyanoferrate ion were measured under varying concentrations of urea and alkylureas (MU, DMU, EU, TMU) at pH 7.0. As [denaturant] is increased, the rate coefficient of CO-association for Ferrocyt *c* (k_{ass}) first decrease in subdenaturing region and then increase on going from subdenaturing to denaturing milieu, which indicates that the low concentrations of denaturants constrain the internal dynamics of Ferrocyt *c*. Within the subdenaturing limit, the denaturant-mediated constrained dynamics of Ferrocyt *c* is found to be more for urea and least for TMU. However, within the subdenaturing limit, such denaturant-mediated constrained dynamics is not observed for Mb. Intermolecular docking between horse Cyt *c* and denaturant molecule (urea, MU, DMU, EU and TMU) reveals that polyfunctional interactions between the denaturant and different groups of Ω-loop of Cyt *c* and other part of protein decrease with an increase of alkyl group on urea molecule, which suggests that the decrease in the extent of restricted dynamics of Ω-loop with a corresponding increase of alkyl groups on urea molecule is due to the decrease of denaturant-mediated cross-linking interactions. These denaturant mediated interactions are expected to reduce the entropy of Ferrocyt *c*. Analysis of rate temperature data shows a progressive decrease in entropy of Ferrocyt *c* in the native to subdenaturing region. Thermodynamic analysis of denaturant (urea, MU, DMU, EU and TMU) effects on the thermal unfolding of Ferrocyt *c* and Mb reveals that (i) thermodynamic stability of proteins decreases with increasing concentration of denaturant or hydrophobicity of urea derivatives, (ii) water activity plays an important role in stabilization of protein, and (iii) destabilization of Ferrocyt *c* and Mb by denaturant occurs through the disturbance of hydrophobic interactions and hydrogen-bonding.

In chapter 4, the effects of glycerol and trehalose were investigated on the structural, kinetic and thermodynamic properties of alkali pH-denatured Cyt *c* (U_B-state). Near-UV CD, far-UV CD, tryptophan fluorescence and 1-anilino-8-napthalene sulfonate (ANS) binding experiments suggest that the glycerol and trehalose transform the base-denatured Cyt *c* to MG-states. The glycerol and trehalose -induced fully populated G_B (glycerol-induced) and T_B (trehalose-induced) conformations

of base-denatured Ferricyt *c* and Cyt-CO are molecular compact states containing native-like secondary structural contents but disordered tertiary interactions. The calculated values of free energy change (ΔG^o) for the $U_B \rightarrow G_B$ (ΔG^o ~1.76 Kcal mol^{-1}) and $U_B \rightarrow T_B$ (ΔG^o ~1.62 Kcal mol^{-1}) transitions are within error almost same, where G_B and T_B are the glycerol and trehalose induced MG states of base-denatured Ferricyt *c*. Both G_B and T_B-states of Ferricyt *c* undergo highly cooperative thermal unfolding transitions and they show cold denaturations at low sugar concentration. As [sugar] is increased, the thermal denaturation temperature increase and the cold denaturation temperature decrease. Thermal unfolding of G_B and T_B states of Ferricyt *c* are characterized by a large heat capacity change, indicating that the hydrophobic effect also contributes substantially toward the energetic stabilization of G_B and T_B states. Kinetic and thermodynamic parameters associated with the measurement of CO-association reactions of alkaline Ferrocyt *c* (pH 12.9) at variable concentrations of glycerol and trehalose indicate substantially restricted overall motion and stiffness of the polypeptide chain in G_B- and T_B-states of Cyt-CO.

In chapter 5, the effect of sugars (glycerol, ribose, glucose, maltose, sucrose and trehalose) was investigated on the structural and thermodynamic properties of Lyz at pH 2.3 and pH 13. Near-UV CD, far-UV CD and ANS binding experiments suggest that the glycerol and trehalose transform the base-denatured Lyz (pH 13) to MG-state. This chapter also evaluated the effect of sugars (glycerol, ribose, glucose, maltose, sucrose and trehalose) on the thermodynamic stability of Lyz at pH 2.3 both in the absence and presence of denaturants (GdnHCl and urea). Thermodynamic analysis of thermal and denaturant-induced unfolding transitions of Lyz at pH 2.3 measured at different concentrations of sugars (glycerol, ribose, glucose, maltose, sucrose and trehalose) reveals that these sugars increase the thermal and conformational stability of Lyz. Among the sugars used, the thermal and conformational stability of Lyz is increased more for trehalose and least for glycerol (trehalose > sucrose > maltose > glucose > ribose > glycerol). Thermodynamic analysis of thermal and urea-induced unfolding transitions of Lyz at pH 2.3 measured at different concentration of GdnHCl or urea in the absence and presence of fixed concentration of sugars (glycerol, ribose, glucose, maltose, sucrose and trehalose) reveals that these sugars counteract the destabilizing effect of the denaturants. The counteraction effect of sugars on the destabilizing effect of the denaturants is more pronounced for trehalose and least for glycerol (trehalose > sucrose > maltose > glucose > ribose > glycerol).

In chapter 6, the effects of pH and electrolytes were investigated on the stability and iron release kinetics of oTf. The role of electrostatic interactions to the stability of iron binding to oTf have been assessed by equilibrium experiments that measure iron retention level of diferric-ovotransferrin (Fe_2oTf) as a function of pH and urea in the presence of varying types and concentrations of salts (NaCl, Na_2SO_4, NaBr and $NaNO_3$) at 25 °C. As [salt] is increased, the pH-midpoint for iron release increases monoexponentially and plateau at ~0.4(±0.05)M NaCl/NaBr/$NaNO_3$ or ~0.15(±0.03)M Na_2SO_4. However, at pH 7.4, the urea-midpoints for iron release (based on fluorescence emission at 340 nm) and for unfolding of Fe_2oTf and apo-ovotransferrin (based on ellipticity values at 222 and 282 nm) are found to decrease at low salts concentrations (≤0.1(±0.02)M Na_2SO_4 or ≤0.35(±0.15) M NaCl) but are increased at higher salts concentrations. Furthermore, Na_2SO_4 has a greater effect than does NaCl in increasing the urea-midpoints for iron release and unfolding. These results indicate that at low salt concentrations, the electrostatic interactions control the stability of the oTf-Fe^{3+} complex and secondary and tertiary structures of protein, while at higher salt concentrations; salt ions behave according to Hofmeister series. At pH 5.6, as [salt] is increased, the rate constants for reductive iron release (Fe^{2+} release) and urea-denaturation induced iron release (Fe^{3+} release) from the N-lobe of oTf (Fe_NoTf) increase monoexponentially and plateau at ~0.4(±0.1)M $NaNO_3$/NaCl or ~0.2(±0.05) M Na_2SO_4. These results suggest that the conformational change-induced by anion binding as well as the electrostatic screening of surface Coulombic interactions plays important role in the accelerating of Fe^{2+} and Fe^{3+} release from Fe_NoTf at endosomal pH conditions.

In chapter 7, the effects of concentration, size, shape, and viscosity of crowding agents on stability and iron release kinetics of sTf-Fe^{3+} complex at physiological pH 7.4 and endosomal pH 5.5-5.7 were investigated. As [crowding agent] is increased, the pH-midpoints for iron release of Fe_2sTf shift towards the lower pH values while the urea-denaturation midpoints for iron release and unfolding of Fe_2sTf shift towards the higher urea concentrations, which suggest that the crowding agent presence in the reaction medium increase the Tf-Fe^{3+} complex and structural stability of Fe_2sTf. Furthermore, the crowding agent mediated increase in Tf-Fe^{3+} complex and structural stability of Fe_2sTf typically follows the order: dextran 70 (rod shaped) > dextran 40 (rod shaped) > ficoll 70 (spherical shaped), which suggests that size, shape and viscosity of crowding agent also control the Tf-Fe^{3+} complex and structural stability of Fe_2sTf. As [NaCl] is increased both in the absence and presence of dextran 40, the pH-midpoints for iron release from Fe_2sTf shift towards the

higher pH values while the urea-denaturation midpoints for iron release and unfolding of Fe_2sTf at pH 7.4 and 5.7 shift towards the lower urea concentrations, which suggest that the salt presence both in the absence and presence of crowding agent decrease the Tf-Fe^{3+} complex and structural stability of Fe_2sTf. At pH 7.4 and pH 5.5, as [crowding agent] is increased, the rate constants for reductive iron release (Fe^{2+} release) and urea denaturation-induced iron release (Fe^{3+} release) from the N-lobe of sTf (Fe_NsTf) decrease, which suggest that the crowding agent presence in the reaction medium retards the iron release from Fe_NsTf. Furthermore, the crowding agent mediated retardation in iron release typically follows the order: dextran 70 > dextran 40 > ficoll 70, which suggest that the size, shape and viscosity of crowding agents control the iron release from Fe_NsTf. The anion mediated acceleration of reduction and urea denaturation induced iron release from Fe_NsTf is also observed both in the absence and presence of crowding agent.

In chapter 8, the mechanism of iron release from diferric ovotransferrin (Fe_2oTf) was evaluated at mildly acidic pH ($3.9 \leq pH \leq 4.3$) in the presence of nonsynergistic anions (Cl^-, SO_4^{2-}). In vitro, iron release from Fe_2oTf at mildly acidic pH in the presence of nonsynergistic anions occurs in at least six kinetically detectable steps. Step 1 involves the proton-assisted loss of the synergistic carbonate anion. In subsequent steps, iron release is controlled by slow proton transfers and anion binding. In Step 2, the N-lobe gains one proton. In Step 3, the N-lobe gains one proton with kinetic linkage to the binding of two monoanions or one dianion. In step 4, iron is released from the N-lobe with kinetic linkage to the uptake of two protons accompanied by the loss of anions. In Step 5, the C-lobe gains one proton with kinetic linkage to the binding of two mono anions or one dianion. In Step 6, iron release from the C-lobe occurs with the gains of two protons accompanied by the loss of anions.

Chapter 1
Introduction

In vivo proteins are nature's gift. To perform various biological functions, the unfolded polypeptide chain must fold into a three dimensional native conformation. In 1970s, Chris Anfinsen revealed that the linear amino acid sequence of a polypeptide chain contains all the necessary information to fold in a three-dimensional structure [1]. Despite a commendable progress has been made in protein folding [2-31], a basic question how proteins fold in vivo and in vitro remains enigmatic? In vitro, the molecular interactions assist folding while in cellular milieu, the cellular helper factors, including, praline isomers, protein-protein disulfide isomerase, and molecular "chaperones" assist folding [32]. The traditional view of the protein folding reaction was based on the existence of a preferred route driving the denatured chain to its native conformation via a sequence of consecutive intermediate. Non native compact conformations during protein folding are called as folding intermediates [33]. Misfolded or partially folded intermediates often tend to aggregate because of exposure of hydrophobic core in unstructured polypeptide chain which is originally buried in the native state of protein [34]. In vivo, the highly crowded environment of the cell can also cause the protein aggregation [32,35]. This may lead to formation of highly ordered, amyloid fibrils. These clumps formation in brain are believed to cause the neurodegenerative diseases (Mad Cow and Alzheimer's disease). The native conformations of proteins must be energetically stable. There are several factors such as hydrophobic interactions, ionic interactions, hydrogen bonding, conformational entropy, metal coordination, and disulfide bonding are accountable for the correct folding and stability of proteins [36-38]. The equilibrium between unfolded and native state of the protein can be altered by varying these factors through the changes in solvent conditions (*i.e.*, changes in cosolvents composition, temperature and pH) [39-41]. The interrelationships between protein function, stability, and dynamics play significant role in many biological processes.

Stabilization of proteins, which are particularly susceptible to osmotic stress, is of key importance to the cell's health. All organisms typically experience various types of water stress, *i.e.*, stresses such as high or low temperature, desiccation, and external osmotic pressure [39]. To avoid osmotic catastrophe under stress conditions, the cell volume is maintained osmotically via carefully controlled changes in the intracellular concentrations of organic osmolytes [39,42-43]. Naturally occurring osmolytes are typically classified as protecting and non-protecting

osmolytes. The non-protecting osmolytes (*i.e.,* urea) generally denature the proteins [44-74]. In contrast, protecting osmolytes generally increase the stability of native proteins but they do not greatly affect the native structure of protein [75]. Protecting osmolytes provide protection against denaturing stresses. Naturally occurring protecting osmolytes mainly include following three chemical classes: (i) the polyols, which include glycerol, sucrose, trehalose, sorbitol and other sugars, (ii) certain amino acids, including glycine and proline and (iii) methylamines, such as sarcosine, betaine and trimethylamine-*N*-oxide [39,42-43,75]. Protecting osmolytes maintain the intracellular proteins in a soluble form in order to maintain cell viability. Intracellular presence of Trimethylamine-*N*-oxide in the cells of rays and sharks is supposed to counteract the deleterious effect of urea [39]. They manage the cell volume regulation under water-stressed conditions that may includes (i) extremes of temperature, (ii) extremes of pressure, (iii) changes in extracellular osmotic condition, (iv) desiccation, or (v) even the intracellular presence of the protein denaturing osmolyte, urea [76-78]. Protecting osmolytes favors the folded conformation through increasing the free energy of the unfolded conformation, whereas non-protecting osmolytes favour the unfolded conformation through lowering the free energy of the unfolded conformation [79-81]. Generally, the non-protecting osmolytes interact favorably with the unfolded conformation, resulting in preferential accumulation of non-protecting osmolytes proximate to the protein surface and protecting osmolytes interact unfavorably with the unfolded conformation, resulting in preferential depletion of osmolytes proximate to the protein surface [79-81]. However, the exact mechanism of osmolytes-proteins interactions is still unknown.

Denaturants like urea (a non-protecting osmolyte) [44-74] and guanidine hydrochloride (GdnHCl) [82-83], alcohols [84-85] are widely used to study the stability and folding of proteins. However, the mechanisms by which these denaturants unfold the proteins in aqueous solution are poorly understood.The molecular mechanisms responsible for urea-induced protein denaturation are not clearly understood. Two classes of interactions are distinguished in the literature- (i) direct hydrogen-bonding interactions between urea and protein molecule [44-53] or (ii) indirect effects via changes in water structure [54-59]. So far it is not clear whether urea forms hydrogen bonds with the polypeptide backbone or the polar residues [50,54-56,60-68]. Calorimetric studies with cyclic dipeptides in urea reveal that both mechanisms can contribute significantly in the denaturant-induced unfolding of proteins [69]. Poklar et al investigated the effect of alkylureas on the thermodynamic stability of β-lactoglobulin A [70-71], α-chymotrypsinogen A [72-73],

and ribonuclease A [74-75]. They reported two important results: (i) the thermodynamic stability of these proteins decrease with increasing hydrophobicity of urea derivatives [70-75], and (ii) depending on the hydrophobicity and concentration of alkylureas, they also destabilize the tertiary structure and can cause rearrangement and distortion of secondary structure of proteins [70-75].

The interrelationships between protein function, stability, and dynamics play significant roles in protein engineering and biological process. In last few years, XRD-technique [86-87] and NMR spectroscopy [87-88] have been vastly used to correlate structure, conformational changes, function, and stability of proteins. Despite a commendable progress has been made in understanding the physics of protein folding, the investigations of protein dynamics are still in its infancy [89]. In particular, internal dynamics that include small amplitude collective motions [90], large amplitude cooperative breathing modes [91], and structural fluctuations at the subglobal level [92] are poorly understood.

The stability and dynamics of proteins in solution are strongly coupled to the dynamics of solvent [89,93-96]. In terms of time scale, protein undergoes structural fluctuations from ultrafast (in the femtoseconds to picoseconds range) to relatively slow (in the range of seconds) [97-101]. Structural fluctuations which occur on the ultrafast time scale eventually facilitate larger scale protein rearrangements that are responsible for modulating the biological functions of proteins [93,102-103]. Although, the fast protein motions that control conformational transitions associated with protein function has been studied extensively [104-108], the relatively slow changes in structural dynamics of proteins across the folding-unfolding transition has received meager attention [109-110]. Equilibrium hydrogen exchange experiments under native to denaturing conditions provide evidence for selective and sequential opening of subglobal strucres in a manner that restricts the possible folding pathways to a limited set [110]. The possible roles of structural dynamics in folding can be determined by studying the changes in thermal fluctuations at both atomic and large-scale collective level. Neutron scattering techniques [111], NMR relaxation and spectral density maps [112-113], and cross-relaxation suppressed exchange NMR spectroscopy (EXSY) [114] have provided valuable insight into the structural dynamics of proteins. Analysis of X-ray data for certain protein crystals soaked in denaturant (urea or GdnHCl) solution indicates that the low concentrations of denaturant reduce the mobility of native proteins [115-116]. Constraints on intramolecular dynamics can also

reduce the amplitudes of thermal fluctuations [115-117]. Analysis of the effect of GdnHCl concentration on the rate of slow dynamic processes such as Y97 ring-flip motions in Ferricytochrome *c* (Ferricyt *c*) and thermal dissociation of CO from natively folded CO-liganded Ferrocytochrome *c* (Ferrocyt *c*) also provides evidence that the low concentrations of denaturant restrict the internal dynamics of protein [109,114]. In order to determine the role of hydrophobic and hydrogen bonding interactions on the stability, folding and dynamics of native proteins, this thesis work investigated the effects of urea and alkylureas on the thermodynamic stability and internal dynamics of horse heart cytochrome *c* (Cyt *c*) and horse heart myoglobin (Mb). To determine the effect of urea and alkylureas on the internal dynamics of heme proteins, the CO-association reaction of Ferrocytochrome *c* (Ferrocyt *c*) and CO-replacement reaction of myoglobin–CO complex (MbCO) by hexacyanoferrate ion were measured under varying concentrations of urea and its alkyl derivatives (MU, DMU, EU, and TMU).

In vitro, sugars are widely used as stabilizing agents for the maintenance of biological activity of biomolecules [118-125]. Glycerol, sucrose, glucose, and trehalose are most widely used sugars due to their protein stabilizing efficiency [120,126]. Sugars also exhibit the function of aiding in protein folding, refolding and in preventing protein aggregation [127-128]. The ability of protecting osmolytes to protect against denaturation is supposed to be generic and independent of the evolutionary history of the proteins [129-130]. Sugars may also strengthen the intermolecular O-H interactions responsible for the stability and structure of proteins [131]. Sugars protect the proteins against dehydration by hydrogen bonding to the dried protein by serving as water substitute [132-133]. Despite its widespread use the molecular basis for sugars ability to stabilize the proteins remains unknown. Sugars protect the protein against thermal denaturation through increasing the thermal denaturation temperature (T_m) [131,134-148]. Higher thermal stability of enzymes advantageous for the industries where thermostable enzymes provide increased rate of reactions, longer shelf-lives at normal storage temperatures and lowered risk of microbial contamination [149]. Sugars have more stabilizing effect on the pH-denatured proteins than the native proteins [136-138]. Sugars have ability to refold and stabilize the acid-denatured protein to molten globule (MG)-state [150-152].

A molten globule (MG) is a molecular compact state with native-like secondary structure but with a disordered tertiary structure [153-155]. On the basis of structural and kinetic studies, MG-state has been assumed to be a major intermediate in protein folding [155-159]. Several

earlier reports suggest that MG-state can occur both in the late stages of folding [154-155,160-161] as well as in the early stages of folding [158,162-164]. The MG-state is also very important for protein function in the living cell [153]. A family of intrinsically disordered proteins that lacks tertiary structure but are MG-like [165-167] have been found to be involved in cell signaling and regulatory functions through their interactions with DNA and other proteins [168-171]. A number of small angle X-ray scattering studies revealed that MG-state adopts a wide range of structures from the relatively disordered to highly ordered [172-173], which imply that the MG-state is a largely fluctuating ensemble with various energy minimum. The effect of electrolytes or charges on the stability of MG-state showed that the reduction of electrostatic repulsion between charged residues of unfolded conformation is the main driving force of MG-state stability [158,174-176].

Timasheff and co-workers demonstrated that sugars stabilize the protein as a result of preferential hydration of the denatured state as compared native state [134-135]. Thus, the folded state of protein is stabilized relative to the unfolded state because it exposes less surface area from which the cosolvents must be excluded. While the effects of sugars on the fast protein dynamics are widely studied [177-179], very little has been done to record the effect of sugars on low-frequency local motions that control the relatively slow changes in structural dynamics of proteins [180]. Furthermore, the effect of sugars on the thermodynamic stability of pH-denatured proteins is not clearly understood [150]. In order to understand the effect of sugars on the pH-denatured proteins, this thesis work investigated the effect of sugars (glycerol, ribose, glucose, maltose, sucrose and trehalose) on the structural and thermodynamic properties of Cyt *c* and Lysozyme (Lyz) at pH 12.9-13 or pH 2.3. To determine the effect of sugars on the internal dynamics of protein, the CO-association reaction of Ferrocyt *c* were measured under varying concentrations of glycerol and trehalose at pH 12.9.

The contribution from ionic interactions in proteins is relatively more complex [181]. For example, the low pH triggers a large conformational change in transferrins (Tfs), which is a critical step for iron release in endosome [182-196]. In general, the pH modulates the protein stability by altering the charges on ionizable groups in the proteins through protonation or deprotonation [197]. Buffer conditions such as pH and electrolyte (salt) can have dramatic effect on biological functions of proteins [182-196,198-210]. The salt ions also modulate the stability of proteins [211-212]. At lower salt concentrations, salt ions affect the stability of proteins by

altering the electrostatic (Debye-Hückel) screening of Coulombic interactions [213-215]. On the other hand, the specific ion binding effects of salt often occurs at less than one millimolar salt concentrations [216] while the hydrophobic effects of salt dominates at molar salt concentrations (>0.5 M) [213-214,217-219]. At relatively higher salt concentrations, the Hofmeister effect, which depends on the nature of added ions, also affects the stability of proteins by increasing the surface tension of solvent that eventually modulates the hydrophobic interactions [212,220-223]. According to Hofmeister series, the anions typically follow the order: $F^- \approx HPO_4^{2-} > SO_4^{2-} > CH_3COO^- > Cl^- > NO_3^- > Br^- > ClO_3^- > I^- > ClO_4^- > SCN^-$ [211]. The species left to the Cl^- are referred to as kosmotropes (ordering of water structures and thus stabilize the protein) and causes salting out effect while those right to the Cl^-, known as chaotropes (breaking of water structure and thus destabilize the proteins), leads to salting-in effects [220-223].

Structurally, transferrins (Tfs; serum transferrin (sTf), ovotransferrin (oTf) and lactoferrin (Lf)) are bi-lobed glyco-proteins proteins, N- and C-terminal domains of approximately similar size, and each can bind one iron (Fe^{3+}) synergistically with a carbonate anion [185, 224-227]. These two domains are connected by a linker sequence [228-229]. The synergistic anion carbonate is an absolute necessary for the interaction of Tfs with the iron [227,230-233]. Carbonate (or bicarbonate) is the dominant synergistic anion *in vivo* that plays a critical role in physiological release and uptake of iron by Tfs [234-241]. The affinity of Tfs for Fe^{3+} is extremely high ($K_a \sim 10^{20}$ M^{-1}) [242-245]. The high affinity for Fe^{3+} gives protection against iron-catalyzed free radical formation and limits the bacterial growth. Tfs can also bind non-ferrous metal ions [246-249], few of them are of therapeutic and diagnostic interest [243,250-252]. sTf is primarily responsible for iron transport from biological fluids to cytosol by receptor-mediated endocytosis [234] while oTf and Lf act as bacteriostatic agents [226]. Few earlier *in-vitro* studies have revealed that the oTf also possesses the cellular iron transport functions [253-255].

Delivery of Fe^{3+} from plasma to tissue cells occurs via pH-dependent receptor-mediated endocytosis [256-258]. At neutral pH, circulating sTf preferentially binds to the extracellular portion of the transferrin receptor (TFR) on the cell surface followed by rapid internalization into an acidic endocytic compartment [259]. In endosome, acid induced conformational change releases the Fe^{3+} from sTf-Fe^{3+} complex [260-261]. Now, there is prerequisite for reduction of Fe^{3+} because only Fe^{2+} is transported out of endosomal lumen to cytoplasm by divalent metal transporter (DMT1) [234]. Reduction of Fe^{3+} is mediated by an endosomal ferrireductase [259-

260]. After iron release, apo-sTf remains bound to the TFR and recycled back to the cell surface. The sTf protein is present at a concentration of ~3 mg mL^{-1} in serum of a healthy human body. It is only ~30% saturated with iron [262], which allowing it to significantly bind and transport other metal ions. More than thirty metal ions can bind to Tfs and some of them are of therapeutic and diagnostic interest [250-252]. Ferritin and sTf manage essential stores of iron in our body. Inside cells, extra iron is locked safely in the protein shell of ferritin [263-264]. At neutral pH, the affinity of Tfs for iron is extremely high but decreases progressively with decreasing pH below neutrality [83,182,184-196,215]. Increasing evidences suggest that both pH and many non-synergistic anions (e.g., SO_4^{2-}, Cl^-, NO_3^-, ClO_4^-, etc.) which do not bind directly to iron but bind to the protein [188,265-270] also play an important role in iron release from Tfs [188,269, 253-255, 263, 265-285]. However, the effect of non-synergistic anions on the chelator-meditated iron release from monoferric- (Fe_NTfs or Fe_CTfs) and differric-Tfs (Fe_2Tfs) remains controversial because it depends on the types of chelator used [269, and reference there in]. The contributions of electrostatic and hydrophobic interactions to the stability of proteins are generally determined by measuring the stability of proteins in the presence of varying types and concentrations of salts often as function of pH [206,286-287]. Although, the effects of salts on the stability of proteins have been studied extensively [203,215,218,288-289], only few studies measured the relative contributions of the electrostatic and hydrophobic interactions to the stability and functional properties of proteins [215,289]. This thesis work investigated the effects of pH and salts on the stability and iron release kinetics of oTf and sTf.

The structures of N- and C-lobes are quite similar in Tfs. However, these lobes are different in: (a) affinity for iron binding [252,290-291], (b) conformational and thermal stability [292-293], (c) interaction with nonsynergistic anions, [294] and (d) kinetics of iron binding and release [279-280, 295-297]. Few earlier reports suggest that protonation and anion binding to the protein control the kinetics of iron release from diferric-sTf (Fe_2sTf) and differic-Lf (Fe_2Lf) [295,298-301]. To understand the mechanisms by which pH and salts influence the biological functions of proteins, by using the methods and techniques of chemical relaxation [295,300,302-304], this thesis work investigated the effects of salts (NaCl and Na_2SO_4) on the kinetics and mechanism of iron release from diferric ovotransferrin (Fe_2oTf) at mildly acidic pH conditions.

The cell is filled with large numbers of macromolecules (nucleic acid, ribosomes, lipids, carbohydrate, and proteins) [305-306]. The concentration of these macromolecules in the

cytoplasm ranges from 50-400 mg ml^{-1} [307-309]. Cumulative excluded volume from all macromolecules inside the cell is generally referred by “macromolecular crowding” [310-311]. The term “macromolecular crowding” coined by Minton implies the nonspecific influence of steric repulsions on specific reactions that occur in high volume occupied media [312]. The macromolecular crowding is generally described as an excluded volume effect [313]. Because of it any reaction that amplifies the available volume will be stimulated by macromolecular crowding [314-315]. According to excluded volume effects, crowding is a nonspecific force that favors processes resulting in the reduction of total volume, such as the folding of proteins [316-317].

Macromolecular crowding has a significant impact on the protein conformational change, structure, folding, stability, activity, binding, mobility, protein-protein interactions, aggregation and protein allostry [312,317-344]. The milieu of cytoplasm is considered as a highly crowded and concentrated that modulates the kinetics and thermodynamics of biochemical reactions [318-320,345-352]. Macromolecular crowding alters the equilibrium constants and reaction rates through: (i) change in reactant molecules mobility [353-356], (ii) depletion interaction (excluded volume effect) that results in attraction between protein and crowder [320,345,357-359], and (iii) non-specific chemical interaction between protein and crowder [349-350,360-361].

The highly crowded intracellular environment alters the thermodynamics of biophysical processes including protein folding, dissociation, association and diffusion [320,362-365]. Generally, the macromolecular crowding effect described in two ways, hardcore repulsions and nonspecific chemical (soft) interactions [349-351,366-369]. Excluded volume effect originates from hardcore repulsions that decreases the volume available to the protein and thus favors the compact conformation of protein. Excluded volume effect generates anisotropic osmotic pressure known as a depletion force that pushes the molecules together [370-371]. The hardcore repulsive effect involves only the arrangement of molecules, not their chemical interaction. The second phenomenon arises because crowders not only exclude volume, but also participate in nonspecific chemical (soft) interaction for which coulombic interactions [369], hydrogen bonds, and the hydrophobic effect are key players [372-373]. Repulsive nonspecific interactions reinforce the hardcore repulsions, whereas attractive nonspecific interactions oppose them. Even though individually weak, the high concentration of macromolecules can lead to a large net

effect [361]. The crowding effects described to arise from entropic and enthalpic contributions; hard-core repulsions are entropic, whereas the consequent nonspecific chemical interactions are enthalpic.

Crowded environment is not confined to cellular interiors but also occurs in the extracellular matrix of tissues and takes place at membrane surfaces [319,374]. The blood plasma contains ~80 mg ml^{-1} of protein, a concentration sufficient to cause significant crowding effect [319]. sTf-Fe^{3+}-receptor complex releases its iron under a highly crowded cellular environment [256-261]. Factor affecting the stability and iron release from Tfs have been well established by different research groups in dilute solutions [182-196,269, 253-255, 263, 265-285]. However, the physiological environment is poorly modeled by such dilute solutions [375]. *In vivo,* the biochemical reactions differ significantly from those studied *in vitro* in dilute solutions [375]. While the effects of macromolecular crowding on the stability [376,377,387-385, and reference there in] and functional properties of proteins [386,387-388,389-391] have been studied extensively, the effects of macromolecular crowding on the functional properties of Tfs are not explored so far Thus, the macromolecular crowding in the blood plasma, on the cell surface and in the endosome may play an important role in the conformational transition during iron release from sTf. In vivo, the environment around sTf is crowded with molecules of different shapes and sizes. Proteins have evolved to function under such crowded environments. To model the iron release from sTf by mimicking the *in vivo* conditions, *in vitro* such a crowded environment can be achieved by adding high concentrations of crowding agents to the system [319-320,326,352,374, 392-395]. In vitro, synthetic crowding agents such as dextran and ficoll are often used to mimic the intracellular crowding [278-285,396-398]. They are chemically inert, non-charged polymers of certain sizes and shapes (i.e., dextran 40, dextran 70 and ficoll 70). They occupy the space in reaction medium but do not interact directly with the proteins [404-406]. Dextran 40 and dextran 70 are polymers of D-glucopyranose and these behave as a quasi random coil due to flexibility and linearity having R_h of ~45 Å and ~63 Å, respectively [399-403]. Ficoll 70 is a compact and highly cross-linked and branched copolymer of sucrose and epichlorohydrin that can be approximated as a semi-rigid sphere having R_h of ~55 Å [401-403]. Dextran has a lower degree of branching than ficoll that adopts a more elongated and flexible shape [404-406]. Thus, the relative studies employing these crowding agents allow us to examine

how the nature and the geometric shape of the respective crowding agent affect the stability and iron release from sTf.

The macromolecular crowding can modulate the structure, stability, and function of sTf.–To understand how sTf executes its biological function in a highly crowded cellular environment, this thesis work evaluated the effects of concentration, size, shape and viscosity of crowding agents (dextran 40, dextran 70 and ficoll70) on stability and iron release kinetics of sTf. This thesis work also evaluated the effect of crowding agent (dextran 40) on the salt (NaCl) dependence of the stability and iron release kinetics of sTf.

Cyt *c* and Mb serve as paradigm for the study of stability and folding of proteins. The heme protein Cyt *c* is known for its role as an electron carrier in the mitochondrial electron transport chain [407]. The structure of Cyt *c* (104 amino acids and 12.4 kDa molecular weight) consists of five *α*-helices connected by Ω loops (Fig. 1.1a) [408]. The presence of covalently bound heme, smaller size and single-domain in Cyt *c* makes it paradigm for examining new concepts and approaches in protein folding [409-411]. Cyt *c* is involved in apoptosis. Nantes et al observed that (de)protonations of ionic residues due to change in pH of mitochondrial intermembrane space alter the binding efficiency of Cyt *c* to Cyt oxidase, Cyt reductase and other components of electron transfer chain, which in result change the normal function of protein and induce the apoptosis [412]. The biological activity of Cyt *c* as a mitochondrial electron transport shuttle strongly depends on maintaining the native HIS18/MET80 heme coordination [413]. Mb is also a heme protein that stores oxygen in cardiac muscle and facilitates the diffusion of oxygen from blood capilliaries to the mitochondria. It can also bind other ligands such as NO and CO [414]. The structure of Mb (153 amino acid and 16.7 kDa molecular weight) consists of eight α-helicies connected by short loops (Fig. 1.1b). Because of its vital role in the muscle metabolism and noncovalently bound heme group, Mb has been the subjects of intensive biophysical research [415-416]. Lyz is found in tears, saliva, human milk, and mucus. Lyz damages the cell walls of bacteria and thus exhibits bacteriolytic functions. Lyz (129 amino acid and 14.3 kDa molecular weight) is a bi-domains (α-helical and β-sheet domains) globular protein (Fig. 1.1c). Owing to its smaller size, high-abundance and well characterized biophysical properties, Lyz has been frequently used in protein science [420-423]. The bi-lobed structcture of Fe_2oTf is shown in Fig. 1.1d.

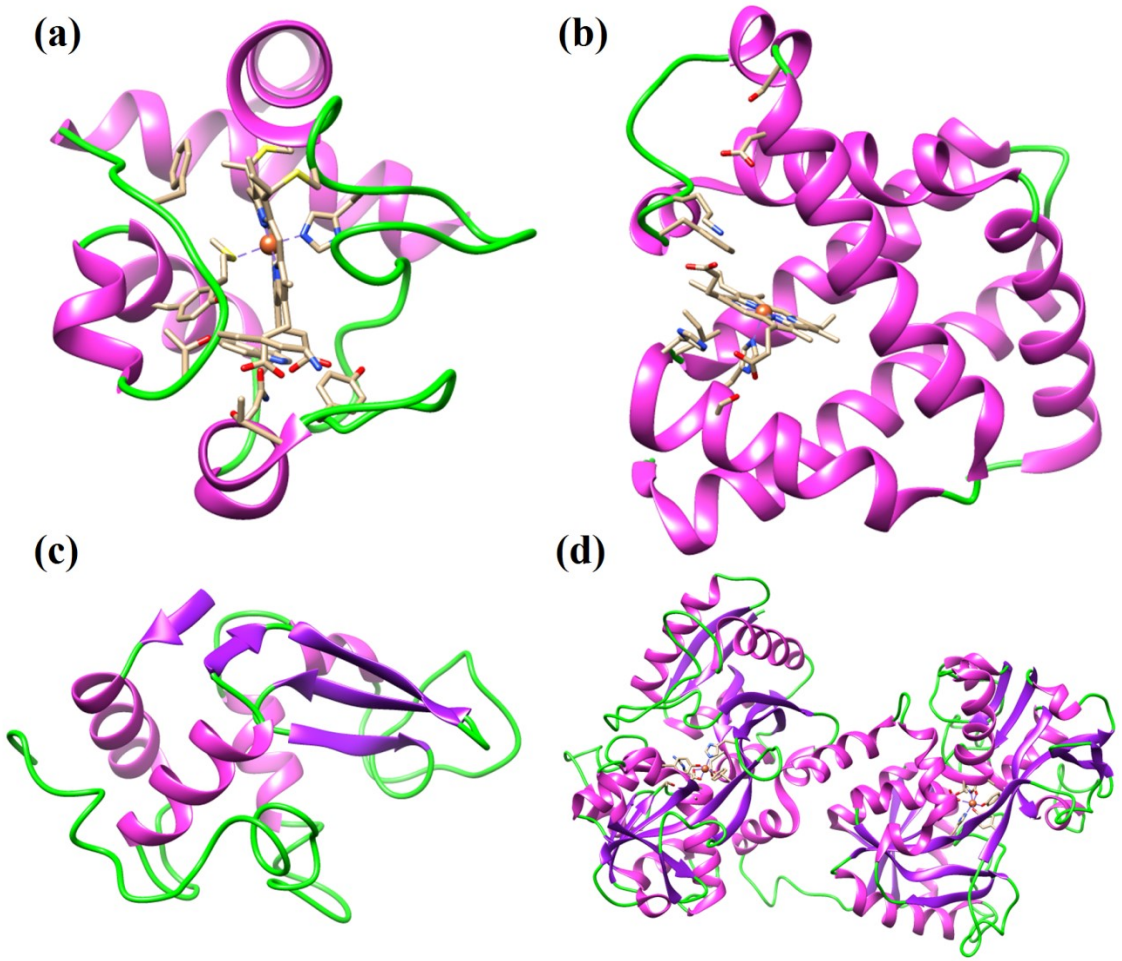

Fig. 1.1 Ribbon models for (a) Cyt *c* (PDB: 1HRC) [408], (b) Mb (PDB: 1YMB) [417], (c) Lyz (PDB: 2LYZ) [418] and (d) oTf (PDB: 1OVT) [419].

References

[1] Anfinsen CB, Science 181:223–230 (1973)
[2] Englander SW, Mayne L, Proc Natl Acad Sci USA 111:15873–15880 (2014)
[3] Adhikari AN, Freed KF, Sosnick TR, Phys Rev Lett 111:028103 (2013)
[4] Pande VS, Adv Exp Med Biol 797:101–106 (2014)
[5] Lindorff–Larsen K, Piana S, Dror RO, Shaw DE, Science 334:517–520 (2011)
[6] Bédard S, Krishna MM, Mayne L, Englander SW, Proc Natl Acad Sci USA 105:7182–7187 (2008)
[7] Bai Y, Englander JJ, Mayne L, Milne JS, Englander SW, Methods Enzymol 259:344–356 (1995)
[8] Onuchic JN, Luthey–Schulten Z, Wolynes PG, Annu Rev Phys Chem 48:545–600 (1997)
[9] Wolynes PG, Onuchic JN, Thirumalai D, Science 267:1619–1620 (1995)
[10] Krishna MM, Englander SW, Protein Sci 16:449–464 (2007)

[11] Levinthal C, J Chim Phys 65:44–45 (1968)
[12] Plotkin SS, Onuchic JN, Q Rev Biophys 35:111–167 (2002)
[13] Chandrayan SK, Guptasarma P, Biochim Biophys Act 1794:905–912 (2009)
[14] Chandrayan SK, Prakash S, Ahmed S, Guptasarma P, PLoS One 9:e80014 (2014)
[15] Kundu B, Guptasarma P, Proteins 37:321–324 (1999)
[16] Shukla A, Guptasarma P, Proteins 55:548–557 (2004)
[17] Chandrayan SK, Guptasarma P, Proteins 72:539–546 (2008)
[18] Arya S, Kumari A, Dalal V, Bhattacharya M, Mukhopadhyay S, Phys Chem Chem Phys 17:22862–22871 (2015)
[19] Bhattacharya M, Mukhopadhyay S, J Phys Chem B 116:520–531 (2012)
[20] Dalal V, Bhattacharya M, Narang D, Sharma PK, Mukhopadhyay S, J Phys Chem Lett 3:1783–1787 (2012)
[21] Singh AK, Manjasetty B, Balasubramani GL, Koul S, Kaushik A, Ekka MK, Singh V, Kumaran S, PLoS One 10:e0124333 (2015)
[22] Singh SM, Cabello–Villegas J, Hutchings RL, Mallela KMG, Proteins 78:2625–2637 (2010)
[23] Assfalg M, Bertini I, Dolfi A, Turano P, Mauk AG, Rosell FI, Gray HB. J Am Chem Soc 125:2913–2922 (2003)
[24] Konermann L, Rosell FI, Mauk AG, Douglas DJ, Biochemistry 36:6448–6454 (1997)
[25] Biswas D, Pandya V, Singh AK, Mondal AK, Kumaran S, PLoS One 7:e45525 (2012)
[26] Rao DK, Bhuyan AK, J Biomol NMR 39:187–196 (2007)
[27] Bhuyan AK, Biochemistry 41:13386–13394 (2002)
[28] Bhuyan AK, Kumar R, Biochemistry 41:12821–12834 (2002)
[29] Kumar R, Bhuyan AK, Biochemistry 44:3024–3033 (2005)
[30] Bhuyan AK, Udgaonkar JB, J Mol Biol 312:1135–1160 (2001)
[31] Bhuyan AK, Udgaonkar JB, Proteins 32:241–247 (1998)
[32] Ellis RJ, Minton AP, Biol Chem 387:485–497 (2006)
[33] Brockwell DJ, Radford SE, Curr Opin Struct Biol 17:30–37 (2007)
[34] Hart FU, Hart MH, Nat Struct Mol Biol 16:574–581 (2009)
[35] Zimmerman SB, Trach SO, J Mol Biol 222:599–620 (1991)
[36] Prabhu N, Sharp K, Chem Rev 106:1616−1623 (2006)
[37] Benseny–Cases N, Cocera M, Cladera J, Biochem Biophys Res Commun 361:916−921 (2007)
[38] Reuveni S, Granek R, Klafter J, Phys Rev Lett 100:208101–208104 (2008)
[39] Yancey PH, Clark ME, Hand SC, Bowlus RD, Somero GN, Science 217:1214−1222 (1982)
[40] Shellman JA, Biophys J 85:108−125 (2003)
[41] Yancey PH, J Exp Biol 208:2819−2830 (2005)
[42] Bolen DW, Baskakov IV, J Mol Biol 310:955–963 (2001)
[43] Chamberlin ME, Strange K, Am J Physiol 257:C159–173 (1989)
[44] Clark ME, In Transport Processes, Iono– and Osmoregulation, ed. R Gilles, M Gilles–Baillien, Berlin/Heidelberg: Springer–Verlag pp. 412–423 (1985)
[45] Åstrand PO, Wallqvist A, Karlström G, J Phys Chem 98:8224–8233 (1994)
[46] Tirado–Rives J, Orozco M, Jorgensen WL, Biochemistry 36:7313–7329 (1997)
[47] Grdadolnik J, Marechal Y, J Mol Struct 615:177–189 (2002)
[48] Mountain RD, Thirumalai D, J Am Chem Soc 125:1950–1957 (2003)

[49] Klimov DK, Straub JE, Thirumalai D, Proc Natl Acad Sci USA 101:14760–14765 (2004)
[50] Tobi D, Elber R, Thirumalai D, Biopolymers 68:359–369 (2003)
[51] O'Brien EP, Dima RI, Brooks B, Thirumalai D, J Am Chem Soc 129:7346–7353 (2007)
[52] Stumpe MC, Grubm€uller H, J Am Chem Soc 129:16126–16131 (2007)
[53] Stumpe MC, Grubm€uller H, PLoS Comput Biol 4:e1000221 (2008)
[54] Das P, Zhou R, J Phys Chem B 114:5427–5430 (2010)
[55] Bennion BJ, Daggett V, Proc Natl Acad Sci USA 100:5142–5147 (2003)
[56] Frank HS, Franks F, J Chem Phys 48:4746–4757 (1968)
[57] Finer EG, Franks F, Tait MJ, J Am Chem Soc 94:4424–4429 (1972)
[58] Hoccart X, Turrell G, J Chem Phys 99:8498–8503 (1993)
[59] Das A, Mukhopadhyay C, J Phys Chem B 113:12816–12824 (2009)
[60] Yang L, Gao YQ, J Am Chem Soc 132:842–848 (2010)
[61] Auton M, Bolen DW, Proc Natl Acad Sci USA 102:15065–15068 (2005)
[62] Courtenay ES, Capp MW, Record TM Jr, Protein Sci 10:2485–2497 (2001)
[63] Moglich A, Krieger F, Kiefhaber T, J Mol Biol 345:153–162 (2005)
[64] Caballero–Herrera A, Nordstrand K, Berndt KD, Nilsson L, Biophys J 89:842–857 (2005)
[65] Oostenbrink C, van Gunsteren WF, Phys Chem Chem Phys 7:53–58 (2005)
[66] Makhatadze GI, Privalov PL, J Mol Biol 226:491–505 (1992)
[67] Lee M–E, van der Vegt NFA, J Am Chem Soc 128:4948–4949 (2006)
[68] Nozaki Y & Tanford C, J Biol Chem 238:4074–4081 (1963)
[69] Zou Q, Habermann–Rottinghaus S, Murphy K, Proteins 31:107–115 (1998)
[70] Poklar N, Lapanje S, Biophys Chem 42:283–290 (1992)
[71] Poklar N, Vesnaver G, Lapanje S, Biophys Chem 47:143–151 (1993)
[72] Poklar N, Vesnaver G, Lapanje S, J Protein Chem 14:709–719 (1995)
[73] Poklar N, Vesnaver G, Lapanje S, Biophys Chem 57:279–289 (1996)
[74] Poklar N, Petrovcic N, Oblak M, Vesnaver G, Protein Sci 8:832–840 (1999)
[75] Poklar N, Lah N, Oblak M, Vesnaver G, Acta Chim Slov 46:315–322 (1999)
[76] Yancey PH, Somero G, Biochem J 183:317–323 (1979)
[77] Somero G, Am J Physiol 251:R197–R213 (1986)
[78] Gillett MB, Suko JR, Santoso FO, Yancey PH, J Exp Zool 279:386–391 (1997)
[79] Lee JC, Timasheff SN, J Biol Chem 256:7193–201 (1981)
[80] Wang A, Bolen DW, Biochemistry 36:9101–9108 (1997)
[81] Street TO, Bolen DW, Rose GD, Proc Natl Acad Sci USA 103:13997–4002 (2006)
[82] Pace CN, Methods Enzymol 131:266–280 (1986)
[83] Schellman JA, Biophys Chem 96:91–101 (2002)
[84] Hirato N, Mizuno K, Goto Y, J Mol Biol 275:365–378 (1998)
[85] Velicelebi G, Sturtevant JM, Biochemistry 18:1180–1186 (1979)
[86] Pellicena P, Kuriyan J, Curr Opin Struct Biol 16:702–709 (2006)
[87] Grishaev A, Wu J, Trewhella J, Bax A, J Am Chem Soc 127:16621–16628 (2005)
[88] Stangler T, Hartmann R, Willbold D, Koenig BW, Z Phys Chem 220:567–613 (2006)
[89] Fenimore PW, Frauenfelder H, McMahon BH, Young RD, Proc Natl Acad Sci USA 101:14408–14413 (2004)
[90] Karplus M, Methods Enzymo l131:283–307 (1986)
[91] Englander SW, Downer NW, Teitelbaum H, Annu Rev Biochem 41:903–924 (1972)

[92] Ansari A, Berendzen J, Bowne SF, Frauenfelder H, Iben IE, Sauke TB, Shyamsunder E, Young RD, Proc Natl Acad Sci USA 82:5000–5004 (1985)
[93] Frauenfelder H, McMahon BH, Austin RH, Chu K, Groves JT, Pro Natl Acad Sci USA 98:2370–2374 (2001)
[94] Fenimore PW, Frauenfelder H, McMahon BH, Parak FG, Proc Natl Acad Sci USA 99:16047–16051 (2002)
[95] Ansari A, Jones CM, Henry ER, Hofrichter J, Eaton WA, Science 256:1796–1798 (1992)
[96] Beece D, Eisenstein L, Frauenfelder H, Good D, Marden MC, Reinisch L, Reynolds AH, Sorensen LB, Yue KT, Biochemistry 19:5147–5157 (1980)
[97] Sottini S, Abbruzzetti S, Viappiani C, Bettati S, Ronda L, Mozzarelli A, J Phys Chem B 109:11411–11413 (2005)
[98] Sawicki CA, Khaleque MA, Biophys J 44:191–199 (1983)
[99] Lim M, Jackson TA, Anfinrud PA, J Am Chem Soc 126:7946–7957 (2004)
[100] Merchant KA, Noid WG, Akiyama R, Finkelstein IJ, Goun A, McClain BL, Loring RF, Fayer MD, J Am Chem Soc 125:13804–13818 (2003)
[101] Rector KD, Jiang J, Berg M, Fayer MD, J Phys Chem B 105:1081–1092 (2001)
[102] Viappiani C, Bettati S, Bruno S, Ronda L, Abbruzzetti S, Mozzarelli A, Eaton WA, Proc Natl Acad Sci USA 101:14414–14419 (2004)
[103] Ansari A, Colleen MJ, Henry ER, Hofrichter J, Eaton WA, Biochemistry 33:5128–5145 (1994)
[104] Austin RH, Beeson KW, Eisenstein L, Frauenfelder H, Gunsalus IC, Biochemistry 14:5355–5373 (1975)
[105] Frauenfelder H, Parak F, Young RD, Ann Rev Biophys Biophys Chem 17:451–479 (1988)
[106] Schlichting I, Berendzen J, Phillips GN, Sweet RM, Nature 371:808–812 (1994)
[107] Parak F, Curr Opin Struct Biol 13:552–557 (2003)
[108] Bourgeois D, Vallone B, Schotte F, Arcovito A, Miele AE, Sciara G, Wulff M, Anfinrud P, Brunori M, Proc Natl Acad Sci USA 100:8704–8709 (2003)
[109] Kumar R, Prabhu NP, Yadaiah M, Bhuyan AK, Biophys J 87:2656–2662 (2004)
[110] Bai Y, Sosnick TR, Mayne L, Englander SW, Science 269:192–197 (1995)
[111] Natali F, Boffi F, Bonincontro A, Bultrini E, Caracciolo G, Cinelli S, Onori G, Pozzi D, Castellano AC, Appl Phys A 74:S1579–S1581 (2002)
[112] Farrow NA, Zhang O, Forman-Kay JD, Kay LE, Biochemistry 34:868–878 (1995)
[113] Akke M, Liu J, Cavanagh J, Erickson HP, Palmer AG, Nat Struct Biol 5:55–59 (1998)
[114] Rao DK, Bhuyan AK, J Biomol NMR 39:187–196 (2007)
[115] Pike AC, Acharya KR, Protein Sci 3:706–710 (1994)
[116] Dunbar J, Yennawar HP, Banerjee S, Luo J, Farber GK, Protein Sci 6:1272–1733 (1997)
[117] Makhatadze GI, Privalov PL, J Mol Biol 226:491–505 (1992)\
[118] Tanford C, Buckley CE, De PK, Lively EP, J Biol Chem 237:1168–1171 (1962)
[119] Utter MF, Keeth DB, Scrutton MC, Adu Enzyme Regul 2:49–68 (1964)
[120] Gerlsma SY, J Biol Chem 243:957–961 (1968)
[121] Gerlsma SY, Eur J Biochem 14:150–153 (1970)
[122] Gerlsma SY, Stuur ER, Int J Peptide Protein Res 4:377–383 (1972)
[123] Gerlsma SY, Stuur ER, Int J Peptide Protein Res 6:65–74 (1974)
[124] Neucere NJ, St Angelo AJ, Anal Biochem 47:80–89 (1972)
[125] Frigon RP, Lee JC, Arch Biochem Biophys 153:587–589 (1972)

[126] Back JF, Oakenfull D, Smith MB, Biochemistry 18:5191–5196 (1979)
[127] Vagenende V, Yap MG, Trout BL, Biochemistry 48:11084–11096 (2009)
[128] Ignatova Z, Gierasch LM, Methods Enzymol 428:355–372 (2007)
[129] Wang A, Bolen DW, Biophys J 71:2117–2122 (1996)
[130] Wang A, Bolen DW, Biochemistry 36:9101-9108 (1997)
[131] Hédoux A, Willart JF, Ionov R, Affouard F, Guinet Y, Paccou L, Lerbret A, Descamps M, J Phys Chem B 110:22886–22893 (2006)
[132] Carpenter JF, Prestrelski SJ, Arakawa T Arch Biochem Biophys 303:456–464 (1993)
[133] Carpenter JF, JH Crowe, Biochemistry 28:3916–3922 (1989)
[134] Xie G, Timasheff SN, Biophys Chem 64:25–43 (1997)
[135] Xie G, Timasheff SN, Protein Sci 6:211–221 (1997)
[136] Poddar NK, Ansari ZA, Singh RK, Moosavi–Movahedi AA, Ahmad F, Biophys Chem 138:120–129 (2008)
[137] Haque I, Singh R, Moosavi–Movahedi AA, Ahmad F, Biophys Chem 117:1–12 (2005)
[138] Kaushik JK, Bhat R, J Phys Chem B 102:7058–7066 (1998)
[139] Gekko K, Timasheff SN, Biochemistry 20:4677–4686 (1981)
[140] Miyawaki O, Biochim Biophys Acta 1774:928–935 (2007)
[141] Saadati Z, Bordbar AK, Protein J 27:455–460 (2008)
[142] D'Alfonso L, Collini M, Baldini G, Eur J Biochem 270:2497–2504 (2003)
[143] Kim YS, Jones LS, Dong A, Kendrick BS, Chang BS, Manning MC, Randolph TW, Carpenter JF, Protein Sci 12:1252–1261 (2003)
[144] Kulmyrzaev A, Bryant C, McClements DJ, J Agric Food Chem 48:1593–1597 (2000)
[145] O'Connor TF, Debenedetti PG, Carbeck JD, Biophys Chem 127:51-63 (2007)
[146] Xie G, Timasheff SN, Protein Sci 6:222–232 (1997)
[147] Beg I, Minton AP, Hassan I, Islam A, Ahmad F, Biochemistry 54:3594−3603 (2015)
[148] Kaushik JK, Bhat R, J Biol Chem 278:26458-26465 (2003)
[149] Asial I, Cheng YX, Engman H, Dollhopf M, Wu B1, Nordlund P, Cornvik T, Nat Commun 4:2901 (2013)
[150] Davis–Searles PR, Morar AS, Saunders AJ, Erie DA, Pielak GJ, Biochemistry 37:17048–17053 (1998)
[151] Zhang N, Liu FF, Dong XY, Sun Y, Biochem Eng J 70:188–195 (2013)
[152] Bongiovanni C, Sinibaldi F, Ferri T, Santucci R, J Protein Chem 21:35–41 (2002)
[153] Ptitsyn OB, Adv Protein Chem 47:83–229 (1995)
[154] Kuwajima K, Arai M, The Molten Globule State: The Physical and Biological Significance in Mechanisms of Protein Folding (Pain, R. H., Ed.) 2nd ed., pp 138–174, Oxford University Press, New York (2000)
[155] Arai M, Kuwajima K, Adv Protein Chem 53:209–282 (2000)
[156] Ohgushi M, Wada A, FEBS Lett 164:21–24 (1983)
[157] Ptitsyn OB, J Protein Chem 6:273–293 (1987)
[158] Kuwajima K, Proteins: Struct, Funct, Genet 6:87–103 (1989)
[159] Kuwajima K, Curr Opin Biotechnol 3:462–467 (1992)
[160] Colón W, Roder H, Nat Struct Biol 3:1019–1025 (1996)
[161] Sosnick TR, Mayne L, Hiller R, Englander SW, Nat Struct Biol 1:149–156 (1994)
[162] Jennings PA, Wright PE, Science 262:892–896 (1993)

[163] Fujiwara K, Arai M, Shimizu A, Ikeguchi M, Kuwajima K, Sugai S, Biochemistry 38:4455–4463 (1999)
[164] Matthews CR, Annu Rev Biochem 62:653–683 (1993)
[165] Uversky VN, Protein Sci 11:739–756 (2002)
[166] Tompa P, Trends Biochem Sci 27:527–533 (2002)
[167] Uversky VN, Eur J Biochem 269:2–12 (2002)
[168] Bychkova VE, Pain RH, Ptitsyn OB, FEBS Lett 238:231–234 (1988)
[169] Dunker AK, Cortese MS, Romero P, Iakoucheva LM, Uversky VN, FEBS J 272:5129–5148 (2005)
[170] Radivojac P, Vucetic S, O'Connor TR, Uversky VN, Obradovic Z, Dunker AK, Proteins 63:398–410 (2006)
[171] Baker BY, Yaworsky DC, Miller WL, J Biol Chem 280:41753–41760 (2005)
[172] Kataoka M, Hagihara Y, Mihata K, Goto Y, J Mol Biol 229:591–596 (1993)
[173] Kataoka M, Nishii I, Fujisawa T, Ueki T, Tokunaga F, Goto Y, J Mol Biol 249:215–228 (1995)
[174] Goto Y, Fink AL, Biochemistry 28:945–952 (1989)
[175] Goto Y, Nishikori S, J Mol Biol 222:679–686 (1991)
[176] Griko YV, Privalov PL, J Mol Biol 235:1318–1325 (1994)
[177] Finkelstein IJ, Massari AM, Fayer MD, Biophys J 92:3652–3662 (2007)
[178] Cicerone MT, Soles CL, Biophys J 86:3836–3845 (2004)
[179] Paciaroni, A, Orecchini A, Cinelli S, Onori G, Lechner RE, Pieper J, Chem Physics 292:397–404 (2003)
[180] Kumar R, Jain R, Kumar R, Chem Physics 418:57–64 (2013)
[181] Kohn WD, Kay CM, Hodges RS, J Mol Biol 267:1039-1052 (1997
[182] Lee DA, Goodfellow JM, Biophysical J 85:2747-2759 (1998)
[183] Rinaldo D, Field MJ, Biophysical J 85:3485-3501 (2003)
[184] Bobst CE, Zhang M, Kaltashov IA, J Mol Biol 388:954-967 (2009)
[185] Aisen P, Listowsky I, Annu Rev Biochem 49:357-393 (1980)
[186] Dewan JC, Mikami B, Hirose M, Sacchettini JC, Biochemistry 32:11963–11968 (1993)
[187] MacGillivray RT, Moore SA, Chen J, Anderson BF, Baker H, Luo Y, Bewley M, Smith CA, Murphy ME, Wang Y, Mason AB, Woodworth RC, Brayer GD, Baker EN, Biochemistry 37:7919–7928 (1998)
[188] He QY, Mason AB, Tam BM, MacGillivray RT, Woodworth RC, Biochemistry 38:9704-9711 (1999)
[189] Byrne SL, Chasteen ND, Steere AN, Mason AB, J Mol Biol 396:130-140 (2010)
[190] Steere AN, Byrne SL, Chasteen ND, Smith VC, MacGillivray RT, Mason AB, J Biol Inorg Chem 15:1341-1352 (2010)
[191] James NG, Byrne SL, Steere AN, Smith VC, MacGillivray RT, Mason AB, Biochemistry 48:2858-2867 (2009)
[192] James NG, Berger CL, Byrne SL, Smith VC, MacGillivray RT, Mason AB, Biochemistry 46:10603-10611 (2007)
[193] Halbrooks PJ, Giannetti AM, Klein JS, Björkman PJ, Larouche JR, Smith VC, MacGillivray RT, Everse SJ, Mason AB, Biochemistry 44:15451-15460 (2005)
[194] Nurizzo D, Baker HM, He QY, MacGillivray RT, Mason AB, Woodworth RC, Baker EN, Biochemistry 40:1616-1623 (2001)

[195] He QY, Mason AB, Tam BM, MacGillivray RT, Woodworth RC, Biochem J 344:881-887 (1999)
[196] Byrne SL, Mason AB, J Biol Inorg Chem 14:771–781 (2009)
[197] Spencer DS, Xu K, Logan TM, Zhou HX, J Mol Biol 351:219-232 (2005)
[198] Hom RA, Vora M, Regner M, Subach OM, Cho W, Verkhusha VV, Stahelin RV, Kutateladze TG, J Mol Biol 373:412–423 (2007)
[199] Schreiber G, Fersht AR, J Mol Biol 248:478–486 (1995)
[200] Olson LJ, Hindsgaul O, Dahms NM, Kim JJ, J Biol Chem 283:10124–10134 (2008)
[201] Chaves FA, Richards KA, Torelli A, Wedekind J, Sant AJ, Biochemistry 45:6426–6433 (2006)
[202] Re F, Sesana S, Barbiroli A, Bonomi F, Cazzaniga E, Lonati E, Bulbarelli A, Masserini M, FEBS Lett 582:215–220 (2008)
[203] Kawai C, Prado FM, Nunes GL, Di Mascio P, Carmona–Ribeiro AM, Nantes IL, J Biol Chem 280:34709–34717 (2005)
[204] Yoo SH, J Biol Chem 269:12001–12006 (1994)
[205] Muga A, Gonzalez–Manas JM, Lakey JH, Pattus F, Surewicz WK, J Biol Chem 268:1553–1557 (1993)
[206] Villa A, Zecca L, Fusi P, Colombo S, Tedeschi G, Tortora P, Biochem J 295:827–831 (1993)
[207] Mauk MR, Mauk AG, J Biol Chem 285:20499–20506 (2010)
[208] Rosell FI, Mauk MR, Mauk AG, Biochemistry 44:1872–1879 (2005)
[209] Aisen P, Listowsky I, Annu Rev Biochem 49:357–393 (1980)
[210] Lee DA, Goodfellow JM, Biophys J 85:2747–2759 (1998)
[211] Hofmeister F, Arch Exp Pathol Pharmakol 24:247-260 (1888)
[212] Baldwin RL, Biophys J 71:2056-2063 (1996)
[213] Elcock AH, McCammon JA, J Mol Biol 280:731-748 (1998)
[214] Perez-Jimenez R, Godoy-Ruiz R, Ibarra-Molero B, Sanchez-Ruiz JM, Biophys J 86:2414-2429 (2004)
[215] Kumar R, Mauk AG, J Phys Chem B 113:12400–12409 (2009)
[216] van Asselt EJ, Dijkstra BW, FEBS Lett 458:429-435 (1999)
[217] Perl D, Holtermann G, Schmid FX, Biochemistry 40:15501-15511 (2001)
[218] Jayaraman S, Gantz DL, Gursky O, Biochemistry 45:4620-4628 (2006)
[219] Nishimura C, Uversky VN, Fink AL, Biochemistry 40:2113-2128 (2001)
[220] Cacace MG, Landau EM, Ramsden JJ, Q ReV Biophys 30:241-277 (1997)
[221] Von Hippel PH, Wong KY, Science 145:577-580 (1964)
[222] Pegram LM, Record MT Jr, J Phys Chem B 112:9428-9436 (2008)
[223] Record MT Jr, Anderson CF, Lohman TM, Q ReV Biophys 11:103-178 (1978)
[224] Baker EN, Baker HM, Kidd RD, Biochem Cell Biol 80:27–34 (2002)
[225] Aasa R, Malmstroem BG, Saltman P, Biochim Biophys Acta 24:203–222 (1963)
[226] Baker EN, Adv Inorg Chem 41:389–463 (1994)
[227] Anderson BF, Baker HM, Norris GE, Rice DW, Baker EN, J Mol Biol 20:711–734 (1989)
[228] Baker EN, Lindley PF, J Inorg Biochem 47:147–160 (1992)
[229] Haridas M, Anderson BF, Baker EN, Acta Crystallogr D Biol Crystallogr 51:629–646 (1995)
[230] Bou-Abdallah, F, El Hage Chahine JM, Eur J Biochem 258:1022−1031 (1998)

[231] Bou-Abdallah, F, El Hage Chahine, JM, Eur J Biochem 263:912−920 (1999)
[232] Anderson BF, Baker HM, Norris GE, Rumball SV, Baker EN, Nature 344:784−787 (1990)
[233] Kurokawa H, Mikami B, Hirose M, J Mol Biol 254:196−207 (1995)
[234] Dautry-Varsat A, Ciechanover A, Lodish HF, Proc Natl Acad Sci USA 80:2258-2262 (1983)
[235] Thorstensen K, Romslo I, Biochem J 271:1-9 (1990)
[236] Hemadi M, Ha-Duong NT, El HageChahine JM, J Mol Biol 358:1125-1136 (2006)
[237] Schlabach MR, Bates GW, J Biol Chem 25:2182-2188 (1975)
[238] Campbell RF, Chasteen ND, J Biol Chem 252:5996-6001 (1977)
[239] Zweier JL, Wooten JB, Cohen JS, Biochemistry 20:3505-3510 (1981)
[240] Aisen P, Leibma A, Pinkowitz RA, Pollack S, Biochemistry 12:3679-3684 (1973)
[241] Aisen P, Brown EB, Prog Hematol 9:25-56 (1975)
[242] Aasa R, Malmstrom BG, Saltman P, Vanngård T, Biochim Biophys Acta 75:203-222 (1963)
[243] Sun H, Li H, Sadler PJ, Chem ReV 99:2817-2842 (1999)
[244] MacGillivray RTA, Mason AB, (Transferrin Templeton, DM Ed) Marcel Dekker, Inc:New York (2002)
[245] He QY, Mason AB, (Templeton, D. M., Ed) Marcel Dekker, Inc:New York (2002)
[246] Sun H, Li H, Sadler PJ, Chem ReV 99:2817-2842 (1999)
[247] Hémadi M, Ha-Duong NT, Plantevin S, Vidaud C, El Hage Chahine JM, J Biol Inorg Chem 15:497–504 (2010)
[248] Chikh Z, Ha-Duong NT, Miquel G, El Hage Chahine JM, J Biol Inorg Chem 12:90–100 (2007)
[249] Zhong W, Parkinson JA, Guo M, Sadler PJ, J Biol Inorg Chem 7:589–599 (2002)
[250] Guo M, Sun H, McArdle HJ, Gambling L, Sadler PJ, Biochemistry 39:10023-10033 (2000)
[251] Tinoco AD, Valentine AM, J Am Chem Soc 127:11218-11219 (2005)
[252] Tinoco AD, Incarvito CD, Valentine AM, J Am Chem Soc 129:3444-3454 (2007)
[253] Mason AB, Woodworth RC, J Biol Chem 259:1866-1873 (1984)
[254] Mason AB, Brown SA, Church WR, J Biol Chem 262:9011-9015 (1987)
[255] Mason AB, Woodworth RC, Oliver RW, Green BN, Lin LN, Brandts JF, Savage KJ, Tam BM, MacGillivray RT, Biochem J 319:361-368 (1996)
[256] Hall DR, Hadden JM, Leonard GA, Bailey S, Neu M, Winn M, Lindley PF, Acta Crystallogr D Biol Crystallogr 58:70–80 (2002)
[257] Mason AB, Halbrooks PJ, James NG, Connolly SA, Larouche JR, Smith VC, MacGillivray RT, Chasteen ND, Biochemistry 44:8013–8021 (2005)
[258] Wally J, Halbrooks PJ, Vonrhein C, Rould MA, Everse SJ, Mason AB, Buchanan SK, J Biol Chem 281:24934–24944 (2006)
[259] Ohgami RS, Campagna DR, Greer EL, Antiochos B, McDonald A, Chen J, Sharp JJ, Fujiwara Y, Barker JE, Fleming MD, Nat Genet 37:1264–1269 (2005)
[260] Aisen P, Enns C, Wessling-Resnick M, Int J Biochem Cell Biol 33:940–959 (2001)
[261] Sendamarai AK, Ohgami RS, Fleming MD, Lawrence CM, Proc Natl Acad Sci USA 105:7410–7415 (2008)
[262] MacGillivray RTA, Mason AB, Transferrin. In Molecular and Cellular Iron Transport; Templeton, D. M., Ed.; Marcel Dekker, Inc.: New York, pp 41−69 (2002)

[263] Crow A, Lawson TL, Lewin A, Moore GR, Le Brun NE, J Am Chem Soc 131:6808–6813 (2009)
[264] Wong S, Grigg J, Le Brun N, Moore G, Murphy M, Mauk G, J Biol Chem 290:3732–3739 (2015)
[265] Folajtar DA, Chasteen ND, J Am Chem Soc 104:5775–5780 (1982)
[266] Bell JD, Brown JD, Kubal G, Sadler PJ, Bio chem Soc Trans 16:714–715 (1988)
[267] Grady JK, Mason AB, Woodworth RC, Chasteen ND, Biochem J 309:403–410 (1995)
[268] Harris WR, Cafferty AM, Abdollahi S, Trankler K, Biochim Biophys Acta 1383:197–210 (1998)
[269] He QY, Mason AB, Nguyen V, MacGillivray RT, Woodworth RC, Biochem J 350:909–915 (2000)
[270] Wishnia A, Weber I, Warner RC, J Am Chem Soc 83:2071–2080 (1961)
[271] Byrne SL, Steere AN, Chasteen ND, Mason AB, Biochemistry 49:4200–4207 (2010)
[272] Egan TJ, Ross DC, Purves LR, Adams PA, Inorg Chem 31:1994–1998 (1992)
[273] Marques HM, Watson DL, Egan TJ, Inorg Chem 30:3758–3762 (1991)
[274] Kretchmar SA, Raymond KN, Inorg Chem 27:1436–1441 (1988)
[275] Williams J, Chasteen ND, Moreton K, Biochem J 201:527–532 (1982)
[276] Harris WR, Bali PK, Inorg Chem 27:2687–2691 (1988)
[277] Baldwin DA, Egan TJ, Marques HM, Biochim Biophys Acta 1038:1–9 (1990)
[278] Egan TJ, Zak O, Aisen P, Biochemistry 32:8162–8167 (1993)
[279] Marques HM, Walton T, Egan TJ, J Inorg Biochem 57:11–21 (1995)
[280] Zak O, Tam B, MacGillivray RT, Aisen P, Biochemistry 36:11036–11043 (1997)
[281] Li Y, Harris WR, Biochim Biophys Acta 1387:89–102 (1998)
[282] Marques HM, Egan TJ, Pattrick G, S Afr J Sci 86:21–24 (1990)
[283] Muralidhara BK, Hirose M, J Biol Chem 275:12463–12469 (2000)
[284] Mizutani K, Muralidhara BK, Yamashita H, Tabata S, Mikami B, Hirose M, J Biol Chem 276:35940–35946 (2001)
[285] Hamilton DH, Turcot I, Stintzi A, Raymond KN, J Biol Inorg Chem 9:936–944 (2004)
[286] Lindman S, Xue WF, Szczepankiewicz O, Bauer MC, Nilsson H, Linse S, Biophys J 90:2911-2921 (2006)
[287] Cavagnero S, Debe DA, Zhou ZH, Adams MW, Chan SI, Biochemistry 37:3369-3376 (1998)
[288] Dominy BN, Perl D, Schmid FX, Brooks CL 3rd, J Mol Biol 319:541–554 (2002)
[289] Apetri AC, Surewicz WK, J Biol Chem 278:22187–22192 (2003)
[290] Aisen P, Leibman A, Zweier J, J Biol Chem 253:1930−1937 (1978)
[291] Lin LN, Mason AB, Woodworth RC, Brandts J, Biochemistry 33:1881−1888 (1994)
[292] Shen ZM, Yang JT, Feng YM, Wu CS, Protein Sci 1:1477−1484 (1992)
[293] Lin L, Mason AB, Woodworth RC, Brandts JF, Biochem J 293:517−522 (1993)
[294] Oe H, Takahashi N, Doi E, Hirose M, J Biochem 106:858−863 (1989)
[295] El Hage Chahine JM, Fain D, Eur J Biochem 223:581−587 (1994)
[296] Zak O, Aisen P, Crawley JB, Joannou CL, Patel KJ, Rafiq M, Evans RW, Biochemistry 34:14428−14434 (1995)
[297] Kretchmar SA, Raymond KN, J Am Chem Soc 108:6212−6218 (1986)
[298] Hemadi M, Ha–Duong NT, El HageChahine JM, J Mol Biol 358:1125–1136 (2006)
[299] Chikh Z, Hemadi M, Miquel G, Ha–Duong N T, El Hage Chahine JM, J Mol Biol 380:900−916 (2008)

[300] El Hage Chahine JM, Pakdaman R, Eur J Biochem 230:1102−1110 (1995)
[301] Kumar R, Mauk AG, J Phys Chem B 116:3795–3807 (2012)
[302] Bou–Abdallah F, El Hage Chahine JM, J Mol Biol 303:255−266 (2000)
[303] Eigen M, deMaeyer L, Relaxation Methods. In Techniques of Organic Chemistry; Friess, S. L., Lewis, E. S., Weissberger, A., Eds.; Interscience: New York, 1963; Vol. 8 (pt. 2), pp 895−1029.
[304] Brouillard R, J Chem Soc Faraday Trans 76:583−587 (1980)
[305] Ellis RJ, Trends Biochem Sci 26:597–604 (2001)
[306] Stagg L, Zhang S, Cheung MS, Wittung–Stafshede P, Proc Natl Acad Sci USA 104:18976−18981 (2007)
[307] Zimmerman SB, Trach SO, J Mol Biol 222:599–620 (1991)
[308] Van den Berg B, Ellis RJ, Dobson CM, EMBO J 18:6927–6933 (1999)
[309] Rivas G, Ferrone F, Herzfeld J, EMBO Rep 5:23–27 (2004)
[310] Minton AP, Curr Opin Struct Biol 10:34–39 (2000)
[311] Minton AP, Curr Opin Biotechnol 8:65–69 (1997)
[312] Minton AP, Wilf J, Biochemistry 20:4821–4826 (1981)
[313] Minton AP, Biopolymers 20:2093–2120 (1981)
[314] Laurent TC, Ogston AG, Biochem J 89:249–253 (1963)
[315] Minton AP, Biophys J 88:971–985 (2005)
[316] Zhou HX, Acc Chem Res 37:123–130 (2004)
[317] Cheung MS, Klimov D, Thirumalai D, Proc Natl Acad Sci USA 102:4753–4758 (2005)
[318] Minton AP, Curr Opin Struct Biol 10:34−39 (2000)
[319] Ellis RJ, Trends Biochem Sci 26:597−604 (2001)
[320] Zhou HX, Rivas G, Minton AP, Annu Rev Biophys 37:375−397 (2008)
[321] Feig M, Sugita Y, J Phys Chem B 116:599−605 (2012)
[322] Martin J, Hartl FU, Proc Natl Acad Sci USA 94:1107–1112 (1997)
[323] Eggers DK, Valentine JS, J Mol Biol 314:911–922 (2001)
[324] Friedel M, Sheeler DJ, Shea J-E, J Chem Phys 118:8106–8113 (2003)
[325] McPhie P, Ni YS, Minton AP, J Mol Biol 361:7–10 (2006)
[326] Du F, Zhou Z, Mo Z-Y, Shi J-Z, Chen J, Liang Y, J Mol Biol 364:469–482 (2006)
[327] Mittal J, Best RB, Proc Natl Acad Sci USA 105:20233–20238 (2008)
[328] Mukherjee S, Waegele MM, Chowdhury P, Guo L, Gai F, J Mol Biol 393:227–236 (2009)
[329] Batra J, Xu K, Qin S, Zhou H-X, Biophys J 97:906–911 (2009)
[330] Charlton LM, Barnes CO, Li C, Orans J, Young GB, Pielak GJ, J Am Chem Soc 130:6826–6830 (2008)
[331] Homouz D, Stagg L, W.-Stafshede P, Cheung MS, Biophys J 96:671–680 (2009)
[332] McGuffee SR, Elcock AH, PLoS Comput Biol 6:e1000694 (2010)
[333] Mittal J, Best RB, Dependence of protein folding stability and dynamics on the density and composition of macromolecular crowders, Biophys J 98:315–320 (2010)
[334] Ross PD, Minton AP, Analysis of non-ideal behavior in concentrated hemoglobin solutions, J Mol Biol 112:437–452 (1977)
[335] Ferrone FA, Ivanova M, Jasuja R, Biophys J 82:399–406 (2002)
[336] Munishkina LA Ahmad A, Fink AL, Uversky VN, Biochemistry 47:8993–9006 (2008)
[337] White DA, Buell AK, Knowles TPJ, Welland ME, Dobson CM, J Am Chem Soc 132:5170–5175 (2010)

[338] Magno A, Caflisch A, Pellarin R, J Phys Chem Lett 1:3027–3032 (2010)
[339] Jarvis TC, Ring DM, Daube SS, von Hippel PH, J Biol Chem 265:15160–15167 (1990)
[340] Rivas G, Fernandez JA, Minton AP, Proc Natl Acad Sci USA 98:3150–3155 (2001)
[341] Kim JS, Yethiraj A, Biophys J 96:1333–1340 (2009)
[342] Phillip Y, Sherman E, Haran G, Schreiber G, Biophys J 97:875–885 (2009)
[343] Kim YC, Best RB, Mittal J, J Chem Phys 133:205101 (2010)
[344] Minh DD, Chang CE, Trylska J, Tozzini V, McCammon JA, J Am Chem Soc 128:6006–6007 (2006)
[345] Minton AP, Mol Cell Bioch (1983) 55:119–40 (1983)
[346] Zimmerman SB, Minton AP, Annu Rev Bioph Biom 22:27–65 (1993)\
[347] Minton AP, J Biol Chem 276:10577–10580 (2001)
[348] Minton AP, J Pharm Sci 94:1668–1675 (2005)
[349] Minton AP, Biopolymers 99:239–244 (2013)
[350] Zhou HX, FEBS Lett 587:1053–1061 (2013)
[351] Phillip Y, Schreiber G, FEBS Lett 587:1046–1052 (2013)
[352] Ellis RJ, Curr Opin Sruc Biol 11:114–119 (2001)
[353] Elowitz M, Surette M, Wolf P, Stock J, Leibler S, J Bacteriol 181:197–203 (1999)
[354] Mika JT, vanden Bogaart G, Veenhoff L, Krasnikov V, Poolman B, Mol Microbiol 77:200–207 (2010)
[355] Kalwarczyk T, Ziebacz N, Bielejewska A, Zaboklicka E, Koynov K, Szymański J, Wilk A, Patkowski A, Gapiński J, Butt HJ, Hołyst R, NanoLett 11:2157–2163 (2011)
[356] Kalwarczyk T, Tabaka M, Holyst R, Bioinformatics 28:2971–2978 (2012)
[357] Asakura S, Oosawa F, J Chem Phys 22:1255–1256 (1954)
[358] Berg OG, Biopolymers 30:1027–1037 (1990)
[359] Marenduzzo D, Finan K, Cook PR, J Cell Biol 175:681–686 (2006)
[360] Sarkar M, Li C, Pielak GJ, Biophys Rev 5:187–194 (2013)
[361] Sarkar M, Smith AE, Pielak GJ, Proc Natl Acad Sci USA 110:19342–19347 (2013)
[362] Dix JA, Verkman AS, Annu Rev Biophys 37:247-263 (2008)
[363] Elcock AH, Curr Opin Struct Biol 20:196-206 (2010)
[364] Gershenson A, Gierasch LM, Curr Opin Struct Biol 21:32-41 (2011)
[365] Mika JT, Poolman B, Curr Opin Biotechnol 22:117-126 (2011)
[366] Wang Y, Sarkar M, Smith AE, Krois AS, Pielak GJ, J Am Chem Soc 134:16614-16618 (2012)
[367] Knowles DB, LaCroix AS, Deines NF, Shkel I, Record MT Jr, Proc Natl Acad Sci USA 108:12699–12704 (2011)
[368] Fodeke AA, Minton AP, J Phys Chem B 115:11261–11268 (2011)
[369] Miklos AC, Sarkar M, Wang Y, Pielak GJ, J Am Chem Soc 133:7116–7120 (2011
[370] Asakura S, Oosawa F, J Polym Sci B 33:183-192 (1958)
[371] Groen J, Foschepoth D, te Brinke E, Boersma AJ, Imamura H, Rivas G, Heus HA, Huck WT, J Am Chem Soc 137:13041-13048 (2015)
[372] Crowley PB, Chow E, Papkovskaia T, Chem Bio Chem 12:1043–1048 (2011)
[373] Wang Q, Zhuravleva A, Gierasch LM, Biochemistry 50:9225–9236 (2011)
[374] Bokvist M, Gröbner G, J Am Chem Soc 129:14848–14849 (2007)
[375] Minton AP, J Cell Sci 119:2863–2869 (2006)
[376] Stagg L, Zhang S, Cheung MS, Wittung–Stafshede P, Proc Natl Acad Sci USA 104:18976−18981 (2007)

[377] Minton AP, Curr Opin Biotechnol 8:65–69 (1997)
[378] Christiansen A, Wang Q, Samiotakis A, Cheung MS, Wittung–Stafshede P, Biochemistry 49:6519–6530 (2010)
[379] Wang Y, Sarkar M, Smith AE, Krois AS, Pielak GJ, J Am Chem Soc 134:16614−16618 (2012)
[380] Malik A, Kundu J, Mukherjee SK, Chowdhury, PK, J Phys Chem B 116:12895−12904 (2012)
[381] Benton LA, Smith AE, Young GB, Pielak GJ, Biochemistry 51:9773−9775 (2012)
[382] Spencer DS, Xu K, Logan TM, Zhou H–X, J Mol Biol 351:219–232 (2005)
[383] McPhie P, Ni YS, Minton AP, J Mol Biol 361:7–10 (2006)
[384] Ai X, Zhou Z, Bai Y, Choy WY, J Am Chem Soc 128:3916–3917 (2006)
[385] Perham M, Stagg L, Wittung–Stafshede P, FEBS Lett 581:5065–5069 (2007)
[386] Ellis RJ, Trends Biochem Sci 26:597–604 (2001)
[387] Minton AP, Curr Opin Struct Biol 10:34–39 (2000)
[388] Zhou HX, Rivas G, Annu Rev Biophys 37:375–397 (2008)
[389] Feig M, Sugita Y, J Phys Chem B 116:599−605 (2012)
[390] Derham BK, Harding JJ, Biochim Biophys Acta 1764:1000–1006 (2006)
[391] Moran–Zorzano MT, Viale A, Munoz F, Alonso–Casajus N, Eydallin GG, Zugasti B, Baroja–Fernández E, Pozueta–Romero J, FEBS Lett 581:1035–1040 (2007)
[392] Bellotti V, Chiti F, Curr Opin Struct Biol 18:771–779 (2008)
[393] van den Berg B, Wain R, Dobson CM, Ellis RJ, EMBO J 19:3870–3875 (2000)
[394] Zhou BR, Liang Y, Du F, Zhou Z, Chen J, J Biol Chem 279:55109–55116 (2004)
[395] Homouz D, Perham M, Samiotakis A, Cheung MS, Wittung-Stafshede P, Proc Natl Acad Sci USA 105:11754–11759 (2008)
[396] Bohrer MP, Patterson GD, Carroll PJ, Macromolecules 17:1170–1173 (1984)
[397] Venturoli D, Rippe B, Am J Physiol Renal Physiol 288:F605–F613 (2005)
[398] Zhou HX, Rivas G, Annu Rev Biophys 37:375–397 (2008)
[399] Goins AB, Sanabria H, Waxham MN, Biophys J 95:5362–5373 (2008)
[400] Ruhlmann C, Thieme M, Helmstedt M, Chem Phys Lipids 110:173–181 (2001)
[401] Wenner JR, Bloomfield VA, Biophys J 77:3234–3241 (1999)
[402] Luby-Phelps K, Castle PE, Taylor DL, Lanni F, Proc Natl Acad Sci USA 84:4910–4913 (1987)
[403] Venturoli D, Rippe B, Am J Physiol 288:F605–F613 (2005)
[404] Bohrer MP, Patterson GD, Carroll PJ, Macromolecules 17:1170–1173 (1984)
[405] Davidson MG, Deen WM, Macromolecules 21:3474-3481 (1988)
[406] Granath KA, J Colloid Sci 13:308–328 (1958)
[407] Alberts B, Johnson A, Lewis J, et al., Molecular Biology of the Cell. 4th edition. New York: Garland Science; (2002)
[408] Bushnell GW, Louie GV, Brayer GD, J Mol Biol 214:585–595 (1990)
[409] Englander SW, Sosnick TR, Mayne LC, Shtilerman M, Qi PX, Bai Y, Acc Chem Res 31:737–744 (1998)
[410] Shastry MC, Roder H, Nat Struct Biol 5:385–392 (1998)
[411] Bai Y, Sosnick TR, Mayne L, Englander SW, Science 269:192–197 (1995)
[412] Kawai C, Prado FM, Nunes GL, Mascio PDi, Carmona-Ribeiro AM, Nantes IL, J Bio Chem 280:34709–34717 (2005)
[413] Moore GR, Pettigrew GW, Cytochrome *c*: Evolutionary, structural and physiochemical

aspects. Berlin: Springer-Verlag (1990)
[414] Cooper CE, Biochimica et Biophysica Acta- Bioenergetics 1411:290–309 (1999)
[415] Frauenfelder H, McMahon BH, Fenimore PW, Proc Natl Acad Sci USA 100:8615–8617 (2003)
[416] Parak FG, Nienhaus GU, Chemphyschem 3:249–254 (2002)
[417] Evans SV, Brayer GD, J Mol Biol 213:885–897 (1990)
[418] Diamond R, J Mol Biol 82:371–391 (1974)
[419] Kurokawa H, Mikami B, Hirose M, J Mol Biol 254:196–207 (1995)
[420] Yasin UM, Sashi P, Bhuyan AK, J Phys Chem B 118:6662-6669 (2014)
[421] Ibarra-Molero B, Sanchez-Ruiz JM, Biochemistry 36:9616−9624 (1997)
[422] Bieri O, Wildegger G, Bachmann A, Wagner C, Kiefhaber T, Biochemistry 38:12460−12470 (1999)
[423] Radford SE, Dobson CM, Evans PA, Nature 358:302−307 (1992)

Chapter 2
Materials and Methods

2.1 Materials

Horse heart Cytochrome *c* (Cyt *c*) (type VI), horse heart Myoglobin (Mb), egg white apo-ovotransferrin (apo-oTf) (C0755) and bovine serum apo-transferrin (apo-sTf) (T0178) were purchased from Sigma. Hen egg white Lysozyme (Lyz) was purchased from Calbiochem. Alkylureas (methylurea (MU), *N*,*N'*-dimethylurea (DMU), ethylurea (EU), tetramethylurea (TMU)), sugars (ribose, glucose, maltose, sucrose, trehalose), salts (NaCl, $NaNO_3$, NaBr, Na_2SO_4, $NaClO_4$), bathophenanthroline disulfonate (BPS), 8-anilino-1-naphthalene sulfonate (ANS), crowding agents (Dextran 40, Dextran 70), NaOH, sodium dithionite, $K_3[Fe(CN)_6]$, and salts of buffers (glycine, dibasic and mono basic sodium phosphate, sodium acetate, 4-(2-Hydroxyethyl)-1-piperazineethanesulfonate (HEPES), 2-(*N*-mopholino) ethanesulfonate (MES) and 3-[Cyclohexylamino]-1-propanesulfonic acid (CAPS)) were purchased from Sigma. Ultra pure GdnHCl and urea were purchased from USB. Glycerol was purchased from Merck. Ficoll 70 was purchased from GE health care. Centricon filter of 10 kDa molecular mass cut-off was purchased from Millipore, Bedford, MA, USA. pH of samples were adjusted by using concentrated NaOH or HCl.

2.2 Methods

2.2.1 Measurements of CO-association kinetics of Ferrocyt c

To evaluate the effect of different cosolvents on internal dynamics of Ferrocyt *c*, the CO-association kinetics of Ferocity *c* were measured at varying concentrations of cosolvent (denaturant (urea, MU, EU, DMU, TMU, GdnHCl (pH 7.0) or sugar (glycerol, trehalose (pH 12.9)) or salt (NaCl (pH 12.9))). Ferrocytochrome *c* (Ferrocyt *c*) can be driven to bind CO when the latter is used in saturating concentration (1 mM). Small volumes of Ferrocyt *c* solution were diluted 101-fold into deaerated CO-saturated buffer containing ~3 mM sodium dithionite and varying concentrations of denaturant (urea, MU, EU, DMU, TMU, GdnHCl (0.1 M phosphate, pH 7.0)) or sugar (glycerol, trehalose (2 mM CAPS, pH 12.9)) or salt (NaCl (2 mM CAPS, pH 12.9)) under anaerobic atmosphere. Final concentration of protein in the reaction medium was ~8-10 μM. Measurements of CO-association kinetics of Ferrocyt *c* were performed on Shimadzu 2450 spectrophotometer at 550 nm (heme absorbance). In the presence of destabilizing

concentrations of denaturant, the kinetics of the fast CO-association reactions were recorded on Shimadzu 2450 spectrophotometer coupled with Applied Photophysics RX 2000 Rapid Kinetics System stopped-flow mixing accessory.

2.2.2 Measurement of CO-replacement kinetics of MbCO by hexacyanoferrate ion

If the internal dynamics of protein changes by addition of denaturant then there should change in the reaction rate of ligand binding or exit. For CO-replacement reaction of CO-liganded myoglobin (MbCO) by hexacyanoferrate ion, MbCO was prepared by dissolving the protein in the deaerated buffer (pH 7.0, 0.1 M phosphate buffer) containing sodium dithionate and then dry CO was passed under anaerobic atmosphere. Small volumes of MbCO were diluted in the degassed $K_3[Fe(CN)_6]$ containing varying concentrations of denaturant (urea, MU, EU, DMU, TMU) (pH 7.0, 0.1 M phosphate buffer). The final concentrations of protein, CO, sodium dithionate, and $K_3[Fe(CN)_6]$ in the reaction medium were ~10, 500, 0.5, 400 mM, respectively. This method permits replacement of CO by $[Fe(CN)_6]^{3-}$ and CO-replacement kinetic measurements were performed on Shimadzu 2450 spectrophotometer at 421 nm.

2.2.3 Measurement of far-UV CD, near-UV CD, fluorescence and absorbance monitored denaturant-induced equilibrium unfolding transitions of proteins

CD spectroscopy is particularly good for the characterization of secondary (far-UV CD) and tertiary (near-UV CD) structures in proteins. Protein conformation can be tracked by fluorescence spectroscopy. CD and fluorescence spectroscopy could be used to study the conformational stability of a protein under stress conditions (extreme pH conditions or high concentration of denaturants). Native protein have good amount of secondary and tertiary structure than the unfolded one. To determine the effect of denaturants on the conformational stability of proteins, the far-UV CD (222 nm), near-UV CD (282 nm) and fluorescence (ex: 280 nm)-monitored denaturant (urea, MU, DMU, EU, TMU and GdnHCl)-induced equilibrium unfolding curves were measured for Ferricytochrome *c* (Ferricyt *c*) (pH 6.0 (±0.5)), CO-liganeded Ferrocyt *c* (Cyt-CO) (pH 7.0 (±1)), Mb (pH 7.0 (±1)) and Ferrocyt *c* (pH 7.0 (±1)) at

25 °C. The final protein concentrations for the fluorescence, far-UV CD and near-UV CD measurements were ~10 (Ferricyt *c*/Ferrocyt *c*/Cyt-CO/Mb/MbCO), ~10-15 (~10 (Ferricyt *c*), ~15 (Mb)) and ~70 μM (Ferricyt *c*), respectively. The absorption spectrum of Ferricyt *c* shows to characterstic heme absorbances centred at around 399 and 695 nm. The urea dependent heme absorbance of Ferricyt *c* at 399 and 695 nm were also measured using 20 and 100 μM concentration of protein, respectively at pH 6.0 (±0.5), 25 °C. Cyt-CO samples were prepared by incubating the Ferrocyt *c* under different concentration of denaturant in the presence of CO (≈1.0 mM) under anaerobic atmosphere. MbCO samples were prepared as described previously and before the measurements were placed in dark place in tightly capped quartz cuvettes. Before the measurements, the protein samples (Ferrocyt *c*, Ferricyt *c*, Cyt-CO, Mb, MbCO) were equilibrated for ~2 hrs. The buffer conditions used for these measurements were 0.1 M phosphate buffer.

To determine the effect of sugars on the conformational stability of proteins, fluorescence (ex: 280) monitored GdnHCl-induced unfolding of Cyt-CO (pH 12.9, 2 mM CAPS) and Lyz (pH 13, 2 mM CAPS), and urea-induced unfolding of Lyz (pH 2.3, 25 mM glycine) were measured in the absence and presence of a desired concentration of sugar (trehalose, sucrose, maltose, glucose, ribose or glycerol) or salt (NaCl). To determine the sugar effect on the denaturant-dependant thermodynamic stability of Lyz, the fluorescence monitored GdnHCl dependent urea-induced unfolding transitions of Lyz (pH 2.3, 25 mM glycine) were also measured in the absence and presence of sugar (trehalose, sucrose, maltose, glucose, ribose or glycerol). The final concentration of Cyt-CO and Lyz was 10 μM for fluorescence measurements. The protein samples were equilibrated for ~60 minutes before the measurements.

To determine the effect of salt or sucrose on thermodynamic stability of Fe_2oTf and apo-oTf, the far-UV CD and near-UV CD monitored urea-induced unfolding curves of diferric-ovotransferrin (Fe_2oTf) and apo-oTf (0.05 M HEPES (pH 7.4) or 0.05 M MES (pH 5.8-5.4)) were measured in the presence of different concentrations of salt (NaCl, Na_2SO_4) or sucrose at 25 °C. To determine the effect of crowding agents on thermodynamic stability of Fe_2sTf at pH 7.4 and pH 5.5, the far-UV CD-monitored urea-induced unfolding curves of Fe_2sTf (0.05 M HEPES (pH 7.4) or 0.05 M MES (pH 5.5)) were measured in the presence of different concentrations of crowding agents (dextran 40, dextran 70 or ficoll70) at 25 °C. To determine the effect of crowding agents on salt-dependence of thermodynamic stability of Fe_2sTf at pH 7.4 and

pH 5.5, the far-UV CD-monitored urea-induced unfolding curves of Fe_2sTf (0.05 M HEPES (pH 7.4) or 0.05 M MES (pH 5.5)) were measured in the presence of different concentrations of NaCl in the absence and presence of 200 mg ml^{-1} dextran 40 at 25 °C. The final concentrations of protein (apo-oTf, Fe_2oTf, Fe_2sTf) for far-UV and near-UV CD measurements were ~5 and ~10 μM, respectively. Prior to data collection, the protein samples (apo-oTf, Fe_2oTf, Fe_2sTf) were incubated for ~5 hrs at 25 °C. The fraction of unfolded protein (apo-oTf, Fe_2oTf, Fe_2sTf), $f_{D,}$ was estimated from the far-UV (222 nm) and near-UV (282 nm) CD data.

CD (far-UV CD (250-200 nm, 1.0 mm cell), near-UV CD (320-240 nm, 5.0 mm cell)), fluorescence emission (320-410 nm, 10.0 mm cell) and absorbance (800-250 nm, 10.0 mm cell) spectra were taken on JASCO (model J810 or J815) spectropolarimeter, Perkin Elmer LS-55 spectrofluorometer and Shimadzu 2450 spectophotometer, respectively. However, the fluorescence emission spectra of Cyt-CO in the presence urea, alkyl ureas (MU, DMU, EU, TMU) and GdnHCl (pH 7.0, 25 °C) were taken on Cary Eclipse Agilent spectrofluorometer. Fluorescence emission intensity used was 358/360 nm, 358 nm, 360 nm and 375 nm for Cyt *c* (Ferricyt *c*, Ferrocyt *c*), Mb, Lyz and Cyt-CO/MbCO, respectively. The concentrations of the urea and GdnHCl solutions before and after measurements were determined by refractive index measurements on an Abbe refractometer. The final concentrations of urea and GdnHCl are those taken after the measurements. The unfolding transitions were analyzed assuming a two state transition between the folded (N) and unfolded (U) conformations by using the procedure of Santoro and Bolen [1] equation (1),

$$S_{obs} = \frac{(c_f + m_f[D]) + (c_u + m_u[D])\exp(\frac{-\Delta G_D + m_g[D]}{RT})}{1 + \exp(\frac{-\Delta G_D + m_g[D]}{RT})} \qquad (1)$$

where S_{obs} is the signals (fluorescence, CD or absorbance) at given denaturant concentration, D, c_f and c_u, and m_f and m_u represent intercepts and slopes of native and denatured states baselines, respectively, ΔG_D is the denaturation free energy in the absence of denaturant, and m_g is the surface area exposed by the solvent.

2.2.4 Measurement of the far-UV CD, near-UV CD, fluorescence and ANS fluorescence spectra of native and pH-denatured proteins in the presence of sugar or salt

Under extreme pH conditions, protein looses its secondary and/or tertiary structures and the addition of stabilizing additive in the pH-denatured proteins may stabilize the the secondary and/or tertiary structures, these changes could be monitored using the CD and intrinsic fluorescence spectroscopy. The far-UV CD, near-UV CD and fluorescence spectra of base denatured Ferricyt *c*, Cyt-CO, Lyz were measured in the absence and presence of sugar (glycerol and trehalose) or salt (NaCl) at pH 12.9/13, 25 °C (2 mM CAPS). The far-UV CD and near-UV CD spectra of native Ferricyt *c*, Ferrocyt *c*, Lyz and GdnHCl-unfolded Ferricyt *c*, Cyt-CO and Lyz were collected at pH 7.0, 25 °C (50 mM phosphate buffer). The far-UV CD and near-UV CD spectra of Lyz were also collected at pH 2.3, 25 °C (25 mM glycine buffer). The fluorescence spectra of native Ferricyt *c*, Ferrocyt *c* and Lyz were also collected at pH 7.0, 25°C (50 mM phosphate buffer). The final concentration of the protein used for the far-UV CD, near-UV CD and fluorescence measurements were 10-30, 50-130 and 10 μM, respectively. ANS-fluorescence is widely used to detect the MG-states of proteins [2-3]. Binding of ANS to hydrophobic regions generally increases the ANS fluorescence intensity of MG-state [2-3]. The ANS fluorescence spectra for the native Lyz and Ferricyt *c* at pH 7.0, 25°C (50 mM phosphate buffer) and base-denatured Ferricyt *c* and Lyz, at pH 12.9/13, 25 °C (2 mM CAPS buffer)) were measured without additive and in the presence of glycerol and trehalose, respectively. The ANS fluorescence spectrum was also recorded for GdnHCl-denatured Lyz at pH 7.0, 25°C (50 mM phosphate buffer). For ANS fluorescence measurements, ratio of ANS (150 μM) and protein (10 μM) were 15:1. The CD (far-UV CD (250-200 nm, 1.0 mm cell), near-UV CD (320-240 nm, 5.0 mm cell)) and fluorescence (fluorescence (ex: 280 and em: 320-410 nm, 10.0 mm cell), ANS-fluorescence (ex: 380 and em: 400-600 nm, 10.0 mm cell)) spectra of proteins were collected on JASCO J815 spectropolarimeter and Perkin Elmer LS-55 spectrofluorometers, respectively. Before the measurements the samples were equilibrated for ~60 minutes.

2.2.5 Measurement of the far-UV CD and absorbance monitored thermal unfolding transitions of proteins

Temperature dependent changes in the proteins conformation could be monitored using the far-UV CD and absorbance signals. To investigate the effects of the denaturants and sugar on the thermal stability of native Ferrocyt *c* and Mb, the visible absorbance monitored (416 and 550 nm for Ferrocyt *c* and 409 nm for Mb) thermal unfolding curves of Ferrocyt *c* and Mb were

collected in the absence and presence of different concentrations of urea, GdnHCl, sucrose, alkylureas (MU, EU, DMU, TMU) at pH 7.0 (0.1 M phosphate buffer). To find out the effect of urea, GdnHCl, and sugar on the acid-denatured Lyz, the absorbance monitored (292 nm) thermal unfolding curves of Lyz were collected at pH 2.3 (25 mM glycine buffer) in the absence and presence of different concentrations of urea, GdnHCl and sugars (glycerol, ribose, glucose, maltose, sucrose, trehalose). To evaluate the effect of sugar on the denaturant dependant thermal stability of acid-denatured Lyz, the absorbance monitored (292 nm) thermal unfolding curves of Lyz were collected at pH 2.3 at different concentration of denaturant in the absence and presence of fixed concentration of sugar (glycerol, ribose, glucose, maltose, sucrose, trehalose) at pH 2.3.

To estimate the effect of sugar (glycerol or trehalose) or salt (NaCl) on the thermal stability of base-denatured Ferricyt *c* and Lyz, the far-UV CD monitored (222 nm) thermal unfolding curves of Ferricyt *c* and Lyz were collected at pH 12.9 (±0.1) (2 mM CAPS buffer) in the absence and presence of different concentrations of sugar (glycerol or trehalose) or salt (NaCl). The far-UV CD monitored (222 nm) thermal unfolding curve of Ferrocyt *c* was collected at pH 7.0 in 0.1 M phosphate buffer. The absorbance and CD monitored thermal denaturation curves of proteins were collected on Shimadzu 2450 spectophotometer (with S-1700 thermoelectric single cell holder) and on Jasco 815 CD spectrophotometer (Peltier controlled), respectively. The temperature of protein solution was raised at a rate of 1 °C/min. The protein concentration used for the absorbance monitored thermal unfolding experiments were 7-10, 5-7 and 5-7 μM for Ferrocyt *c*, Mb and Lyz, respectively. For CD measurements ~15 μM of protein (Ferricyt *c*, Ferrocyt *c*, Lyz) was used. These thermal unfolding curves were analyzed by using two-state van′t Hoff equation (equation (2)) [4] or Gibbs Helmholtz equation (equation (3)),

$$S_{obs}\ (T) = \frac{(y_N + m_N T) + (y_U + m_U T)\exp\left[\dfrac{-\Delta H_m}{R}\left(\dfrac{1}{T} - \dfrac{1}{T_m}\right)\right]}{1 + \exp\left[\dfrac{-\Delta H_m}{R}\left(\dfrac{1}{T} - \dfrac{1}{T_m}\right)\right]} \qquad (2)$$

$$S_{obs}\ (\mathrm{T}) = \frac{(\mathrm{y_N} + \mathrm{m_N}T) + (\mathrm{y_U} + \mathrm{m_U}T)\exp\left(\dfrac{\Delta H_{\mathrm{m}}\left(\dfrac{T}{T_{\mathrm{m}}} - 1\right) - \Delta C_{\mathrm{p}}\left(T_{\mathrm{m}} - T + T\ln\left(\dfrac{T}{T_{\mathrm{m}}}\right)\right)}{RT}\right)}{1 + \exp\left(\dfrac{\Delta H_{\mathrm{m}}\left(\dfrac{T}{T_{\mathrm{m}}} - 1\right) - \Delta C_{\mathrm{p}}\left(T_{\mathrm{m}} - T + T\ln\left(\dfrac{T}{T_{\mathrm{m}}}\right)\right)}{RT}\right)} \qquad (3)$$

where S_{obs} (T) is the observed signal (absorbance or CD), y_N and y_U, and m_N and m_U, represent intercepts and slopes of the native (pre-transition) and unfolded (post-transition) baselines, respectively, R is the gas constant, T is absolute temperature ΔC_p represent heat capacity change, R is a gas constant, and ΔH_m represent the van't Hoff enthalpy at thermal denaturation midpoint (T_m). Thermodynamic stability, expressed in terms of free energy of denaturation, ΔG_T was calculated using the equation (4),

$$\Delta G_T = \Delta H_{\mathrm{m}}\left(1 - \frac{T}{T_{\mathrm{m}}}\right) + \Delta C_{\mathrm{p}}\left(T - T_{\mathrm{m}} - T\ln\left(\frac{T}{T_{\mathrm{m}}}\right)\right) \qquad (4)$$

2.2.6 Preparation of Fe_2Tf and Fe_NTf

Diferric-transferrin (Fe_2Tf; Fe_2oTf and Fe_2sTf) was prepared by well known procedure used earlier for Fe_2sTf [5-7]. Briefly, an iron nitrilotriacetate solution was prepared by dissolving nitriloacetic acid (~100 μmol) and $FeCl_3.6H_2O$ (~50 μmol) in 2 mL solution of 6 M HCl. The pH of this solution was adjusted to 4.0 with the concentrated NaOH solution. The solution was finally diluted to 10 mL. Apo-transferrin (apo-oTf and apo-sTf) (80 mg, 1 μmol) was dissolved in 3 mL of buffer (50 mM HEPES, pH 7.4, 20 mM $NaHCO_3$). Protein solution was then diluted upto 5 mL by adding the freshly prepared iron nitrilotriacetate solution. Protein solution thus prepared was incubated overnight at ~37 °C. To remove the unbound iron, protein solution was exchanged at least five times with original buffer (50 mM HEPES, pH 7.4) by using a Centricon filter of 10 kDa molecular mass cut-off. The iron saturation of Tf was checked by urea–polyacrylamide gel electrophoresis. The concentration of Fe_2Tf was determined spectrophotometrically on the basis of $\varepsilon_{465\ nm} = 5\times10^3\ M^{-1}\ cm^{-1}$ [8]. The percentage of protein iron saturation was above 95%.

N-lobe of Tf (Fe_NTf; oTf (Fe_NoTf) and N-lobe of sTf (Fe_NsTf)) was prepared by well known procedure used earlier for Fe_NsTf [7,9]. The perchlorate ion enhances the rate of iron release from the C-lobe 260 times more than the N-lobe of Tf. Therefore, the concept of selective release of iron from C-lobe of Fe_2Tf is used to prepare the Fe_NTf. For this, Fe_2Tf (250 μM) was incubated at 37 °C for ~2 hrs in 0.1 M HEPES buffer that also contained 0.1 M EDTA and 2.7 M $NaClO_4$. To remove the EDTA and $NaClO_4$ from the protein solution, the protein solution was exchanged at least five times with original buffer (50 mM HEPES, pH 7.4) by using a Centricon filter of 10 kDa. The iron saturation of Fe_NTf was checked by urea–polyacrylamide gel electrophoresis. The concentration of Fe_NTf was determined spectrophotometrically on the basis of $\varepsilon_{465\ nm} = 2150\ M^{-1}\ cm^{-1}$ [5].

2.2.7 Measurement of the absorbance and fluorescence monitored iron release profiles of Fe_2Tf as a function of pH and urea

Low pH and high concentration of denaturant promote the iron release from Fe_2Tf. To determine the effect of salt or sucrose on the pH-induced iron release from Fe_2oTf, the samples of Fe_2oTf (~10 μM) were prepared in mixture of buffers (0.02 M HEPES + 0.02 M MES, pH ~8.0-3.0) containing different concentrations of salts (NaCl, $NaNO_3$, NaBr, Na_2SO_4) or sucrose at 25 °C. To determine the effect of crowding agents on the pH-induced iron release from Fe_2oTf, the samples of Fe_2sTf (~6 μM) were prepared in mixture of buffers (0.1 M HEPES + 0.05 M MES, pH 7.5-2.0) that contained different concentrations of crowding agent (dextran 40, dextran 70, ficoll70) at 25 °C. To determine the effect of crowding agents on the salt-dependence of pH-induced iron release from Fe_2Tf, the samples of Fe_2sTf (~6 μM) were prepared in mixture of buffers (0.1 M HEPES + 0.05 M MES, pH 7.5-2.0) that contained different concentrations of salt (NaCl) in the absence and presence of 200 mg ml^{-1}dextran 40 at 25 °C. Before the data collections, the Fe_2oTf and Fe_2sTf samples were incubated for ~4 hrs and ~6 hrs at 25 °C, respectively. The pH of protein samples were measured both before and after the experiments. The reported pH values are those determined after taking the data. The decrease in absorbance maximum at 465 nm and increase in fluorescence emission intensity at 340 nm (ex: 280 nm) were used as the reliable markers for iron release from Fe_2Tf [10-13]. The pH equilibrium profiles for Fe_2Tf were measured by monitoring changes in the fluorescence emission at 340 nm (ex: 280 nm) or absorbance at 465 nm. The pH profiles of Fe_2Tf were fitted to equation (5) [14]:

$$y = \left[\frac{c_f + c_u \left[10^{(Cm-pH)} \right]}{1+10^{(Cm-pH)}} \right] \quad (5)$$

where c_f and c_u are the normalized absorbance or fluorescence signals for the iron-loaded native state and the iron-free acid-denatured state, respectively, and C_m is the pH midpoint where the Fe_2Tf lost its half of the metal ions.

To determine the effect of salt or sucrose on the urea-induced iron release from Fe_2oTf, the samples of Fe_2oTf (10 μM) were prepared in a buffer (0.05 M HEPES, pH 7.4 or 0.05 M MES, pH 5.8-5.4) containing different concentrations of urea and a desired concentration of salt (NaCl, Na_2SO_4) or sucrose. Before the data collection, the protein samples were incubated for ~5 hrs at 25 °C. To determine the effect of crowding agent on the urea-induced iron release from Fe_2oTf, the samples of Fe_2sTf (~6 μM) were prepared in a buffer (0.1 M HEPES, pH 7.4 or 0.1 M MES, pH 5.7) containing different concentrations of urea and a desired concentration of crowding agent (dextran 40, dextran 70, ficoll 70) at 25 °C. To determine the effect of crowding agents on the salt-dependence of urea-induced iron release from Fe_2Tf, the samples of Fe_2sTf (~6 μM) were prepared in different concentrations of urea contained variable concentrations of salt (NaCl) in the absence and presence of 200 mg ml^{-1}dextran 40 at 25 °C. Before the data collection, Fe_2sTf samples at 7.4 and pH 5.7 were incubated for ~20 and ~3 hrs (25 °C), respectively. On the basis of fluorescence emission at 340 nm (ex: 280 nm) and absorbance at 465 nm, the fraction of iron released was estimated. The normalized urea-induced denaturation curves for the iron release were fitted to equation (1). Fluorescence emission spectra (320-410 nm) were collected on Perkin Elmer LS-55 spectrofluorometer or visible absorbance spectra (390-710 nm) were collected on Shimadzu 2450 spectrophotometer.

2.2.8 Stopped-flow measurement of folding-unfolding kinetics of Ferrocyt c

To establish the connection between the denaturant dependent CO-association rates and global folding and unfolding rates the folding-unfolding kinetics of Ferrocyt *c* were measured under different conditions of GdnHCl. For refolding kinetics, Ferricyt *c* (0.35 mM) unfolded in 7.5 M GdnHCl was reduced under N_2 by the sodium dithionite (3.2 mM). Thus prepared unfolded Ferrocyt *c* was mixed with the refolding buffer in the stopped flow in the desired ratio to record the folding kinetics. For unfolding kinetics, Ferrocyt *c* (0.35 mM) was prepared by

reducing the Ferricyt *c* with sodium dithionite added to a final concentration of 3.2 mM. Thus prepared native Ferrocyt *c* was mixed with the unfolding buffer in the stopped flow in the desired ratio to record the unfolding kinetics. Samples were equilibrated for 10 min before mixing. Stopped-flow experiments used a Biologic SFM400 module regulated at 25 °C by the use of an external water bath. The spectrometer was configured for fluorescence detection (ex: 280 nm, em: 358 nm). A two syringe mixing at a total flow rate of 8 ml s^{-1} was employed (1:7, protein/buffer). Typically, 10–20 shots were averaged.

2.2.9 Measurement of urea denaturation-induced and sodium dithionite reduction-induced iron release kinetic profiles of Fe_NTf

When Fe_NoTf was incubated with 9.0 M urea at pH 7.4 or 6.0 M urea at pH 5.6, the absorbance of 465 nm band is decreased significatenly with time [15]. To determine the effect of salt or sucrose on the urea-induced iron release from Fe_NTf**,** Fe_NoTf solution (40 μL, 110 μM, pH 7.4) was mixed rapidly to HEPES buffer (0.05 M, 0.8 mL, pH 7.4) that contained 9.0 M urea and a desired concentration of salt (NaCl or Na_2SO_4) or sucrose at 37 °C. At pH 5.6, iron release reaction is relatively faster, therefore, the kinetics of iron release at this pH was measured by a Shimadzu 2450 spectrophotometer coupled with applied photophysics RX 2000 rapid kinetics stopped-flow mixing accessory. Fe_NoTf (pH 7.4) was placed in one syringe and MES buffer (0.05 M, pH 5.6) that contained 6.0 M urea and a desired concentration of salt (NaCl or Na_2SO_4) or sucrose was placed in other stopped flow syringe. For kinetic experiments of urea denaturation-induced iron release the final concentrations of Fe_NoTf were ~5.5 μM and ~10 μM at pH 7.4 and 5.6, respectively. To determine the effect of crowding agents on the urea-induced iron release from Fe_NTf**,** Fe_NsTf solution (50 μL, pH 7.4) was mixed rapidly to HEPES buffer (0.1 M, 950 μL, pH 7.4) (for measurement at pH 7.4) or MES buffer (0.1 M, 950 μL, pH 5.5) (for measurement at pH 5.5) that contained 10.0 M (pH 7.4) or 6.0 M (pH 5.5) urea and a desired concentration of crowding agent (dextran 40 or dextran 70 or ficoll 70) at 37 °C. To determine the effect of crowding agents on the salt-dependence of urea-induced iron release from Fe_NTf, Fe_NsTf solution (50 μL, pH 7.4) was mixed rapidly to HEPES buffer (0.1 M, 950 μL, pH 7.4) (for measurement at pH 7.4) or MES buffer (0.1 M, 950 μL, pH 5.5) (for measurement at pH 5.5) that contained 10.0 M (pH 7.4) or 6.0 M (pH 5.5) urea and different concentrations of NaCl in the absence and presence of 200 mg ml^{-1} dextran 40 at 37 °C. For kinetic experiments of urea

denaturation-induced iron release, the final concentration of Fe_NsTf was ~15.0 μM. The kinetics of iron release from the Fe_NTf was measured by monitoring the change in absorbance at 465 nm, 37 °C.

To determine the effect of salt or sucrose on the reduction induced Fe^{2+} release from Fe_NoTf at pH 7.4, a small volume of Fe_NoTf solution (40 μL, 110 μM, pH 7.4) was mixed rapidly to a degassed HEPES (0.05 M, 0.8 mL, pH 7.4) buffer that contained 10 mM sodium dithionite, 0.25 mM BPS and a desired concentration of salt ($NaNO_3$ or Na_2SO_4) or sucrose (25 °C). At pH 5.6, the reductive iron release reaction is relatively faster, therefore, the kinetics of reductive iron release at this pH was measured by a Shimadzu 2450 spectrophotometer coupled with applied photophysics RX 2000 rapid kinetics stopped-flow mixing accessory. Fe_NoTf (pH 7.4) was placed in one syringe and MES buffer (0.05 M, pH 5.5) that contained sodium dithionite, BPS, and a desired concentration of salt ($NaNO_3$ or Na_2SO_4) or sucrose was placed in other stopped flow syringe (25 °C). For kinetic experiments of reduction induced Fe^{2+} release at pH 5.6 and 7.4, the final Fe_NoTf concentration was ~5 μM. To determine the effect of crowding agents on the reduction induced Fe^{2+} release from Fe_NsTf at pH 7.4 or pH 5.5, 20 μL (pH 7.4) of Fe_NsTf solution was mixed rapidly to a deaerated HEPES buffer (0.1 M, 980 μL, pH 7.4) or MES buffer (0.1 M, pH 5.4) that contained sodium dithionite, BPS and a desired concentration of crowding agent (dextran 40 or dextran 70 or ficoll 70) at 25 °C. To determine the effect of crowding agents on the salt-dependence of reduction induced Fe^{2+} release from Fe_NsTf at pH 7.4 or pH 5.5, 20 μL (pH 7.4) of Fe_NsTf solution was mixed rapidly to a deaerated HEPES buffer (0.1 M, 980 μL, pH 7.4) or MES buffer (0.1 M, pH 5.4) that contained sodium dithionite, BPS and different concentrations of NaCl in the absence and presence of dextran 200 mg ml^{-1} 40 at 25 °C. 8 μM and 10 μM concentration of Fe_NsTf was used for reduction induced Fe^{2+} release kinetic experiments at pH 7.4 and pH 5.5, respectively. The final concentration of sodium dithionite and BPS were 10 and 0.25 mM, respectively. The reductive iron release kinetics was measured by Fe^{2+}-BPS complex absorbance at 538 nm [16-17].

2.2.10 Measurements of mildly acidic pH-triggered iron release kinetic profiles of Fe_2oTf

Manual mixing kinetics experiments were performed by thorough mixing of a neutral aqueous solution of Fe_2Tf (pH 7.4, 50 mom HEPES buffer) with acetate buffer (pH≤4.2)

containing a desired concentrations of NaCl or Na_2SO_4 to achieve a final pH of 3.9≤pH≤4.3 at 25 °C. To capture the fast process, the kinetics experiments were also measured by Shimadzu 2450 spectrophotometer coupled with rapid kinetics stopped-flow mixing accessory (applied photophysics RX 2000). Fe_NoTf (pH 7.4) was placed in one syringe and acetate buffer (pH≤4.2) that containing desired concentrations of NaCl or Na_2SO_4 was placed in other stopped flow syringe at 25 °C. The final concentration of Fe_2oTf was 8−10 μM. The resulting change in absorbance at 465 nm was monitored with a Shimadzu 2450 spectrophotometer or Cary Model 6000i spectrophotometer (25.0 ± 0.1 °C).

2.2.11 Measurement of water activity (a_W) in the presence of denaturants and sugars

Water activity (a_W) plays an important role on protein stability [18-21]. In the presence of denaturants and sugars to determine the effect of water activity (a_W) on proteins stability the water activity analysis were performed. When cosolute Y is urea, GdnHCl, and sugar (trehalose, sucrose, maltose, glucose, ribose, glycerol) water activity (a_W) of a protein solution was calculated by equation (6) [18-21],

$$a_W = (1 - X_Y)\exp(\alpha X_Y + \beta X_Y^2 + \gamma X_Y^3) \qquad (6)$$

where X_Y is the mole fraction of cosolute. The experimental parameters, α, β and γ were reported for urea, GdnHCl, and (trehalose, sucrose, maltose, glucose, ribose, glycerol) in the literature [18-20] and are provided in Table (1). The values of a_w for alkylureas (MU, EU, and DMU) were calculated by an expression, $\phi = -55.51/m \ln a_w$, where m is molality of a given alkylurea. The experimental osmotic coefficient ϕ for the MU, DMU, and EU were taken from the literature [22].

Table 1 Parameters in Equation (6) to describe water activity of denaturants and sugars solutions.*

Solute	α	β	γ
Urea	-	0.8309	-
GdnHCl	-0.6462	6.560	-20.97
Sucrose	-	-7.405	-
Trehalose	-	−6.646	164.72
Maltose	-	−9.549	-
Glucose	-	−2.734	-
Ribose	-	−1.699	-
Glycerol	-	−2.22	-

* From reference [18-21]

2.2.12 Docking experiments of Cyt c and MbCO with denaturants

In order to gain insight into the protein-denaturants interactions, docking between the horse cyt *c* (PDB: 1HRC [23]) or horse MbCO (PDB: 1DWR [24]) and denaturant molecule (urea, MU, DMU, EU and TMU) was performed on SwissDock server using the default parameters [25-26]. Different binding modes of denaturant-protein hydrogen bonding were analyzed using UCSF chimera [27].

2.2.13 Urea concentration correction in the presence of crowding agent

Inert crowding agent increases the activity coefficient of other small species through decreasing its available volume through pure steric repulsion [28-31]. To calculate the effective concentrations of urea in the presence of crowding agent (dextran 40, dextran 70, ficoll 70), the partial specific volume of dextran 40, dextran 70 and ficoll 70 were determined in the absence and presence of urea. The partial specific volume is same in the absence and presence of crowding agent suggest that no interaction between crowding agent and urea. The value partial specific volume for all the crowding agents is 0.670 (±0.004) ml gm^{-1} and did not dependent on the concentration of crowding agent. The effective concentration of urea was calculated as described previously [28-31]. Urea concentration denotes the corrected effective concentration.

2.3 References

[1] Santoro MM, Bolen DW, Biochemistry 27:8063–8068 (1988)
[2] Kumar R, Prabhu NP, Rao DK, Bhuyan AK, J Mol Biol 364:483–495 (2006)
[3] Ptitsyn, OB, Semisotnov GV, The mechanism of protein folding. In: Nall BT, Dill KA, editors. Conformations and forces in protein folding. AAAS; Washington, DC. pp. 155–168 (1991)
[4] Engelhard M, Evans PA, Protein Sci 4:1553–1562 (1995)
[5] Bali PK, Harris WR, Arch Biochem Biophys 281:251–256 (1990)
[6] Turcot I, Stintzi A, Xu J, Raymond KN, J Biol Inorg Chem 5:634–641 (2000)
[7] Hissen AHT, Moore MM, J Biol Inorg Chem 10:211–220 (2005)
[8] Aasa R, Malmstrom BG, Saltman P, Vanngård T, Biochim Biophys Acta 75:203–222 (1963)
[9] Baldwin DA, de Sousa DM, Biochem Biophys Res Commun 99:1101–1107 (1981)
[10] James NG, Berger CL, Byrne SL, Smith VC, MacGillivray RT, Mason AB, Biochemistry 46:10603–10611 (2007)
[11] Lehrer SS, J Biol Chem 244:3613–3617 (1969)
[12] Bali PK, Harris WR, J Am Chem Soc 111:4457–4461 (1989)
[13] Halbrooks PJ, Mason AB, Adams TE, Briggs SK, Everse SJ, J Mol Biol 339:217–226 (2004)

[14] Kumar R, Mauk AG, J Phys Chem B 113:12400–12409 (2009)
[15] Nakazato K, Yamamura T, Satake K, J Biochem 103:823–828 (1988)
[16] Baldwin DA, Egan TJ, Marques HM, Biochim Biophys Acta 1038:1–9 (1990)
[17] Kojima N, Bates GW, J Biol Chem 254:8847–8854 (1979)
[18] Miyawaki O, Saito A, Matsuo T, Nakamura K, Biosci Biotechnol Biochem 61:466–469 (1997)
[19] Miyawaki O, Biochim Biophys Acta 1774:928–935 (2007)
[20] Miyawaki O, Biophys Chem 144:46–52 (2009)
[21] Miyawaki O, Tatsuno M, J Biosci Bioeng 111:198–203 (2011)
[22] Barone G, Rizzo E, Volpe V, J Chem and Engin Data 21:59–61 (1976)
[23] Bushnell GW, Louie GV, Brayer GD, J Mol Biol 214:585–595 (1990)
[24] Chu K, Vojtchovský J, McMahon BH, Sweet RM, Berendzen J, Schlichting I, Nature 403:921–913 (2000)
[25] Grosdidier A, Zoete V, Michielin O, Nucl Acids Res 39:W270–W277 (2011)
[26] Grosdidier A, Zoete V, Michielin O, J Comput Chem 32:2149–2159 (2011)
[27] Pettersen EF, Goddard TD, Huang CC, Couch GS, Greenblatt DM, Meng EC, Ferrin TE, J Comput Chem 13:1605–1612 (2004)
[28] Hall D, Minton AP, Biochim Biophys Acta 1649:127–139 (2003)
[29] Record MT Jr, Courtenay ES, Cayley S, Guttman HJ, Trends Biochem Sci 23:190–194 (1998)
[30] Hong J, Gierasch LM, J Am Chem Soc 132:10445–10452 (2011)
[31] Christiansen A, Wang Q, Samiotakis A, Cheung MS, Wittung-Stafshede P, Biochemistry 49:6519–6530 (2010)

Chapter 3
Effects of Urea and Alkylureas on Thermodynamic Stability and Internal Dynamics of Heme Proteins

3.1 Introduction

Although, the effect of urea and GdnHCl on the stability and local dynamics of M80-containing Ω-loop of native cytochrome *c* (Cyt *c*) have been investigated [1-3], the molecular mechanism by which these denaturants influence the local dynamics of M80-containing Ω-loop of Cyt *c* is not clearly understood. Moreover, the influence of alkylureas (methylurea (MU), dimethyl urea (DMU), ethylurea (EU) and tetramethylurea (TMU)) on the internal dynamics of Cyt c and myoglobin (Mb) is not studied before. In order to unravel the underlying mechanism by which these denaturants control the local dynamics of M80-containing Ω-loop of Cyt *c*, the effect of urea, GdnHCl, MU, DMU, EU and TMU on the structural fluctuations of the M80-containing Ω-loop of Cyt *c* was examined by measuring the rate of thermally-driven CO interaction with Ferrocyt *c* with varying concentrations of these denaturants. To determine the effect of denaturants on the internal dynamics of Mb, the rate of CO-replacement reaction of CO-liganded Mb (MbCO) was examined in the presence of varying concentrations of urea, MU, DMU, EU and TMU. It is known that CO interaction with Ferrocyt *c* replaces the native Fe^{2+}-M80 bond of protein with the non-native Fe^{2+}-CO bond [4-5]. Within the subdenaturing limit, the CO-association reaction data shows a substantial reduction in the amplitudes of thermal motions of the M80-containing Ω-loop of Ferrocyt *c*. The amplitudes of thermal motions of Ω-loop are found to be more reduced for urea and least for TMU. These results in conjugation with the docking results between the horse Cyt *c* and denaturant molecule (urea, MU, DMU, EU and TMU) show that the decrease in the extent of denaturant-mediated restricted dynamics of Ω-loop with a corresponding increase of alkyl groups on urea molecule is due to the decrease of denaturant-mediated cross-linking interactions with different groups of Ω-loop or other parts of the protein. On going from subdenaturing to unfolding milieu, the constraints on intramolecular dynamics of Ferrocyt *c* are subdued by the chaotropic action of the denaturant. However, within the subdenaturing conditions, as the concentration of denaturant is increased in the reaction medium, the rate of CO-replacement from MbCO increases and found to be more increased in the presence of TMU and least for urea. These results suggest that (i) the subdenturing concentrations of these denaturants unable to restrict the internal dynamics of Mb and, (ii)

chaotropic action of the denaturant increases as the hydrophobicity increases on the urea molecule.

The understanding of factors governing protein stability is important for biopharmaceutical and vaccines development efforts. In order to determine the exact effects of denaturants on the thermal stability of native proteins, the effects of urea and alkylureas were investigated on the thermal unfolding of Ferrocyt *c* and Mb. Water plays a fundamental and important role on protein stabilization [6]. Pioneering works by Miyawaki et al have revealed that water activity also plays an important role in protein stability [7-9]. Thermodynamic analysis of urea, MU, DMU, EU and TMU effects on the thermal unfolding of Ferrocyt *c* and Mb reveals that (i) thermal denaturation free energy change (ΔG_T), thermal unfolding midpoint temperature (T_m), and van′t Hoff enthalpy change (ΔH_m) of protein decrease with increasing the concentration of denaturant and hydrophobicity of urea derivatives, (ii) water activity plays an important role in Ferrocyt *c* and Mb stability and (iii) the disturbance of hydrophobic interactions and the hydrogen-bonding play crucial role in the destabilization of Ferrocyt *c* and Mb by denaturant.

3.2 Results

3.2.1 Denaturants dependence rate constant and activation parameters of CO-association and CO-replacement reactions

Fig. 3.1a typifies the kinetics of CO-association reaction of Ferrocyt *c* in the absence of denaturant at pH 7.0, 25 °C. The kinetics of CO-replacement reaction of MbCO in the absence of denaturant at pH 7.0, 22 °C is shown in Fig. 3.1b. The CO-association (Fig. 3.1a) and CO-replacement (Fig. 3.1b) kinetics are best described by single exponential decay with time constant, τ_{ass} = 18 min and τ_{off} = 0.6 min, respectively. The exponential decay in absorbance at 550 nm (the heme π→π* α-band) is due to association of CO to the protein. The CO replacement reaction of MbCO by hexacyanoferrate ions ($K_3[Fe(CN)_6]$) can be described as [10]:

$$\mathrm{MbCO} + \mathrm{CN}^- \underset{k_{on}}{\overset{k_{off}}{\rightleftharpoons}} \mathrm{Mb} + \mathrm{CO} + \mathrm{CN}^- \underset{k_{-CN}}{\overset{k_{+CN}}{\rightleftharpoons}} \mathrm{MbCN} + \mathrm{CO}$$

As described earlier [10-11], the observed rate constant $k_{app,}$ can be given as,

$$k_{app} = \frac{k_{off}k_{+CN} + k_{-CN}k_{on} + k_{off}k_{-CN}}{k_{on} + k_{+CN} + k_{-CN}} \quad (1)$$

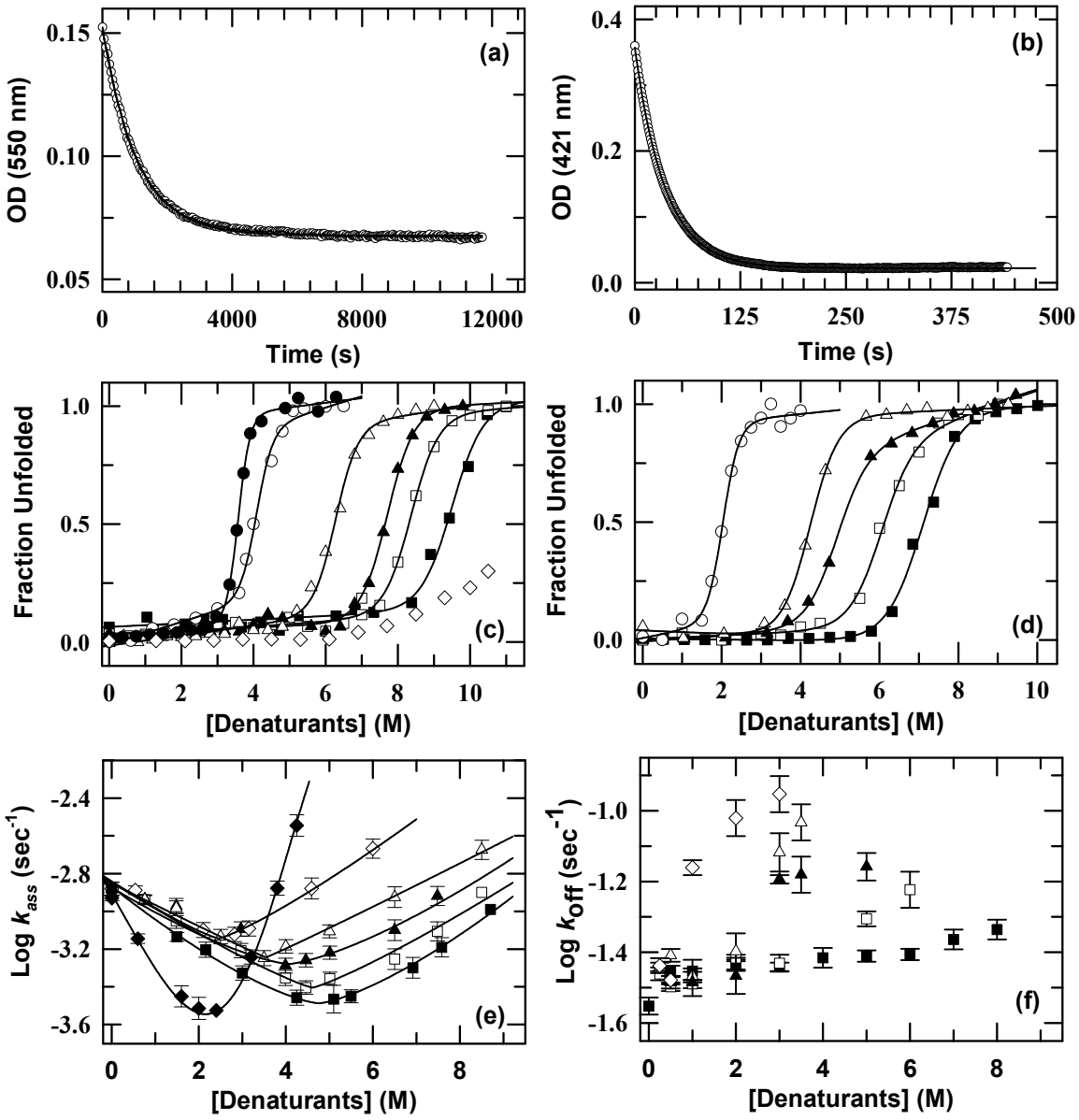

Fig. 3.1 (a) Represents the slow single-phase CO-association reaction, Ferrocyt *c*+CO → Ferrocyt *c*-CO (τ = 18.0 min, 25 °C) monitored by 550 nm heme absorbance. (b) Represents the slow single-phase CO replacement reaction, MbCO+CN^- → MbCN+CO (τ = 0.6 min, 22 °C) monitored at 421 nm. (c) Represents fluorescence monitored urea (■), MU (□), DMU (▲), EU (Δ), TMU (o), and GdnHCl (●) induced unfolding transitions of Cyt-CO at pH 7.0, 25 °C. Panel (c) also shows the urea-induced partial denaturation of Ferrocyt *c* (◊). (d) Represents fluorescence monitored urea (■), MU (□), DMU (▲), EU (Δ), and TMU (o) induced unfolding transitions of MbCO at pH 7.0, 25 °C. The solid lines in panel (c) and panel (d) represent the iterated least-squares fit of the data to a two-state unfolding transition (equation (1), chapter 2). The fitted parameters are summarized in Tables 1 and 2. (e) Denaturants dependence of Log k_{ass} (urea (■), MU (□), DMU (▲), EU (Δ), TMU (◊) and GdnHCl (♦)) at 25(±1) °C, pH 7.0. The lines through the data in panel (e) have been drawn by inspection only. (f) Denaturants dependence of Log k_{off} (urea (■), MU (□), DMU (▲), EU (Δ), and TMU (◊) at 22(±1) °C, pH 7.0.

Because CO dissociates much slower and CN^- binds much faster, therefore, $k_{+CN} \gg k_{on}$, and $k_{-CN} \ll k_{off}$. Furthermore, $k_{-CN} \ll k_{+CN}$. The equation (1) then simplifies to $k_{app} \sim k_{off}$. After the addition of CN^-, the kinetics of CO replacement by CN^- was monitored at 421 nm. Figs. 3.1c and 3.1d show the denaturant (urea, MU, DMU, EU, TMU or GdnHCl)-induced fluorescence monitored unfolding transitions of the CO-liganded Ferrocyt *c* (Cyt-CO) and MbCO, respectively at pH 7.0, 25 °C. Fig. 3.1c also presents the urea-denaturation transition of Ferrocyt *c* at pH 7.0, 25 °C, which clearly suggests that within the limit of the aqueous solubility of urea, Ferrocyt *c* exhibits incomplete unfolding [12]. Two-state analysis [13] (equation (1), Chapter 2) of the denaturant-induced unfolding transition curves of the Cyt-CO and MbCO provided the free energy of denaturation (ΔG_D) and surface area exposed by solvent (m_g) for denaurants. The resulting, ΔG_D, m_g and C_m for different denaturants for Cyt-CO and MbCO are summarized in Tables 1 and 2, respectively. Figs. 3.2a and 3.2b show the effect of denaturants (urea, MU, EU, DMU, TMU, and GdnHCl) on the relative free energies of native and unfolded states in Cyt-CO and MbCO. The difference between the relative free energies of native and unfolded states typically follows the trend: urea > MU > DMU > EU > TMU > GdnHCl (Figs. 3.2a and 3.2b).

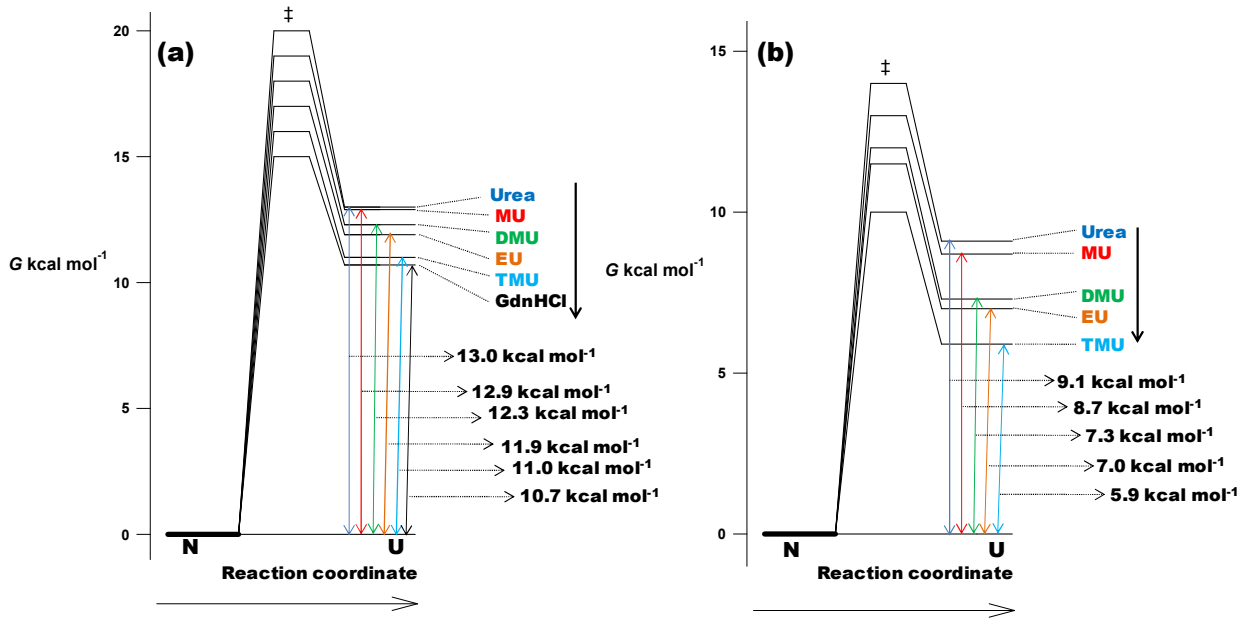

Fig. 3.2 Diagram illustrating the effect of denaturants (urea, MU, EU, DMU, TMU, and GdnHCl) on the relative free energies of native and unfolded states in Cyt-CO (a) and MbCO (b). The thermodynamic parameters derived from equilibrium unfolding experiments (Fig. 3.1c and 3.1d, Tables 1 and 2). The free energy of the native state of proteins is arbitrarily set to zero. The energy levels of transition states may not appear scaled exactly.

Table 1 ΔG_D, m_g, and C_m values for denaturants for unfolding of Cyt-CO monitored by fluorescence (ex: 280 nm, em: 375 nm).

denaturant (M)	ΔG_D	m_g	C_m	denaturant (M)	ΔG_D	m_g	C_m
Urea	13.0	1.37	9.5	EU	11.9	1.90	6.3
MU	12.9	1.54	8.4	TMU	11.0	2.70	4.1
DMU	12.3	1.60	7.7	GdnHCl	10.7	3.00	3.6

*m_g and ΔG_D (25 °C) are reported as kcal mol^{-1} M^{-1} and kcal mol^{-1}, respectively. The uncertainties of m_g and ΔG_D values reported here are ±0.2 kcal mol^{-1} M^{-1} and ±1.0 kcal mol^{-1}, respectively. C_m is reported in M. The uncertainty of C_m values reported here is ±0.3 M.

Table 2 ΔG_D, m_g, and C_m values for denaturants for unfolding of MbCO monitored by fluorescence (ex: 280 nm, em: 375 nm).

denaturant (M)	ΔG_D	m_g	C_m	denaturant (M)	ΔG_D	m_g	C_m
Urea	9.1	1.28	7.1	EU	7.0	1.65	4.2
MU	8.7	1.45	6.0	TMU	5.9	2.92	2.0
DMU	7.3	1.49	4.9				

*m_g and ΔG_D (25 °C) are reported as kcal mol^{-1} M^{-1} and kcal mol^{-1}, respectively. The uncertainties of m_g and ΔG_D values reported here are ±0.2 kcal mol^{-1} M^{-1} and ±1.0 kcal mol^{-1}, respectively. C_m is reported in M. The uncertainty of C_m values reported here is ±0.3 M.

Figs. 3.1e and 3.1f show the logarithm of rate coefficient for CO-association reaction and CO-replacement reaction in the presence of different concentration of urea, MU, EU, DMU, TMU, and GdnHCl. Data in Fig. 3.1e provides two major results: (i) "Chevron-like" feature of the Log k_{ass}-denaturants space: As the final concentration of denaturant is raised starting from strongly native-like conditions, the value of Log k_{ass} initially decreases and then increases, showing the inflections centered around 5.0, 4.5, 4.0, 3.1, 2.8, and 2.3 M for urea, MU, DMU, EU, TMU, and GdnHCl, respectively, (ii) The variation in magnitudes of k_{ass} with denaturants: As the denaturants concentrations are increased from 0.0 to 5.0 M urea, 4.5 M MU, 4.0 M DMU, 3.1 M EU, 2.8 M TMU, and 2.3 M GdnHCl, the value of k_{ass} decreases to about 4.0, 3.3, 2.5, 2.3, 1.7, and 4.5 folds, respectively.

In the subdenaturing limit of denaturants, the decrease in the Log k_{ass} value is more pronounced for GdnHCl and urea and least for TMU (GdnHCl > urea > MU > DMU > EU > TMU) (Fig. 3.1e), which suggests that CO-association with Ferrocyt *c* is controlled by some specific interactions of denaturant molecules with the protein groups. At relatively higher concentrations of denaturant, the unfolding action of denaturant dominants that eventually

facilitates the CO-association process, and hence the values of Log k_{ass} increase sharply (Fig. 3.1e). Data in Fig. 3.1f clearly shows that within the subdenaturing limit of denaturants, the Log k_{off} continuously increases, indicating that subdenaturing concentrations of denaturants are unable to reduce the thermal motions of Mb. The increase in Log k_{ass} and Log k_{off} values at higher denaturant concentration (Figs. 3.1e and 3.1f) are more pronounced for longer chain monosubstituted urea and tetramethyl-substituted urea, which suggests that the hydrophobic interactions and hydrogen-bonding may play important roles in controlling the CO-association reaction of Ferrocyt *c* and the CO-replacement reaction of MbCO.

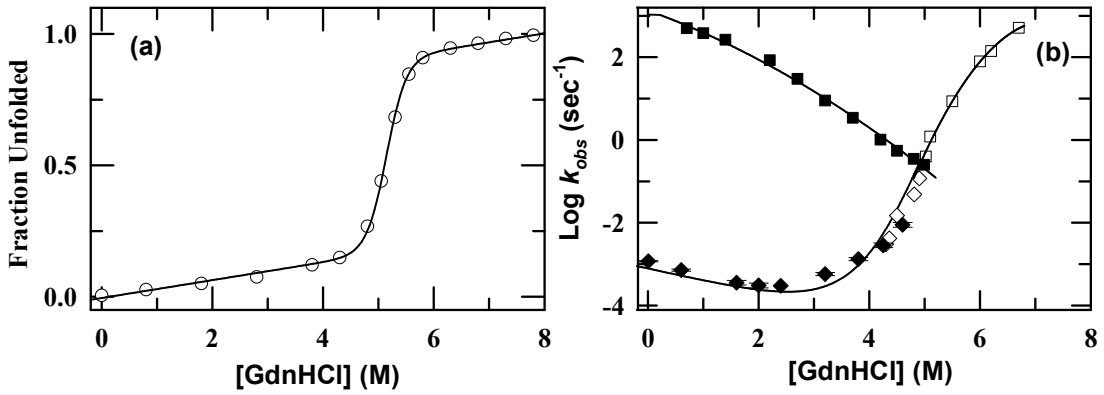

Fig. 3.3 (a) Represents the GdnHCl-induced equilibrium unfolding curve of Ferrocyt *c* (pH 7.0, 25 °C) probed by fluorescence (ex: 280 nm, em: 358 nm). The solid lines in panel (a) represent the iterated least-squares fit of the data to a two-state unfolding transition (equation (1), chapter 2). (b) GdnHCl dependence of the CO-association reaction rates presented in the perspective of global folding-unfolding kinetic rates. GdnHCl dependence of Log k_{obs} for the CO-association reaction (slow (♦) (manually and with stopped flow rapid mixing accessory) and fast (◊) (conventional stopped flow), Log k_{ass}), and global folding (■, Log k_f) and unfolding (□, Log k_u) rates of Ferrocyt *c*. The lines through the data in panel (b) have been drawn by inspection only.

The observation that the values of Log k_{ass} are increasingly promoted in progressively destabilizing conditions (Fig. 3.1e) leads one to examine the nature of the unfolding mode that controls the CO-association reaction. Fig. 3.3a presents the GdnHCl-induced unfolding transition of Ferrocyt *c* at 25 °C. Given C_m ~5.1 M GdnHCl for the equilibrium unfolding, the rate-[GdnHCl] data in Fig. 3.3b warrant a dynamical analysis of the protein in subdenaturing and denaturing limits. To establish the connection between the Log k_{ass}-labeled unfolding event and the global unfolding, Fig. 3.3b also presents the millisecond folding/unfolding rates of Ferrocyt *c*. As GdnHCl concentration is increased stating from 0.0 to 5.0 M, Log k_{ass} initially decrease

upto ~2.3 M GdnHCl and then increase and finally merge with the Log k_u values at ~4.9 M GdnHCl. This finding indicates that the motional mode of Ferrocyt *c* that controls CO-association reaction preserves its identity as a local mode (thermal fluctuations) in the subdenaturing limit but is dominated by the global unfolding motions under denaturing or unfolding conditions.

To further investigate the effect of denaturants on the internal dynamics of native Ferrocyt *c* and MbCO, the denaturants dependence of the activation enthalpy ($\Delta H_{ass}^{\ddagger}$) and activation entropy ($\Delta S_{ass}^{\ddagger}$) was examined for the CO-association reaction of Ferrocyt *c* and CO-replacement reaction of MbCO. If internal dynamics of protein is restricted at some concentration of denaturant, then the activation enthalpy for the CO-association reaction would be comparatively higher. Fig. 3.4a shows the Eyring plots for CO-association reaction of Ferrocyt *c* in the absence and presence of 5.0 M urea, 4.5 M MU, 4.0 M DMU, 3.1 M EU, 2.8 M TMU, and 2.3 M GdnHCl. Fig. 3.4b shows the Eyring plots for CO-replacement reaction of MbCO in the absence and presence of 8.0 M urea, 6.0 M MU, 3.5 M DMU, 3.5 M EU, and 3.0 M TMU. To determine the denaturants dependency of activation enthalpy and activation entropy, the plots in Figs. 3.3a and 3.3b were analyzed by using the Eyring equation (equation (1)) [14].

$$\ln(k_{ass/off} h/k_B T) = (\Delta S_{ass/off}^{\ddagger}/R) - (\Delta H_{ass/off}^{\ddagger}/RT) \qquad (1)$$

Tables 3 and 4 summarize the values of the activation enthalpies and activation entropies at varying concentrations of denaturants for Ferrocyt *c* and MbCO, respectively. The data in Table 3 clearly shows that in the presence of low concentrations of denaturants, the activation enthalpy for CO-association reaction of Ferrocyt *c* increases. The data in Table 4 clearly shows that in the presence of denaturants, the activation enthalpy for CO-replacement reaction of MbCO decreases. The extent of increase in the activation enthalpy for CO-association reaction of Ferrocyt *c* is most marked for GdnHCl and urea, and least for TMU (Table 3). The extent of decrease in the activation enthalpy for CO-replacement reaction is most marked for TMU and least for urea for (Table 4).

Both entropy and fluctuations have the same origin, and the entropy of the system is a measure of atomic fluctuations [10,12]. This entropy appears to be local, owing to less freedom of the bonded residues and restrictions on the rotations of pertinent dihedral angles (φ, ψ and ω).

Table 3 Activation enthalpy ($\Delta H_{ass}^{\ddagger}$), activation entropy ($\Delta S_{ass}^{\ddagger}$) and entropy reduction ($\Delta\Delta S_{ass}^{\ddagger}$) for CO-association reaction of Ferrocyt *c* in 0.1 M sodium phosphate buffer, pH 7.*

Stabilizing Additive	additive concentration (M)	$\Delta H_{ass}^{\ddagger}$	$\Delta S_{ass}^{\ddagger}$	$\Delta\Delta S_{ass}^{\ddagger}$
no additive	0.0	24.9 (±0.2)	10.1 (±1.0)	0.0
Urea	5.0	28.5 (±0.4)	21.9 (±1.2)	11.8 (±0.2)
GdnHCl	2.3	28.6 (±0.4)	21.8 (±1.2)	12.7 (±0.2)
MU	4.5	28.1 (±0.1)	21.0 (±0.3)	10.9 (±0.7)
DMU	4.0	26.7 (±0.2)	16.8 (±0.6)	6.7 (±0.4)
EU	3.1	25.4 (±0.1)	12.6 (±0.6)	2.5 (±0.4)
TMU	2.8	25.1 (±0.4)	11.6 (±1.2)	1.5 (±0.2)

*$\Delta H_{ass}^{\ddagger}$, $\Delta S_{ass}^{\ddagger}$, and $\Delta\Delta S_{ass}^{\ddagger}$ are reported as kcal mol^{-1}, cal mol^{-1} K^{-1}, and cal mol^{-1} K^{-1}, respectively. The uncertainty (standard error) is indicated in parenthesis.

Table 4 Activation enthalpy ($\Delta H_{off}^{\ddagger}$) and activation entropy ($\Delta S_{off}^{\ddagger}$) for CO-replacement reaction of MbCO in 0.1 M sodium phosphate buffer, pH 7.*

Additive	additive concentration (M)	$\Delta H_{off}^{\ddagger}$	$\Delta S_{off}^{\ddagger}$
no additive	0.0	19.0 (±0.3)	-1.5 (±1.1)
Urea	8.0	15.2 (±0.5)	-13.7 (±1.6)
MU	6.0	14.5 (±0.3)	-15.6 (±1.1)
DMU	3.5	13.4 (±0.5)	-19.0 (±1.7)
EU	3.5	13.1 (±0.7)	-19.4 (±2.0)
TMU	3.0	12.0 (±0.5)	-22.9 (±1.8)

*$\Delta H_{off}^{\ddagger}$, and $\Delta S_{off}^{\ddagger}$ are reported as kcal mol^{-1}, and cal mol^{-1} K^{-1}, respectively. The uncertainty (standard error) is indicated in parenthesis.

Thus, a reduction in the vibrational entropy in the presence of denaturants correlates with decreased spatial displacements of vibration (thermal) fluctuations of heme and the surrounding atoms responsible for the CO-association to Ferrocyt *c*. A previous study revealed that the low frequency local motions of M80 containing Ω-loop of Ferrocyt *c* controls the CO-dissociation process from natively folded CO-liganded Ferrocyt *c* [15]. The entropy reduction for the protein

in the presence of denaturant relative to that in the absence of denaturant ($\Delta\Delta S_{ass}^{\ddagger}$) was calculated according to equation,

$$\Delta\Delta S_{ass}^{\ddagger} = S_{ass\,(x)}^{\ddagger} - S_{ass\,(ref)}^{\ddagger} \qquad (2)$$

where, $\Delta S_{ass\,(ref)}^{\ddagger}$ and $\Delta S_{ass\,(x)}^{\ddagger}$ are the activation entropies for CO-association reaction in the absence and the presence of *x* concentration of denaturant. Table 3 summarizes values of $\Delta\Delta S_{ass}^{\ddagger}$ in the presence of 5.0 M urea, 4.5 M MU, 4.0 M DMU, 3.1 M EU, and 2.8 M TMU. The entropy reduction for CO-association reaction is apparently positive in the presence of denaturant and this positive entropy loss is found higher for urea and GdnHCl and least for TMU (Table 3).

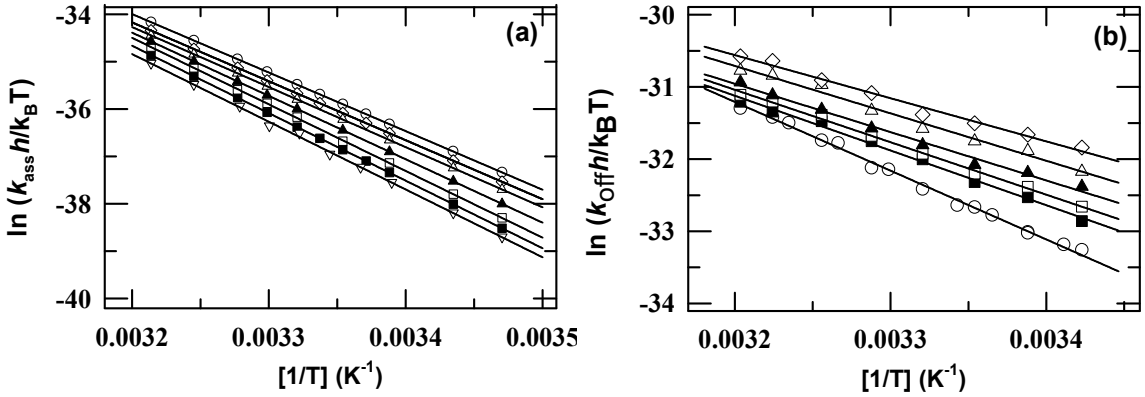

Fig. 3.4 (a) Eyring plots for the CO-association reaction, 0.1 M sodium phosphate buffer, pH 7 with no additive (o), 5.0 M urea (■), 4.5 M MU (□), 4.0 M DMU (▲), 3.1 M EU (Δ), 2.8 M TMU (◊), and 2.3 M GdnHCl (∇). Activation enthalpies ($\Delta H_{ass}^{\ddagger}$) and activation entropies ($\Delta S_{ass}^{\ddagger}$) are listed in Table 3. (b) Eyring plots for the CO-replacement reaction, 0.1 M sodium phosphate buffer, pH 7 with no additive (o), 8.0 M urea (■), 6.0 M MU (□), 3.5 M DMU (▲), 3.5 M EU (Δ) and 3.0 M TMU (◊). Activation enthalpies ($\Delta H_{off}^{\ddagger}$) and activation entropies ($\Delta S_{off}^{\ddagger}$) are listed in Table 4.

Fig. 3.5a shows the urea distribution of $\Delta H_{ass}^{\ddagger}$ determined from temperature dependence of the CO-association reaction. The peak value of $\Delta H_{ass}^{\ddagger}$ appears at 5.0 M of urea, which is also the concentration at which the Log k_{ass} *vs* [Denaturant] profile exhibits the minimum (Fig. 3.1e). This finding reveals that in the presence of urea (≤5.0 M), the free energy of the protein is lowered, leading to decrease of Log k_{ass}. Above 5.0 M urea, the denaturing action of denaturant beats its own protein stabilizing effect, therefore, the Log k_{ass} now increases because of an increase in entropy reduction of the protein that leads to a decrease in $\Delta H_{ass}^{\ddagger}$ and $\Delta S_{ass}^{\ddagger}$. Fig. 3.5b

shows the $\Delta\Delta S_{ass}^{\ddagger}$ *vs* [Urea] plot. The increase in $\Delta\Delta S_{ass}^{\ddagger}$ with [Urea] exhibits a peak value of ~12 cal $mol^{-1}K^{-1}$ at 5.0 M urea, suggesting a dramatic loss of motional freedom of the protein.

The data in Figs. 3.4a and 3.4b suggest strong enthalpy-entropy compensation, this correlation was confirmed by plotting $\Delta H_{ass}^{\ddagger}$ against $\Delta S_{ass}^{\ddagger}$ (Fig. 3.5c). Linear least-squares fits to the data in Fig. 3.5c provided a compensation temperature around 293 K, which suggests that water plays important role in controlling the CO-association dynamics of Ferrocyt *c*.

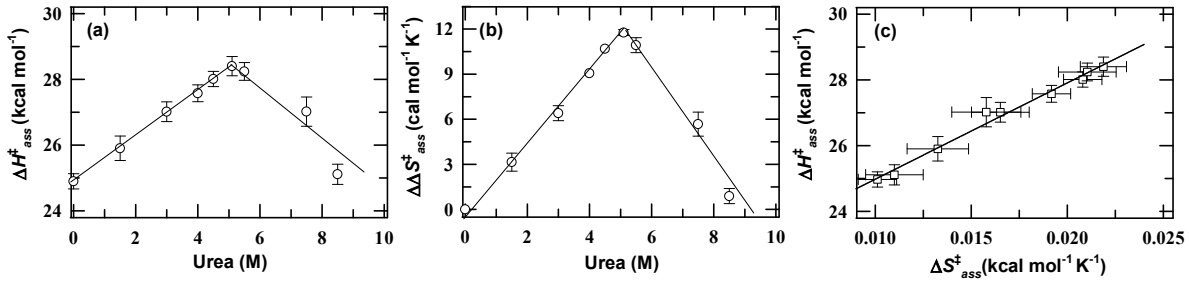

Fig. 3.5 (a) Urea distribution of $\Delta H_{ass}^{\ddagger}$ for CO-association reaction (b) Urea distribution of entropy reduction ($\Delta\Delta S_{ass}^{\ddagger}$) by protein relative to the entropy of the protein in the absence of denaturant ($\Delta S_{ass}^{\ddagger}{}_{(ref)}$) for CO-association reaction. (c) Presents the $\Delta H_{ass}^{\ddagger}$ against $\Delta S_{ass}^{\ddagger}$ plot for urea. The solid line in panel (c) presents linear least-squares fits to the data.

3.2.2 In silico identification of denaturants binding sites on Cyt c and MbCO

The different clusters of denaturants (urea, MU, DMU, EU, and TMU) that are involved in binding with Cyt *c* and MbCO at the same site are screened through their fullfitness strength. Docking results reveal that these denaturants can form multiple variable length hydrogen bonds with the backbone-backbone or backbone-side chain atoms of the Cyt *c* and MbCO molecule that are distant from each other (Figs. 3.5 and 3.6, and Tables 5 and 6). In the subdenaturing limit of denaturants, such polyfunctional interactions between the denaturant and different groups of Ω-loop and other part of the Cyt *c* (Fig. 3.6 and Table 5) restrict the internal dynamics of protein or part of it (Fig. 3.1e). As the alkyl group is increased on the urea molecule, the number of denaturant molecules that involved in polyfunctional interactions with different groups of Ω-loop and other part of the Cyt *c* decrease (Fig. 3.6 and Table 5). Figs. 3.5b and 3.5c clearly indicate that about seven urea molecules and four DMU molecules form multiple variable length hydrogen bonds with backbone and side chain atoms of the Ω-loop. Docking results further revealed that the denaturant molecules also form variable length hydrogen bonds with the side chain or peptide bond (C=O or N-H group) of single amino acid (Tables 5 and 6). These

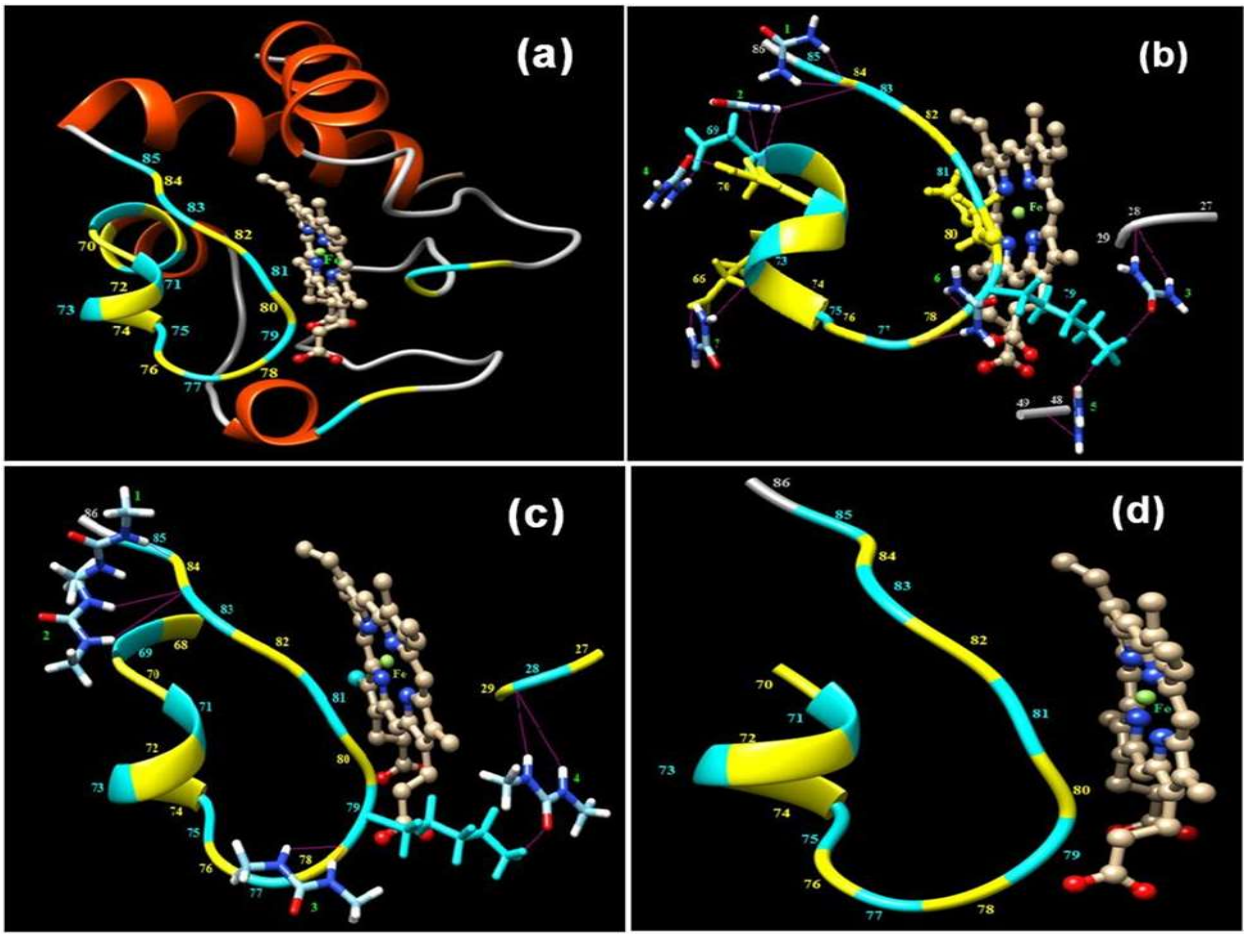

Fig. 3.6 (a) A ribbon model for horse Cyt *c* (PDB: 1HRC) [18]. Heme atoms are shown in ball and stick form. The Ω-loop residues (70-85) are marked according to their position. (b) Shows the hydrogen bonding network established by seven urea molecules in which ASN70, LYS73, LYS79, ALA83, GLY84 residues of Ω-loop are involved. Panel (b) clearly shows that these seven urea molecules establish nine hydrogen bonds with different residues of Ω-loop (ASN70, LYS73, LYS79, ALA83, GLY84) and seven hydrogen bonds with other different residues of the protein (THR28, TYR48, GLU66, GLU69). (c) Represents the hydrogen bonding network established by four DMU molecules in which 6 hydrogen bonds forms with different residues of Ω-loop (THR78, LYS79, ALA83, GLY84) and two hydrogen bonds with other different residue of protein (THR28). Panel (d) shows that TMU molecules do not form any hydrogen bond with Ω-loop. For better visualization, the side chains of those residues are shown only which eventually involved in hydrogen bonding with denaturant molecules (panels (b) and (c)). Panel (b) also shows the side chain of MET80 in ball and stick form. The other residues (as appear in panel (a)) have been removed in panels (b), (c) and (d) to better expose the denaturant binding sites on Ω-loop. Image processing was performed using UCSF Chimera [19].

Table 5 Classification of denaturant-protein hydrogen bonding interactions determined by using SwissDock server [16-17].

denaturant hydrogen bonding interactions sites of horse Cyt *c*	number of denaturant molecules involved in hydrogen bonding with Cyt *c*					number of denaturant molecules involved in hydrogen bonding with Ω-loop of Cyt *c*			
	urea	MU	DMU	EU	TMU	Urea	DMU	EU	TMU
with side chain of single amino acid only	8	10	6	10	6	0	0	1	0
with C=O group of single peptide bond only	1	6	9	8	0	0	3	1	0
with N-H group of single peptide bond only	0	0	2	2	2	0	0	0	0
with C=O group of peptide bond and side chain of different amino acid	7	1	3	2	0	3	1	0	0
with N-H group of peptide bond and side chain of different amino acid	2	1	0	0	0	0	0	0	0
with two C=O groups of different peptide bonds	6	3	2	1	0	3	0	0	0
with C=O and N-H groups of two different peptide bonds	1	0	1	1	0	0	0	0	0
with side chains of two amino acids	7	8	3	4	0	1	0	0	0
total denaturants molecules involved in hydrogen bonding with protein	32	29	26	28	8	7	4	2	0
total denaturant molecules that involved in poly functional cross-linking interactions	23	13	9	8	0	7	1	0	0
total denaturant molecules that not involved poly functional cross-linking interactions	9	16	17	20	8	0	3	2	0
ratio of denaturant molecules that involved and not involved in poly functional cross-linking interactions	2.55	0.81	0.52	0.4	0				

Table 6 Classification of denaturant-MbCO hydrogen bonding interactions determined by using SwissDock server [16-17].

denaturant hydrogen bonding interactions sites of MbCO	number of denaturant molecules involved in hydrogen bonding with MbCO				
	Urea	MU	DMU	EU	TMU
with side chain of single amino acid only	8	14	8	9	2
with C=O group of single peptide bond only	6	5	4	6	0
with N-H group of single peptide bond only	0	0	0	1	1
with C=O group of peptide bond and side chain of different amino acid	2	3	1	4	0
with N-H group of peptide bond and side chain of different amino acid	1	1	0	0	0
with two C=O groups of different peptide bonds	0	0	1	0	0
with C=O and N-H groups of two different peptide bonds	2	0	0	0	0
with side chains of two amino acids	1	1	1	3	0
total denaturants molecules involved in hydrogen bonding with protein	20	24	15	23	3
total denaturant molecules that involved in poly functional cross-linking interactions	6	5	3	7	0
total denaturant molecules that not involved poly functional cross-linking interactions	14	19	12	16	3
ratio of denaturant molecules that involved and not involved in poly functional cross-linking interactions	0.30	0.26	0.25	0.43	0

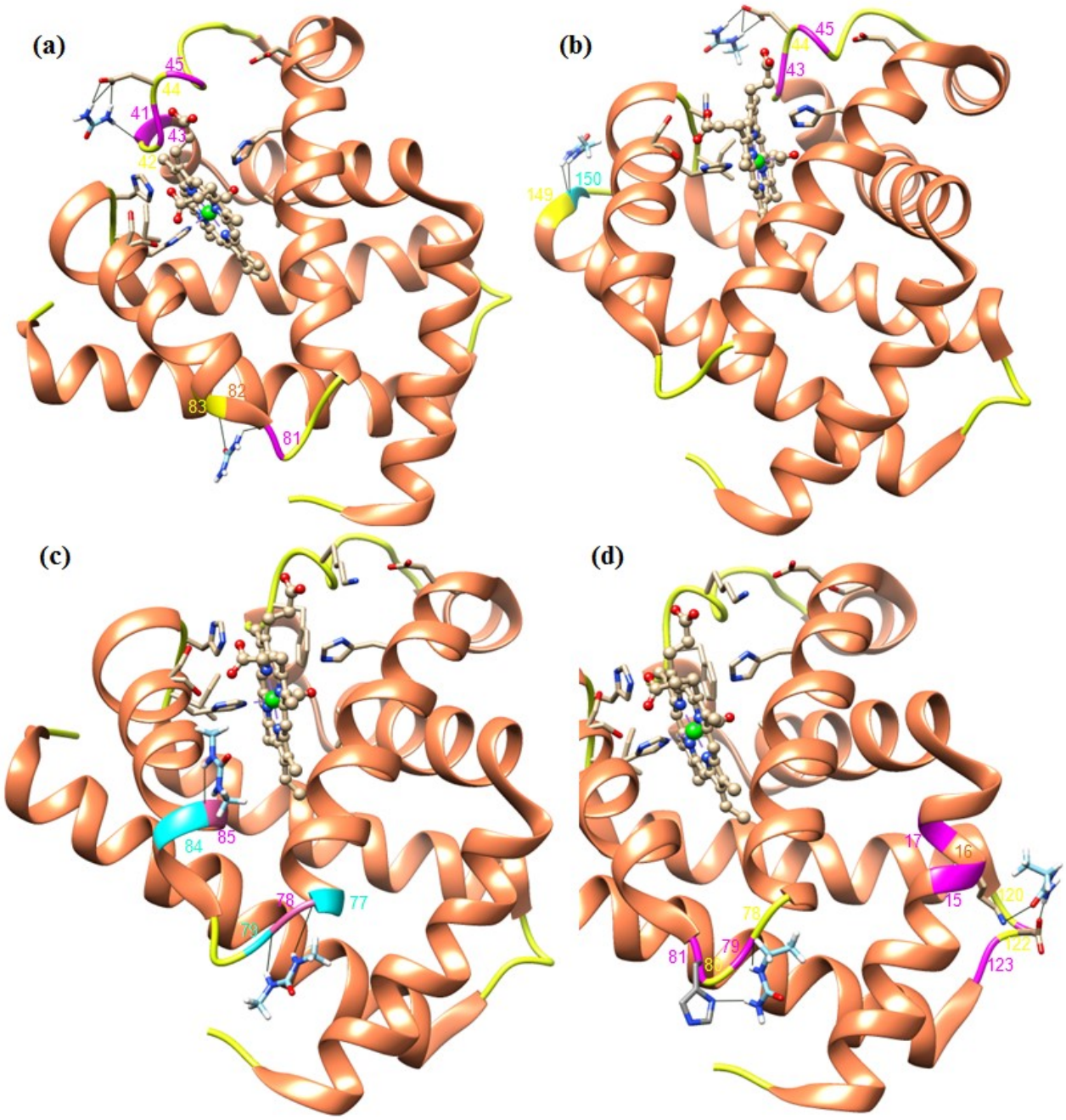

Fig. 3.7 (a) Shows the hydrogen bonding network established by two urea molecules with GLU41, ASP44, HSE81 and GLU83 residues of protein. (b) Shows the hydrogen bonding network established by two MU molecules with ASP44 and LEU149 residues of protein. (c) Shows the hydrogen bonding network established by two DMU molecules with LYS77, LYS78 and ALA84 residues of protein. (d) Shows the hydrogen bonding network established by two EU molecules with LYS16, ASP122, LYS78 and HIS81 residues of protein. Panels (a) to (d) show the ribbon model for horse MbCO with heme atoms and CO in ball and stick form. Residues are marked according to their position. Image processing was performed using UCSF Chimera [19].

hydrogen bonding interactions do not crosslink the different atoms of the protein. However, their contributions toward the denaturant-mediated restricted dynamics of Cyt *c* cannot be neglected

since denaturant like TMU does not involve in polyfunctional interactions with different groups of Cyt *c* or Ω-loop of it (Table 5) but it restricts the internal dynamics of protein (Fig. 3.1e). It is also observed that TMU does not form any hydrogen bond on the Ω-loop of Cyt *c* (Fig. 3.6d). Figs. 3.6a, 3.6b, 3.6c, and 3.6d show the multiple variable length hydrogen bonding network established by the urea, MU, DMU and EU with the different groups on MbCO, respectively. However, as compared to Cyt *c* the lesser denaturant molecules are involved in polyfunctional cross-linking interactions in the case of MbCO (Table 6). Therefore, in the subdenaturing limit, the polyfunctional interactions between the denaturant and different groups of MbCO are not enough to restrict the internal dynamics of MbCO (Fig. 3.1f).

3.2.3 Denaturant dependence of far-UV CD, near-UV CD, heme absorbance, and fluorescence

Aqueous stability of Ferrocyt c is extremely high (~18 kcal mol^{-1} at 25 °C) [5], and within the limit of the aqueous solubility of urea, Ferrocyt *c* exhibits incomplete unfolding [12]. Ferrocyt *c* and Ferricyt *c* are nearly identical both structurally and conformationally [20-23], so to determine the effect of urea and alkylureas on the conformational stability of protein, the denaturant induced unfolding transitions were measured for Ferricyt *c*. The far-UV CD spectra of Ferricyt *c* and Mb exhibit two negative bands at 208 and 222 nm, which reflects the secondary structure of the protein. Fig. 3.8a presents the far-UV CD spectra of Ferricyt *c* without additive and in the presence of 5.0 M urea, MU, EU, and GdnHCl. Fig. 3.8b presents the far-UV CD spectra of Mb without additive and in the presence of 4.6 M urea, 4.8 M MU, 4.3 M DMU, 4.3 M EU, and 9.0 M urea. Figs. 3.7a and 3.7b clearly show that in the presence of denaturants, the two negative bands at 208 and 222 nm are eliminated, which reflects that the denaturants disrupt the secondary structure of protein [5,12,24-28]. These two negative bands (peptide bands) of Ferricyt *c* are not greatly affected in the presence of 5.0 M urea but are significantly lost in the presence of 5.0 M of EU (Fig. 3.8a). The peptide bands of Mb also do not greatly affected in the presence of 4.6 M urea but significantly lost in the presence of 4.3 M of EU (Fig. 3.8b).

The near-UV CD spectrum of native Ferricyt *c* exhibits two sharp negative bands between 280 and 295 nm, associated with the packing of the Trp59 side chains [29]. Fig. 3.8c presents the near-UV CD spectra of Ferricyt *c* without additive and in the presence of 5.0 M of urea, MU, DMU, EU, and GdnHCl. Fig. 3.8c clearly shows that in the presence of 5.0 M

urea/MU/DMU, the two negative bands at 282 and 289 nm are disrupted, indicating that denaturants disrupt the tertiary structure of folded proteins [12,30]. The two negative bands at 282 and 289 nm are not greatly affected in the presence of 5.0 M urea but are significantly lost in the presence of 5.0 M of EU, indicating that the efficiency for the disruption of tertiary structure also vary with the hydrophobicity of denaturant.

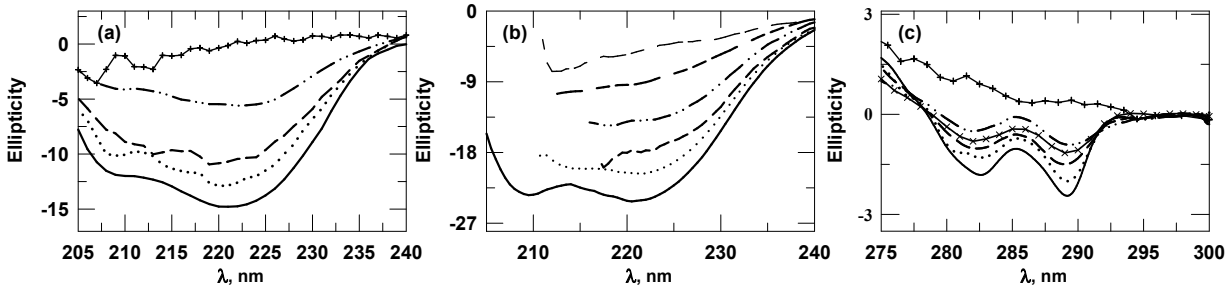

Fig. 3.8 (a) Represent the far-UV CD (in the absence of denaturant (——) and in 5.0 M aqueous solutions of urea (·····), MU (–––), EU (— · · —), and GdnHCl (++++++)) spectra of Ferricyt *c*, at pH 6.0 (±0.5), 25 °C. (b) Represent the far-UV CD (in the absence of denaturant (——) and in aqueous solutions of 4.6 M urea (·····), 4.8 M MU (– – –), 4.3 M DMU (— · · —), 4.3 M EU (–– – –), and 9.0 M urea (– ––) spectra of Mb, pH 7.0 (±0.1), 25 °C. (c) Represent the near UV-CD (in the absence of denaturant (——) and in 5.0 M aqueous solutions of urea (·····), MU (– – –), DMU (–×××–), EU (— · · —), and GdnHCl (++++++)) spectra of Ferricyt *c* at pH 6.0 (±0.5), 25 °C.

Figs. 3.8a and 3.8b represent the the far-UV CD (222 nm) monitored various denaturants-induced equilibrium unfolding transitions of Ferricyt *c* and Mb, respectively. Figs. 3.8c and 3.8d represent the fluorescence-monitored various denaturants-induced equilibrium unfolding transitions of Ferricyt *c* and Mb, respectively. Fig. 3.9e represents near-UV CD (282 nm) monitored various denaturants-induced equilibrium unfolding transitions of Ferricyt *c.* These unfolding transitions were analyzed assuming a two state transition between the folded (N) and unfolded (U) conformations by using the procedure of Santoro and Bolen [13] (equation (1), chapter 2). The resulting free energy of denaturation (ΔG_D), surface area exposed by solvent (m_g), and midpoint denaturant concentration (C_m) for unfolding of Ferricyt *c* and Mb by various denaturants monitored by CD (far-UV CD (222 nm) and near-UV CD (282 nm)), and fluorescence (ex: 280 nm) are provided in Tables 7 and 8, respectively.

Table 7 ΔG_D, m_g, and C_m values for denaturants for unfolding of Ferricyt *c* monitored by far-UV CD (222 nm), near-UV CD (282 nm), and fluorescence (ex: 280 nm, em: 358 nm).

	far-UV CD (222 nm)			near-UV CD (282 nm)			Fluorescence		
denaturant (M)	ΔG_D	m_g	C_m	ΔG_D	m_g	C_m	ΔG_D	m_g	C_m
Urea	9.02	1.20	7.52	10.1	1.3	7.8	8.4	1.1	7.8
MU	7.02	1.02	6.85	8.8	1.25	7.0	6.9	0.97	7.1
DMU	-	-	-	6.7	1.1	6.2	6.4	0.95	6.7
EU	5.50	1.16	4.75	5.1	1.0	5.1	3.0	0.65	4.6
TMU	-	-	-	-	-	-	2.8	0.80	3.5
GdnHCl	4.96	1.77	2.80	5.60	2.0	2.8	5.5	2.2	2.5

*m_g and ΔG_D (25°C) are reported as kcal mol^{-1} M^{-1} and kcal mol^{-1}, respectively. The uncertainties of m_g and ΔG_D values reported here are ±0.2 kcal mol^{-1} M^{-1} and ±1.0 kcal mol^{-1}, respectively. C_m is reported in M. The uncertainty of C_m values reported here is ±0.3 M.

Table 8 ΔG_D, m_g, and C_m values for denaturants for unfolding of Mb monitored by far-UV CD (222 nm), and fluorescence ((ex: 280 nm, em: 358 nm).

	far-UV CD (222 nm)			Fluorescence		
denaturant (M)	ΔG_D	m_g	C_m	ΔG_D	m_g	C_m
Urea	8.4	1.47	5.7	8.6	1.43	6.0
MU	8.0	1.59	5.0	8.1	1.67	4.9
DMU	6.5	1.48	4.4	7.8	1.76	4.4
EU	6.3	1.90	3.3	7.0	2.30	3.0
TMU	-	-	-	6.3	3.03	2.1
GdnHCl	6.0	3.74	1.6	6.5	4.11	1.6

*m_g and ΔG_D (25°C) are reported as kcal mol^{-1} M^{-1} and kcal mol^{-1}, respectively. The uncertainties of m_g and ΔG_D values reported here are ±0.3 kcal mol^{-1} M^{-1} and ±1.5 kcal mol^{-1}, respectively. C_m is reported in M. The uncertainty of C_m values reported here is ±0.3 M.

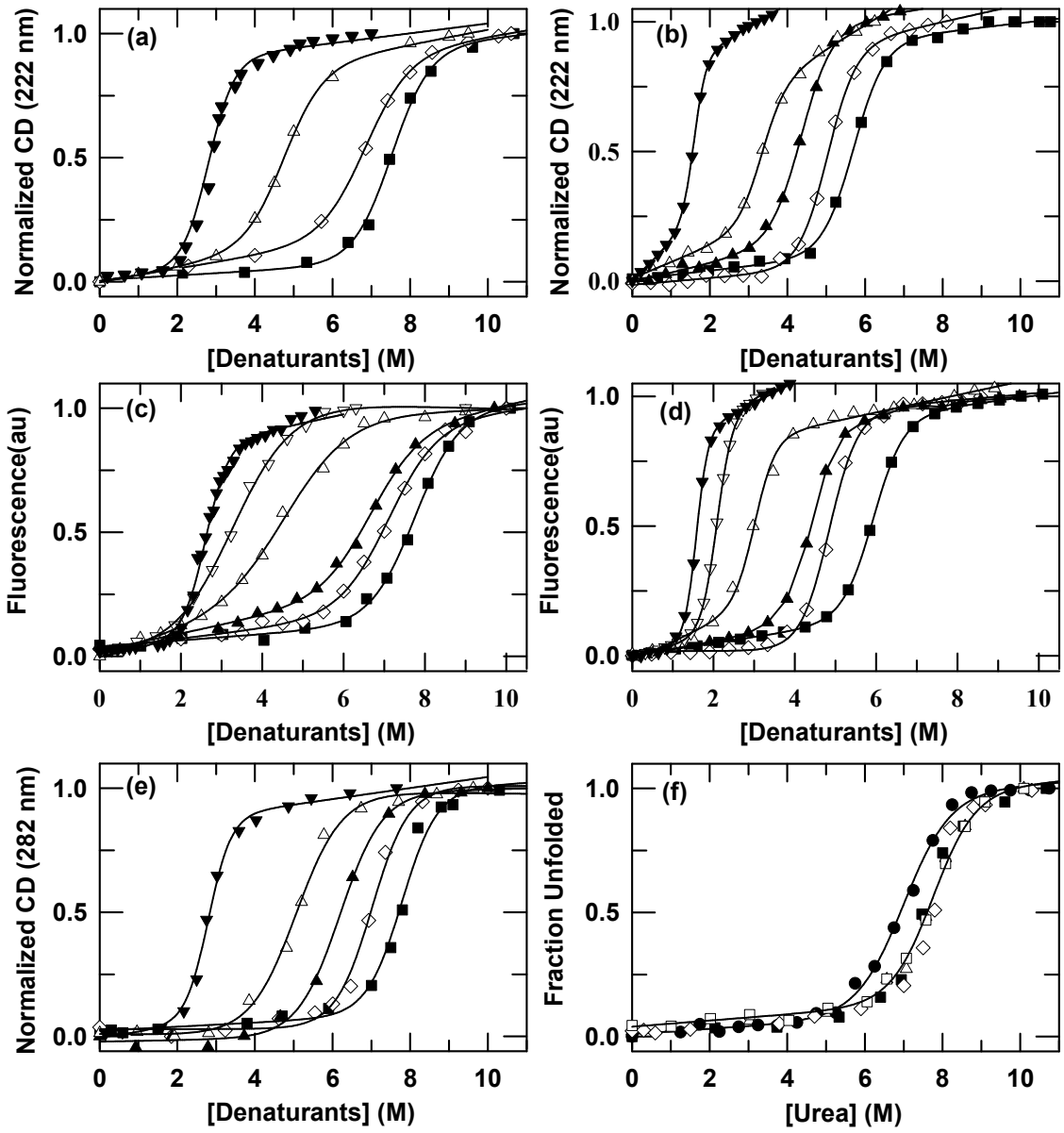

Fig. 3.9 (a) Denaturants dependence of the far-UV CD at 222 nm (urea (■), MU (◊), EU (Δ), and GdnHCl (▼)) for Ferricyt *c*. (b) Represent the denaturants dependence of the far-UV CD at 222 nm (urea (■), MU (◊), DMU (▲), EU (Δ), and GdnHCl (▼)) for Mb. (c) Shows the denaturants dependence of the fluorescence (ex: 280 nm, em: 358 nm) (urea (■), MU (◊), DMU (▲), EU (Δ), TMU (∇), and GdnHCl (▼)) for Ferricyt *c*. (d) Shows the denaturants dependence of the fluorescence (ex: 280 nm, em: 358 nm) (urea (■), MU (◊), DMU (▲), EU (Δ), TMU (∇), and GdnHCl (▼)) for Mb. (e) Represent the denaturants dependence of the near-UV CD at 282 nm (urea (■), MU (◊), DMU (▲), EU (Δ), and GdnHCl (▼)) for Ferricyt *c*. (f) Represents fraction of Ferricyt *c* unfolded as function of urea (pH 6.0 (±0.5), 25 °C) probed by CD signals at 222 nm (■), 282 nm (◊), heme absorbance at 399 nm (Δ) and 695 nm (•), and fluorescence at 358 nm (□). All transitions in panels (a), (c), (e) and (f) were measured at 25 °C, 0.1 M phosphate, pH 6.0 (±0.5). All transitions in panels (b) and (d) were measured at 25 °C, 0.1 M phosphate, pH 7.0 (±0.1), 25 °C. The solid lines in panels (a) to (f), represent the iterated least-squares fit of the data to a two-state unfolding transition (equation (1), chapter 2). The fitted parameters are summarized in Tables 5 and 6 for Ferricyt *c* and Mb, respectively.

The effectiveness of the urea and three alkylureas (MU, DMU, and EU) was investigated for disruption in helical secondary structure and tertiary structure of Ferricyt *c* and secondary structure of Mb as a function of increasing hydrocarbon chain size and branching. For Ferricyt *c*, this is shown in Figs. 3.8a and 3.8e where almost 7.5 M of urea is required to disrupt one half of the secondary structure as well as tertiary structure while the corresponding figures are only 7.0 M for MU, 6.0 M for DMU, and 5.0 M for EU (Table 7). For Mb, this is shown in Fig. 3.9b where almost 5.7 M of urea is required to disrupt one half of the secondary structure while the corresponding figures are only 5.0 M for MU, 4.4 M for DMU, and 3.3 M for EU (Table 8). Fig. 3.9f compares the urea-induced normalized equilibrium unfolding transitions of Ferricyt *c* probed by employing the far-UV CD at 222 nm, near-UV CD at 282 nm, fluorescence emission at 358 nm, and heme absorption at 399 nm and 695 nm. This comparison shows that the transitions measured by far-UV CD at 222 nm, near-UV CD at 282 nm, fluorescence emission at 358 nm, and heme absorbance at 399 nm are, within error, nearly superimposable but they are non-coincidence with the transition measured by heme absorbance at 695 nm (Fig. 3.9f).

3.2.4 Thermal denaturation of Ferrocyt c and Mb in the presence of denaturants

The Soret, α, and β peaks are the main characteristics of the Ferrocyt *c* absorption spectrum. The maxima of the Soret, α, and β bands are ~416, 550, and 520.5 nm, respectively at 293 K , pH 7.0 [31-32]. These values correspond to native HIS18/MET80 axial coordination of the heme [31-32]. A recent thermal unfolding study of Ferrocyt *c* (pH 7) have shown that when the temperature is increased from 20 to 100 °C, the intensities of the Soret (416 nm) and α (550 nm) bands decrease significantly, indicating that the protein is substantially denatured [15]. For Mb the absorbance maxima at 409 nm decreases at higher temperature suggests temperature induced protein denaturation [10]. Recently, pioneering works by Schweitzer-Stenner group have revealed accumulation of intermediates during the thermal unfolding of Ferricyt *c* [33-34]. In search of intermediates for thermal unfolding of Ferrocyt *c*, the thermal unfolding transition for Ferrocyt *c* was probed by employing the far-UV CD (222 nm) (Fig. 3.10a) and heme absorption (416 nm (Fig. 3.10b) and 550 nm (Fig. 3.10c)) are, within error, nearly superimposable and cooperative (Fig. 3.10d). The observation of indistinct thermal unfolding transition curves fails

the basic test for accumulation of intermediates to a detectable level for the thermal unfolding of Ferrocyt *c*. Thermal unfolding of Ferrocyt *c*/Mb in the presence of different concentrations of urea, GdnHCl, MU,EU, DMU, and TMU should be verifiable by far-UV CD (222 nm) as well. However, in the presence of alkylureas at high temperatures, the far-UV CD spectra show very large noise signal due to an elevation of the HT voltage; especially, peptide signals are increasingly obscured with the alkylureas content.

Figs. 3.11a and 3.11b show that the intensities of the α (550 nm) and Soret (416 nm) bands recorded at 320 K in the presence of 6.0 M MU (pH 7.0) were decreased significantly when the temperature was increased up to 380 K. This allows us to evaluate the effect of urea, alkylureas, and GdnHCl on the thermal unfolding of Ferrocyt *c*. Previous reports revealed the temperature dependence shifts in the Soret bands of heme proteins with increasing temperature [32,35-37]. However, at low denaturant concentrations [0.0-4.0 M GdnHCl], the temperature-induced shift was not observed in α-band (550 nm) of Ferrocyt *c* [32]. Similarly, the temperature-induced shift was not observed in α-band (550 nm) of Ferrocyt *c* (Fig. 3.11b) but was observed in the Soret band (416 nm) of Ferrocyt *c* (Fig. 3.11a). So the linear behavior depicted in Fig. 3.10c is not due to temperature-induced blueshift. Figs. 3.10c and 3.10d show the thermal denaturation curves for Ferrocyt *c* monitored at λ = 550 nm and 416 nm taken in different MU concentrations. For comparison these denaturation curves were normalized and expressed as a fraction unfolded in Figs. 3.10e and 3.10f for λ = 550 nm and 416 nm, respectively. Fig. 3.12a shows that the intensity of 409 band of Mb recorded at 298.15 K in the absence of denaturant (pH 7.0) was decreased significantly when the temperature was increased up to 373.15 K. This allows us to evaluate the effect of urea and alkylureas on the thermal unfolding of Mb. Fig. 3.12b presents the thermal denaturation curves for Mb monitored at λ = 409 nm under different concentrations of TMU. For comparison these denaturation curves were normalized and expressed as a fraction unfolded in Fig. 3.11c.

To determine the denaturants dependency of denaturation enthalpy change (ΔH_m) and thermal denaturation midpoint T_m, the thermal denaturation data were analyzed by using two-state van′t Hoff equation (equation (2), chapter 2) [38]. The resulting, T_m and ΔH_m for unfolding of Ferrocyt *c* and Mb under various denaturant concentrations are summarized in Tables 9 and 10, respectively. Thermodynamic stability, expressed in terms of free energy of denaturation, ΔG_T at 25 °C for various denaturant concentrations was calculated from equation (4) (chapter 2)

using a constant value of heat capacity, ΔC_P ~1.34 kcal mol^{-1} K^{-1} and ~2.20 kcal mol^{-1} K^{-1} for Ferrocyt *c* and Mb, respectively [32]. The resulting ΔG_T for unfolding of Ferrocyt *c* and Mb under va rious denaturant concentrations are provided in Tables 9 and 10, respectively.

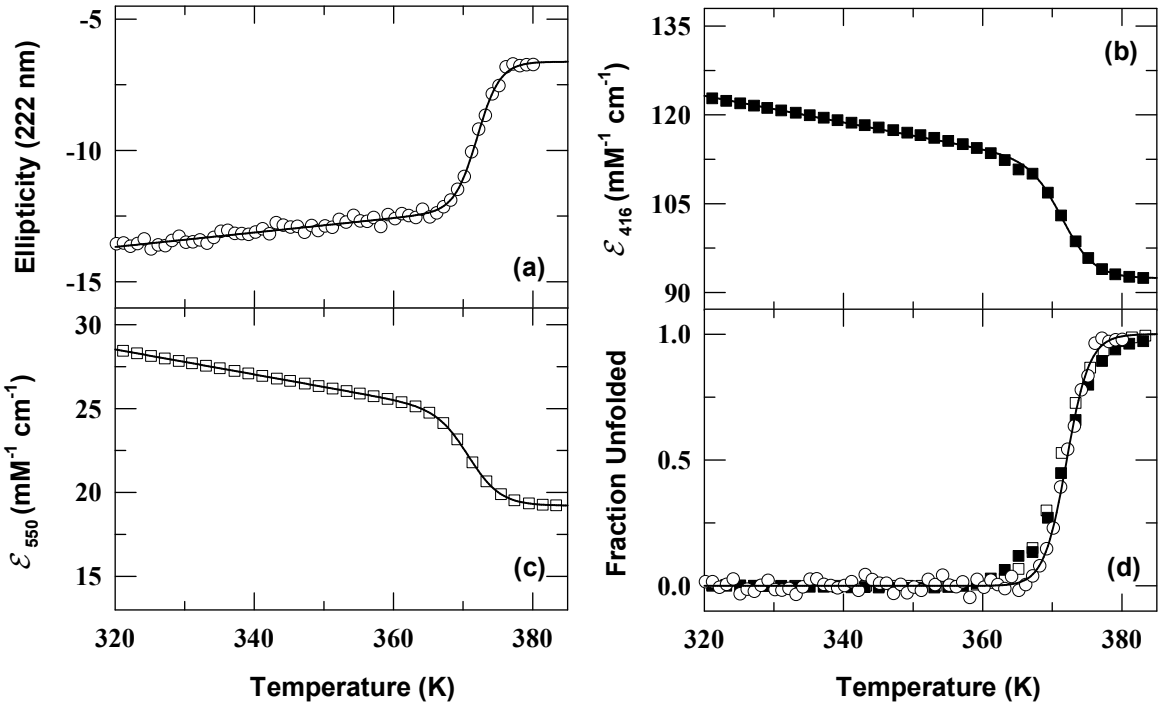

Fig. 3.10 (a) Represents the thermal unfolding transition of Ferrocyt *c* monitored by far-UV CD at 222 nm. Panels (b) and (c) present the thermal unfolding transition of Ferrocyt *c* monitored by heme absorption at 416 nm and 550 nm, respectively. (d) Presents the thermal unfolding transitions measured by different optical probes, presented as a fraction of unfolded protein (CD signal at 222 nm (o) and heme absorptions at 416 nm (■) and 550 nm (□)). All transitions in panels (a), (b), and (c) were measured in the absence of denaturant at pH 7.0. The solid curves in panels (a), (b), and (c) represent nonlinear least-squares fits to equation (2) (chapter 2).

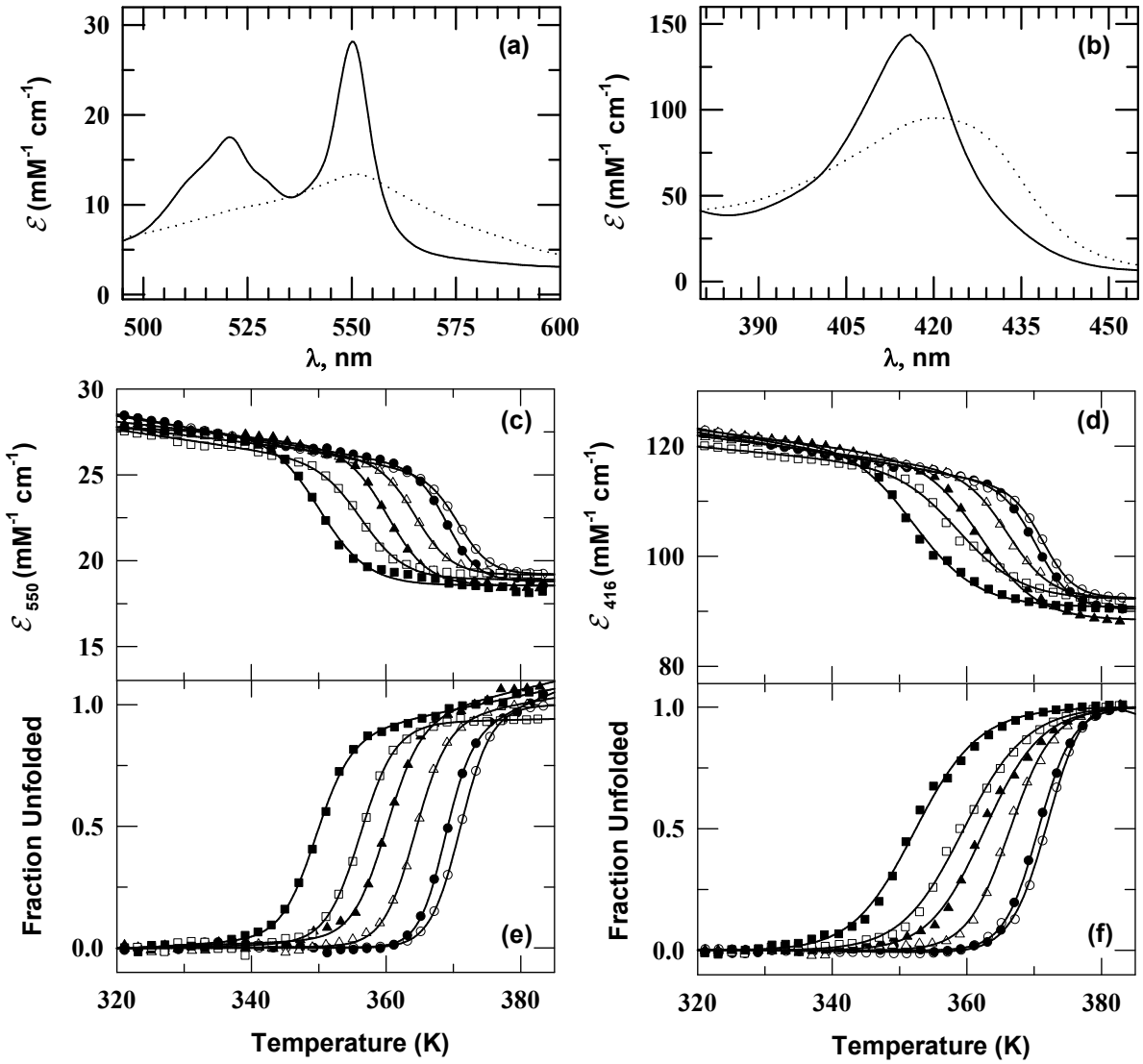

Fig. 3.11 Panels (a) and (b) represent the absorption spectra of Ferrocyt *c* at 320 K (solid line) and 380 K (dotted line) recorded in the presence of 6.0 M MU (pH 7.0). Panels (c) and (d) show thermally induced unfolding of Ferrocyt *c* monitored at 550 nm (panel (c)) and 416 nm (panel (d)) as the change in excitation coefficient in the presence of 0.0 (o), 1.29 (•), 3.06 (Δ), 4.72 (▲), 6.75 (□) and 10.8 (■) molal solution of MU. The solid curves in panels (c) and (d) represent nonlinear least-squares fits to equation (2) (chapter 2). To simplify the comparison of various thermal transitions, the extent of protein denaturation is presented as a fraction of unfolded protein (550 nm, panel (e); and 416 nm (panel (f)). The solid curves in panels (e) and (f) represent nonlinear least-squares fits to equation (2) (chapter 2).

Table 9 Denaturant (urea, MU, DMU, EU, TMU, GdnHCl) and sucrose dependence of thermodynamic parameters for thermal denaturation of Ferrocyt *c* as monitored by absorbance at 550 and 416 nm.

550 nm

urea (*m*)	T_m	ΔH_m	ΔG_T	MU (*m*)	T_m	ΔH_m	ΔG_T	DMU (*m*)	T_m	ΔH_m	ΔG_T
0.0	371.6	120	13.3	0.0	371.6	120	13.3	0.0	371.6	120	13.3
1.60	369.0	117	12.7	1.29	368.5	117	12.7	1.73	364.4	114	12.1
2.65	366.6	114	12.1	3.06	363.3	112	11.7	3.51	359.3	108	11.0
3.69	364.4	113	11.9	4.72	361.0	107	10.8	5.76	353.9	101	9.7
5.04	361.9	108	11.0	6.75	355.3	101	9.7	7.46	350.2	95	8.7
6.86	357.6	103	10.1								

550 nm

EU (*m*)	T_m	ΔH_m	ΔG_T	TMU (m)	T_m	ΔH_m	ΔG_T	GdnHCl (*m*)	T_m	ΔH_m	ΔG_T
0.0	371.6	120	13.3	0.0	371.6	120	13.3	0.0	371.6	120	13.3
1.33	365.5	114	12.1	2.18	351.8	108	10.7	0.3	367.4	103	10.1
3.71	355.8	102	9.9	3.28	342.7	100	8.9	0.6	364.4	96	8.8
5.56	350.6	95	8.7	4.60	336.1	90	7.2	1.0	360.4	86	7.2
6.46	348.2	92	8.2	5.25	331.2	80	5.7	1.5	355.4	75	5.5
								2.0	350.6	73	5.4
								2.8	342.9	65	4.4

550 nm

Sucrose (*m*)	T_m	ΔH_m	ΔG_T
0.0	371.6	120	13.3
0.7	374.3	128	14.9
1.3	376.8	136	16.5
2.0	382.0	145	18.5

416 nm

MU (*m*)	T_m	ΔH_m	ΔG_T	DMU (*m*)	T_m	ΔH_m	ΔG_T
0.0	372.0	117	12.7	0.0	372.0	117	12.7
1.29	368.6	113	11.9	1.73	363.2	113	11.9
3.06	364.2	108	11.0	3.51	359.3	108	11.0
4.72	360.0	100	9.6	5.76	355	90	8.0
6.75	356.2	96	8.9	7.46	352	75	5.6

416 nm

EU (*m*)	T_m	ΔH_m	ΔG_T	TMU (*m*)	T_m	ΔH_m	ΔG_T
0.0	372.0	117	12.7	0.0	372.0	117	12.7
1.33	366.8	100	9.5	2.18	354.4	109	11.0
3.71	357.8	85	7.1	3.28	345.0	105	9.8
5.56	352.5	75	5.6	4.60	338.0	99	8.4
6.46	350.2	70	4.9	5.25	333.0	96	7.5

*ΔH_m and ΔG_T (25 °C) are reported as kcal mol^{-1}. The uncertainties of ΔH_m and ΔG_T (25 °C) values reported here are ±5 and ±1.0 kcal mol^{-1}, respectively. T_m is reported in *K*. The uncertainty of T_m values reported here is ±0.5 °C.

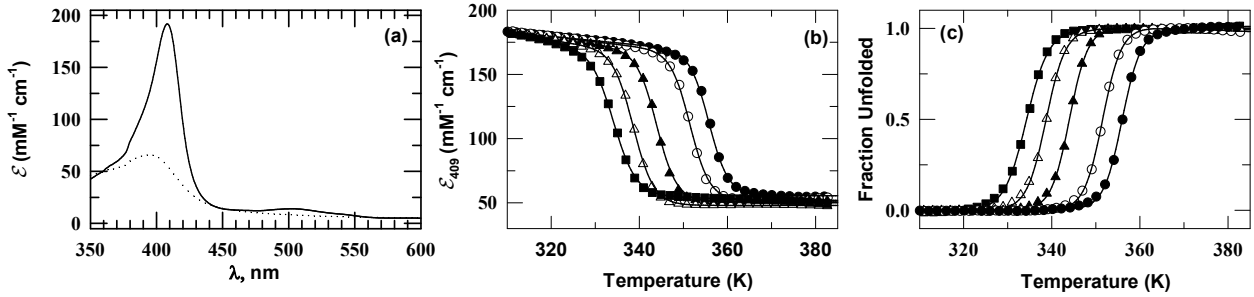

Fig. 3.12 Panel (a) represents the absorption spectra of Mb at 298.15 K (solid line) and 373.15 K (dotted line) recorded in the absence of denaturant (0.1 M phosphate buffer, pH 7.0). Panel (b) shows thermally induced unfolding of Mb monitored at 409 nm as the change in excitation coefficient in the presence of 0.0 (●), 0.25 (○), 0.53 (▲), 0.82 (Δ), 1.13 (■) molal solution of TMU. To simplify the comparison of various thermal transitions, the extent of protein denaturation is presented as a fraction of unfolded protein (panel (c). The solid curves in panels (b) and (c) represent nonlinear least-squares fits to equation (2) (chapter 2).

Table 10 Denaturant (urea, MU, DMU, EU, TMU, GdnHCl) and sucrose dependence of thermodynamic parameters for thermal denaturation of Mb as monitored by absorbance at 409 nm.

urea (*m*)	T_m	ΔH_m	ΔG_T	MU (*m*)	T_m	ΔH_m	ΔG_T	DMU (*m*)	T_m	ΔH_m	ΔG_T
0.00	355.9	115	7.8	0.00	355.9	115	7.8	0.00	355.9	115	7.8
0.95	351.4	106	6.8	0.51	350.9	106	6.8	0.45	351.4	106	6.7
2.01	347.1	94	5.3	1.08	347.1	93	5.2	0.96	347.7	92	4.9
3.21	342.2	83	4.3	1.68	342.7	86	4.6	1.09	345.3	90	4.8
4.58	337.1	75	3.6	2.34	338.5	74	3.3	1.49	341.2	81	4.9
				3.06	333.4	66	2.7	2.08	336.0	66	2.5
								2.73	330.4	56	1.9
EU (*m*)	T_m	ΔH_m	ΔG_T	TMU (m)	T_m	ΔH_m	ΔG_T	Gdn HCl (*m*)	T_m	ΔH_m	ΔG_T
0.00	355.9	115	7.8	0.00	355.9	115	7.8	0.00	355.9	115	7.8
0.66	346.6	95	5.5	0.25	351.6	106	6.8	0.10	353.8	112	7.5
1.40	338.3	70	2.9	0.53	344.0	87	4.6	0.25	350.2	102	6.2
2.24	329.3	50	1.5	0.82	338.7	77	3.7	0.52	344.9	89	4.8
				1.13	334.2	66	2.8	0.80	340.7	78	3.7
								1.10	336.0	69	2.9
Sucrose (*m*)	T_m	ΔH_m	ΔG_T								
0.00	355.9	115	7.8								
1.00	358.6	117	7.9								
3.08	360.4	121	8.2								

*ΔH_m and ΔG_T (25 °C) are reported as kcal mol^{-1}. The uncertainties of ΔH_m and ΔG_T (25 °C) values reported here are ±5 and ±1.0 kcal mol^{-1}, respectively. T_m is reported in *K*. The uncertainty of T_m values reported here is ±0.5 °C.

3.2.5 Denaturant dependence of the thermal denaturation midpoint (T_m), enthalpy of denaturation (ΔH_m), and free energy of denaturation (ΔG_T)

Fig. 3.13 shows the effects of various denaturants on the T_m, ΔH_m and ΔG_T for Ferrocyt *c* and Mb, respectively. The T_m, ΔH_m, and ΔG_T decrease linearly with increasing concentration of denaturants and the number of hydrophobic groups substituted on urea molecule (Tables 9 and 10). Among the denaturants used in this study, the decrease in T_m is most pronounced for GdnHCl (Fig. 3.13a), which suggests that the GdnHCl is a most effective denaturant. When the number of the carbon is fixed in the alkylureas, the decrease in T_m, ΔH_m, and ΔG_T are most pronounced for the normal alkylurea than the branched one (Fig. 3.13). The order of effectiveness towards the decrease in T_m, ΔH_m, and ΔG_T is similar as reported in the literature for other proteins (urea < MU < DMU < EU < TMU) [39-43].

3.2.6 Analysis of thermal unfolding of Ferrocyt c and Mb in denaturants and sugar solutions with varied water activity

The reciprocal form of Wyman-Tanford (WT) equation (equation (3)) can be applied to determine the change in the hydration number per protein molecule (Δi) upon unfolding of Ferrocyt *c* and Mb in different denaturants and sugar solutions [8,15,44],

$$dlnK_{D,S}/dlna_W = \left[\Delta i - \left(X_W/X_Y\right)\Delta j\right] \quad (3)$$

where $K_{D,S}$ (=[D]/[N]), a_W is water activity, $(X_w/X_Y)\Delta j$ is the cosolute-binding terms, X_w and X_Y are the mole fractions of water and cosolute, respectively, and Δj is the change in bound-cosolute molecules per protein molecule. Figs. 3.13a and 3.13b present the $lnK_{D,S}$ *vs* lna_W plots for unfolding of Ferrocyt *c* and Mb, respectively under different concentrations of denaturants and sugar. For each denaturant, the slope of reciprocal WT plot (Δi- $(X_w/X_Y)\Delta j$) was derived from linear least square fitting of data in Figs. 3.13a and 3.13b to equation (3) for Ferrocyt *c* and Mb, respectively. The slope was dependent upon the type of denaturant and sugar (Tables 11 and 12). The positive and negative slopes were obtained for sucrose and denaturants (urea, MU, DMU, EU, and GdnHCl), respectively. For sucrose, the term $(X_W/X_Y)\Delta j$ in equation (3) is negligible [7-9], which provides the value of Δi = 68.8 mol/mol-protein and 32.1 mol/mol-protein for Ferrocyt *c* and Mb, respectively. From these Δi values, the binding term, $(X_W/X_Y)\Delta j$ for each denaturant was calculated from the slope in Figs. 3.13a and 3.13b for Ferrocyt *c* and Mb, respectively.

When the concentration of the cosolute is fixed, the term Δj can be easily determined from the solute binding term, $(X_W/X_Y)\Delta j$ (Tables 13 and 14). As compared to urea, MU, and DMU, the Δj value is found more for EU (2.83 for Ferrocyt *c* and 4.8 for Mb). However, among urea, MU, DMU, EU, and GdnHCl, the Δj value is found highest for GdnHCl (4.26 for Ferrocyt *c* and 6.7 for Mb), indicating that as compared to urea and alkylureas molecules, the GdnHCl molecules bind more strongly to proteins upon their unfolding.

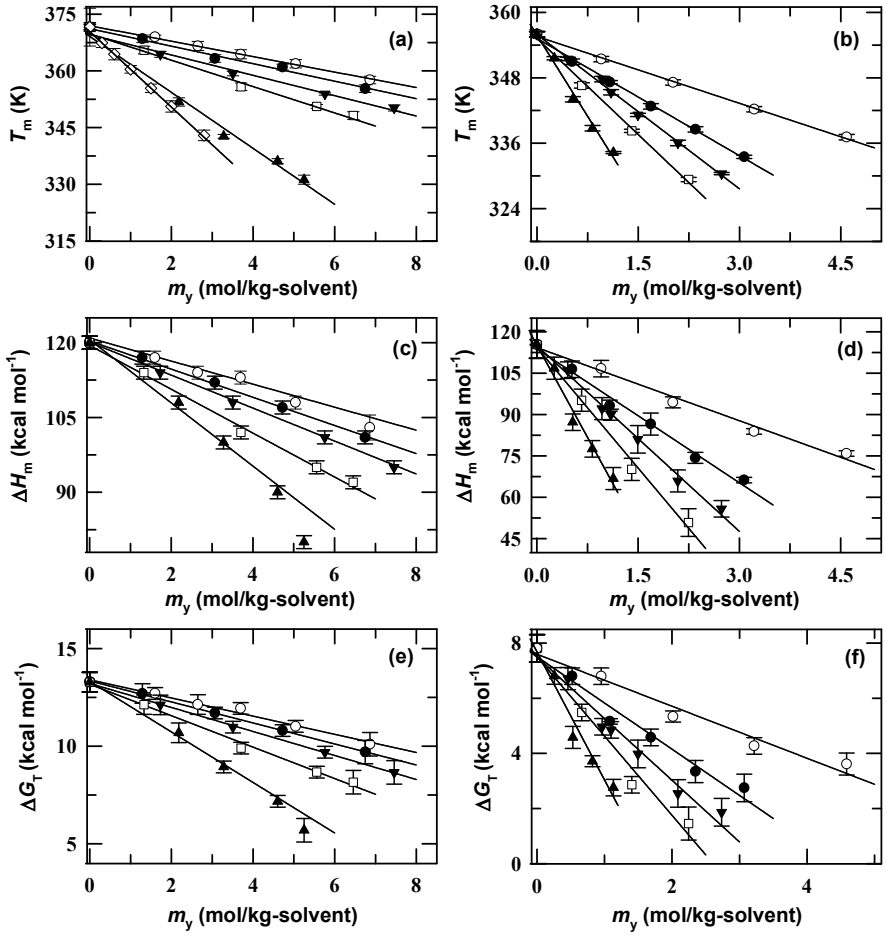

Fig. 3.13 (a) Effect of denaturants concentration (urea (○), MU (●), DMU (▼), EU (□), TMU (▲) and GdnHCl (◊)) on melting temperature (T_m) (550 nm) of Ferrocyt *c* at pH 7. (b) Effect of denaturants concentration (urea (○), MU (●), DMU (▼), EU (□), TMU and (▲) on melting temperature (T_m) (409 nm) of Mb at pH 7. (c) Denaturants (urea (○), MU (●), DMU (▼) EU (□) and TMU (▲)) dependence of enthalpy change, ΔH_m for Ferrocyt *c* at pH 7 (550 nm). (d) Denaturants (urea (○), MU (●), DMU (▼) EU (□) and TMU (▲)) dependence of enthalpy change, ΔH_m for Mb at pH 7 (409 nm). (e) Denaturants (urea (○), MU (●), DMU (▼), EU (□) and TMU (▲)) dependence of denaturation free energy change (ΔG_T) for Ferrocyt *c* at pH 7 (550 nm). (f) Denaturants (urea (○), MU (●), DMU (▼), EU (□) and TMU (▲)) dependence of denaturation free energy change (ΔG_T) for Mb at pH 7 (409 nm). In panels (a) to (f) the solid curves represent linear least-squares fitting.

Table 11 Slope of the reciprocal Wyman-Tanford plot for Ferrocyt *c* (equation (3)).

Cosolute	Urea	MU	DMU	EU
	-50.0	-56.5	-72.9	-91.3
Cosolute	GdnHCl	Sucrose		
	-171.2	68.8		

Table 12 Slope of the reciprocal Wyman-Tanford plot for Mb (equation (3)).

Cosolute	Urea	MU	DMU	EU
	-70.7	-128.7	-176.7	-235.2
Cosolute	GdnHCl	Sucrose		
	-337.3	32.1		

Table 13 Number of change in bound-cosolute molecules upon protein unfolding, Δj, at cosulute concentration of 1 mol/kg-solvent for Ferrocyt *c*.

Cosolute	Urea	MU	DMU	EU
	2.1	2.2	2.5	2.83
Cosolute	GdnHCl	Sucrose		
	4.26	0.00		

Table 14 Number of change in bound-cosolute molecules upon protein unfolding, Δj, at cosulute concentration of 1 mol/kg-solvent for Mb.

Cosolute	Urea	MU	DMU	EU
	1.9	2.9	3.8	4.8
Cosolute	GdnHCl	Sucrose		
	6.7	0.0		

3.2.7 Thermodynamic analysis for protein conformational stability in the presence of denaturants

The linear extrapolation model (LEM) (equation (6)) [45-53] does not theoretically provide the direct effect of [cosolute] on $\Delta\Delta G$,

$$\Delta\Delta G = m[m_Y] \quad (4)$$

where $\Delta\Delta G$ is the free energies difference for protein unfolding in denaturant solution and water, m_Y is the concentration of cosolute (mol/kg-solvent), and m is an empirical parameter. The m-value is negative for chaotropic cosolvents (*i.e.* denaturants) while it is positive for kosmotropic cosolvents (*i.e.,* sugars). To determine the exact effect of [cosolute] on $\Delta\Delta G$, equation (4) can be applied for analyzing the value of Δi for protein unfolding in sugar and denaturant solutions [9,15,54],

$$\Delta lnK_D - \Delta lnK_{D,0} = \left[\Delta i - \left(X_W/X_Y\right)\Delta j\right] lna_W \quad (5)$$

By relating the $\Delta\Delta G$ to $[\Delta i\text{-}(X_w/X_Y)\Delta j]$ and $\ln a_W$, one can obtain the possible role of water activity in protein stability [9,51],

$$\Delta\Delta G = -RT\left(\Delta lnK_D - \Delta lnK_{D,0}\right) = -RT\left[\Delta i - \left(X_W/X_Y\right)\Delta j\right] lna_W \quad (6)$$

Since $\ln a_W$ is zero or negative ($a_W \leq 1$), so the term Δi should always stabilize the protein (equation (6)). In contrast, the term, $(X_W/X_Y)\Delta j$, always destabilize the proteins unless Δj is negative [55-56]. Equation (5) also provides a theoretical basis for the LEM model. From equation (6), the $\Delta\Delta G$ was obtained as a function of [cosolute]. Figs. 3.13c and 3.13d show the plots of $\Delta\Delta G$ against [cosolutes] (m_Y (mol/kg-solvent)) for Ferrocyt *c* and Mb, respectively. $\Delta\Delta G$ was found to depend linearly on [cosolutes]. This indicates the applicability of LEM model. For each denaturant and sucrose, the slope (*m*-value) was calculated from the $\Delta\Delta$G *vs* m_Y plots (Figs. 3.13c and 3.13d). The *m*-values for urea, MU, DMU, EU, GdnHCl, and sucrose were summarized in Tables 15 and 16. Tables 15 and 16 clearly indicate that the *m*-value depends on the type of denaturant used.

Table 15 *m*-value of denaturants and sucrose for Ferrocyt *c* unfolding (equation (6)).

Cosolute	Urea	MU	DMU	EU
	-0.53	-0.59	-0.71	-0.90
Cosolute	GdnHCl	Sucrose		
	-3.1	1.1		

The m-value is reported as kcal $mol^{-1}m^{-1}$. The uncertainties of *m*-value reported here is ± 0.2 kcal $mol^{-1}m^{-1}$.

Table 16 *m*-value of denaturants and sucrose for Mb unfolding (equation (6)).

Cosolute	Urea	MU	DMU	EU
	-0.92	-1.45	-1.85	-2.54
Cosolute	GdnHCl	sucrose		
	-7.50	0.24		

The m-value is reported as kcal $mol^{-1}m^{-1}$. The uncertainties of *m*-value reported here is ± 0.2 kcal $mol^{-1}m^{-1}$.

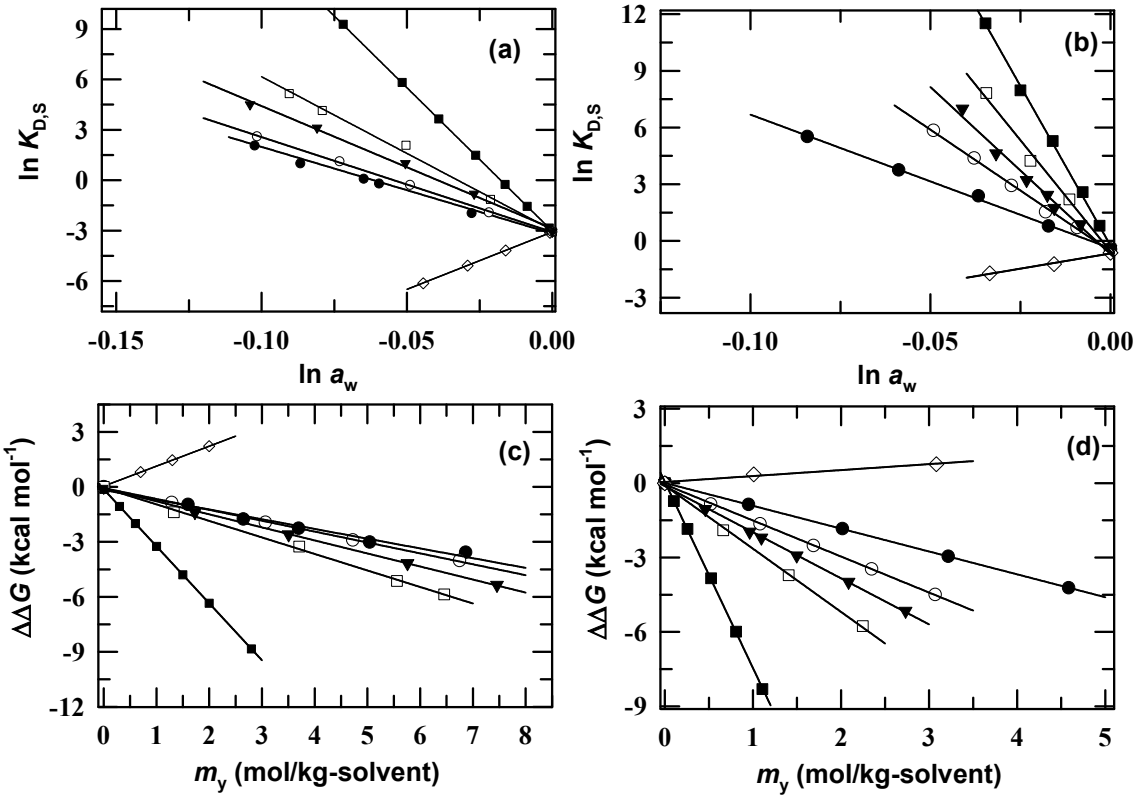

Fig. 3.14 (a) Reciprocal form of Wyman–Tanford plot: Effect of water activity on unfolding ratio of Ferocity *c* in aqueous solution of denaturants (urea (•), MU (○), DMU (▼), EU (□) and GdnHCl (■)), and sugar (sucrose (◊)) at pH 7.0, 363.15 K. (b) Reciprocal form of Wyman–Tanford plot: Effect of water activity on unfolding ratio of Mb in aqueous solution of denaturants (urea (•), MU (○), DMU (▼), EU (□) and GdnHCl (■)), and sugar (sucrose (◊)) at pH 7.0, 355.00 K. (c) $\Delta\Delta G$ is plotted as a function of cosolute concentration (m_y) (urea (•), MU (○), DMU (▲), EU (□), GdnHCl (◊) and sucrose (■)) for thermal unfolding of Ferrocyt *c* at pH 7.0. (d) $\Delta\Delta G$ is plotted as a function of cosolute concentration (m_y) (urea (•), MU (○), DMU (▲), EU (□), GdnHCl (■) and sucrose (◊)) for thermal unfolding of Mb at pH 7.0. The solid curves in Panels (a) to (d) represent linear least-squares fitting.

3.3 Discussion

The internal motions of the heme protein vary in response to the solvent conditions. The M80-contaning Ω-loop of cyt *c* comprises the residues 70 to 85 (Fig. 3.6a) [57]. This Ω-loop was recognized as a partially unfolded subglobal part of the protein [58-59]. The collective motions of this loop are the main determinant of the CO-association (Fe^{2+}-M80 + CO → Fe^{2+}-CO + M80) and dissociation (Fe^{2+}-CO + M80 → Fe^{2+}-M80 + CO) processes [1,23,60-61]. Furthermore, the denaturant modulation of CO-association rate reveals how collective motions of this Ω-loop vary in response to the denaturants in the reaction medium [1]. The rationale for studying CO-replacement experiments of carbonmonoxymyoglobin (MbCO) as a function of denaturant is

based on the fact that entry and exit of ligands to and from the protein and the reaction rate parameters characterizing the binding of the ligand to the heme iron are all governed by Mb motions [62-64]. Previous reports revealed that the barrier for binding of CO and O_2 to Mb are dynamic in nature and involves large structural motions [63-64]. The denaturant-protein interactions control internal motions of MbCO which are responsible for the CO-replacement from it. The kinetic and thermodynamic studies of Ferrocyt *c* in the presence of various denaturants (urea, MU, DMU, EU, TMU, and GdnHCl) have provided significant evidence for internal motional constraints and entropy reduction of the Ω-loop of Ferrocyt *c* in the subdenaturing region of these denaturant. However, such kind of internal motional constraints on MbCO are not observed under subdenaturing concentration of denaturant. The probable explanations for the constrained dynamics of the Ω-loop of Ferrocyt *c* in the presence of subdenaturing concentrations of denaturants and increased Log k_{off} in the presence of denaturants are also discussed. The thermodynamic stability of Ferrocyt *c* and Mb decreases with increasing the denaturant concentration in the reaction medium. The role of water activity on protein stabilization is discussed.

3.3.1 Motional constraints and entropy reduction due to denaturant binding

Isothermal calorimetry [65] and x-ray crystallography [66-68] studies have provided evidence for direct interactions between protein groups and urea or guanidinium ion. At lower concentrations, guanidinium ion or urea molecule can interact with protein molecule through multiple hydrogen bonds and van der Waals interactions [66-68]. Docking results between the Cyt *c* and urea also reveal that about seven urea molecules form multiple variable length hydrogen bonds with the backbone-backbone or backbone-side chain atoms of the Ω-loop of Cyt *c* (Fig. 3.6b). Such denaturant-mediated nonspecific polyfunctional interactions may reduce the motional freedom and internal motions of the native proteins [1,66-67]. These additional interactions may also reduce the number of conformations accessible to the unfolded state and thus decrease the configurational entropy of local unfolding [69]. The superior stability of reduced Cyt *c* over oxidized Cyt *c* was explained on the basis of entropy reduction [22-23 ,70-71]. However, as compared to Cyt *c* the lesser denaturant molecules are involved in polyfunctional cross-linking interactions with MbCO (Tables 5 and 6). In the subdenaturing limit

of denaturants, these weaker polyfunctional interactions between the denaturant and different groups of the MbCO are not enough for the motional constraints on MbCO (Fig. 3.1f).

3.3.2 Kinetic and thermodynamic consequences of protein-denaturant interactions

For the CO-association reaction, the intramolecular thermal collisions between the reactant molecules provide the energy for barrier crossing [1]. Due to some form of denaturant-protein interactions, there must be a reduction in the amplitude of thermal fluctuations [1-2]. The restricted thermal fluctuations then lower the rates of the CO-association reaction by increasing the activation energy barrier (Table 3). The decrease in the crystallographic B-factor conformations of the several proteins crystals soaked in low concentrations of denaturant solutions [66-67] could be due to reduction in amplitude of thermal fluctuations [103] As previously described [10,12], both local entropy and atomic fluctuations have the same physical origin, therefore, the restricted dynamics in the subdenaturing limit of denaturants must alter the entropy reduction of the protein. For Mb, within the subdenaturing limit, such denaturant-mediated constrained dynamics is not observed and a continuous increase in the rate of CO-replacement reactions occurs as the denaturant concentration is increased in the reaction medium (Fig. 3.1f).

The CO-association reaction of Ferocity *c* has been designed to underline the changes in activation enthalpy and entropy reduction of proteins in the presence of denaturants (urea, MU, DMU, EU, TMU, and GdnHCl). The data in Table 3 clearly shows that in the presence of subdenaturing concentrations of denaturants, both activation enthalpy and entropy reduction increases, which supports the reduced motional freedom of Cyt *c* in the presence of subdenaturing concentrations of denaturant relative to that in the absence of denaturant. The sizeable decrease in amplitudes of thermal motions in the subdenturing limit of denaturants must also reduce the magnitude of subglobal unfolding motions and entropy reduction of the system [1]. In the presence of subdenaturing concentration of denaturants, the increase in activation enthalpy suggests the increase in barrier height between the native-state and transition state for the CO-association (Fe^{2+}-M80+CO→Fe^{2+}-CO + M80) process. It is more likely that the numbers of denaturants molecules that interact with the protein in the subdenaturing limit are insufficient to cross-link a large part of the molecule. This suggests that the observed restricted dynamics is localized to a subglobal part of the protein and the dynamics of which affect the CO-association

reactions. The extent of entropy reduction of Ferrocyt *c* for GdnHCl is found slightly higher as compared to that by urea (Table 3). Furthermore, the extent of entropy reduction of Ferrocyt *c* for urea is also found to decrease with increasing the number of hydrophobic groups substituted on urea molecule (Table 3).

3.3.3 How could the increase in hydrophobic groups on urea molecule decrease the extent of denaturant-mediated constrained dynamics of Ω-loop of Ferrocyt c?

An earlier study with Ferrocyt *c* has shown that the subdenaturing concentrations of urea constrain the internal dynamics of the Ω-loop of Ferrocyt *c* [2]. The present study shows that the subdenaturing concentrations of alkylureas (MU, DMU, EU, and TMU) also constrain the internal dynamics of the Ω-loop (Fig. 3.1e). It is also observed that with increase in the number of hydrophobic groups on urea molecule, the extent of denaturant-mediated constrain in the internal dynamics of Ω-loop of Ferrocyt *c* decrease (Fig. 3.1e). How could the increase in hydrophobic groups on urea molecule decrease the extent of denaturant-mediated constrained dynamics of Ω-loop of Ferrocyt *c*? The fact that, alkyl substituted urea molecule has lower ability to form hydrogen bonds, therefore, they may not produce as extensive cross-linking as the urea does. Makhatadze et al have calculated the total number of binding sites for urea in the folded and unfolded state of Cyt *c* [65]. From the obtained number of native state binding sites, one can approximately estimate that about 26 urea molecules interact to the protein in the presence of 5.0 M urea. If one urea molecule interacts with about two to three amino acid residues, assuming at least two hydrogen bonds per urea molecule [65-67], then in the presence of 5.0 M urea, approximately 52 residues of protein would experience restricted dynamics.

Docking results between the Cyt *c* and urea, MU, DMU, EU, and TMU reveal that with increasing hydrophobic groups on urea molecule, polyfunctional interactions between the denaturant and different groups of Ω-loop and other part of the protein decrease (Fig. 3.6 and Table 5). This finding confirms that the decrease in the extent of denaturant-mediated restricted dynamics of Ω-loop with a corresponding increase of alkyl groups on urea molecule is due to the decrease of denaturant-mediated cross-linking interactions. It can be speculated that with increasing number of hydrophobic groups substituted on urea molecule, the less number of free N-H moieties in urea molecular framework are available to cross-link different groups of Ω-loop and protein. As a consequence, the denaturant-mediated cross-linking interactions decreases,

therefore, in the subdenaturing limit of alkyl substituted urea, the less number of residues would experience restricted dynamics. When all the N-H moieties in the urea molecule are methyl substituted, the denaturant-mediated constrain in the internal dynamics of Ferrocyt *c* is still noticeable (Fig. 3.1e). The current docking results reveal that the denaturant molecules also form variable length hydrogen bonds with the side chain or peptide bond (C=O or N-H group) of single amino acid (Figs. 3.5b, 3.5c, 3.5d and Table 5). Although, they do not crosslink with the different groups of the protein (Figs. 3.5b, 3.5c, 3.5d and Table 5) but their contributions toward the denaturant-mediated restricted dynamics of protein cannot be neglected since denaturant like TMU is not involved in cross linking with different groups of Ω-loop and protein (Fig. 3.6d and Table 5) but it restricts the internal dynamics of Ω-loop (Fig. 3.1e).

In the presence of subdenaturing concentration of denaturant (urea, MU, DMU, EU and GdnHCl, the denaturant-mediated polyfunctional cross-linking interactions between different groups of proteins are responsible for the "disorder-to-order" structural transition of the Ferrocyt *c,* relative to that in an aqueous solution. This "disorder-to-order" transition is responsible for the constrained internal dynamics of protein because of this the amplitudes of thermal fluctuations responsible for the CO-association reaction also be reduced. The solvent-slaving model of protein dynamics [73-75] has two components: first, global and larger-scale diffusive motions of the protein are linked to the bulk solvent and are viscosity-dependent also known as α-fluctuations, whereas internal dynamics the second component are coupled to motions in the hydration shell also known as β-fluctuations. β-fluctuations are essentially independent of the bulk solvent fluctuations [73-75]. These additional β-fluctuations are local protein motions that are essentially independent of the bulk solvent fluctuations and may be relevant at late stages of folding [73-75]. Since TMU does not involve in the polyfunctional cross-linking interactions between different groups of proteins but slows down the rate of CO-association to Ferrocyt *c*. This result warrants the role of solvent fluctuation on the protein internal dynamics. In the subdenaturing region in addition to polyfunctional cross-linking interactions between different groups of proteins, solvent fluctuations (solvent viscosity) exert its effect in controlling the internal dynamics of protein. However, at higher concentration denaturing action of denaturant controls the internal motions of Ω-loop of Ferrocyt *c* which eventually controls the CO-association process.

The current results thus reveal that subdenaturing concentrations of urea and alkylureas stabilize the Ferrocyt *c* conformation. These results are inconsistent with earlier hydrogen-deuterium exchange study of Ferrocyt *c* probed by real time NMR [76] and equilibrium NMR [59] methods. The results obtained from hydrogen-deuterium exchange study of Ferrocyt *c* revealed a gradual denaturation of protein by GdnHCl [59,76]. The folding models of Englander consider partial unfolded forms (PUFs) detectable under subdenaturing conditions [59,77-79]. The present results cannot directly be related to stabilization of PUFs, because urea and alkylurea-mediated cross-linking are not localized at certain parts of the protein. Because the denaturant molecules can interact with many functional groups including the backbone, the motional constraints are felt more or less globally. These results suggest that the hydrophobicity on urea molecule plays an important role in the internal motion of Ferrocyt *c*.

3.3.4 Why subdenaturing concentrations of denaturants not constraint the internal dynamics of MbCO?

The effect of subdenaturing concentrations of urea and alkylureas on the internal dynamics of the Mb has not been studied before. The present study showed that the denaturant mediated constrain is not observed on the internal dynamics of MbCO (Fig. 3.1f). Why subdenaturing concentrations of denaturants are unable to constrain the internal dynamics of MbCO? In comparison to Cyt *c*, docking results between the MbCO and urea, MU, DMU, EU, and TMU reveal that with increasing hydrophobic groups on urea molecule, polyfunctional interactions between the denaturant and different groups of the protein do not follow any trend (Table 6). However in each case the ratio of denaturant molecules that are involved or not in polyfunctional cross-linking interactions is small (Table 6). These weaker polyfunctional interactions between the denaturant and different groups of the MbCO are not enough for the motional constraints of MbCO (Fig. 3.1f). The present study also shows that the extent of denaturant-mediated structural fluctuations of MbCO increases with increase in the number of hydrophobic groups on urea molecule. This finding indicates that the hydrophobicity of denaturant molecule controls the internal dynamics of MbCO.

3.3.5 Denaturant-induced entropic and electrostatic contributions

Subdenaturing concentrations of both urea and GdnHCl stabilize [80-85] and constrain the internal dynamics of proteins [1,2,10,80-82,86]. How could subdenaturing concentrations of urea and GdnHCl stabilize and constrain the internal dynamics of proteins? The ionic denaturant, GdnHCl constrain the internal dynamics of the native and partially denatured states of proteins by both entropic effect due to intramolecular protein cross linking actions of guanidinium ions [1,2,10,81] and electrostatic effect due to the interactions of chloride and guanidinium ions with the charged groups of the proteins [1,2,28,80-85]. The electrostatic effect of denaturants stabilizes the proteins under conditions favorable for charge screening. On the other hand, the entropic effect of denaturant operates invariably and is expected to stabilize all proteins through lowering the entropy reduction of protein. The stabilization of Ferrocyt *c* by subdenaturing concentrations of non-ionic urea is purely entropic [2].

3.3.6 Effect of denaturants on the thermodynamic stability of Ferrocyt c and Mb

Thermodynamic stability (ΔG_T) of Ferrocyt *c* (Fig. 3.13e) and Mb (Fig. 3.13f) decrease with increasing the concentration of denaturant and the size of hydrophobic group substituted on the urea molecule. Poklar et al had also studied the thermal denaturation of α-chymotrypsinogen and RNAase A in aqueous mixture of urea, MU, EU, and DMU by DSC and observed that ΔG_T decrease with increasing concentration of denaturant and the size of hydrophobic group substituted on the urea molecule [41,87]. Several previous studies on urea, alkylureas, and GdnHCl denaturation of proteins have shown that over the full range of denaturant concentration, ΔG_T decreases linearly with denaturant concentration as [53,88-89],

$$\Delta G_T = \Delta G_T^\circ - m^* m_Y \qquad (7)$$

where ΔG_T° is the Gibbs free energy of denaturation in the absence of denaturant, and m^* is the rate of change of ΔG_T with concentration of cosolute (denaturant), m_Y (mol/kg-solvent). Although, the physical importance of the factor m^* is not clearly understood, but few previous studies suggested that it reflects the difference between the accessibility of surface areas of native and denatured states of the polypeptide chain for a given denaturant [90-93]. ΔG_T for Ferrocyt *c* (Fig. 3.13e) and Mb (Fig. 3.13f) varies linearly with denaturants concentrations. The parameters, m^* and ΔG_T° were derived from linear least-squares fitting of the data (ΔG_T vs m_Y) to equation (7). The values of m^* and ΔG_T° are summarized in Tables 17 and 18. The high m^*

value for EU suggests high effectiveness of this denaturants towards protein denaturation as compared to the other denaturants, urea, MU, and DMU.

Table 17 m^* and ΔG_T°-values of denaturants for Ferrocyt *c* unfolding (equation (7)).

Cosolute	Urea	MU	DMU	EU
Parameters				
ΔG_T°	14.5	14.3	14.2	13.8
m^*	-5.1	-5.8	-6.7	-8.5

m^* and ΔG_T° (25°C) are reported as kcal $mol^{-1}m^{-1}$ and kcal mol^{-1}, respectively. The uncertainties of m^* and ΔG_T° values reported here are ± 0.2 kcal $mol^{-1}m^{-1}$ and ± 0.5 kcal mol^{-1}, respectively.

Table 18 m^* and ΔG_T°-values of denaturants for Mb unfolding (equation (7)).

Cosolute	Urea	MU	DMU	EU
Parameters				
ΔG_T°	7.6	7.5	7.5	7.5
m^*	-1.0	-1.7	-2.2	-2.9

m^* and ΔG_T° (25°C) are reported as kcal $mol^{-1}m^{-1}$ and kcal mol^{-1}, respectively. The uncertainties of m^* and ΔG_T° values reported here are ± 0.2 kcal $mol^{-1}m^{-1}$ and ± 0.5 kcal mol^{-1}, respectively.

3.3.7 Urea and alkylurea-induced structural unfolding of Cyt c and Mb

There is a general interest in determining the mechanism by which denaturants disrupt the protein secondary and tertiary interactions. The efficiencies for the disruption of secondary and tertiary structures vary significantly depending on the type of denaturant used. For Ferricyt *c* and Mb, the order of effectiveness towards the disruption of secondary and tertiary structures typically follows as: EU > DMU > MU > urea (Figs. 3.8a, 3.8b and 3.8e). This finding suggests that with increasing the hydrophobicity of urea derivatives, the ability of denaturant towards the structural unfolding increases. Within the experimental errors, the disruption of secondary and tertiary structures of Ferricyt *c* occurs at same denaturant concentration, for example the disruption of secondary and tertiary structures of native Ferricyt *c* is almost over at 9.0 M urea (Figs. 3.8a and 3.8e). However, the urea unfolding transitions of Ferricyt *c* measured by the far-UV CD at 222 nm, near-UV CD at 282 nm, fluorescence emission at 358 nm, and heme absorption at 399 nm are non-coincidence with the urea unfolding transition measured by heme absorbance at 695 nm (Fig. 3.9f), which suggests the presence of an equilibrium intermediate in the N- to U-state transition of Ferricyt *c*. Recent thermodynamic studies on Ferricyt *c* have also

revealed the presence of intermediates in the N-to U-state thermal transition of Ferricyt *c* [33-34].

3.3.8 The role of water activity on protein stability

Equation (6) presents an important role of water activity in protein stability. $\Delta\Delta G$ was linearly dependent on urea, alkylureas (MU, DMU, and EU), and GdnHCl concentrations (Figs. 3.13c and 3.13d). The *m*-values for these denaturants for protein unfolding were determined from the slopes of $\Delta\Delta G$ *vs* m_y plots in Figs. 3.13c and 3.13d (Tables 15 and 16). The *m*-value is considered to be a reliable indicator of denaturant efficiency towards its unfolding action. From all of the denaturants used in this study, GdnHCl gave the highest negative *m*-value (Tables 15 and 16). The destabilizing power of GdnHCl, which is a typical protein denaturant, is stronger than the urea and alkylureas used in this study. Among urea and alkylureas, EU gave the highest negative *m*-value while the urea gave the lowest negative *m*-value (Tables 15 and 16). The hydrophobicity of urea and alkyl substituted urea typically decrease in the order EU > DMU > MU > urea. These findings suggest that the disturbance of hydrophobic interactions as well as the hydrogen-bonding play significant role in denaturant-mediated destabilization of Ferrocyt *c* and Mb.

3.4. Conclusion

It is important to understand the effects of denaturants (urea, alkylureas, and GdnHCl) on the structural fluctuation of the M80 containing Ω-loop of Cyt *c* across the folding/unfolding transition, since subglobal unfolding units of Cyt *c* appear to determine the limited set of folding pathways [94]. On going from native to unfolding conditions, the thermal motion of the Ferrocyt *c* first decreases in the subdenaturing milieu and then increases as subdenaturing to unfolding conditions are approached. Within the subdenaturing limit, the extent of decrease in amplitudes of thermal motions of the Ferrocyt *c* is found to be higher for urea and least for TMU. These results in conjugation with the docking results between the Cyt *c* and denaturant molecule (urea, MU, DMU, EU and TMU) reveal that the decrease in the extent of restricted dynamics of Ω-loop with a corresponding increase of alkyl groups on urea molecule is results from the decrease of denaturant-mediated cross-linking interactions. The denaturant-mediated cross-linking interactions also results in entropy reduction, and thus stiffens the Ferrocyt *c*. As compared to

TMU, the extent of entropy reduction is more for urea. As in the case of Cyt *c*, the thermal motion of MbCO was not found to decrease under subdenaturing concentrations of denaturants. The extent of increase in internal motions of the MbCO is found to be lower for urea and highest for TMU, which indicates that hydrophobicity on urea molecule controls the internal dynamics of MbCO. These results in conjugation with the docking results between the MbCO and denaturant molecule (urea, MU, DMU, EU and TMU) reveal that the denaturant-mediated cross-linking in MbCO are not sufficient to constrain the internal dynamics of MbCO. Thermodynamic analysis of denaturants (urea, MU, DMU, EU, TMU) effects on the thermal unfolding of Ferrocyt *c* and Mb shows that the thermodynamic stability of protein decreases with increasing concentration of denaturant and hydrophobicity of urea derivatives. The reciprocal form of WT equation has been also utilized to evaluate the effect of water activity on Ferrocyt *c* and Mb stability. By this, the stabilization free energy of the protein in denaturant solution was calculated. The *m*-values were also obtained from the slope of the stabilization free energy *vs* [denaturant] plot. The *m*-values were found to be more negative for longer chain monosubstituted urea and di-methyl-substituted urea, which indicates that the destabilization of proteins by denaturants occur through the disturbance of hydrophobic interactions and hydrogen-bonding.

3.5 References

[1] Kumar R, Prabhu NP, Yadaiah M, Bhuyan AK, Biophys J 87:2656–2662 (2004)
[2] Bhuyan AK, Biochemistry 41:13386–13394 (2002)
[3] Varhac R, Biochemica biophysica acta 1834:739–744 (2013)
[4] Latypov RF, Maki K, Cheng H, Luck SD, Roder H, J Mol Biol 383:437–453 (2008)
[5] Bhuyan AK, Kumar R, Biochemistry 41:12821–12834 (2002)
[6] Bellissent-Funel M, Hydration Processes in Biology: Theoretical and Experimental Approaches, IOS Press, Amsterdam. (1999)
[7] Miyawaki O, Saito A, Matsuo T, Nakamura K, Biosci Biotechnol Biochem 61:466–469 (1997)
[8] Miyawaki O, Biochim Biophys Acta 1774:928–935 (2007)
[9] Miyawaki O, Biophys Chem 144:46–52 (2009)
[10] Kumar R, Bhuyan AK, J Biol Inorg Chem 14:11–21 (2009)
[11] Olson JS, Methods Enzymol 76:631–651 (1981)
[12] Kumar R, Bhuyan AK, Biochemistry 44:3024–3033 (2005)
[13] Santoro MM, Bolen DW, Biochemistry 27:8063–8068 (1988)
[14] Miksovská J, Day JH, Larsen RW, J Biol Inorg Chem. 8:621–625 (2003)
[15] Jain R, Sharma D, Kumar R, J Biochem 154:341–354 (2013)
[16] Grosdidier A, Zoete V, Michielin O, Nucl Acids Res 39:W270-W277 (2011)

[17] Grosdidier A, Zoete V, Michielin O, J Comput Chem 32:2149–2159 (2011)
[18] Bushnell GW, Louie GV, Brayer GD, J Mol Biol 214:585–595 (1990)
[19] Pettersen EF, Goddard TD, Huang CC, Couch GS, Greenblatt DM, Meng EC, Ferrin TE, J Comput Chem 13:1605–1612 (2004)
[20] Takano T, Dickerson RE, J Mol Biol 153:79–94 (1981)
[21] Takano T, Dickerson RE, J Mol Biol 153:95–115 (1981)
[22] Banci L, Bertini I, Gray HB, Luchinat C, Reddig T, Rosato A, Turano P, Biochemistry 36:9867–9877 (1997)
[23] Banci L, Bertini I, Huber JG, Spyroulias GA, Turano P, J Biol Inorg Chem 4:21–31 (1999)
[24] Bhuyan AK, Udgaonkar JB, J Mol Biol 312:1135–1160 (2001)
[25] Thomas YG, Goldbeck RA, Kliger DS, Biopolymers 57:29–36 (2000)
[26] Latypov RF, Cheng H, Roder NA, Zhang J, Roder H, J Mol Bio 357:1009–1025 (2006)
[27] Tanford C, Adv Protein Chem 23:121–282 (1968)
[28] Timasheff SN, Acc Chem Res 3:62–68 (1970)
[29] Davies AM, Guillemette JG, Smith M, Greenwood C, Thurgood AGP, Mauk AG, Moore GR, Biochemistry 32:5431–5435 (1993)
[30] Elove GA, Chaffotte AF, Roder H, Goldberg ME, Biochemistry 31:6876–6883 (1992)
[31] Margoliash E, Frohwirt N, Biochem J 71:570–572 (1959)
[32] Varhac R, Antalik M, Bano M, J Biol Inorg Chem 9:12–22 (2004)
[33] Hagarman A, Duitch L, Schweitzer-Stenner R, Biochemistry 47:9667–9677 (2008)
[34] Schweitzer-Stenner R, Hagarman A, Verbaro D, Soffer JB, Methods Enzymol 466:109–153 (2009)
[35] Cupane A, Leone M, Vitrano E, Cordone L, Eur Biophys J 23:385-398 (1995)
[36] Leone M, Cupane A, Cordone L, Eur Biophys J 24:117-124 (1996)
[37] Cupane A, Leone M, Vitrano E, Eur Biophys J 21:385-391 (1995)
[38] Santoro MM, Bolen DW, Biochemistry 31:4901–4907 (1992)
[39] Poklar N, Lapanje S, Biophys Chem 42:283–290 (1992)
[40] Poklar N, Vesnaver G, Lapanje S, Biophys Chem 47:143–151 (1993)
[41] Poklar N, Vesnaver G, Lapanje S, J Protein Chem 14:709–719 (1995)
[42] Poklar N, Vesnaver G, Lapanje S, Biophys Chem 57:279–289 (1996)
[43] Poklar N, Petrovcic N, Oblak M, Vesnaver G, Protein Sci 8:832–840 (1999)
[44] Jenkins WT, Protein Sci 7:376–382 (1998)
[45] Pace CN, Methods Enzymol 131:266–280 (1986)
[46] Schellman JA, Biophys Chem 96:91–101 (2002)
[47] Bennion BJ, Daggett V, Proc Natl Acad Sci USA 100:5142–5147 (2003)
[48] Timasheff SN, Xie G, Biophys Chem 105:421–448 (2003)
[49] Hirato N, Mizuno K, Goto Y, J Mol Biol 275:365–378 (1998)
[50] Velicelebi G, Sturtevant JM, Biochemistry 18:1180–1186 (1979)
[51] Tanford C, Adv Protein Chem 24:l–95 (1970)
[52] Prakash V, Loucheux C, Scheuffle S, Gorbunoff J, Timasheff SN, Arch Biochem Biophys 210:455–464 (1981)
[53] Greene RF, Pace CN, J Biol Chem 249:5388–5393 (1974)
[54] Miyawaki O, Tatsuno M, J Biosci Bioeng 111:198–203 (2011)
[55] Xie G, Timasheff SN, Biophys Chem 64:25–43 (1997)
[56] Kaushik JK, Bhat R, J Biol Chem 278:26458–26465 (2003)

[57] Leszczynski JF, Rose GD, Science 234:849-855 (1986)
[58] Hoang L, Maity H, Krishna MMG, Lin Y, Englander SW, J Mol Biol 331:37–43 (2003)
[59] Xu Y, Mayne LC, Englander SW, Nature Struct Biol 5:774–778 (1998)
[60] Morgan JD, McCammon JA, Biopolymers 22:1579–1593 (1983)
[61] Berghuis AM, Brayer GD, J Mol Bio 223:959–976 (1992)
[62] Beece D, Eisenstein L, Frauenfelder H, Good D, Marden MC, Reinisch L, Reynolds AH, Sorensen LB, Yue KT, Biochemistry 19:5147–5157 (1980)
[63] Fenimore PW, Frauenfelder H, McMahon BH, Young RD, Proc Natl Acad Sci USA 101:14408–14413 (2004).
[64] Austin RH, Beeson KW, Eisenstein L, Frauenfelder H, Gunsalus IC, Biochemistry 14:5355–5373 (1975)
[65] Makhatadze GI, Privalov PL, J Mol Biol 226:491–505 (1992)
[66] Pike AC, Acharya KR, Protein Sci 3:706–710 (1994)
[67] Dunbar J, Yennawar HP, Banerjee S, Luo J, Farber GK, Protein Sci 6:1272–1733 (1997)
[68] Hibbard LS, Tulinsky A, Biochemistry 17:5460–5468 (1978)
[69] Dill KA, Biochemistry 29:7133–7155 (1990)
[70] Trewhella J, Carlson VA, Curtis EH, Heidorn DB, Biochemistry 27:1121–1125 (1988
[71] Cohen DS, Pielak GJ, J Am Chem Soc 117:1675–1677 (1995)
[72] Petsko GA, Ringe D, Ann Rev Biophys Bioeng 13:331–371 (1984)
[73] Fenimore PW, Frauenfelder H, McMahon BH, Young RD, Proc Natl Acad Sci U S A 101:14408-14413 (2004)
[74] Fenimore PW, Frauenfelder H, McMahon BH, Parak FG, Proc Natl Acad Sci U S A 99:16047-16051 (2002)
[75] Frauenfelder H, Fenimore PW, Chen G, McMahon BH, Proc Natl Acad Sci U S A 103:15469-15472 (2006)
[76] Bhuyan AK, Udgaonkar JB, Proteins: Struct, Funct, Genet 32:241–247 (1998)
[77] Maity H, Maity M, Krishna MM, Mayne L, Englander SW, Proc Natl Acad Sci USA 102 4741–4746 (2005)
[78] Maity H, Maity M, Englander SW, J Mol Biol 343:223–233 (2004)
[79] Krishna MM, Maity H, Rumbley JN, Lin Y, Englander SW, J Mol Biol 359:1410–1419 (2006)
[80] Zarrine-Afsar A, Mittermaier A, Kay LE, Davidson AR, Protein Sci 15:162–170 (2006)
[81] Jain R, Kaur S, Kumar R, J Biochem 153:161–177 (2013)
[82] Makhatadze GI, J Phys Chem B 103:4781–4785 (1999)
[83] Makhatadze GI, Lopez MM, Richardson JM, Thomas ST, Protein Sci 7:689–697 (1998)
[84] Mayr LM, Schmid FX, Biochemistry 32:7994–7998 (1993)
[85] Hagihara Y, Aimoto S, Fink AL, Goto Y, J Mol Biol 231:180–184 (1993)
[86] [114] Natali F, Moretti L, Boffi F, Bianconi A, Della Longa S, Castellano AC, Eur Biophys J 27:1–7 (1998)
[87] Poklar N, Lah N, Oblak M, Vesnaver G, Acta Chim Slov 46:315–322 (1999)
[88] Tanford C, Aune KC, Biochemistry 9:206–211 (1970)
[89] Poklar N, Vesnaver G, Lapanje S, J Protein Chem 13:323–331 (1994)
[90] Schellman JA, Biopolymers 26:549–559 (1987)
[91] Alonso DO, Dill KA, Biochemistry 30:5974–5985 (1991)
[92] Mayo SL, Baldwin RL, Science 262:873–876 (1993)
[93] Knapp JA, Pace CN, Biochemistry 13:1289–1294 (1974)

[94] Hoang L, Bédard S, Krishna MMG, Lin Y, Englander SW, Proc Natl Acad Sci USA 99 12173–12178 (2002)

Chapter 4
Structural, Kinetic and Thermodynamic Characterizations of the Sugar-Induced Molten Globule States of the Alkali pH-Denatured Horse Cytochrome *c*

4.1 Introduction

Few earlier reports showed that a MG-like intermediate also play an important role in the Ferrocytochrome *c* (Ferrocyt *c*) folding [1-8]. Several previous reports suggest that anions arising from salts transform the acid-denatured protein (U_A-state) to MG-state (A-state) [9-17]. Few other previous reports suggest that cations also transform the base-denatured protein (U_B-state) to MG-state (B-state) [16,18-21]. In general, a balance between the electrostatic interactions of charged residues and the opposing forces like hydrogen bonding and hydrophobic interactions determine the stability of MG-state [22-24]. However, the thermal denaturation studies of U_A or U_B-state of Ferricytochrome *c* (Ferricyt *c*) [14,19,25-26] showed that the hydrophobic interactions also contribute to the MG-state stability. Few previous reports showed that protecting osomolytes such as sugars and polyols also transform the U_A-state of Ferricyt *c* to MG-state [27-30]. In the former case, the main driving force for MG formation is the increase in steric repulsion between the protein and sugar solution [28-29], while in the latter case it is the enhanced hydrophobic interactions that overcome electrostatic repulsion among charged side chains [27]. A Previous study showed that the NaCl induced A-state of Ferricyc *c* is partially folded state, consisting of the heme, C-terminal, N-terminal, and 60s helices, which is stabilized by nonbonding interactions between helices and with the heme [31]. A previous Trp fluorescence and resonance Raman spectroscopies study suggests that charge screening effect of KCl accelerates the early polypeptide chain collapse and introduces heterogeneity into the subsequent folding processes [32].

Previous studies have shown that Na^+ ions arising from NaCl transform the U_B-state of Cytochrome *c* (Cyt *c*) to MG-state (B-state) by charge-screening mechanism [18-19]. A previous report revealed that (i) sugar (stachyose, melezitose, trehalose, glucose and glycerol) and salt (NaCl) transform the highly positively charged acid-denatured Ferricyt *c* (U_A-state) to MG-state [28,33], and (ii) the heme environment near PHE82 is more native like in sugar than in salt [28,33]. Glycerol also transforms the native (N-state) state of Ferricyt *c* to MG-state that lacks the native Fe^{3+}-M80 axial bond [34]. An earlier report showed that trehalose stabilizes the global

conformation of Ferricyt *c* under alkaline conditions [35]. The current study showed that glycerol and trehalose transform the highly negatively charged base-denatured Ferricyt *c* and CO-liganded Ferrocyt *c* (Cyt-CO) (U_B-states) to G_B and T_B-states, respectively, (where G_B and T_B are the glycerol and trehalose-induced MG states of U_B-state of Ferricyt *c* and Cyt-CO), presumably mainly by the steric repulsion between solution components, that favors the compact state relative to unfolded state. The results from Circular dichroism (CD), tryptophan (Trp) fluorescence and 1-anilino-8-napthalene sulfonate (ANS) binding experiments suggest that the G_B and T_B-states resemble the generic properties of molten globules. A matter of our concern is to find out the source of G_B and T_B-states stability. The present work also determined the effects of glycerol and trehalose on (i) thermal unfolding of U_B-state of Ferricyt *c* (pH 12.9), and (ii) kinetics of CO-association to alkaline Ferrocyt *c* (pH 12.9)

4.2 Results and Discussion

4.2.1 Sugar-induced molecular compaction of the base-denatured Ferricyt c and Cyt-CO

Native-states (N-states) of Ferricyt *c* and Ferrocyt *c* (pH 7.0) are fluorescence-silent while the U_B-states of Ferricyt *c* and Cyt-CO at pH ~12.9 are fluorescent (Figs. 4.1a and 4.1b). Previous pH dependent Trp fluorescence and far-UV CD studies of Ferricyt *c* and Cyt-CO also revealed that Ferricyt *c* and Cyt-CO are substantially denatured at extreme basic pH ~12.9 [18-21]. Unfolding results in an increase in the heme-Trp distance due to molecular expansion [36-37]. Molecular compaction of the U_B-states of Ferricyt *c* (Fig. 4.1a) and Cyt-CO (Fig. 4.1b) occurs when 6.0 M glycerol or 1.5 M trehalose or 1.5 M NaCl is included.

Figs. 4.1c and 4.1d show the ANS fluorescence spectra of N- and U_B-states of Ferricyt *c* without additive and in the presence of different concentrations of glycerol and trehalose, respectively. Clearly, the ANS fluorescence intensity of U_B-state of Ferricyt *c* is significantly increased in the presence of high concentration of sugar (6.0 M glycerol and 1.5 M trehalose) than in its absence. This finding indicates that in the G_B and T_B-states of Ferricyt *c*, the hydrophobic clusters, which were originally buried inside, are now solvent exposed. Figs. 4.1e and 4.1f present the fluorescence monitored titration of the U_B-state of Ferricyt *c* with glycerol and trehalose, respectively. Data in Figs. 4.1e and 4.1f clearly suggests that glycerol and trehalose-drive the $U_B \rightarrow G_B$ and $U_B \rightarrow T_B$ transitions, where G_B and T_B are glycerol and trehalose-induced molecular compact state of alkali-denatured Ferricyt *c*, respectively.

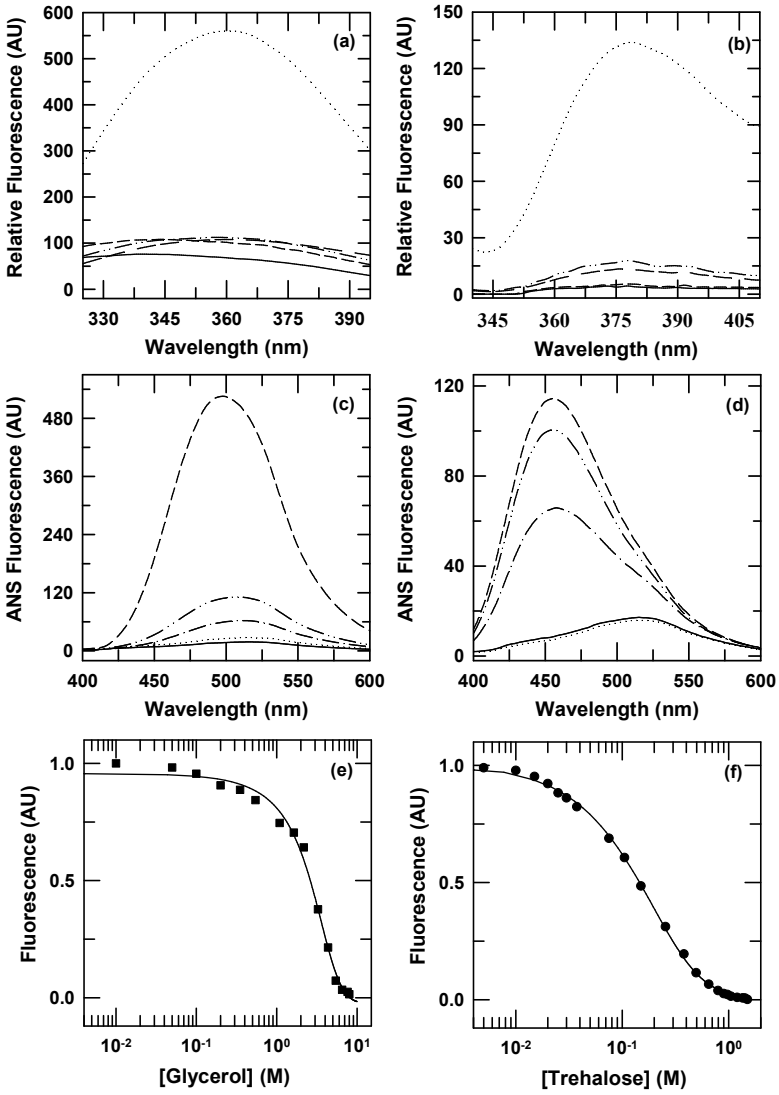

Fig. 4.1 (a) Fluorescence emission spectra for N-state of Ferricyt *c* at pH 7 in the absence of additive (solid line) and U_B-state of Ferricyt *c* at pH 12.9 absence of additive (dotted line), and presence of 6.0 M glycerol (medium dash line), 1.5 M trehalose (short dash line) and 1.5 M NaCl (dash dot dot line). (b) Fluorescence emission spectra for N-state of Ferrocyt *c* at pH 7 in the absence of additive (solid line) and U_B-state of Cyt-CO at pH 12.9 in the absence of additive (dotted line), and presence of 6.0 M glycerol (medium dash line), 1.5 M trehalose (short dash line) and 1.5 M NaCl (dash dot dot line). (c) ANS fluorescence spectra (ex: 380) of N-state of Ferricyt *c* in the absence of additive (pH 7.0) (solid line) and U_B-state of Ferricyt *c* (pH 12.9) in the absence of additive (dotted line) and in the presence of 2.0 M (dash dote line), 3.0 M (dash dot dot line) and 6.0 M (short dash line) of glycerol. (d) ANS fluorescence spectra (ex: 380) of N-state of Ferricyt *c* at pH 7 in the absence of additive (solid line) and U_B-state of Ferricyt *c* at pH 12.9 in the absence of additive (dotted line) and in the presence of 0.25 M (dash dote line), 1.0 M (dash dot dot line) and 1.5 M (short dash line) of trehalose. (e) Relative quenching of Trp59 fluorescence (ex: 280 nm, em: 360 nm) of Ferricyt *c* as a function of glycerol, pH 12.9. (f) Relative quenching of Trp59 fluorescence (ex: 280 nm, em: 360 nm) of Ferricyt *c* as a function of trehalose, pH 12.9. The solid line through the data in panels (e) and (f) has been drawn by inspection only. The final proteins concentrations for Trp and and ANS fluorescence measurements were 10 μM.

4.2.2 Sugar-induced folding of the U_B-state

The MG-states generally have native-like secondary structures [9,22]. Figs. 4.2a, 4.2b, 4.2c and 4.2d show the far-UV CD spectra of different states of Cyt *c*. The MRE observed for the U_B-states of Ferricyt *c* (Figs. 4.2a and 4.2b) and Cyt-CO (Figs. 4.2c and 4.2d) at 222 nm decrease when 6.0 M glycerol (Figs. 4.2a and 4.2c), 1.5 M trehalose (Figs. 4.2b and 4.2d) and 1.5 M NaCl (Figs. 4.2b and 4.2d) are included, indicating the $U_B \rightarrow G_B$, $U_B \rightarrow T_B$ and $U_B \rightarrow B$ transitions, where G_B, T_B and B-states are the glycerol, trehalose and salt-induced refolded state of U_B-state of the Ferricyt *c*/Cyt-CO. It is observed that the MRE values for the G_B (Figs. 4.2a and 4.2c), T_B and B-states (Figs. 4.2b and 4.2d) of Ferricyt *c*/Cyt-CO are comparable with the MRE value of the N-states of Ferricyt *c* (Figs. 4.2a and 4.2c)/Ferrocyt *c* (Figs. 4.2b and 4.2d), respectively. Figs. 4.3a and 4.3b show the normalized far-UV CD (222 nm) monitored $U_B \rightarrow G_B$ and $U_B \rightarrow T_B$ transitions for the U_B-state of Ferricyt *c*, respectively. Figs. 4.3c and 4.3d show the normalized far-UV CD (222 nm) monitored $U_B \rightarrow G_B$ and $U_B \rightarrow T_B$ transitions for the U_B-state of Cyt-CO, respectively. Clearly, base-denatured U_B-states of Ferricyt *c* and Cyt-CO acquire extensive secondary structure and molecular compaction in the presence of high concentrations of glycerol and trehalose.

The Gibbs free energy change, ΔG, for the two-state transitions, $U_B \rightarrow G_B$ and $U_B \rightarrow T_B$ of Ferricyt *c* was calculated by the equation (1):

$$\Delta G = -RT \ln K = -RT \ln\left[(Y_{obs} - Y_{UB}) / (Y_{GB} - Y_{obs})\right] \qquad (1)$$

where, Y_{obs} is the observed value of the CD signal, Y_{UB} and Y_{GB} are the CD signal intensities for the U_B and G_B-states, respectively. By assuming a linear dependence of ΔG on glycerol and trehalose concentration [38], the least-squares fit of the data to equation (2),

$$\Delta G = \Delta G^0 + m[osmolyte] \qquad (2)$$

provides, $\Delta G^o = \sim 1.76\ (\pm 0.1)$ Kcal mol^{-1} and *m* (slope reflecting the cooperativity of the

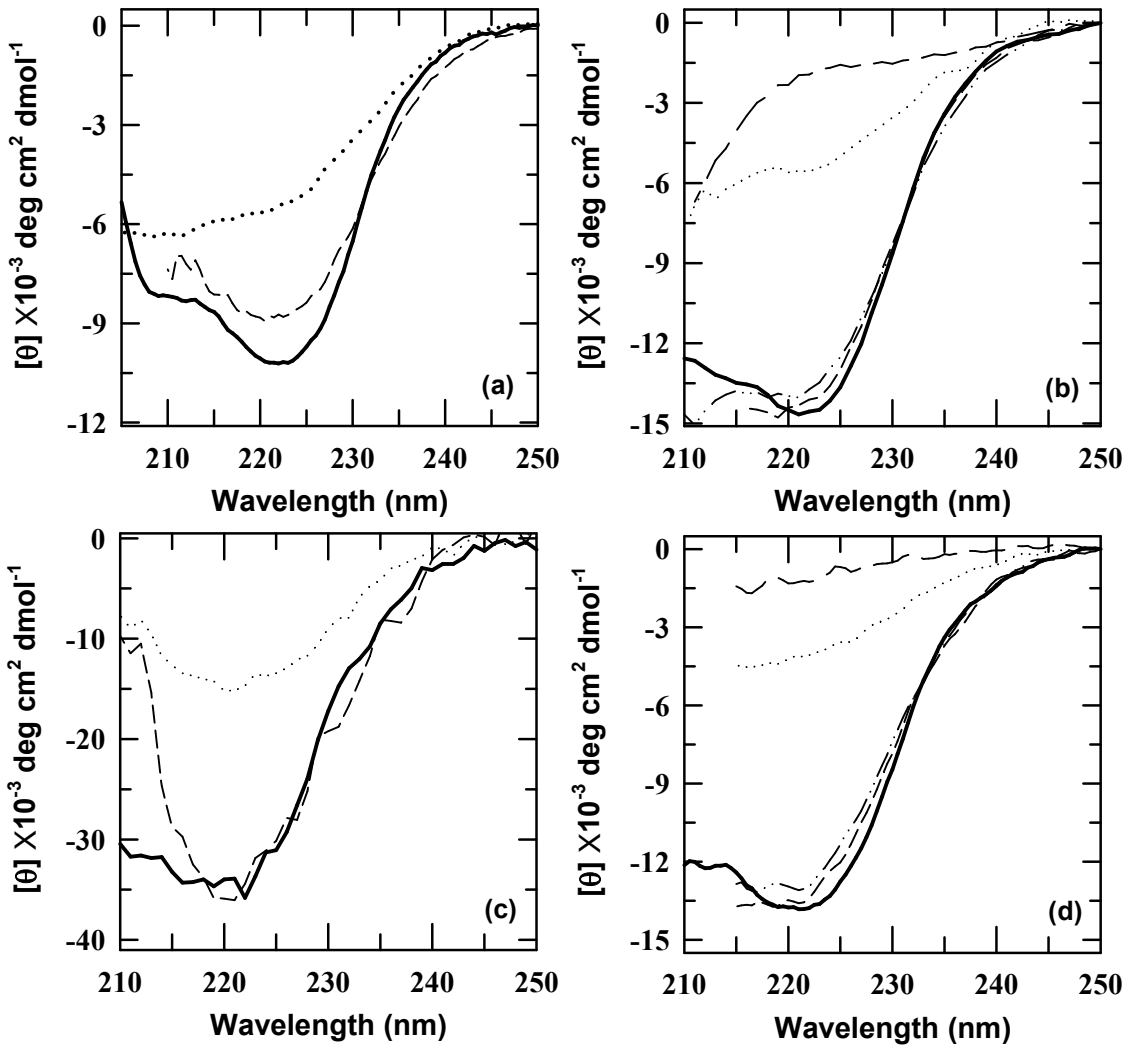

Fig. 4.2 (a) Far-UV CD spectra for N-state of Ferricyt *c* at pH 7 in the absence of additive (solid line) and U_B-state of Ferricyt *c* at pH 12.9 in the absence of additive (dotted line) and in the presence of 6.0 M glycerol (short dash line). (b) Far-UV CD spectra for N-state of Ferricyt *c* at pH 7 in the absence of additive (solid line), GdnHCl-unfolded (5.0 M GdnHCl) Ferricyt *c* at pH 7 (long dash line) and U_B-state of Ferricyt *c* at pH 12.9 in the absence of additive (dotted line) and in the presence of 1.5 M trehalose (short dash line) and 1.5 M NaCl (dash dot dot line). (c) Far-UV CD spectra for N-state of Ferrocyt *c* at pH 7 in the absence of additive (solid line) and U_B-state of Cyt-CO at pH 12.9 in the absence of additive (dotted line) and presence of 6.0 M glycerol (short dash line). (d) Far-UV CD spectra for N-state of Ferrocyt *c* at pH 7 in the absence of additive (solid line), GdnHCl-unfolded (5.0 M GdnHCl) Cyt-CO at pH 7 (long dash line) and U_B-state of Cyt-CO at pH 12.9 in the absence of additive (dotted line) and in the presence of 1.5 M trehalose (short dash line) and 1.5 M NaCl (dash dot dot line). The final concentrations of the protein were 10 μM, 15 μM, 30 μM and 15 μM in panels (a), (b), (c) and (d), respectively.

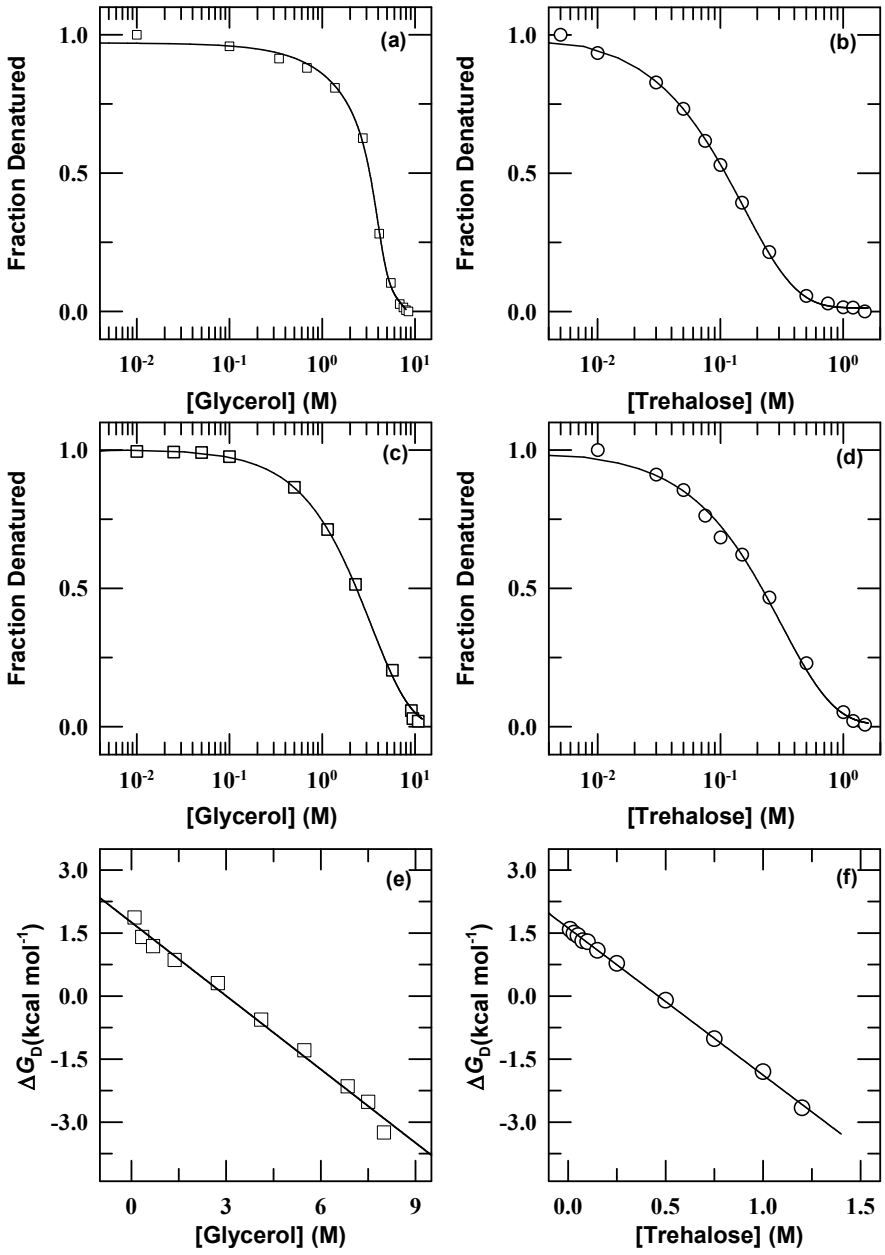

Fig. 4.3 (a) The glycerol-induced folding transition (CD 222 nm) of U_B-state of Ferricyt *c* (10 μM) at pH 12.9. (b) The trehalose-induced folding transition (CD 222 nm) of U_B-state of Ferricyt *c* (15 μM) at pH 12.9. (c) The glycerol-induced folding transition (CD 222 nm) of U_B-state of Cyt-CO (30 μM) at pH 12.9. (d) The trehalose-induced folding transition (CD 222 nm) of U_B-state of Cyt-CO (15 μM) at pH 12.9. The solid lines through the data in panels (a) to (d) have been drawn by inspection only. (e) Shows unfolding free energy changes in the transition region calculated from the equilibrium curve (panel (a)). The linear least-squares best fit of the data to equation (2) [38] provided, ΔG^o = ~1.76 kcal mol^{-1}, m = ~0.58 kcal mol^{-1} M^{-1}.(f) Shows unfolding free energy changes in the transition region calculated from the equilibrium curve (panel (b)). The linear least-squares best fit of the data to equation (2) [38] provided, ΔG^o = ~1.62 kcal mol^{-1} and m = ~3.5 kcal mol^{-1} M^{-1}.

transition) = ~0.58 kcal mol^{-1} M^{-1} for $U_B \rightarrow G_B$ transition (Fig. 4.3e), and ΔG^o= ~1.62 (±0.1) Kcal mol^{-1} and *m*= ~3.5 kcal mol^{-1} M^{-1} for $U_B \rightarrow T_B$ transition (Fig. 4.3f), respectively. Clearly the ΔG^o values for glycerol and trehalose are almost identical, suggesting that ΔG^o is independent of the nature of the protecting osmolyte and thus it is a property of the protein alone. The calculated values of ΔG^o for the $U_B \rightarrow G_B$ (ΔG^o = ~1.76 Kcal mol^{-1}) and $U_B \rightarrow T_B$ (ΔG^o = ~1.62 Kcal mol^{-1}) transitions are lower than the free energy change for the already known $U_A \rightarrow A$ transition (ΔG^o = ~2.63 kcal mol^{-1}) [28,39] and $U_A \rightarrow G_A$ transition (ΔG^o = ~2.25 kcal mol^{-1}) [30], where A and G_A are the anions and glycerol-induced MG-states of U_A-state of Ferricyt *c*. Although, the physical importance of the factor *m* is not clearly understood, but few previous studies of protein denaturation by denaturants suggested that it reflects the difference between the accessibility of surface areas of native and denatured states of the polypeptide chain for a given denaturant [40-43]. The high *m* value for trehalose (~3.5 kcal mol^{-1} M^{-1}) than glycerol (~0.58 kcal mol^{-1} M^{-1}) suggests high effectiveness of trehalose towards refolding of U_B-state to MG-state as compared to glycerol.

4.2.3 Moderately rigid tertiary structure in the G_B and T_B-states

In general, the MGs are characterized by disordered tertiary structure [9,44]. Fig. 4.4 shows the far-UV CD spectra of different states of Ferricyt *c* (Fig. 4.4a-4.4b) and Cyt-CO (Figs. 4.4c-4.4d). U_B-states of Ferricyt *c* (Fig. 4.4a-4.4b) and Cyt-CO (Figs. 4.4c-4.4d) do not show the CD absorption at 282 and 289 nm, which suggest that it lack the tertiary structure. The aromatic CD spectra for the GdnHCl unfolded Ferricyt *c* and Cyt-CO at pH 7.0 and U_B-states of Ferricyt *c* and Cyt-CO at pH 12.9 are almost same (Figs. 4.4b and 4.4d). When 6.0 M glycerol or 1.5 M trehalose or 1.5 NaCl is included in the U_B-states of Ferricyt *c*/Cyt-CO, the base-denatured protein is apparently not acquired sufficient near-UV CD signal, indicating not much gain of tertiary interactions (Fig. 4.4).

4.2.4 GdnHCl-induced stabilization and subsequent unfolding of the G_B-state of Cyt-CO and GdnHCl-induced unfolding of the T_B and B-states of Cyt-CO

Previous pH-dependent absorbance and fluorescence emission studies of Ferrocyt *c* showed that the CO ligation to Ferrocyt *c* at extreme basic pH (pH 13) unfolds the protein [18,20,45].

Furthermore, the inclusion of salt transforms the base-denatured Cyt-CO to B-state [18,20,45].

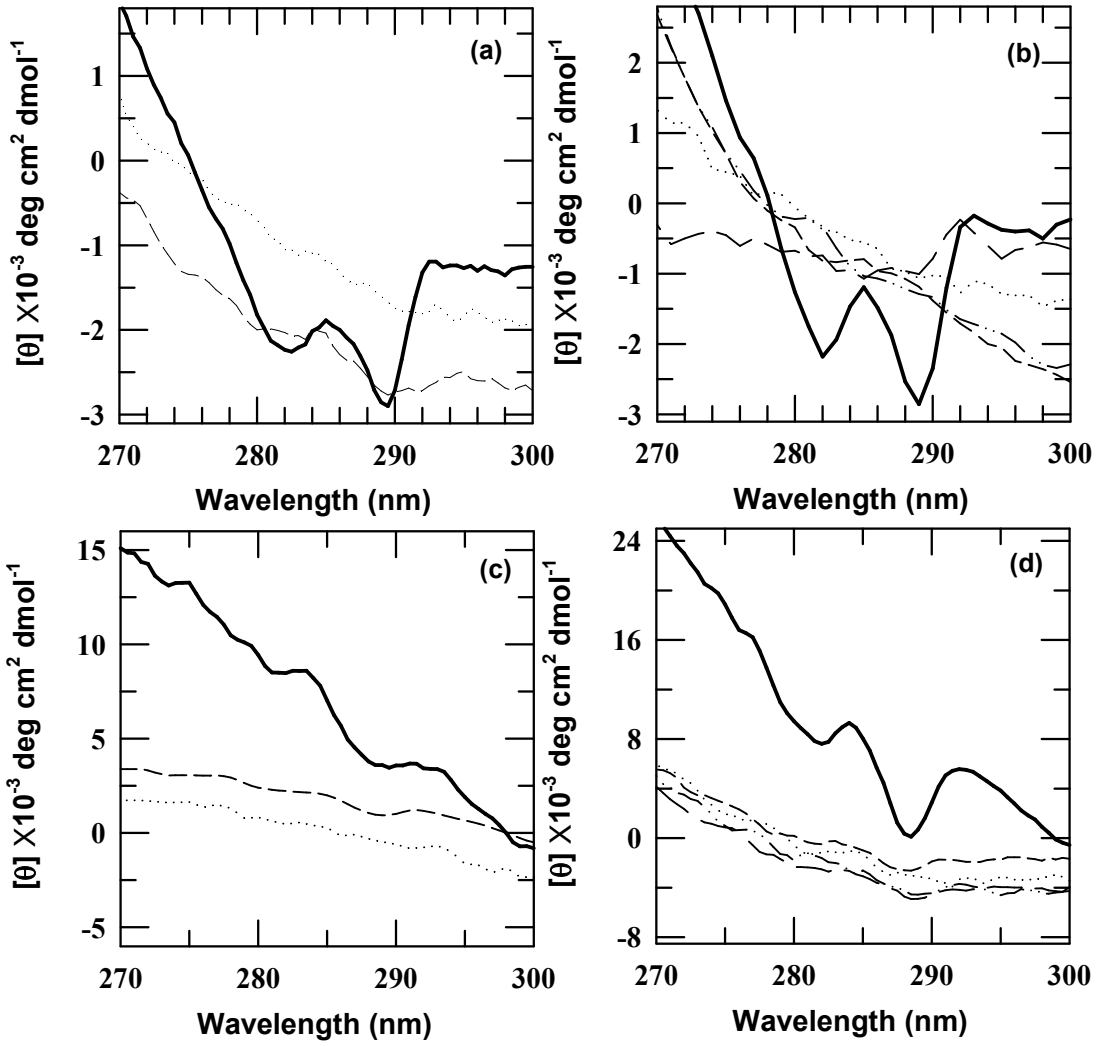

Fig. 4.4 (a) Near-UV CD spectra for N-state of Ferricyt *c* at pH 7 in the absence of additive (solid line) and U_B-state of Ferricyt *c* at pH 12.9 in the absence of additive (dotted line) and in the presence of 6.0 M glycerol (short dash line). (b) Near-UV CD spectra for N-state of Ferricyt *c* at pH 7 in the absence of additive (solid line), GdnHCl-unfolded (5.0 M GdnHCl) Ferricyt *c* at pH 7 (long dash line) and U_B-state of Ferricyt *c* at pH 12.9 in the absence of additive (dotted line) and in the presence of 1.5 M trehalose (short dash line) and 1.5 M NaCl (dash dot dot line). (c) Near-UV CD spectra for N-state of Ferrocyt *c* at pH 7 in the absence of additive (solid line) and U_B-state of Cyt-CO at pH 12.9 in the absence of additive (dotted line) and in the presence of 6.0 M glycerol (short dash line). (d) Near-UV CD spectra for N-state of Ferrocyt *c* at pH 7 in the absence of additive (solid line), GdnHCl-unfolded (5.0 M GdnHCl) Cyt-CO at pH 7 (long dash line), U_B-state of Cyt-CO at pH 12.9 in the absence of additive (dotted line) and in the presence of 1.5 M trehalose (short dash line) and 1.5 M NaCl (dash dot dot line). The final concentrations of the protein used were 90 μM in panels (a), (b), (c) and 130 μM in panel (d).

The U_B-state of Cyt-CO becomes compact in the presence of 6.0 M glycerol, 1.5 M trehalose or 1.5 M NaCl (Fig. 4.1b), indicating $U_B \rightarrow G_B$, $U_B \rightarrow T_B$, $U_B \rightarrow B$ transitions, where G_B,

T_B and B-states are glycerol, trehalose and NaCl-induced molecular compact state of alkali-denatured Cyt-CO, respectively. Few earlier reports have shown that the low concentrations of GdnHCl (≤ 0.5 M) transform the U_A-state and U_B-state of Cyt *c* to MG-states [19,45-46]. Figs. 4.5a and 4.5b present the fluorescence emission spectra of Cyt-CO at pH 12.9 in the presence of 6 M glycerol (Fig. 4.5a) or 1.5 M trehalose (Fig. 4.5b) with 0.0 M, 0.4 M and 3.0 M of GdnHCl. Clearly, the low concentrations of GdnHCl compact the G_B-state of Cyt-CO but not the T_B-state of Cyt-CO.

The GdnHCl titration of the G_B and T_B-states of Cyt-CO are shown in Figs. 4.5c and 4.5d, respectively. Data in Fig. 4.5c show that the low concentration of GdnHCl (≤ 0.4 M) transforms the G_B-state to an intermediate, I_G. Fig. 4.5c clearly shows two consecutive transitions, first is the $GdnH^+$-induced refolding transition of the G_B-state (≤ 0.4 M GdnHCl) and second is the $GdnH^+$-induced unfolding transition of the I_G-state (> 0.4 M GdnHCl). However, this type of $GdnH^+$-induced refolding transition is not observed for T_B-state of Cyt-CO (Fig. 4.5d). The GdnHCl-induced refolding transition of G_B-state is fitted to the equation (3) [39],

$$K_{app} = K(1 + K_b\, a_x)^{\Delta n} \qquad (3)$$

which yields Δn (the difference of the number of $GdnH^+$ ions bound to U_B and G_B-states)= 3.7, K_b (the binding constant) = 4.9 M^{-1}, and K (the true equilibrium constant for the $GdnH^+$ ions-induced refolding transition in the absence of $GdnH^+$) = 2.8. At 25 °C, the value of free energy was found to be ~0.62 kcal mol^{-1} ($\Delta G^o = -RT\ln K$). The increase in the GdnHCl concentration above 0.4 M results in the unfolding of the I_G-state (Fig. 4.5c). The fit of the unfolding transition data (Fig. 4.5c) to the equation (4) [47],

$$\Delta G = \Delta G° - RT \ln\left(\frac{1 + K^{u}_{bind}[GdnHCl]}{1 + K^{G}_{bind}[GdnHCl]}\right)^{n} - m[GdnHCl] \qquad (4)$$

yields m = 0.26(±0.01) kcal mol^{-1} M^{-1} and $\Delta G°$ = 1.0(±0.02) kcal mol^{-1}. The terms K^{u}_{bind}, K^{G}_{bind}, n, m, and $\Delta G°$ in equation (4) have their usual meaning as described earlier [18]. However, this type of $GdnH^+$-induced refolding transition is also not observed for B-state of Cyt-CO (Fig. 4.5f), indicating that glycerol is unable to diminish electrostatic repulsion between the charged residues of the U_B-state (Fig. 4.5d). The $GdnH^+$-induced unfolding transitions of T_B (Fig. 4.5d) and B-states (Fig. 4.5f) were analyzed using standard two state equation (equation (1), chapter 2).

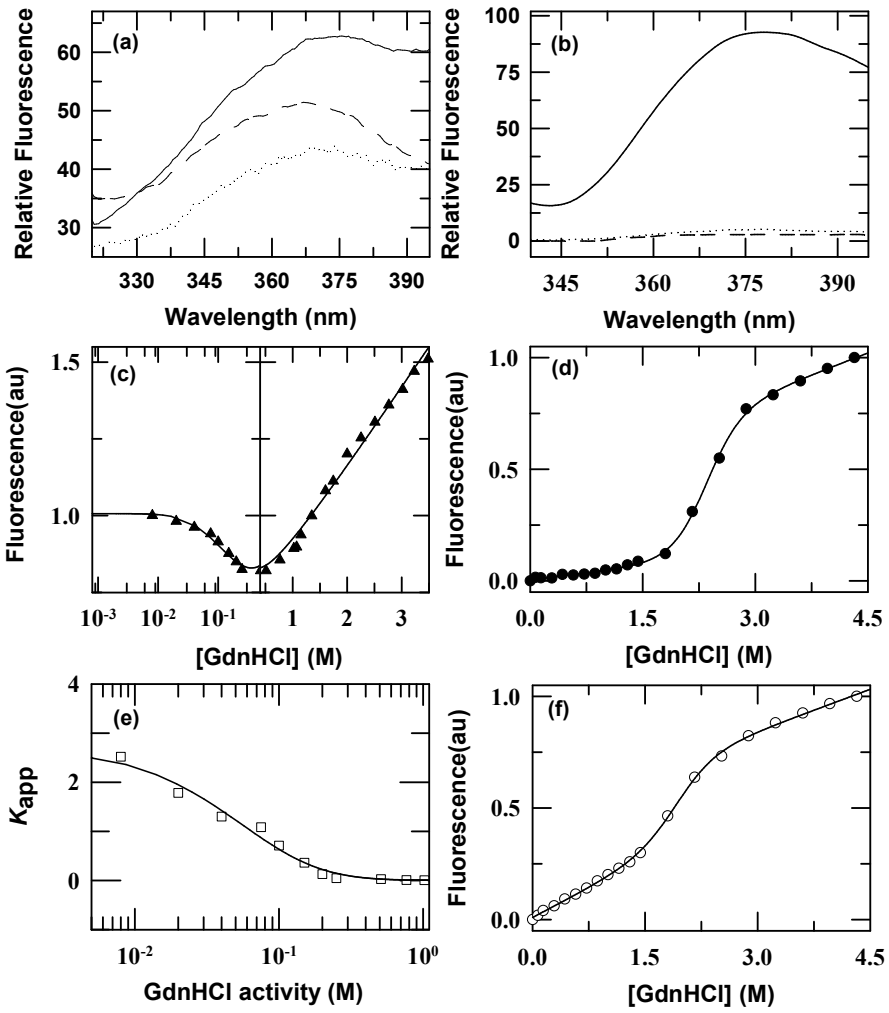

Fig. 4.5 (a) Fluorescence emission spectra of Cyt-CO at pH 12.9 in the presence of 6 M glycerol with 0.0 M (short short line), 0.4 M (dotted line) and 3.0 M (solid line) of GdnHCl. (b) Fluorescence emission spectra of Cyt-CO at pH 12.9 in the presence of 1.5 M trehalose with 0.0 M (short short line), 0.4 M (dotted line) and 3.0 M (solid line) of GdnHCl. (c) The GdnHCl-induced (fluorescence monitored, ex: 280 nm, em: 375 nm) folding-unfolding transition of the G_B-state of Cyt-CO at pH 12.9. The continuous line represents the fit to the experimental data by the use of equation (4). The fit yields m = 0.26(±0.01) kcal mol^{-1} M^{-1} and $\Delta G°$ = 1.0(±0.02) kcal mol^{-1}. (d) The GdnHCl-induced (fluorescence monitored, ex: 280 nm, em: 375 nm) equilibrium unfolding transition of the T_B-state of Cyt-CO at pH 12.9, 1.5 M trehalose. The solid line is the standard two state fit to data (equation (1), chapter 2). The fit yields $\Delta G°_D$ = 5.88 (±0.42) kcal mol^{-1} and m_g= 2.52(±0.18) kcal mol^{-1} M^{-1}. (e) In the presence of low concentrations of GdnHCl, guanidinium ions drive the $G_B \rightarrow I_G$ transition. The observable equilibrium constant, K_{app}, for the $G_B \rightleftharpoons I_G$ is plotted against the molar activity of GdnHCl. The values of K_{app} were calculated from equation, $K_{app} = [(Y_{obs} - Y_{IG}) / (Y_{GB} - Y_{obs})]$, where Y_{obs} is the observed value of the signal, Y_{GB} and Y_{IG} are the corresponding values for the G_B and I_B-states, respectively [39]. The solid line is the fit to data according to equation (3) (see text). The fit yields Δn = 3.7, K_b = 4.9 M^{-1}, and K = 2.8. At 25 °C, the value of K corresponds to the free energy of 0.62 kcal mol^{-1}. (f) The GdnHCl-induced (fluorescence monitored, ex: 280 nm, em: 375 nm) equilibrium unfolding transition of the Cyt-CO at pH 12.9, 1.5 M NaCl. The solid line is the standard two state fit to data (equation (1), chapter 2). The fit yields $\Delta G°_D$ = 4.42 (±0.52) kcal mol^{-1} and m_g = 2.27 (±0.26) kcal mol^{-1} M^{-1}.

The measured $\Delta G°$ for the fully populated $G_{B,}$ T_B and B-states of Cyt-CO against GdnHCl are 1.0(±0.02), 5.88(±0.42) and 4.42(±0.52) kcal mol^{-1}, which indicates that the T_B and B-states are more thermodynamically stable than the G_B-state. However, the $G_{B,}$ T_B and B-states of Cyt-CO are comparably less thermodynamically stable than the N-state of Cyt-CO ($\Delta G°$ = 11.65(±0.2) kcal mol^{-1} for the N-state of Cyt-CO [48]). The m_g-value for $G_{B,}$ T_B and B-states of Cyt-CO are 0.26(±0.01), 2.52 (±0.18), and 2.27(±0.26) kcal mol^{-1} M^{-1}, respectively which indicates that the T_B and B-states of Cyt-CO are more ordered as compared to the G_B-state of Cyt-CO. However, $G_{B,}$ T_B and B-states of Cyt-CO are comparably less ordered as compared to the N-state of Cyt-CO (the m_g-value (2.95(±0.28) kcal mol^{-1}) for the N-state of Cyt-CO [48].

4.2.5 Sugars and salt dependent CO-association kinetics of alkaline Ferrocyt c reveals that the $G_{B,}$ T_B and B-states of Cyt-CO are stiff and dynamically constrained

To determine qualitatively, how dynamic the interior of the $G_{B,}$ T_B and B-states, the CO-association reaction of Ferrocyt *c* were conducted at alkaline pH 12.9 containing the variable concentration of glycerol, trehalose and NaCl. In CO saturated (~1 mM) buffer, the Ferrocyt *c* binds CO [18,45]. The CO-association kinetics is slow, which is a denaturation reaction, because the very stable intrinsic native Fe^{2+}-M80 bond is broken, creating a 5-coordinate heme capable of binding to CO. This slowness of the reaction has allowed accurate determination of CO-association rate constant, k_{ass} by spectrophotometric method (decrease in absorbance at the heme $\pi \rightarrow \pi^*$ α-band (550 nm). Fig. 4.6a represents the CO-association kinetic trace of Ferrocyt *c* in the absence of additive at 25 °C (pH 12.9). This kinetic trace fitted well in a single-exponential function with time constant τ_{ass}= 0.7 min.

Fig. 4.6b shows the variation of k_{ass} with [glycerol] and [trehalose] for alkaline Ferrocyt *c* at pH 12.9. Fig. 4.6b also shows the variation of k_{ass} with [NaCl] for alkaline Ferrocyt *c* at pH 12.9. At pH 12.9, as [glycerol] is raised starting from 0.0 to 5.6 M glycerol, the k_{ass} for Ferrocyt *c* decrease monoexponentially and plateau at ~4.0 M glycerol (Fig. 4.6b). At pH 12.9, the k_{ass} for Ferrocyt *c* also decreases monoexponentially with [trehalose] or [NaCl] and plateau at ~1.0 M [trehalose] or ~ 1.0 M [NaCl] (Fig. 4.6b). CO-association to Ferrocyt *c* is essentially a Fe^{2+}-M80→Fe^{2+}-CO displacement reaction, where the collisions between structural elements or different groups of atoms afforded by internal dynamics of the protein provide the energy necessary for CO-association. Because the local mobility of heme ring is suppressed by intrinsic

size and rigidity of ring system [49], and the neighboring residues of M80 have significantly higher thermal factors [50], so the collective motions of the M80-contaning Ω-loop should control the CO-association reaction [51]. The facts that k_{ass} decrease in the presence of stabilizing additive imply that the structural fluctuations of the M80 containing Ω-loop of Ferrocyt *c* are decreased [18]. The decrease in structural fluctuations of the Ω-loop in the presence of glycerol, trehalose and NaCl clearly demonstrates that the internal dynamics of alkaline Ferrocyt *c* is substantially constrained by glycerol, trehalose and NaCl.

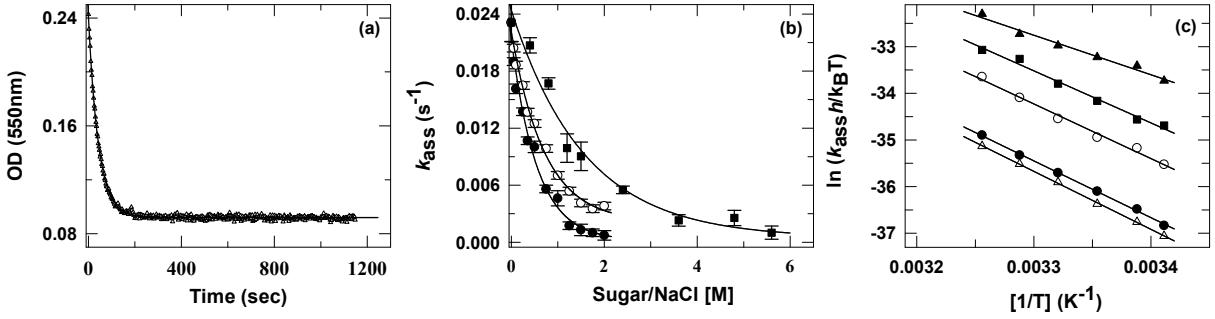

Fig. 4.6 Panel (a) represents the single phase CO-association kinetic trace of alkaline Ferrocyt *c* (τ = 0.7 min, pH 12.9, 25 °C). (b) Dependence of the rate of the CO-association of alkaline Ferrocyt *c* on different concentrations of glycerol (■), trehalose (●) and NaCl (○) at pH 12.9, 25 °C. The lines through the data in panel (b) have been drawn by inspection only. Panel (c) shows the Eyring plots for the CO-association reaction of alkaline Ferrocyt *c* in the absence (▲) and presence of 1.5 M glycerol (■),1.5 M trehalose (●) and 1.5 M NaCl (○) at pH 12.9. Panel (c) also shows the Eyring plot for the CO-association reaction of native Ferrocyt *c* in the absence of additive (Δ) at pH 7. The solid lines in panel (c) were fitted according to Eyring equation (equation (5)) [52]. The resulting values of $\Delta H_{ass}^{\ddagger}$, $\Delta S_{ass}^{\ddagger}$ and $-T\Delta S_{ass}^{\ddagger}$ are provided in Table 1.

Table 1 The effect of trehalose and NaCl on activation parameters for CO-association reaction of Ferrocyt *c*.*

	Additive	$\Delta G_{ass}^{\ddagger a}$ (kcal mol^{-1})	$\Delta H_{ass}^{\ddagger}$ (kcal mol^{-1})	$\Delta S_{ass}^{\ddagger}$ (cal mol^{-1} K^{-1})	$-T\Delta S_{ass}^{\ddagger a}$ (kcal mol^{-1} K^{-1})
pH 12.9	Control	19.8 (0.1)	16.9(1.2)	-9.6(3.9)	2.9(1.2)
	1.5 M glycerol	20.3(0.2)	22.3(1.3)	6.6(3.5)	-2.0(1.0)
	1.5 M trehalose	21.5(0.1)	24.3(0.4)	9.4(1.5)	-2.8(0.4)
	1.5 M NaCl	20.7(0.1)	23.4(1.2)	8.9(3.9)	-2.7(1.2)
pH 7	Control	21.7(0.3)	24.9(0.3)	10.7(0.9)	-3.2(0.3)

[a] Activation free energy ($\Delta G_{ass}^{\ddagger}$) and entropy changes ($-T\Delta S_{ass}^{\ddagger}$) are given at 25 ºC.
*The uncertainties (standard error) in $\Delta H_{ass}^{\ddagger}$, $-T\Delta S_{ass}^{\ddagger a}$ and $\Delta S_{ass}^{\ddagger}$ are indicated in parenthesis.

To test whether the glycerol, trehalose and NaCl influence the structural-fluctuation of

M80 containing Ω-loop entropically or enthalpically, the Eyring plots for CO-association reaction of alkaline Ferrocyt *c* obtained in the absence and presence of 1.5 M sugar (glycerol or trehalose) or NaCl at pH 12.9 (Fig. 4.6c) were analyzed using equation (5) [52],

$$\ln(k_{ass}h/k_B T) = (\Delta S_{ass}^{\ddagger}/R) - (\Delta H_{ass}^{\ddagger}/RT) \quad (5)$$

The estimated activation enthalpies ($\Delta H_{ass}^{\ddagger}$) and activation entropies ($\Delta S_{ass}^{\ddagger}$) are summarized in Table 1. By using the Gibbs free energy function, the corresponding activation free energies ($\Delta G_{ass}^{\ddagger}$) and $-T\Delta S_{ass}^{\ddagger}$ values were also estimated at 25 °C (Table 1). The data in Table 1 clearly suggests that the inclusion of glycerol, trehalose or NaCl in reaction medium increases the enthalpic barrier ($\Delta H_{ass}^{\ddagger}$) for CO-association reaction. This effect attributes to restricted internal dynamics of G_B, T_B and B-states as compared to the U_B-state. The $\Delta H_{ass}^{\ddagger}$ values obtained for CO-association to alkaline Ferrocyt *c* in the presence of 1.5 M glycerol, 1.5 M trehalose and 1.5 M NaCl approaches towards the value measured for the native protein at pH 7. However, these values of $\Delta H_{ass}^{\ddagger}$ are less than the value measured for the CO-association to native Ferrocyt *c* at pH 7, which indicates that the internal dynamics of G_B, T_B and B-states are less constrained as compared to the native Ferrocyt *c*. The data in Table 1 also give following important information, (i) the increase of $\Delta H_{ass}^{\ddagger}$ due to sugar (glycerol and trehalose) and salt (NaCl) is accompanied by a decrease in the entropy change $-T\Delta S_{ass}^{\ddagger}$ and (ii) the enthalpic effect is more dominant than the entropic effect in the presence of sugar (glycerol and trehalose) and salt (NaCl).

As described earlier [53-54], the enthalpy-entropy plot could be used to determine enthalpic and entropic contributions toward the stability, folding and dynamics of proteins. The enthalpy-entropy plot has four sectors (Fig. 4.7). Sectors 1 and 2 correspond to stabilizing cosolutes while sectors 3 and 4 correspond to destabilizing cosolutes. Furthermore, sectors 1 and 3 represent the enthalpically dominated effect while sector 2 and 4 represent entropically dominated effect [53]. Fig. 4.7 presents the $T\Delta\Delta S$ vs $\Delta\Delta H$ plots for 1.5 M glycerol and 1.5 M trehalose. Clearly, the data points for sugar lie in sector 1 (Fig. 4.7), which is in general agreement with the models that describe enthalpically dominated stabilization [53-55].

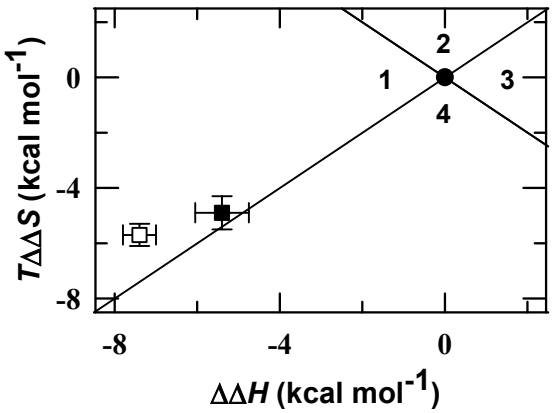

Fig. 4.7. The $T\Delta\Delta S$ and $\Delta\Delta H$ plot at pH 12.9. Data points correspond to in the absence (●) and presence of 1.5 M glycerol (■) and 1.5 M trehalose (□).

4.2.6 Heat and cold denaturation of the G_B and T_B-states of Ferricyt c

To determine the contribution of hydrophobic interactions in the thermal stability of the G_B and T_B-states, the thermal unfolding (CD 222 nm) transitions of protein were collected in the wide range of glycerol and trehalose concentrations. A previous study has shown that the base-denatured Ferricyt *c* in the presence of 1.0 M NaCl attains native-like peptide CD signals at −4 °C while they get unfolded at ~70 °C [19]. At very low salt concentration (0.01 M NaCl), the thermal melt of base-denatured protein exhibits two temperature transitions, the first correspond to cold denatutation and the second correspond to heat denaturation (Figs. 4.8a and 4.8b).

Figs. 4.8a and 4.8b show the thermal melts of base-denatured protein containing different concentrations of glycerol and trehalose, respectively. Since the low temperature CD signal varies with the stabilizing additive (glycerol and trehalose) concentration but the high temperature CD signal remained constant on varying the concentration of the stabilizing additive, hence, the thermal melts were normalized as described earlier [19]. Thermal denaturation of the U_B-state shows substantially reversibility [19], therefore, the normalized thermal unfolding transitions (Figs. 4.8a and 4.8b) were analyzed for thermal denaturation midpoint (T_m), enthalpy of denaturation (ΔH_m), and heat capacity change (ΔC_p) by using a non-linear least squares method according to the Gibbs Helmholtz equation (equation (3), chapter 2). The resulting T_m, ΔH_m and ΔC_p under various glycerol and trehalose concentrations are provided in Table 2. As glycerol and trehalose concentration is increased, both T_m and ΔH_m values

increase but the value of ΔC_p decreases (Table 2). At low glycerol and trehalose concentrations, the G_B and T_B-states undergoes cold denaturation (Figs. 4.8a and 4.8b). With increasing glycerol and trehalose concentrations, the low temperature unfolding transition becomes less obvious (Figs. 4.8a and 4.8b). Figs. 4.8c and 4.8d present the temperature dependent stability curves containing various glycerol and trehalose concentrations, respectively. These stability curves were calculated according to equation (4) (Chapter 2).

Table 2 Effect of glycerol and trehalose on the thermodynamic parameters (transition temperature, enthalpy and heat capacity) for unfolding of base-denatured Ferricyt *c* calculated from 222 nm CD data (pH 12.9).

	Gibbs-Helmholtz equation				van't Hoff equation[#]	
Additive (M)	T_m	ΔH_m	ΔC_p	T_c	T_m	ΔH_m
0.01 NaCl	288.3	20.1	1.11	256	290.6	25.9
Glycerol						
0.1	295.1	20.2	0.90	253	297.7	26.1
0.5	298.8	24.5	0.92	249	302.2	30.3
2.0	305.4	40.1	0.98	231	306.4	38.2
4.5	311.1	40.3	0.88	228	312.1	44.1
5.5	317.2	43.1	0.85	226	321.5	48.2
Trehalose						
0.1	292.8	24.5	1.04	249	295.9	31.7
0.25	304.7	38.7	1.01	235	305.0	37.6
0.5	309.1	47.2	0.99	224	309.7	46.6
1.0	319.3	54.2	0.95	219	319.5	55.0
1.5	333.1	63.4	0.90	211	333.6	65.5

* ΔH_m, ΔC_p, and T_m/T_c are reported as kcal mol^{-1}, kcal mol^{-1} K^{-1}, and K, respectively. The uncertainties of ΔH_m, T_m, T_c and ΔC_p values reported here are ±2 kcal mol^{-1}, ±0.5 K, ±0.5 K and ±0.2 kcal mol^{-1} K^{-1}, respectively.

[#] The normalized thermal unfolding transitions were analyzed using equation (2) (chapter 2).

Table 2 lists the midpoint temperature, T_c for the low temperature denaturation at different concentrations of glycerol and NaCl, obtained from the stability curves. It is observed that even very small concentration of glycerol and trehalose has a profound effect on the temperature dependent stability curve. In all cases, addition of glycerol and trehalose makes the stability curves wider, raises the maxima, and shifts them to lower temperatures (Figs. 4.8c and 4.8d). As glycerol and trehalose concentration are increased, the T_m increases and the T_c decreases (Figs. 4.8c and 4.8d and Table 2).

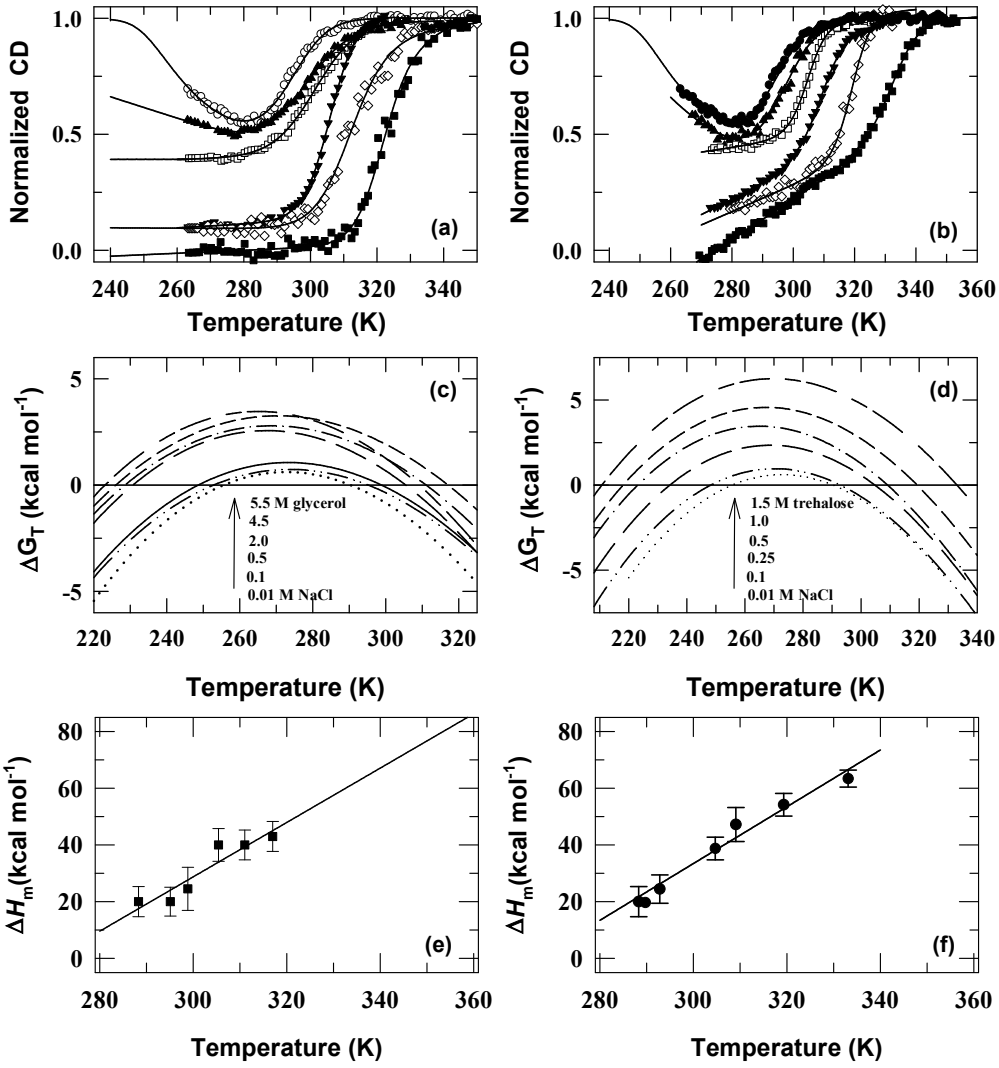

Fig. 4.8 (a) Temperature dependence of normalized peptide CD (222 nm) of base-denatured Ferricyt *c* in the presence of 0.01 M NaCl (○), 0.1 (▲), 0.5 (□), 2.0 (▼), 4.5 (◊), and 5.5 M glycerol (■) at pH 12.9. (b) Temperature dependence of normalized peptide CD (222 nm) of base-denatured Ferricyt *c* in the presence of 0.01 M NaCl (●), 0.1 (▲), 0.25 (□), 0.5 (▼), 1.0 (◊), and 1.5 M trehalose (■) at pH 12.9. The solid lines in panels (a) and (b) are fits according to equation (3) (chapter 2). The thermodynamic parameters derived from fits to CD data are listed in Table 2. (c) Temperature dependent stability curves of the base-denatured Ferricyt *c* in the presence of glycerol concentrations at pH 12.9, calculated by the use of equation (4) (chapter 2). Panel (d) show the temperature dependent stability curves of the base-denatured Ferricyt *c* in the presence of trehalose concentrations at pH 12.9, calculated by the use of equation (4) (chapter 2). (e) Determination of ΔC_p for thermal unfolding of the G_B-state by linear analysis of ΔH_m as a function of T_m. The ΔH_m values were obtained from fits of thermal data by the use of equation (3) (chapter 2). Slope of the straight line (ΔC_p) is ~0.96 (±0.1). (f) Determination of ΔC_p for thermal unfolding of the T_B-state by linear analysis of ΔH_m as a function of T_m. The ΔH_m values were obtained from fits of thermal data by the use of equation (3) (chapter 2). Slope of the straight line (ΔC_p) is ~1.00 (±0.1).

In general, the extreme pH or denaturants-induced partially denatured proteins show cold denaturation [19,56-57] but the molecular basis for this is not completely understood.An earlier report by Kuroda et al (1992) showed that the acid-denatured A-state of Ferricyt *c* in acid medium exhibit cold denaturation [14]. The current study shows that G_B and T_B-states exhibit cold denaturation in highly basic medium. According to an earlier report, cold denaturation of proteins is thought to arise from decrease in hydrophobic interactions at lower temperatures [58]. However, few earlier reports suggest that both hydrophobic and hydrophilic interactions play an important role in the cold denaturation process [59-60].

4.2.7 ΔC_p for the unfolding of the G_B and T_B-states

Figs. 4.8e and 4.8f show the ΔH_m *vs* T_m plot for the G_B and T_B-states of Ferricyt *c*, respectively. The linear least-squares fitting of the ΔH_m *vs* T_m plots provided the ΔC_p value 0.96(±0.1) (Fig. 4.8e) and 1.00(±0.1) (Fig. 4.8f) for the G_B and T_B-states of Ferricyt *c*, respectively. Within error, the ΔC_p values for the G_B and T_B-states are comparable to that of the already reported ΔC_p value of B-state (ΔC_p = 0.91(±0.17) but lower than the N-state (ΔC_p = 1.26±0.21 kcal mol^{-1} K^{-1}) [19,47]. Remarkably, the ΔC_p values for the G_B and T_B-states are significantly higher than the already reported ΔC_p value of A-state of Ferricyt *c* (ΔC_p = 0.38 (±0.03) [47]. The higher ΔC_p values for the unfolding of G_B and T_B-states, suggest significant contribution of hydrophobic interactions toward the stability of the G_B and T_B-states of Ferricyt *c*. Therefore, the weakening of the hydrophobic effect by low temperature is the likely reason for cold denaturation. The comparison of ΔC_p value for the N, G_B, T_B, B, U_B, and A states thus suggests that the degree of the hydrophobic interactions in G_B , T_B and B-states are higher than that of A-and U-states but are less than that of N-state (*i.e.*, N > T_B ~ G_B ~ B > A > U). The higher value of ΔC_p for the $U_B \rightarrow G_B$ and $U_B \rightarrow T_B$ transition (Table 2) further confirms that the hydrophobic interactions contribute significantly to the G_B and T_B states thermal stability.

4.2.8 Mechanism of MG formation by sugars

Several equilibrium and kinetic techniques have been used to determine the structure and stabilizing mechanism of A-and B-states of proteins [9-11, 12-21,23,59,44]. These studies showed that the salt drives the U_A and U_B-states of protein to MG state through the reduction of

the electrostatic repulsion between the charged groups of the protein. Few previous studies also showed that a balance between the electrostatic interactions of charged residues and the opposing forces such as hydrophobic interactions and hydrogen bonding determine the stability of MG-state [22,23,24]. At low salt concentrations, salt does not show much effect on the hydrogen bonding and hydrophobic interactions. These findings suggests that the electrostatic effects govern the formation of the MG-state [22,23,24].

Few previous studies showed that sugars can transform the U_A-state to MG-state [27-30]. The current study showed that the sugar such as glycerol and trehalose also transforms the U_B-states of Ferricyt *c* and Cyt-CO to MG-states. Both steric repulsions and protein-sugar binding interactions modulate the sugar-induced stabilization of proteins, where the steric repulsions are always stabilizing [28-29] while the binding interactions may be stabilizing or destabilizing, depending on the type and nature of the protein and sugar [28-29]. The contribution from steric repulsion is generally categorized as "excluded-volume effect" [28-29]. Among sugars, glycerol has an affinity for the protein [62], other sugars have minimal for proteins and therefore, water–protein interactions are possibly most important for them [29]. Saunderes et al reported that the stabilizing effect of glycerol and trehalose on acid-unfolded protein results from excluded-volume effect, with sugar-protein interactions reducing this stabilization effect [29]. Although, the molecular size of the larger polyol molecules determined the excluded volume effect [63], however, the electrostatic orientation of smaller polyol molecule such as glycerol also contributes towards the increase in the excluded volume effect [64]. In fact, for larger polyol molecules, the excluded volume will be predominantly determined by the molecular size of the polyol [64]. For G_B-state, the electrostatic orientation of glycerol at the protein surface should be considered, because for smaller polyols the increase in the excluded volume due to the electrostatic orientation of polyol molecules cannot be ignored [64]. Therefore, to explain the polyol-induced molecular compaction and increased conformational stability of protein requires assessment of the preferential hydration taking into consideration of the molecular size of the polyol, the electrostatic orientation of polyol molecules at the protein surface, and the volume increments of the local domain upon protein expansion. In the present study, the $T\Delta\Delta S$ vs $\Delta\Delta H$ plots for CO-association reaction of alkaline Ferrocyt *c* in the absence and presence of 1.5 M glycerol and 1.5 M trehalose reveal that in controlling the CO-association to alkaline Ferrocyt *c* in the presence of sugars, the enthalpic effect is more dominated than the

entropic effect (Fig. 4.7). These results contrast mechanisms that rely on direct steric repulsion between protein and sugar, and this enthalpic dominated mechanism cannot be explained by purely excluded volume effect [53]. Current results suggest that both excluded volume effect (hard-core repulsions) and nonspecific chemical (soft) interactions must be considered to understand the effects of sugar on the protein stability. The hydrophobic interactions also contribute to the G_B and T_B-states because thermal unfolding of G_B and T_B-states occurred through a positive heat capacity change.

4.3 Conclusion

In extreme basic medium, the glycerol and trehalose molecules stabilize the U_B-state of Cyt *c* to G_B and T_B-states. Current results suggest that both excluded volume effect and nonspecific chemical interactions contribute toward the glycerol and trehalose-induced stabilization and refolding of base-denatured Cyt *c* to G_B and T_B-states. The G_B and T_B-states meet with the basic molecular and structural organizational definition of the MGs (*i.e.,* molecular compact state containing native-like secondary structures and disordered tertiary structures). Thermal unfolding transitions of G_B and T_B-states are highly cooperative and are characterized by a large heat capacity change. This finding reveals that the hydrophobic effect also appears to contribute significantly toward the energetic stabilization of the G_B and T_B-states. The energetic stability of the G_B and T_B-states are reduced with decreasing temperature, and it undergoes cold denaturation. Analysis of the CO-association rate to the base-denatured Ferrocyt *c* in the presence of variable concentrations of glycerol and trehalose indicate substantially restricted overall motion and stiffness of the polypeptide chain in the G_B and T_B-states.

4.4 References

[1] Pabit SA, Roder H, Hagen SJ, Biochemistry 43:12532–12538 (2004)
[2] Jones CM, Henry ER, Hu Y, Chan CK, Luck S, Bhuyan AK, Roder H, Hofrichter J, Eaton WA, Proc Natl Acad Sci USA 90:11860–11864 (1993)
[3] Hagen SJ, Latypov RF, Dolgikh DA, Roder H, Biochemistry 41:1372–1380 (2002)
[4] Pascher T, Chesick JP, Winkler JR, Gray HB, Science 271:1558–1560 (1996)
[5] Telford JR, Wittung-Stafshede P, Gray HB, Winkler JR, Acc Chem Res 31:755–763 (1998)
[6] Chen E, Wittung-Stafshede P, Kliger DS, J Am Chem Soc 121:3811–3817 (1999)
[7] Chen E, Goldbeck RA, Kliger DS, J Phys Chem A 107:8149–8155 (2003)
[8] Chen E, Vranken VV, Kliger DS, Biochemistry 47:5450–5459 (2008)
[9] Ptitsyn OB, Adv Protein Chem 47:83–229 (1995)

[10] Kuwajima K, Arai M, The Molten Globule State: The Physical and Biological Significance in Mechanisms of Protein Folding (Pain, R. H., Ed.) 2nd ed., pp 138–174, Oxford University Press, New York (2000)
[11] Arai M, Kuwajima K, Adv Protein Chem 53:209–282 (2000)
[12] Kataoka M, Hagihara Y, Mihata K, Goto Y, J Mol Biol 229:591–596 (1993)
[13] Kataoka M, Nishii I, Fujisawa T, Ueki T, Tokunaga F, Goto Y, J Mol Biol 249:215–228 (1995)
[14] Kuroda Y, Kidokoro S, Wada A, J Mol Biol 223:1139–1153 (1992)
[15] Nishii I, Kataoka M, Tokunaga F, Goto Y, Biochemistry 33:4903–4909 (1994)
[16] Goto Y, Fink AL, Biochemistry 28:945–952 (1989)
[17] Nakamura S, Seki Y, Katoh E, Kidokoro S, Biochemistry 50:3116–3126 (2011)
[18] Rao DK, Kumar R, Yadaiah M, Bhuyan AK, Biochemistry 45:3412–3420 (2006)
[19] Kumar R, Prabhu NP, Rao DK, Bhuyan AK, J Mol Biol 364:483–495 (2006)
[20] Bhuyan AK, Biochemistry 49:7774–7782 (2010)
[21] Bhuyan AK, Biochemistry 49:7764–7773 (2010)
[22] Kuwajima K, Proteins: Struct, Funct, Genet 6:87–103 (1989)
[23] Goto Y, Nishikori S, J Mol Biol 222:679–686 (1991)
[24] Xie D, Freire E, Proteins 19:291–301 (1994)
[25] Potekhin S, Pfeil W, Biophys Chem 34:55–62 (1989)
[26] Hamada D, Kidokoro S, Fukada H, Takahashi K, Goto Y, Proc Natl Acad Sci USA 91:10325–10329 (1994)
[27] Kamiyama T, Sadahide Y, Nogusa Y, Gekko K, Biochim Biophys Acta 1434:44–57 (1999)
[28] Davis-Searles PR, Morar AS, Saunderes AJ, Erie DA, Pielak GJ, Biochemistry 37:17048–17053 (1998)
[29] Saunderes AJ, Davis-Searles PR, Allen DL, Pielak GJ, Erie DA, Biopolymers 53:293–307 (2000)
[30] Bongiovanni C, Sinibaldi F, Ferri T, Santucci R, J Protein chem 21:35–41 (2002)
[31] Jordan T, EADS JC, Spiro TG, Protein Science 4:716-728 (1995)
[32] Zhong S, Rousseau DL, Syun-Ru Yeh*J Am Chem Soc 126:13934-13935 (2004)
[33] Pielak GJ, Oikawa K, Mauk AG, Smith M, Kay CM, J Am Chem Soc 108:2724–2727 (1986)
[34] Santucci R, Polizio F, Desideri A, Biochimie 81:745–751 (1999)
[35] Bonincontro A, Bultrini E, Calandrini V, Cinelli S, Onori G, J Phys Chem B 104:6889–6893 (2000)
[36] Vanderkooi JM, Erecinska M, Eur J Biochem 60:199–207 (1975)
[37] Tsong TY, J Biol Chem 249:1988–1990 (1974)
[38] Pace CN, CRC Crit Rev Biochem 3:1–43 (1975)
[39] Goto Y, Takahashi N, Fink AL, Biochemistry 29:3480–3488 (1990)
[40] Schellman JA, Biopolymers 26:549–559 (1987)
[41] Alonso DO, Dill KA, Biochemistry 30:5974–5985 (1991)
[42] Mayo SL, Baldwin RL, Science 262:873–876 (1993)
[43] Knapp JA, Pace CN, Biochemistry 13:1289–1294 (1974)
[44] Goto Y, Calciano LJ, Fink AL, Proc Natl Acad Sci USA 87:573–577 (1990)
[45] Jain R, Kaur S, Kumar R, J Biochem 153:161–177 (2013)
[46] Hagihara Y, Aimoto S, Fink AL, Goto YJ, J Mol Biol 231:180–184 (1993)

[47] Hagihara Y, Tan Y, Goto Y, J Mol Biol 237:336–348 (1994)
[48] Bhuyan AK, Kumar R, Biochemistry 41:12821–12834 (2002)
[49] Morgan JD, McCammon J, Biopolymers 22:1579–1593 (1983)
[50] Berghuis, AM, GD Brayer, J Mol Biol 223:959–976 (1992)
[51] Kumar R, Prabhu NP, Yadaiah M, Bhuyan AK, Biophys J 87:2656–2662 (2004)
[52] Miksovská J, Day JH, Larsen RW, J Biol Inorg Chem 8:621–625 (2003)
[53] Sukenik S, Sapir L, Harries D, Curr Opin Colloid Interface Sci 18:495–501 (2013)
[54] Kumar R, Sharma D, Jain R, Kumar S, Kumar R, Biophys Chem 207:61–73 (2015)
[55] Sapir L, Harries D, Curr Opin Colloid Interface Sci 20:3–10 (2015)
[56] Privalov PL, Crit Rev Biochem Mol Biol 25:281–305 (1990)
[57] Privalov PL, Adv Protein Chem 33:167–241 (1979)
[58] Murphy KP, Freire E, Adv Protein Chem 43:313–361 (1992)
[59] Makhatadze GI, Privalov PL, Adv Protein Chem 47:307–425 (1995)
[60] Spolar RS, Livingstone JR, Record MT Jr, Biochemistry 31:3947–3955 (1992)
[61] Nakamura S, Kidokoro S, Biophys Chem 113:161–168 (2005)
[62] Timasheff SN, Annu Rev Biophys Biomol Struct 22:67–97 (1993)
[63] O'Connor TF, Debenedetti PG, Carbeck JD, Biophys Chem 127:51–63 (2007)
[64] Vagenende V, Yap MGS, Trout BL, Biochemistry 48:11084–11096 (2009)

Chapter 5
Effect of Sugars on the Thermodynamic Stability of pH-Denatured Hen Lysozyme Both in the Absence and Presence of Denaturants

5.1 Introduction

The effect of protecting osmolytes (glycerol, sugars, amino acids and methyl amines) and denaturants (Urea and GdnHCl) on protein stability are widely studied [1-50]. Urea and GdnHCl are widely used as denaturants [19-22]. They typically unfold the proteins through directly binding to them [23-26]. Timasheff and co-workers demonstrated that protecting osmolyte sugars stabilize the protein as a result of preferential hydration of the denatured state as compared to native state [27-28]. Thus, the folded state of the protein is stabilized relative to the unfolded state because it exposes less surface area from which the cosolvent must be excluded. Whereas, denaturants binds to, and stabilizes, the unfolded conformation, thereby favoring unfolding of proteins. Thermodynamically the protein stability is expressed as a free energy change (ΔG_D) between the native and unfolded states. Sugar favors the folded conformation through increasing the free energy of the unfolded conformation, whereas denaturant favors the unfolded conformation through lowering the free energy of the unfolded conformation. Generally, the protein denaturant interact favorably with the unfolded conformation, resulting in preferential accumulation of protein denaturant proximate to the protein surface and sugars interact unfavorably with the unfolded conformation, resulting in preferential depletion of protein stabilizer proximate to the protein surface. It is clear that sugars and denaturant act oppositely against protein stability by increasing and decreasing the ΔG_D between the native and unfolded states, respectively.

It is established that ΔG_D decreases linearly as a function of denaturant (urea and GdnHCl) [47-50] and increases as a function of sugars [27-28,30-33,35-37,39-40,42]. However, the ΔG_D as a function of denaturant in the presence of sugars has not been studied so far. To better understand the forces responsible for the sugar-induced increase in protein stability, this chapter evaluated the effect of sugars (glycerol, ribose, glucose, maltose, sucrose and trehalose) on the structural and thermodynamic properties of hen egg white lysozyme (Lyz) at pH 2.3 and pH 13. Fluorescence, near-UV CD, far-UV CD and 1-anilino-8-napthalene sulfonate (ANS) binding experiments suggest that the glycerol and trehalose transform the base denatured Lyz (pH 13) to MG-state. The effect of sugars (glycerol, ribose, glucose, maltose, sucrose and

trehalose) on the thermodynamic stability of Lyz at pH 2.3 was evaluated both in the absence and presence of denaturants (GdnHCl and urea). Thermodynamic analysis of thermal and denaturant-induced unfolding transitions of Lyz at pH 2.3 measured at different concentrations of sugars (glycerol, ribose, glucose, maltose, sucrose, and trehalose) reveals that these sugars increase the thermal and conformational stability of Lyz. Among the sugars used, the thermal and conformational stability of Lyz is increased more for trehalose and least for glycerol (trehalose > sucrose > maltose > glucose > ribose > glycerol). Thermodynamic analysis of thermal and denaturant-induced unfolding transitions of Lyz at pH 13 measured at different concentrations of sugars (glycerol and trehalose) reveals that the thermal and conformational stability of Lyz is increased more for trehalose than glycerol (trehalose > glycerol). Thermodynamic analysis of thermal and urea-induced unfolding transitions of Lyz at pH 2.3 measured at different concentration of GdnHCl or urea in the absence and presence of fixed concentration of sugars (glycerol, ribose, glucose, maltose, sucrose and trehalose) reveals that these sugars counteract the destabilizing effect of the denaturants. The counteraction effect of sugars on the destabilizing effect of the denaturants is more pronounced for trehalose and least for glycerol (trehalose > sucrose > maltose > glucose > ribose > glycerol).

5.2 Results and discussion

5.2.1 Base-denatured Lyz in the presence of sugars shows the generic properties of the MG-state

The fluorescence intensity of the Lyz decreases with a red shift in emission maxima on increasing the pH from neutral to alkaline [51-52] which suggests unfolding of protein [52]. Fig. 5.1a shows that fluorescence intensity of the Lyz decreases with a red shift in emission maxima from 350 to 360 nm on increasing the pH from 7 to 13 suggests protein unfolds under alkaline conditions. Base-denatured Lyz becomes molecular compact in the presence of high concentrations of trehalose and glycerol (Fig. 5.1a).

The far-UV CD spectrum (200-250 nm) of native Lyz exhibits two negative bands at 208 and 222 nm reflects the secondary structure of the protein [53-55]. Fig. 5.2a clearly shows that in the presence of 7 M GdnHCl, the negative ellipticity is completely disrupted, which suggests that the denaturant disrupt the secondary structure of native Lyz. However, the negative ellipticity of Lyz at 208 nm and 222 nm is not significantly affected at pH 2.3.

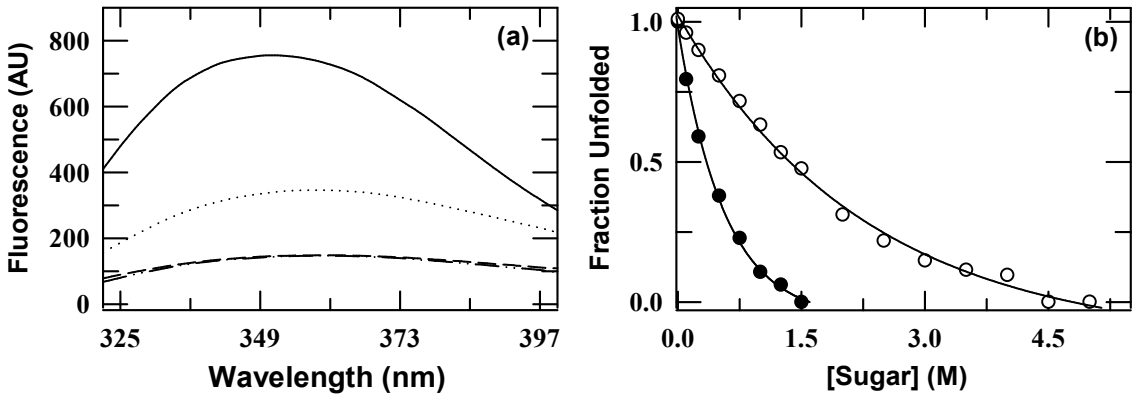

Fig. 5.1 (a) Fluorescence emission (ex: 280 nm) spectra of native Lyz at pH 7 (solid line), base denatured Lyz at pH 13 in the absence (dotted line) and presence of 5.0 M glycerol (short dash line) and 1.5 M trehalose (dash dot dot line). (b) The glycerol (○) and trehalose (●) dependent fluorescence monitored (ex: 280 nm, em: 360 nm) normalized folding transition of base-denatured Lyz at pH 13 (25 °C). The solid line through the data in panel (b) has been drawn by inspection only. The final proteins concentrations for fluorescence measurements in panels (a) and (b) were 10 μM.

The negative ellipticity of Lyz at 208 nm and 222 nm is significantly lost at pH 13 (Fig. 5.2a), indicating loss of secondary structure of Lyz at pH 13. Interestingly, the inclusion of sugars (trehalose and glycerol) in the base-denatured Lyz (pH 13) produces significant gain of the negative ellipticity of Lyz at 208 nm and 222 nm (Fig. 5.2a). This finding indicates that the sugars strengthen the secondary structures of base-denatured Lyz.

The near-UV CD spectrum (250-300 nm) of native Lyz exhibits sharp positive peak intensities between 290 and 280 nm [53-55], associated with the packing of tryptophan residues and with shorter wavelength contributions arising from tyrosine residues. Fig. 5.2b clearly shows that in the presence of 7.0 M GdnHCl, the positive peak intensities between 290 and 280 nm are completely disrupted, which reflects denaturant-induced loss of tertiary structure of native Lyz. The positive peak intensities between 290 and 280 are also significantly lost at pH 13 with the emergence of new positive peak ~252 nm (Fig. 5.2b), indicating significant loss of tertiary structure of Lyz at pH 13. However, the positive peak intensities between 290 and 280 nm are not greatly affected at pH 2.3. The inclusion of sugar (1.5 M trehalose or 5.0 M glycerol) in the base-denatured Lyz does not changes the peak intensities between 290 and 280 nm (Fig. 5.2b), which suggests that the presence of trehalose or glycerol does not lead to any change in the tertiary structure of base-denatured Lyz. The far-UV CD (Fig. 5.2a) and near-UV CD (Fig. 5.2b) results suggest that in the presence of high concentration of sugar, the base-denatured Lyz contains native-like secondary structure but disordered tertiary structure, a characteristic feature

of MG-state [56-58].

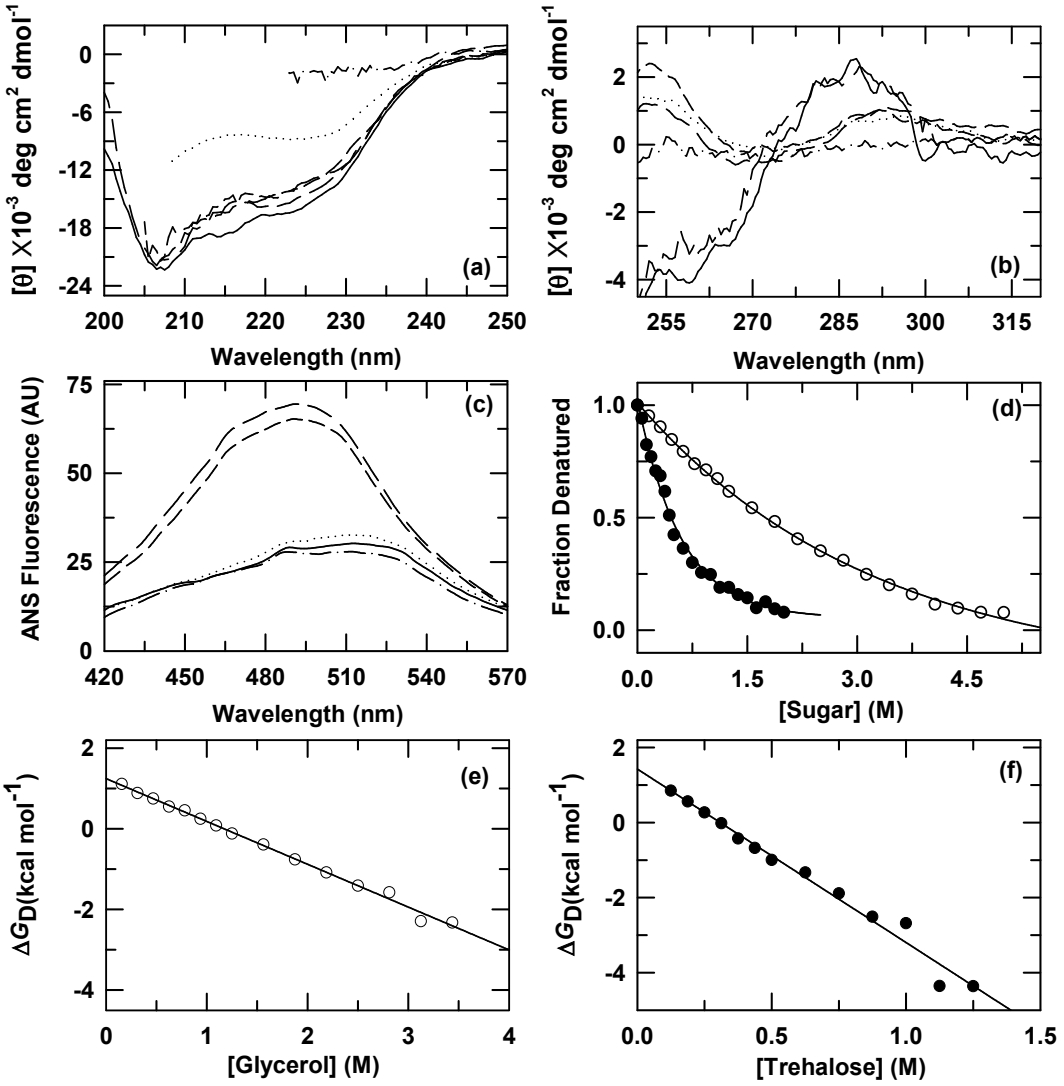

Fig. 5.2 Panels (a) and (b) show the far-UV CD and near-UV CD spectra for native (solid line) Lyz at pH 7, GdnHCl-denatured (7 M GdnHCl) Lyz at pH 7 (dash dot line), Lyz at pH 2.3 (long dash line) and base-denatured Lyz at pH 13 in the absence (dotted line) and presence of 5.0 M glycerol (short dash line) and 1.5 M trehalose (medium dash line), respectively. The final concentrations of Lyz used for the far-UV CD and near-UV CD measurements were 10 μM and 50 μM, respectively. (c) ANS fluorescence spectra of native Lyz at pH 7 (solid line), GdnHCl-denatured (7 M GdnHCl) Lyz at pH 7 (dash dot line) and base-denatured Lyz at pH 13 in the absence (dotted line) and presence of 5.0 M glycerol (short dash line) and 1.5 M trehalose (medium dash line). For ANS fluorescence measurements final concentrations of Lyz was 10 μM. (d) The glycerol (○) and trehalose (●)-induced folding transition (CD 222 nm) of base-denatured Lyz (10 μM) at pH 13. The solid line through the data in panel (d) has been drawn by inspection only. (e) Shows unfolding free energy changes in the transition region calculated from the equilibrium curve (panel (d)) for glycerol. The linear least-squares best fit of the data to equation (2) provided, ΔG^{o} = 1.25 Kcal mol^{-1} and m = 1.07 kcal mol^{-1} M^{-1}. (f) Shows unfolding free energy changes in the transition region calculated from the equilibrium curve (panel (d)) for trehalose. The linear least-squares best fit of the data to equation (2) provided, ΔG^{o} = 1.45 Kcal mol^{-1} and m = 4.67 kcal mol^{-1} M^{-1}.

The binding of ANS to the hydrophobic regions of MG-state of proteins generally increases the ANS fluorescence intensity [56,59–61]. Fig. 5.2c presents the ANS fluorescence spectra of the native and GdnHCl-denatured Lyz at pH 7, and base-denatured Lyz at pH 13 in the absence and presence of sugar (1.5 M trehalose and 5.0 M glycerol). Fig. 5.2c clearly suggests that the ANS fluorescence intensity of the base-denatured Lyz is significantly increased in the presence of sugar (1.5 M trehalose and 5.0 M glycerol) then its absence, which indicates that in the presence of sugar there are sizeable amounts of exposed hydrophobic regions in the base-denatured Lyz. Intrinsic fluorescence, near-UV CD, far-UV CD and ANS binding experiments suggest that the glycerol and trehalose-induced MG-states of base-denatured Lyz are molecular compact states containing native-like secondary structural contents but disordered tertiary interactions.

Fig. 5.2d presents the glycerol and trehalose titration (CD 222 nm) of base-denatured Lyz at pH 13. The Gibbs free energy change, ΔG, for the two-state transition, can be calculated by the equation (1),

$$\Delta G = -RT \ln K = -RT \ln\left[(Y_{obs} - Y_U) / (Y_{MG} - Y_{obs}) \right] \quad (1)$$

where, Y_{obs} is the observed value of the CD signal, Y_U and Y_{MG} are the CD signal intensities for the base-denatured Lyz and MG-states, respectively. By assuming a linear dependence of ΔG on sugar concentration [62], the least-squares fit of the data to equation (2),

$$\Delta G = \Delta G^0 + m[\text{sugar}] \quad (2)$$

provides, ΔG^o = ~1.25 Kcal mol^{-1} and m (slope reflecting the cooperativity of the transition) = ~1.07 kcal mol^{-1} M^{-1} for glycerol (Fig. 5.2e) and ΔG^o = ~1.45 Kcal mol^{-1} and m = ~4.67 kcal mol^{-1} M^{-1} for trehalose (Fig. 5.2f). Clearly the ΔG^o values for glycerol and trehalose are almost identical, suggesting that ΔG^o is independent of the nature of the protecting osmolyte and thus it is a property of the protein alone. The high m value for trehalose (~4.67 kcal mol^{-1} M^{-1}) than glycerol (~1.07 kcal mol^{-1} M^{-1}) suggests high effectiveness of trehalose towards refolding of base-denatured Lyz to MG-state as compared to glycerol.

5.2.2 Sugars increase the thermal stability of Lyz

To find out the effect of sugars on the thermal stability of Lyz, the absorbance (292 nm) and far-UV CD (222 nm) monitored thermal denaturation curves were collected in the absence and presence of different concentrations of sugar (trehalose, sucrose, maltose, glucose, ribose,

glycerol) at pH 2.3 and pH 13, respectively. Fig. 5.3a shows the representative absorbance (292 nm) monitored thermal denaturation curves as the change in extinction coefficient in the absence and presence of different concentration of trehalose at pH 2.3. Figs. 5.3b and 3c show the absorbance (292 nm) and far-UV CD (222 nm) monitored normalized thermal denaturation curves in the absence and presence of different concentration of trehalose at pH 2.3 and pH 13, respectively. Figs. 5.3b and 5.3c show that thermal denaturation curves shift to higher temperature with the increment in trehalose concentration. To determine the sugar dependency of denaturation enthalpy change (ΔH_m) and thermal denaturation midpoint (T_m), the normalized thermal denaturation data were analyzed by using equation (2) (chapter 2). The resulting T_m and ΔH_m of Lyz at pH 2.3 and pH 13 as a function of sugars are summarized in Tables 5.1 and 5.2 (appendix), respectively. Figs. 5.4a and 5.4b show the variation in T_m as a function of sugar at pH 2.3 and pH 13, respectively which suggests that T_m increases linearly with increasing concentration of sugar. Fig. 5.4a shows that among the sugar used (trehalose, sucrose, maltose, glucose, ribose, glycerol), the thermal stability of Lyz at pH 2.3 is increased more for trehalose and least for glycerol (trehalose > sucrose > maltose > glucose > ribose > glycerol). Fig. 5.4b shows that the T_m of Lyz at pH 13 is increased more for trehalose than glycerol. This result is consistent with the earlier reports that found that the sugars increase the thermal stability of proteins [27-42].

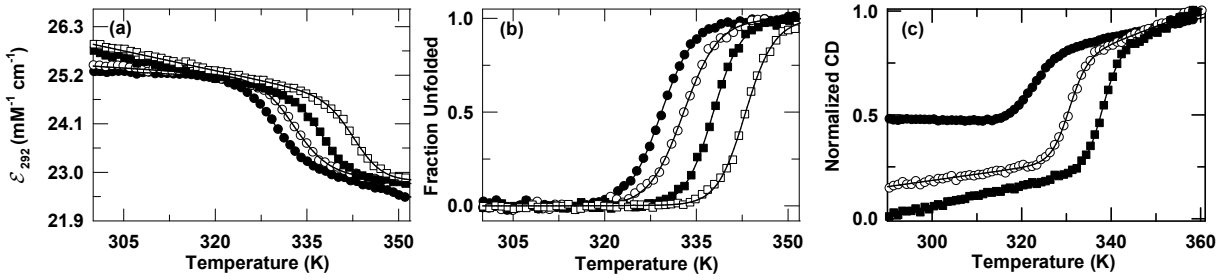

Fig. 5.3 Panel (a) shows thermally-induced unfolding of Lyz monitored at 292 nm as the change in extinction coefficient in the absence (•) and presence of 0.5 (o), 1.0 (■), and 1.5 M (□) solution of trehalose at pH 2.3. Panel (b) shows the normalized thermal-induced unfolding of Lyz monitored at 292 nm in the absence (•) and presence of 0.5 (o), 1.0 (■), and 1.5 (□) M solution of trehalose at pH 2.3. (c) Temperature dependence of normalized peptide CD (222 nm) of Lyz in the absence (●) and presence of 0.5 M trehalose (o) and 1.0 M trehalose (■) at pH 13. The solid curves in panels (a) to (c) represent nonlinear least-squares fit to equation (2) (chapter 2).

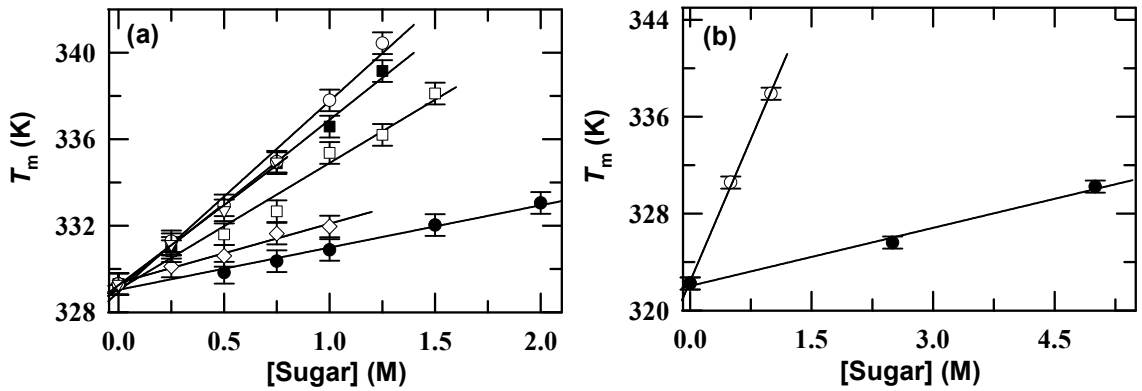

Fig. 5.4 (a) T_m of Lyz at pH 2.3 as a function of sugar (glycerol (●), ribose (◊), glucose (□), maltose (■), sucrose (∇) and trehalose (○)). (b) T_m of Lyz at pH 13 as a function of sugar (glycerol (●) and trehalose (○)). In panels (a) and (b) the solid curves represent linear least-squares fitting.

Among the glycerol, ribose, glucose, maltose, sucrose and trehalose, the stabilization effect is stronger for trehalose and weaker for glycerol (trehalose > sucrose > maltose > glucose > ribose > glycerol), which suggests that the size of sugar plays an important role in the sugar-induced stabilization of protein. Among the disaccharides, trehalose, sucrose and maltose, the stabilizing effect of trehalose dominates over the maltose. This variable effect of these disaccharides suggests that the physico-chemical properties of sugar also play an important in the sugar-induced protein stabilization. Previously, the size dependent stabilizing effect of sugar was explained on the basis of increased steric repulsion between the protein and sugar using sphere particle theory [44]. A previous report also revealed that the addition of sugar of larger molecular size results in increased total packing fraction of the solution, leading to the more stability of the native state relative to that of the unfolded state [63]. Present study shows that the observed effect of sugar on thermal stability of Lyz is a combination of a repulsive excluded volume effect between protein and sugar and attractive chemical interaction. The preferential interactions of cosolvent molecules with the native and denatured state of protein govern their stabilization effect [64]. Sugar plays a crucial role in the stabilization of proteins because they induce preferential hydration for protein and therefore excluded from the immediate vicinity of the protein.

5.2.3 Sugar counteracts the destabilizing effect of the denaturants against thermal denaturation

To find out the effect of sugar on the destabilizing effect of the denaturants against

thermal denaturation of Lyz, the absorbance (292 nm) monitored denaturant (GdnHCl and urea) dependent thermal denaturation curves were collected in the absence and presence of 0.75 M sugar (glycerol, ribose, glucose, maltose, sucrose and trehalose) at pH 2.3 Figs. 5.5a and 5.5b show the representative absorbance monitored GdnHCl (Fig. 5.5a) and urea (Fig. 5.5b)-dependent thermal denaturation curves as the change in extinction coefficient of Lyz at pH 2.3 in the absence and presence of 0.75 M trehalose, respectively. Figs. 5.5c and 5.5d show the representative absorbance (292 nm) monitored GdnHCl and urea-dependent normalized thermal denaturation curves of Lyz at pH 2.3 in the absence and presence of 0.75 M trehalose, respectively. The thermal denaturation curve shifts to lower temperatures in the presence of denaturant (Figs. 5.5c and 5.5d). Figs. 5.5c and 5.5d also show that in the presence of 0.75 M trehalose, the denaturant-mediated shift in the thermal denaturation curve is less pronounced. To find out the effect of sugar on the denaturant dependent thermodynamic parameters (T_m and ΔH_m), the thermal denaturation curves collected as a function of denaturant (GdnHCl and urea) were analyzed by equation (2) (chapter 2). The resulting parameters T_m, and ΔH_m, are given in Tables 5.3 and 5.4 (appendix).

Figs. 5.5e and 5.5f show that T_m decreases linearly with increasing concentration of GdnHCl and urea, respectively. Interestingly, in the presence of 0.75 M sugar, the T_m versus denaturant concentration plot shifts upward (Figs. 5.5e and 5.5f). These results thus suggest that the sugar shift the denaturant-dependent thermal denaturation curve toward the higher temperature, which signifies the counteracting ability of sugar against deleterious effect of denaturant on the temperature-induced protein denaturation. This counteracting ability of sugar is found to be more for trehalose and least for glycerol (trehalose > sucrose > maltose > glucose > ribose > glycerol) (Figs. 5.5e and 5.5f). Timasheff et al have reported that protecting osmolyte counteracts the denaturing effect of denaturant mainly by altering the balance between preferential binding of denaturant and preferential exclusion of protecting osmolytes, resulting in the increased hydration of the protein [65-66]. Similarly, in case of Lyz, it is expected that the addition of sugar alters the balance between the preferential binding of denaturant (GdnHCl and urea) and preferential exclusion of sugar, results in the increased hydration of the protein and helps in the counteraction of the destabilizing action of the denaturant.

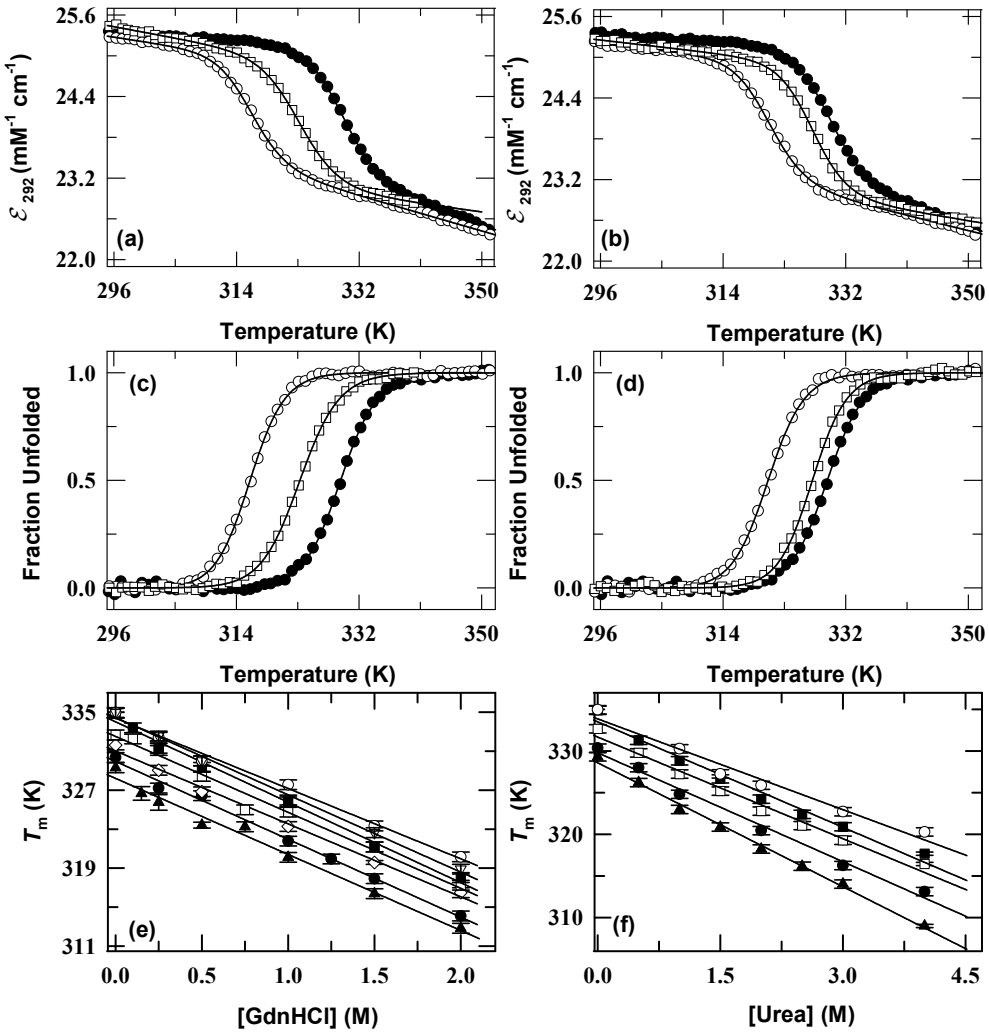

Fig. 5.5 Panel (a) shows thermally-induced unfolding of Lyz monitored at 292 nm as the change in extinction coefficient in the absence (•) and in the presence of 1.5 M GdnHCl (o) and 1.5 M GdnHCl with 0.75 M trehalose (□) at pH 2.3. Panel (b) show thermally-induced unfolding of Lyz monitored at 292 nm as the change in extinction coefficient in the absence (•) and in the presence of 1.5 M urea (o) and 1.5 M urea with 0.75 M trehalose (□) at pH 2.3. Panel (c) shows the normalized thermal-induced unfolding of Lyz monitored at 292 nm in the absence (•) and in the presence of 1.5 M GdnHCl (o) and 1.5 M GdnHCl with 0.75 M trehalose (□) at pH 2.3. Panel (d) shows the normalized thermal-induced unfolding of Lyz monitored at 292 nm in the absence (•) and in the presence of 1.5 M urea (o) and 1.5 M urea with 0.75 M trehalose (□) at pH 2.3. The solid curves in panels (a) to (d) represent nonlinear least-squares fit to equation (2) (chapter 2). (e) T_m of Lyz at pH 2.3 as a function of GdnHCl both in the absence (▲) and presence of 0.75 M sugar (glycerol (●), ribose (◊), glucose (□), maltose (■), sucrose (▽) and trehalose (○)). (f) T_m of Lyz at pH 2.3 as a function of urea both in the absence (▲) and presence of 0.75 M sugar (glycerol (●), glucose (□), maltose (■) and trehalose (○)). In panels (e) and (f), the solid curves represent linear least-squares fitting.

5.2.4 Sugars increases the conformational stability of Lyz

To find out the effect of sugars on conformational stability of Lyz, the fluorescence monitored denaturant (urea and GdnHCl)-induced unfolding curves were collected in the absence and presence of different sugar (glycerol, ribose, glucose, maltose, sucrose and trehalose) at pH 2.3 and pH 13. Fig. 5.6a shows the representative fluorescence monitored urea-induced normalized unfolding curves of Lyz in the absence and presence of 1.5 M sugar (glycerol, ribose, glucose, maltose, sucrose and trehalose) at pH 2.3. Fig. 5.6b shows the representative fluorescence-monitored GdnHCl-induced normalized unfolding curves of Lyz in the absence and presence of 1.5 M trehalose and 5.0 M glycerol at pH 13. Figs. 5.6a and 5.6b show that the denaturant-induced unfolding curve shifts to higher concentrations of denaturant in the presence of sugar. The unfolding transitions were analyzed using equation (1) (chapter 2) assuming a two state transition between the folded and unfolded conformations. The resulting free energy of denaturation (ΔG_D), surface area exposed by solvent (m_g), and midpoint denaturant concentration (C_m) for unfolding of Lyz at pH 2.3 and pH 13 in the presence of different concentration of sugar are provided in Tables 5.5 and 5.6 (appendix). Figs. 5.6c and 5.6d show the C_m as a function of sugars at pH 13 and pH 2.3, respectively.

Fig. 5.6c shows that among the sugars used, the C_m for Lyz at pH 2.3 is increased more for trehalose and least for glycerol (trehalose > sucrose > maltose > glucose > ribose > glycerol). Fig. 5.6d shows that the C_m for Lyz at pH 13 is increased more for trehalose than glycerol. The increase in ΔG_D in the presence of sugar at pH 13 and pH 2.3 indicates that sugar increase the conformational stability of the Lyz (Tables 5.5 and 5.6) (appendix). The ΔG_D for Lyz at pH 2.3 is increased more for trehalose and least for glycerol (trehalose > sucrose > maltose > glucose > ribose > glycerol) (Table 5.5) (appendix). At pH 13, the ΔG_D for Lyz is increased more for trehalose than glycerol (Table 5.6) (appendix).

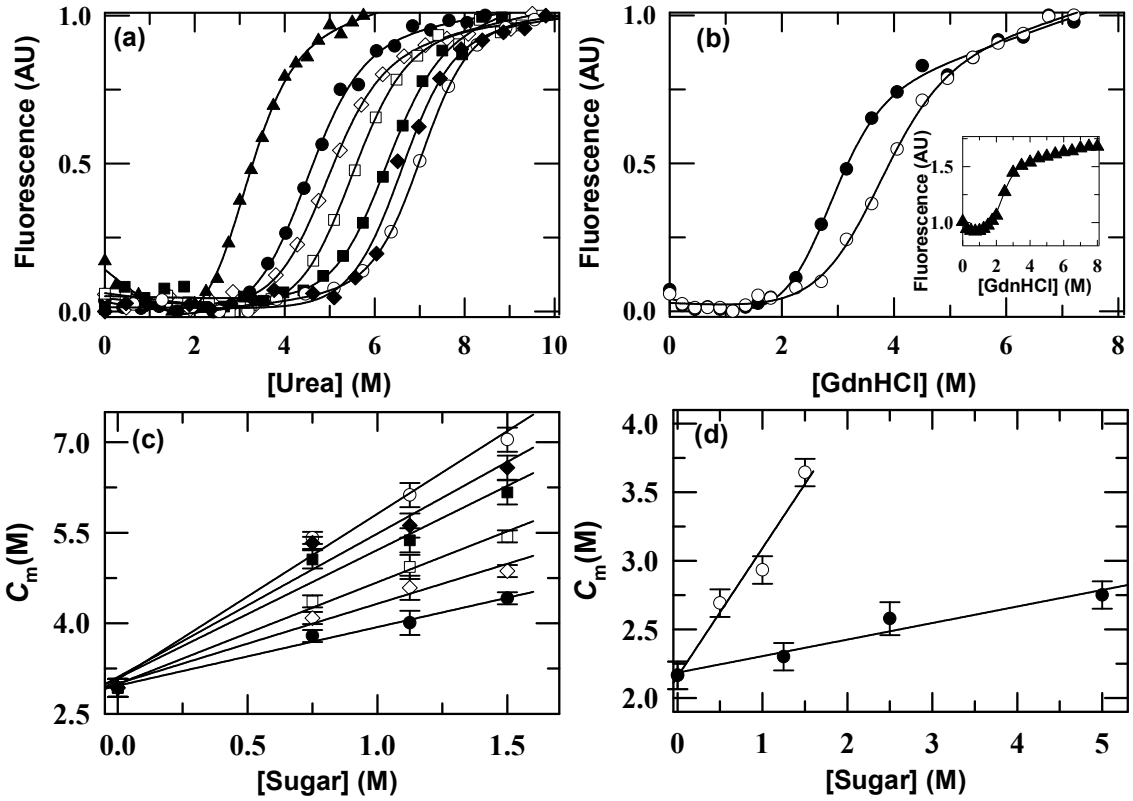

Fig. 5.6 Panel (a) represents fluorescence monitored (ex: 280 nm, em: 360 nm) urea-induced normalized unfolding transitions of Lyz in the absence (▲) and presence of 1.5 M sugar (glycerol (●), ribose (◊), glucose (□), maltose (■), sucrose (♦) and trehalose (○)) at pH 2.3. Panel (b) represents fluorescence monitored (ex: 280 nm, em: 360 nm) GdnHCl-induced normalized unfolding transitions of Lyz in the absence (▲) (Inset) and presence of sugar (5.0 M glycerol (●) and 1.5 M trehalose (○)) at pH 13. The solid lines in panels (a) and (b) represent the iterated least-squares fit of the data to a two-state unfolding transition (equation (1), chapter 2). Panel (c) shows C_m (urea) as a function of sugar (glycerol (●), ribose (◊), glucose (□), maltose (■), sucrose (♦) and trehalose (○)) at pH 2.3. Panel (d) shows C_m (GdnHCl) as a function of sugar (glycerol (●) and trehalose (○)) at pH 13. In panels (c) to (d) the solid curves represent linear least-squares fitting.

5.2.5 Sugars counteract the destabilizing effect of the denaturants against chemical denaturation of Lyz

To find out the effect of sugars on the destabilizing effect of the denaturants against chemical denaturation of Lyz, the fluorescence-monitored GdnHCl dependent urea-denaturation curves were collected in the absence and presence 0.75 M sugars (glycerol, ribose, glucose, maltose, sucrose and trehalose) at pH 2.3. Fig. 5.7a shows that the urea-induced unfolding curve shifts to lower concentration in the presence of 1.5 M GdnHCl. However, when 0.75 M trehalose is included in the presence of 1.5 M GdnHCl, the urea-induced unfolding curve shifts to higher

urea concentration, which indicates sugars counteract the destabilizing effect GdnHCl. To find out the effect of sugars on GdnHCl dependent ΔG_D and C_m of Lyz, the urea-denaturation curves collected in the absence and presence of 0.75 M sugars were analyzed by using equation (1) (chapter 2). The resulting ΔG_D and C_m are provided in Table 5.7 (appendix).

Figs. 5.7b and 5.7c clearly show that C_m and ΔG_D decrease linearly with increasing GdnHCl concentration and in the presence of 0.75 M sugars the ΔG_D and C_m versus [denaturant] plot shifts upward. These results suggest the counteracting ability of sugars against the deleterious effect of denaturant on the denaturant-induced protein unfolding. The denaturant dependent C_m and ΔG_D of Lyz are increased more for trehalose and least for glycerol suggests the counteraction effect of sugars against the destabilizing action of the denaturants is more pronounced for trehalose and least for glycerol (trehalose > sucrose > maltose > glucose > ribose > glycerol). These results indicates that in the sugar-denaturant solution, sugar alters the balance between the preferential binding of denaturant (GdnHCl and urea) and preferential exclusion of sugar, resulting in the increased hydration of the protein and counteracts the destabilizing action of the denaturant.

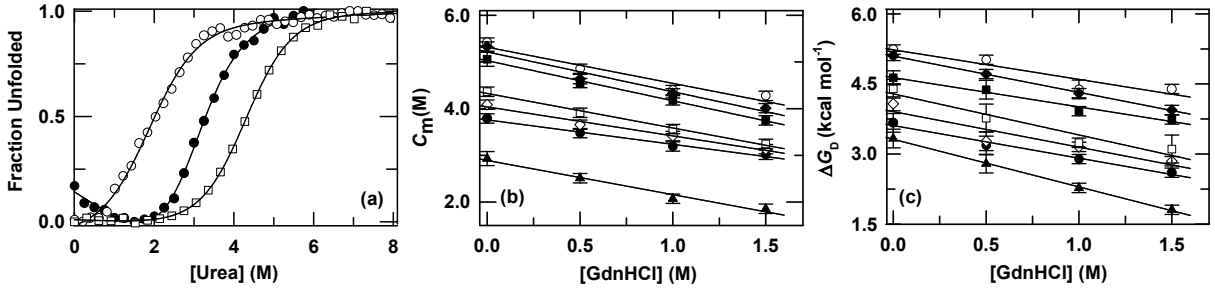

Fig. 5.7 Panel (a) shows the fluorescence monitored (ex: 280 nm, em: 360 nm) urea-induced normalized unfolding transitions of Lyz in the absence (●) and in the presence of 1.5 M GdnHCl (o) and 1.5 M GdnHCl with 0.75 M trehalose (□). The solid lines in panel (a) represent the iterated least-squares fit of the data to a two-state unfolding transition (equation (1), chapter 2). (b) Shows urea midpoint concentration (C_m) as a function of GdnHCl in the absence (▲) and presence of 0.75 M sugar (glycerol (●), ribose (◊), glucose (□), maltose (■), sucrose (♦) and trehalose (○)). (c) Shows free energy of denaturation (ΔG_D) as a function of GdnHCl in the absence (▲) and presence of 0.75 M sugar (glycerol (●), ribose (◊), glucose (□), maltose (■), sucrose (♦) and trehalose (○)). In panels (b) to (c) the solid curves represent linear least-squares fitting.

5.2.6 Analysis of thermal denaturation of Lyz at pH 2.3 in different denaturant and sugar with varied water activity

The reciprocal form of Wyman-Tanford (WT) equation (equation (1)) can be applied to determine the change in the hydration number per protein molecule (Δi) upon unfolding of Lyz in different denaturant and sugars solutions [67-69],

$$dlnK_{D,S}/dlna_W = \left[\Delta i - \left(X_W/X_Y\right)\Delta j\right] \quad (1)$$

where $K_{D,S}$ (=[D]/[N]), a_W is water activity, $(X_w/X_Y)\Delta j$ is the cosolute-binding terms, X_w and X_Y are the mole fractions of water and cosolute, respectively, and Δj is the change in bound-cosolute molecules per protein molecule. Fig. 5.8a presents the $lnK_{D,S}$ *vs* lna_W plots for unfolding of Lyz at pH 2.3 in different concentrations of denaturants and sugar. For each denaturant and sugar, the slope of reciprocal WT plot (Δi- $(X_w/X_Y)\Delta j$) was derived from linear least square fitting of data in Fig. 5.8a to equation (1) for Lyz at pH 2.3. The slope was dependent upon the type of denaturant and sugar (Table 1). The positive and negative slopes were obtained for sugar (glycerol, ribose, glucose, maltose, sucrose and trehalose) and denaturant (urea and GdnHCl), respectively. Sucrose and trehalose are nonreducing sugars thus no chemical interaction with the protein would be expected. For sucrose, the term $(X_W/X_Y)\Delta j$ in equation (1) is negligible [67,70-71], which provides the value of Δi = 130.3 mol/mol-protein for Lyz at pH 2.3. Using this Δi value, the binding term, $(X_W/X_Y)\Delta j$ for each denaturant and sugar was calculated from the slope in Fig. 5.8a. When the concentration of the cosolute is fixed, the term Δj can be easily determined from the solute binding term, $(X_W/X_Y)\Delta j$ (Table 2). As compared to urea, the Δj value is found more for GdnHCl. Reducing sugars (maltose, glucose and ribose) and glycerol showed small Δj suggesting that these sugars weakly bind to proteins upon unfolding. The negative value of Δj for trehalose suggests that it binds preferentially to a folded protein than an unfolded one [27,42].

Table 1 Slope of the reciprocal Wyman-Tanford plot for Lyz at pH 2.3 (equation (1)).

Cosolute	Urea	GdnHCl	glycerol	Ribose
	-87.4	-133.0	29.0	47.1
Cosolute	Glucose	Maltose	sucrose	Trehalose
	103.9	120.7	130.3	160.5

Table 2 Number of change in bound-cosolute molecules upon protein unfolding, Δj, at cosulute concentration o 1 mol/kg-solvent for Lyz at pH 2.3.

Cosolute	Urea	GdnHCl	glycerol	Ribose
	3.9	4.7	1.8	1.5
Cosolute	Glucose	maltose	sucrose	Trehalose
	0.5	0.2	00	-0.5

Green and Pace [72-73] proposed a linear extrapolation model (LEM) for $\Delta\Delta G$:

$$\Delta\Delta G = m[m_Y] \quad (2)$$

where $\Delta\Delta G$ is the free energies difference for protein unfolding in denaturant solution and water, m_Y is the concentration of cosolute (mol/kg-solvent), and m is an empirical parameter. The m-value is negative for chaotropic cosolvents (*i.e.* denaturants) while it is positive for kosmotropic cosolvents (*i.e.,* sugars). To determine the exact effect of [cosolute] on $\Delta\Delta G$, equation (2) can be applied for analyzing the value of Δi for protein unfolding in sugar and denaturant solutions [68,71,74],

$$\Delta lnK_D - \Delta lnK_{D,0} = \left[\Delta i - \left(X_W/X_Y\right)\Delta j\right] lna_W \quad (3)$$

By relating the $\Delta\Delta G$ to $[\Delta i-(X_w/X_Y)\Delta j]$ and $\ln a_W$, one can obtain the possible role of water activity in protein stability [71,74],

$$\Delta\Delta G = -RT\left(\Delta lnK_D - \Delta lnK_{D,0}\right) = -RT\left[\Delta i - \left(X_W/X_Y\right)\Delta j\right] lna_W \quad (4)$$

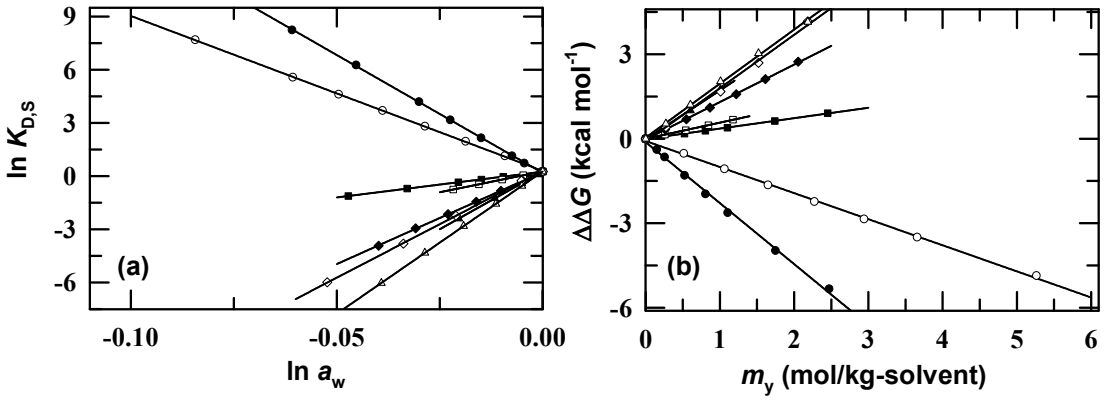

Fig. 5.8 (a) Reciprocal form of WT plot: Effect of water activity on unfolding ratio of Lyz in denaturant (urea (o), GdnHCl (●)) and sugar (glycerol (■), ribose (□), glucose (♦), maltose (◊), sucrose (▲), trehalose (Δ)) solution at pH 2.3, 333.0 K. (b) $\Delta\Delta G$ is plotted as a function of denaturant and sugar concentration (m_y) (denaturant (urea (o), GdnHCl (●)) and sugar (glycerol (■), ribose (□), glucose (♦), maltose (◊), sucrose (▲), trehalose (Δ)) at pH 2.3. The solid curves represent linear least-squares fitting.

Table 3 m-value of denaturants and sucrose for Lyz unfolding (equation (4)).

cosolute	urea	Gdnhcl	glycerol	ribose
	-0.9	-2.2	0.4	0.6
cosolute	glucose	maltose	Sucrose	trehalose
	1.3	1.9	1.7	1.9

The m-value is reported as kcal mol$^{-1}m^{-1}$. The uncertainties of m- value reported here is ± 0.2 kcal mol$^{-1}m^{-1}$.

Since $\ln a_W$ is zero or negative ($a_W \leq 1$), so the term Δi should always stabilize the protein (equation (3)). In contrast, the term, $(X_W/X_Y)\Delta j$, always destabilize the proteins unless Δj is negative [27,42]. Equation (2) also provides a theoretical basis for the LEM model. From equation (4), the $\Delta\Delta G$ was obtained as a function of [cosolute]. Fig. 5.8b shows the plots of $\Delta\Delta G$ against [cosolutes] (m_Y (mol/kg-solvent)) for Lyz at pH 2.3. $\Delta\Delta G$ was found to depend linearly on [cosolutes]. This indicates the applicability of LEM model. For each denaturant and sugar, the slope (m-value) was calculated from the $\Delta\Delta$G *vs* m_Y plots (Fig. 5.8b). The m-values for denaturant and sugar were summarized in Table 3. Table 3 clearly indicates that the m-value depends on the type of denaturant and sugar used.

5.3 Conclusion

Fluorescence, near-UV CD, far-UV CD and ANS binding experiments suggest that the glycerol and trehalose transform the base denatured Lyz at pH 13 to MG-state. The sugar-induced MG-state of base-denatured Lyz (pH 13) exhibits the generic properties of MG-state. Thermodynamic analysis of thermal and denaturant-induced unfolding transitions of Lyz at pH 2.3 and pH 13 measured at different concentrations of sugars (glycerol, ribose, glucose, maltose, sucrose and trehalose) reveals that these sugars increase the thermal and conformational stability of Lyz. Among the sugars used, the thermal and conformational stability of Lyz is increased more for trehalose and least for glycerol (trehalose > sucrose > maltose > glucose > ribose > glycerol). Thermodynamic analysis of thermal and urea-induced unfolding transitions of Lyz at pH 2.3 measured at different concentration of GdnHCl or urea in the absence and presence of fixed concentration of sugar (glycerol, ribose, glucose, maltose, sucrose and trehalose) reveals that these sugars counteract the destabilizing effect of the denaturants. The counteraction effect of sugar on the destabilizing action of the denaturants is more pronounced for trehalose and least for glycerol (trehalose > sucrose > maltose > glucose > ribose > glycerol). The stabilizing effect of sugar is mainly due to preferential exclusion of sugar from the protein surface. Interestingly, in the sugar-denaturant solution, denaturant-induced unfolding of Lyz is found to be offset by sugar in a manner that is roughly the combined effects of both the denaturant and sugar. These results suggest preferential accumulation of denaturant proximate to the protein surface and sugar interacts unfavorably with the unfolded conformation, resulting in preferential depletion of protein stabilizer proximate to the protein surface. The m-values were found to be most negative

for denaturants and positive for sugar consistent with their destabilization and stabilizing effect on protein, respectively.

5.4 References

[1] Yancey PH, Clark ME, Hand SC, Bowlus RD, Somero GN, Science 217:1214–1222 (1982)
[2] Yancey PH, Am Zool 41:699–709 (2001)
[3] Yancey PH, Somero G, Biochem J 183:317–323 (1979)
[4] Somero G, Am J Physiol 251:R197–R213 (1986)
[5] Gillett MB, Suko JR, Santoso FO, Yancey PH, J Exp Zool 279:386–391 (1997)
[6] Tanford C, Buckley CE, De PK, Lively EP, J Biol Chem 237:1168–1171 (1962)
[7] Utter MF, Keeth DB, Scrutton MC, Adu Enzyme Regul 2:49–68 (1964)
[8] Gerlsma SY, J Biol Chem 243:957–961 (1968)
[9] Gerlsma SY, Eur J Biochem 14:150–153 (1970)
[10] Gerlsma SY, Stuur ER, Int J Peptide Protein Res 4:377–383 (1972)
[11] Gerlsma SY, Stuur ER, Int J Peptide Protein Res 6:65–74 (1974)
[12] Neucere NJ, St Angelo AJ, Anal Biochem 47:80–89 (1972)
[13] Frigon RP, Lee JC, Arch Biochem Biophys 153:587–589 (1972)
[14] Back JF, Oakenfull D, Smith MB, Biochemistry 18:5191–5196 (1979)
[15] Vagenende V, Yap MG, Trout BL, Biochemistry 48:11084–11096 (2009)
[16] Ignatova Z, Gierasch LM, Methods Enzymol 428:355–372 (2007)
[17] Wang A, Bolen DW, Biophys J 71:2117–2122 (1996)
[18] Wang A, Bolen DW, Biochemistry 36:9101-9108 (1997)
[19] Pace CN, Methods Enzymol 131:266–280 (1986)
[20] Schellman JA, Biophys Chem 96:91–101 (2002)
[21] Bennion BJ, Daggett V, Proc Natl Acad Sci USA 100:5142–5147 (2003)
[22] Timasheff SN, Xie G, Biophys Chem 105:421–448 (2003)
[23] Bhuyan AK, Biochemistry 41:13386−13394 (2002)
[24] Hibbard LS, Tulinsky A, Biochemistry 17:5460−5468 (1978)
[25] Pike AC, Acharya KR, Protein Sci 3:706−710 (1994)
[26] Dunbar J, Yennawar HP, Banerji S, Luo J, Farber GK, Protein Sci 6:1727−1733 (1997)
[27] Xie G, Timasheff SN, Biophys Chem 64:25–43 (1997)
[28] Xie G, Timasheff SN, Protein Sci 6:211–221 (1997)
[29] Hédoux A, Willart JF, Ionov R, Affouard F, Guinet Y, Paccou L, Lerbret A, Descamps M, J Phys Chem B 110:22886–22893 (2006)
[30] Poddar NK, Ansari ZA, Singh RK, Moosavi–Movahedi AA, Ahmad F, Biophys Chem 138:120–129 (2008)
[31] Haque I, Singh R, Moosavi–Movahedi AA, Ahmad F, Biophys Chem 117:1–12 (2005)
[32] Kaushik JK, Bhat R, J Phys Chem B 102:7058–7066 (1998)
[33] Gekko K, Timasheff SN, Biochemistry 20:4677–4686 (1981)
[34] Miyawaki O, Biochim Biophys Acta 1774:928–935 (2007)
[35] Saadati Z, Bordbar AK, Protein J 27:455–460 (2008)
[36] D'Alfonso L, Collini M, Baldini G, Eur J Biochem 270:2497–2504 (2003)
[37] Kim YS, Jones LS, Dong A, Kendrick BS, Chang BS, Manning MC, Randolph TW, Carpenter JF, Protein Sci 12:1252–1261 (2003)

[38] Kulmyrzaev A, Bryant C, McClements DJ, J Agric Food Chem 48:1593–1597 (2000)
[39] O'Connor TF, Debenedetti PG, Carbeck JD, Biophys Chem 127:51-63 (2007)
[40] Xie G, Timasheff SN, Protein Sci 6:222–232 (1997)
[41] Beg I, Minton AP, Hassan I, Islam A, Ahmad F, Biochemistry 54:3594−3603 (2015)
[42] Kaushik JK, Bhat R, J Biol Chem 278:26458-26465 (2003)
[43] Asial I, Cheng YX, Engman H, Dollhopf M, Wu B1, Nordlund P, Cornvik T, Nat Commun 4:2901 (2013)
[44] Davis–Searles PR, Morar AS, Saunders AJ, Erie DA, Pielak GJ, Biochemistry 37:17048–17053 (1998)
[45] Zhang N, Liu FF, Dong XY, Sun Y, Biochem Eng J 70:188–195 (2013)
[46] Bongiovanni C, Sinibaldi F, Ferri T, Santucci R, J Protein Chem 21:35–41 (2002)
[47] Liu Z, Reddy G, Thirumalai D, J Phys Chem B 116:6707−6716 (2012)
[48] Greene RF, Pace CN, J Biol Chem 249:5388−5393 (1974)
[49] Tanford C, Aune KC, Biochemistry 9:206−211 (1970)
[50] Poklar N, Vesnaver G, Lapanje S, J Protein Chem 13:323−331 (1994)
[51] Lehrer SS, Fasman GD, J Biol Chem 242:4644-4651 (1967)
[52] Ansari MA, Zubair S, Atif SM, Kashif M, Khan N, Rehan M, Anwar T, Iqbal A, Owais M, Protein Pept Lett 17:11-17 (2010)
[53] Venyaminov SYu, Yang JT, In: circular dichroism and the conformational analysis of biomolecules. Fasman GD, editor. New York: Plenum, pp. 69–104 (1996)
[54] Kuwajima K, Hiraoka Y, Ikeguchi M, Sugai S, Biochemistry 24:874–881 (1985)
[55] Buck M, Radford SE, Dobson CM, Biochemistry 32:669–678 (1993)
[56] Ptitsyn OB, Adv Protein Chem 47:83–229 (1995)
[57] Kuwajima K, Arai M, The molten globule state: The physical and biological significance in mechanisms of protein folding (Pain RH, Ed.) 2nd ed., pp 138-174, Oxford University Press, New York. (2000)
[58] Arai M, Kuwajima K, Adv Protein Chem 53:209–282 (2000)
[59] Ptitsyn, OB, Semisotnov GV, The mechanism of protein folding. In: Nall BT, Dill KA, editors. Conformations and forces in protein folding. AAAS; Washington, DC. pp. 155–168 (1991)
[60] Engelhard M, Evans PA, Protein Sci 4:1553–1562 (1995)
[61] Uversky VN, Winter S, Löber G, Biophys Chem 60:79-88 (1996)
[62] Pace CN, CRC Crit Rev Biochem 3:1-43 (1975)
[63] Oshima H, Kinoshita M, J Chem Phys 138:245101 (2013)
[64] Timasheff SN, Adv Protein Chem 51:355-432 (1998)
[65] Lin TY, Timasheff SN, Biochemistry 33:12695–12701 (1994)
[66] Arakawa T, Timasheff SN, Biophys J 47:411–414 (1985)
[67] Miyawaki O, Biochim Biophys Acta 1774:928–935 (2007)
[68] Jain R, Sharma D, Kumar R, J Biochem 154:341-354 (2013)
[69] Jenkins WT, Protein Sci 7:376–382 (2013)
[70] Miyawaki O, Saito A, Matsuo T, Nakamura K, Biosci Biotechnol Biochem 61:466–469 (1997)
[71] Miyawaki O, Biophys Chem 144:46-52 (2009)
[72] Greene RF, Pace N, J Biol Chem 249: 5388–5393 (1974)
[73] Pace CN, Meth Enzymol 131:266–280 (1986)
[74] Miyawaki O, Tatsuno M, J Biosci Bioeng 111:198-203 (2011)

Chapter 6
Electrostatic Effects Control the Stability and Iron Release Kinetics of Ovotransferrin

6.1 Introduction

In the absence of chelators, iron release from the monoferric- and diferric-Tfs can be stimulated by a number of factors that can operate individually or together. *In vitro*, these includes, the acid lability of the two sites, which results in iron release at low pH [1-2], the reduction of Fe^{3+} to the much more weakly bound Fe^{2+} [3-5], the thermal denaturation of holoprotein, which results in iron release above melting temperature [6], and the chemical denaturation of holoprotein, which results in iron release above denaturation midpoint [7]. To assess the role of molecular interactions in stabilizing the oTf-Fe^{3+} complex and secondary and tertiary structures of Fe_2oTf, we have carried out the pH- and urea-denaturations equilibrium experiments for Fe_2oTf in the absence of chelators as a function of various salts (NaCl, $NaNO_3$, NaBr, and Na_2SO_4) or sucrose concentrations at 25 °C. Interestingly, the low concentrations of salts (≤0.1(±0.02) M Na_2SO_4 or ≤0.35(±0.15) M NaCl/$NaNO_3$/NaBr) destabilize the oTf-Fe^{3+} complex and also decrease the structural stability of Fe_2oTf. The present work also reveals that the destabilization of Fe_2oTf appears to result from, (i) destabilization of oTf-Fe^{3+} complex, and (ii) ionic screening of electrostatic interactions because low concentrations of these salts were also found to destabilize the secondary and tertiary structures of apo-ovotransferrin (apo-oTf).

To understand underlying mechanism by which noncovalent molecular interactions control the dynamics of iron release from Tfs, we have also studied the kinetics of Fe^{2+} and Fe^{3+} release from the Fe_NoTf at pH 7.4 and 5.6 in the absence of chelators as a function of various salts (NaCl, $NaNO_3$, and Na_2SO_4) or sucrose concentrations. At pH 7.4, with increasing the salt concentration from 0.0 to 1.0 M NaCl/$NaNO_3$ or 0.5 M Na_2SO_4, the rate constants for the reductive iron release (*i.e.,* Fe^{2+} release) and the urea denaturation-induced iron release (*i.e.,* Fe^{3+} release) from the Fe_NoTf increase initially when the salt concentration is low (≤0.12(±0.05) M NaCl or Na_2SO_4), but decrease at high concentration of salt. At pH 5.6, as salt concentration is increased, the rate constants for the Fe^{2+} and Fe^{3+} release from the Fe_NoTf increase mono-exponentially and plateau at ~0.4(±0.1) M $NaNO_3$/NaCl or ~0.2(±0.05) M Na_2SO_4, suggesting that the conformational change induced by anion binding and electrostatic destabilization of

Fe_NTf complex by salt regulates the kinetics of iron release from Fe_NoTf at endosomal pH conditions.

6.2 Results

6.2.1 pH dependence of the absorbance and fluorescence emission spectra of Fe_2oTf

At pH 7.4, the electronic absorption spectrum of Fe_2oTf shows a maximum at 465 nm (Fig. 6.1a), which indicates that iron is fully associated with protein. When pH is lowered from 7.4 to 3.5, the absorbance maximum at 465 nm is completely lost (Fig. 6.1a). This suggests that iron is fully released from the both sites of Fe_2oTf. Upon lowering the pH from 7.4 to 3.5, the quenching of Trp fluorescence by bound Fe^{3+} also diminishes (Fig. 6.1b), confirming that the both sites of Fe_2oTf completely released the bound iron.

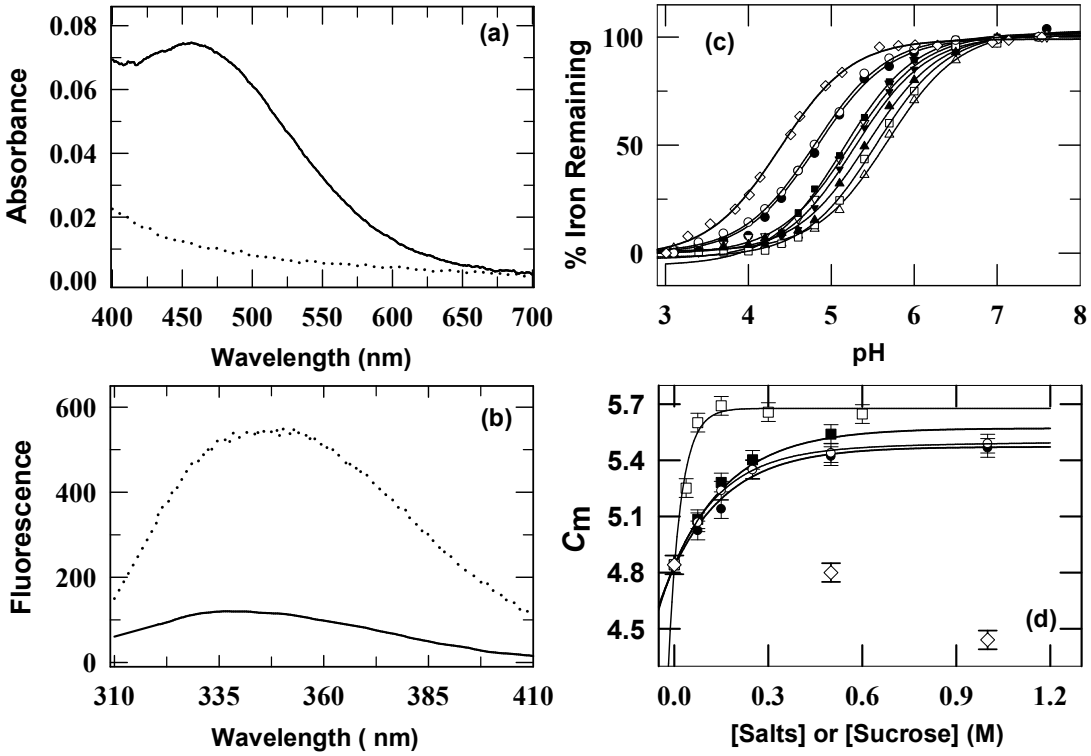

Fig. 6.1. pH dependence of iron release from Fe_2oTf in the presence of salts and sucrose. (a) Absorbance and (b) fluorescence emission spectra of Fe_2oTf ((solid line) 0.05 M HEPES, pH 7.4; (dotted line) 0.05 M MES, pH 3.5). (c) pH equilibrium profiles of Fe_2oTf monitored by fluorescence (ex: 280 nm). All experiments were performed at 25 °C: (●) no salt; (■) 0.15 M NaBr; (▽) 0.15 M NaCl; (▼) 0.15 M $NaNO_3$; (▲) 0. 5 M NaCl; (□) 0.5 M $NaNO_3$; (Δ) 0.25M Na_2SO_4; (○) 0.5 M and (◊) 1.0 M sucrose. The solid lines in panel (c) are fits according to equation 5 (chapter 2). (d) The dependence of the pH-midpoint at which half of the iron is released from Fe_2oTf on [Salts] ((●) NaBr, (○)NaCl, (■) $NaNO_3$, (□) Na_2SO_4) and [Sucrose] ((◊) sucrose). The solid lines in panel (d) represent non-linear least squares fits of the data to a single-exponential function.

6.2.2 Salt dependence of the pH-midpoint for iron release, C_m of Fe_2oTf

To determine the effect of salts or sucrose on the oTf-Fe^{3+} complex stability, the pH-titrations for Fe_2oTf were obtained by monitoring fluorescence emission at 340 nm and absorbance at 465 nm in the presence of various concentrations of salts (NaCl, $NaNO_3$, NaBr, Na_2SO_4) and sucrose at 25 °C. For brevity, we present the fluorescence-monitored pH titrations of Fe_2oTf in the absence of additive and in the presence of ~0.15 and 0.5 M NaCl, 0.15 and 0.5 M $NaNO_3$, 0.15 M NaBr, 0.25 M Na_2SO_4, and 0.5 and 1.0 M sucrose (Fig. 6.1c). As salt concentration is increased, the transition midpoint shift towards higher pH (Figs. 6.1c and 6.1d), which reveals that the salt reduces the oTf-Fe^{3+} complex stability. On contrary, as sucrose concentration is increased, the transition midpoint shift towards to lower pH (Fig. 6.1c), indicating that sucrose increases the oTf-Fe^{3+} complex stability.

To determine the role of molecular interactions responsible for oTf-Fe^{3+} complex stability, the pH profiles of Fe_2oTf measured at various concentrations of salts (NaCl, $NaNO_3$, NaBr, Na_2SO_4) and sucrose were fitted to equation 5 (chapter 2) [6]. As salt concentration is increased, the C_m for iron release increases mono-exponentially and plateau at ~0.4(±0.05) M NaCl/NaBr/$NaNO_3$ or ~0.15(±0.03) M Na_2SO_4 (Fig. 6.1d). On contrary, as sucrose concentration is increased from 0.0 to 1.0 M, the value of C_m decreases ~0.4 unit (Fig. 6.1d). Fig. 6.1d also shows that the increase in C_m for Fe_2oTf is more pronounced for Na_2SO_4 and least for NaBr. The salt-induced increase in C_m for Fe_2oTf typically follows the order, Na_2SO_4 > $NaNO_3$ > NaCl > NaBr. These finding indicates that Na_2SO_4 has a greater effect than does NaBr/$NaNO_3$/NaCl in destabilizing the oTf-Fe^{3+} complex.

6.2.3 Urea dependence of the absorbance and fluorescence emission spectra of Fe_2oTf

At pH 7.4, when the urea concentration is increased from 0.0 to 10.0 M, the maximum at 465 nm in the absorption spectrum of Fe_2oTf is almost eliminated (Fig. 6.2a), indicating that both sites of Fe_2oTf completely released their bound metal ions. At 10.0 M urea, the quenching of Trp fluorescence by bound Fe^{3+} is also diminished (Fig. 6.2b), indicating that the iron is fully dissociated from the both sites of Fe_2oTf complex.

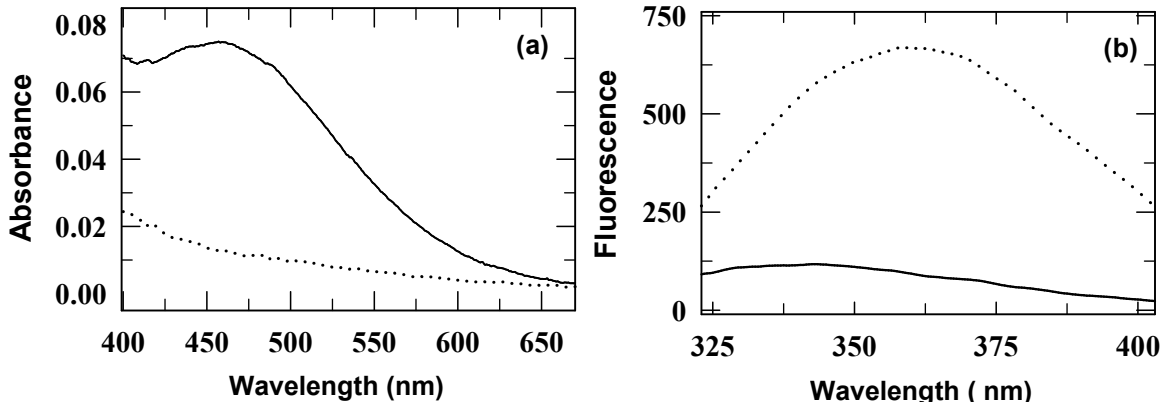

Fig. 6.2. Urea dependence of absorbance and fluorescence emission spectra of Fe_2oTf. Panels (a), (b), show the absorbance and fluorescence emission spectra of Fe_2oTf, respectively, at pH 7.4, 25 °C in the absence (solid line) and presence of 10.0 M urea (dotted line).

6.2.4 Effects of salt on the secondary and tertiary structures of Fe_2oTf and apo-oTf

The far-UV CD spectra (200-250 nm) of native Fe_2oTf (pH 7.4) in the absence and presence of ~0.3 M NaCl show the negative extrema at 208 nm and shoulder around 215-225 nm (Fig. 6.3a), which reflects the secondary structure of the protein. Fig. 6.3a also presents the far-UV CD spectra of Fe_2oTf (pH 7.4) measured at ~10 M urea without salt and at ~7.5 M urea in the absence and presence of ~0.3 M NaCl. Irrespective of exclusion of salt, at ~10.0 M urea, the negative extrema at 208 nm and shoulder around 215-225 nm are substantially disrupted (Fig. 6.3a), indicating that the secondary structure of protein is significantly lost. However, in the absence of salt, at ~7.5 M urea, the negative extrema at 208 nm and shoulder around 215-225 nm are only partially disrupted (Fig. 6.3a). Interestingly, in the presence of ~0.3 M NaCl, these partially disrupted peptide bands are substantially disrupted (Fig. 6.3a), indicating that the low concentration of salt significantly destabilizes the secondary structure of the partially denatured state of protein.

The near-UV CD spectra (250-300 nm) of native Fe_2oTf (Fig. 6.3b) and apo-oTf (Fig. 6.3c) in the absence and presence of ~0.3 M NaCl show the three aromatic residue bands at 255–270 nm (phenylalanine), 282 nm (tyrosine) and 291 nm (tryptophan), which reflects the tertiary structures of Fe_2oTf and apo-oTf. The near-UV CD spectroscopy can be used to probe the structural changes induced by metal binding to Tfs [8]. Upon iron binding, the shapes and intensities of the aromatic bands of apo-oTf alter significantly (Figs. 6.3b and 6.3c), indicating that the metal binding to apo-oTf produces significant changes in the tertiary structure of protein.

Fig. 6.3b also presents the near-UV CD spectra of Fe_2oTf (pH 7.4) measured at 10 M urea without salt and at ~7.5 M urea in the absence and presence of ~0.3 M NaCl. The near-UV CD spectra of apo-oTf measured at ~10 M urea without salt and at ~3.5 M urea in the absence and presence of ~0.3 M NaCl are shown in Fig. 6.3c. Irrespective of exclusion of salt, at ~10.0 M urea, the aromatic bands at 282 and 291 nm are substantially disrupted for both apo-oTf and Fe_2oTf (Figs. 6.3b and 6.3c), indicating that the tertiary structures of the proteins are significantly lost. However, in the absence of salt, at ~7.5 M urea for Fe_2oTf and at ~3.5 M urea for apo-oTf, the aromatic bands at 282 and 291 nm are only partially disrupted (Figs. 6.3b and 6.3c). Interestingly, in the presence of ~0.3 M NaCl, these partially disrupted aromatic bands are substantially lost (Figs. 6.3b and 6.3c), indicating that the low concentration of salt significantly destabilizes the tertiary structures of the partially denatured state of protein.

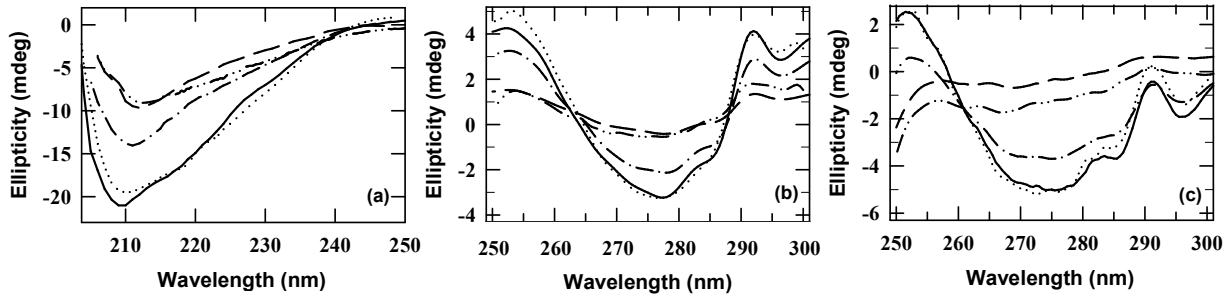

Fig. 6.3. Panel (a) and panel (b) present the far-UV and near-UV CD spectra of Fe_2oTf, respectively measured at ~0.05 M HEPES (solid line) and 0.05 M HEPES with 0.3 M NaCl (dotted line); 0.05 M HEPES with 10.0 M urea (short dash line); 0.05 M HEPES with 7.5 M urea (dash dot line); and 0.05 M HEPES with 7.5 M urea and 0.3 M NaCl (dash double dot line). Panel (c) present the near-UV CD spectra of apo-oTf measured at ~0.05 M HEPES (solid line) and 0.05 M HEPES with 0.3 M NaCl (dotted line); 0.05 M HEPES with 10.0 M urea (short dash line); 0.05 M HEPES with 3.5 M urea (dash dot line); and 0.05 M HEPES with 3.5 M urea and 0.3 M NaCl (dash double dot line).

6.2.5 Effect of pH on the urea-denaturation-induced iron release and unfolding of Fe_2oTf

Figs. 6.4a and 6.4b show the urea-induced denaturation curves for iron release (based on fluorescence emission at 340) and unfolding of Fe_2oTf (based on CD at 222 nm), respectively, at pH 7.4, 5.8, 5.6, and 5.4. The normalized urea-induced denturation curves for the iron release and unfolding collected at pH 7.4, 5.8, 5.6, and 5.4 (Figs. 6.4a and 6.4b) were fitted to equation 1 (chapter 2) [9]. The resulting m_g and ΔG_D for iron release and unfolding are provided in Table 1. Although, the physical importance of the factor m_g is not clearly understood, but an earlier study has suggested that it reflects the difference between the accessibility of surface areas of native

and denatured states of the polypeptide chain for a given denaturant [10]. With decreasing the pH from 7.4 to 5.4, the m_g values for iron release and unfolding of Fe_2oTf become larger (Table 1), suggesting that the more surface area is exposed to solvent upon iron release and unfolding at low pH. At each pH, the ΔG_D value determined by far-UV CD is larger than the ΔG_D value measured by fluorescence (Table 1). This is presumably because the Fe_2oTf responds to increased urea concentration by means of a coupled process in which the urea-induced iron release precedes the unfolding reaction (Fe_2oTf $\rightarrow$ $2Fe^{3+}$ + apo-oTf$\rightarrow$ unfolding). The far-UV CD monitored urea-denaturation of Fe_2oTf reflects this coupled process (iron release and unfolding) while the fluorescence or absorbance (465 nm) monitored urea-denaturation of Fe_2oTf reflects the iron release process of Fe_2oTf. The urea mid-points for iron release and unfolding ($C_m = \Delta G_D/m_g$) were calculated as a function of pH. The plots of C_m for iron release and unfolding of Fe_2oTf as function of pH are shown in Figs. 6.4c and 6.4d, respectively. Upon lowering the pH from 7.4 to 5.4, there is a large decrease in the C_m values for both iron release and unfolding is occurred (Figs. 6.4c and 6.4d). The finding indicates that the electrostatic interactions play vital roles in the destabilizations of the oTf-Fe^{3+}complex and secondary structure of the protein.

Table 1. pH dependence of C_m, ΔG_D, and m_g for urea-induced iron release and unfolding of Fe_2oTf derived as monitored by fluorescence at 340 nm and ellipticity at 222 nm.*

	Iron release			Unfolding		
pH	C_m	ΔG_D	m_g	C_m	ΔG_D	m_g
7.4	6.0	3.0	0.50	7.7	5.6	0.73
5.8	5.1	2.3	0.45	6.0	4.1	0.68
5.6	3.7	2.0	0.54	5.2	3.8	0.73
5.4	2.4	1.9	0.80	4.6	3.7	0.80

*C_m, ΔG_D, and m_g are reported as M, kcal mol^{-1}, and kcal mol^{-1} M^{-1}. The uncertainty of C_m, ΔG_D, and m_g values reported here is ±0.1 M, ± 0.2 kcal mol^{-1}, and 0.02 kcal mol^{-1} M^{-1}.

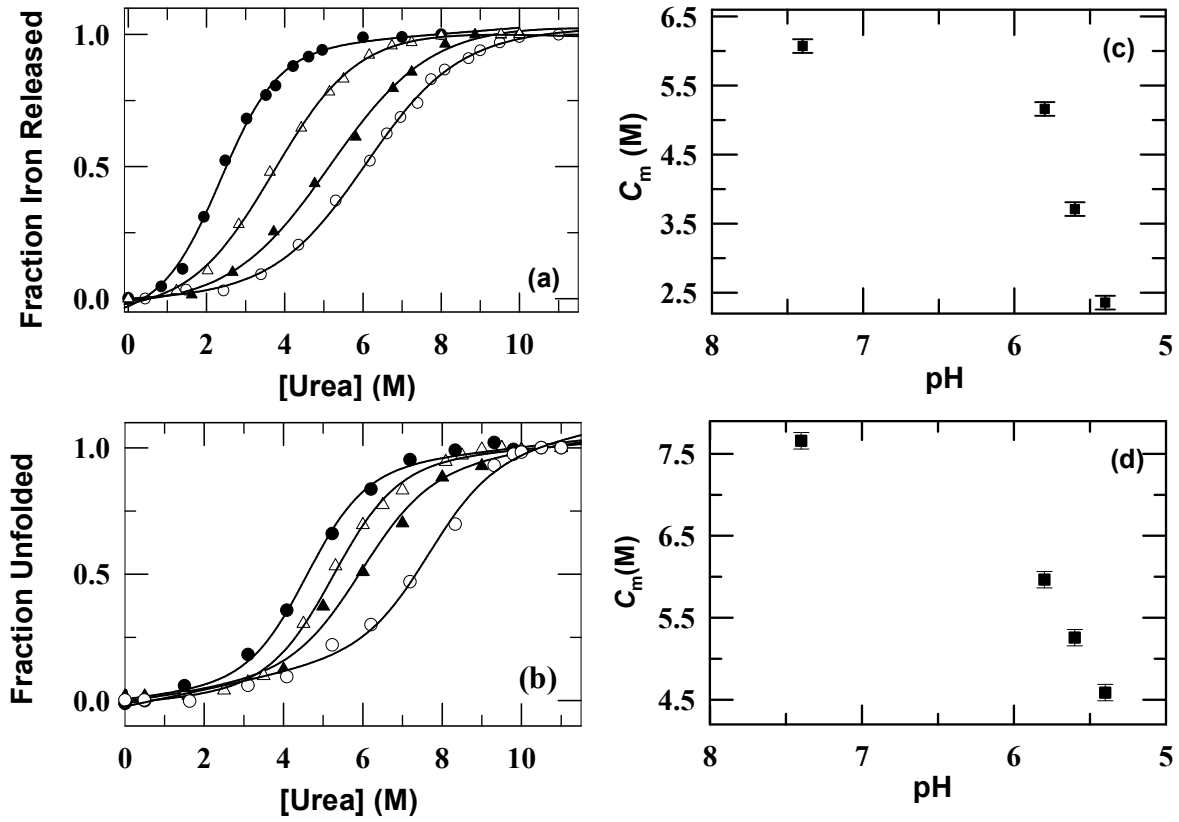

Fig. 6.4 (a) The pH dependence of the urea-induced release of iron from Fe_2oTf as evaluated from the change in fluorescence emission at 340 nm ((●), pH 5.4; (Δ), pH 5.6; (▲), pH 5.8; and (○), pH 7.4). (b) The pH dependence of the urea-induced unfolding of Fe_2oTf as evaluated from the change in far-UV CD at 222 nm ((●), pH 5.4; (Δ), pH 5.6; (▲), pH 5.8; and (○), pH 7.4). The solid lines in panel (a) and (b), represent a non-linear least squares fit of the data to equation 1 (chapter 2). The urea-induced iron release and unfolding mid-point, C_m (=$\Delta G_D/m_g$) was calculated as a function of pH. Panels (c) and (d) show pH-dependence of urea-induced iron release and unfolding midpoints, respectively.

6.2.6 Effects of salt and sucrose on urea denaturation-induced iron release from Fe_2oTf and unfolding of Fe_2oTf and apo-oTf

Fig. 6.5a shows urea-denaturation curves for iron release (based on fluorescence emission at 340) of Fe_2oTf at various salts (NaCl and Na_2SO_4) and sucrose concentration at pH 7.4. The far-UV (222 nm) CD monitored urea-induced unfolding curves of Fe_2oTf and apo-oTf measured at various salts (NaCl and Na_2SO_4) and sucrose concentrations at pH 7.4 are shown in Figs. 6.5b and 6.5c, respectively. Fig. 6.6 shows the near-UV (282 nm) CD monitored urea-induced unfolding curves of Fe_2oTf (Fig. 6.6a) and apo-oTf (Fig. 6.6b) measured at various salts

(NaCl and Na_2SO_4) and sucrose concentrations at pH 7.4. To determine the molecular interactions that control the stability of the oTf-Fe^{3+} complex and secondary and tertiary structures of protein, the urea-denaturation curves collected at various salts and sucrose concentrations for iron release from Fe_2oTf and unfolding of Fe_2oTf and apo-oTf were analyzed by using equation 1 (chapter 2) [9]. The resulting values of ΔG_D and m_g for iron release and unfolding are provided in Table 2 and Table 3, respectively.

Table 2. Salt and sucrose dependence of C_m, ΔG_D, and m_g derived for urea-induced iron release from Fe_2oTf at pH ~7.4 as monitored by flourescence.*

	ΔG_D	m_g	C_m
Control	3.0	0.50	6.0
[NaCl] (M)			
0.1	2.7	0.47	5.7
0.25	3.5	0.75	4.7
0.5	2.7	0.51	5.3
1.0	3.2	0.45	7.1
[Na_2SO_4] (M)			
0.025	3.0	0.51	5.9
0.1	3.1	0.60	5.2
0.15	3.1	0.54	5.7
0.25	3.2	0.50	6.4
0.5	3.5	0.46	7.6
[Sucrose] (M)			
0.15	3.2	0.47	6.8
0.25	3.3	0.49	6.7
0.5	3.8	0.50	7.6

*C_m, ΔG_D, and m_g are reported as M, kcal mol^{-1}, and kcal mol^{-1} M^{-1}. The uncertainty of C_m, ΔG_D, and m_g values reported here is ±0.1 M, ±0.2 kcal mol^{-1}, and 0.02 kcal mol^{-1} M^{-1}.

At each salt concentration, the ΔG_D value for unfolding is larger for Fe_2oTf than the apo-oTf (Table 3), which suggests that the conformational stability of apo-oTf increase upon complex formation with iron. At each salt concentration, the ΔG_D value for unfolding of Fe_2oTf (based on ellipticity values at 222 and 282 nm) is also larger than the ΔG_D value measured for iron release (based on fluorescence emission at 340 nm). Fig. 6.7 suggests that free energy difference between native and unfolded state for iron release from Fe_2oTf and unfolding of Fe_2oTf and apo-oTf in the absence and presence of 0.1 M NaCl typically follows the order: iron release < apo-oTf unfolding < holo-oTf unfolding. This finding further confirms that the Fe_2oTf responds to increased urea concentration by means of a coupled process in which the urea-

induced iron release reaction occurs prior to the unfolding reaction. The urea mid-points for iron release and unfolding ($C_m = \Delta G_D/m_g$) were calculated as a function of salts (NaCl and Na_2SO_4) and sucrose concentration (Table 2 and Table 3). The plots of C_m for iron release of Fe_2oTf as function of salts or sucrose concentration is shown in Fig. 6.5d. Figs. 6.5e and 6.5f show the plots of C_m for unfolding of secondary structures of Fe_2oTf and apo-Tf, respectively, as function of salts or sucrose concentration.

Table 3. Salt and sucrose dependence of C_m, ΔG_D, and m_g for unfolding of Fe_2oTf and apo-oTf at pH ~7.4 derived as monitored by CD at 222 and 282 nm.*

	222 nm						282 nm					
	Fe_2oTf			Apo-oTf			Fe_2oTf			Apo-oTf		
	ΔG_D	m_g	C_m	ΔG_D	m_g	C_m	ΔG_D	m_g	C_m	ΔG_D	m_g	C_m
Control	5.6	0.73	7.7	4.0	1.1	3.6	5.7	0.82	7.0	4.2	1.1	3.8
NaCl (M)												
0.1	4.9	0.80	6.1	3.8	1.1	3.4	5.0	0.80	6.3	3.9	1.1	3.5
0.25	4.6	0.85	5.4	3.8	1.2	3.2	4.6	0.85	5.4	3.5	1.2	2.9
0.5	4.6	0.88	5.2	4.2	1.1	3.8	5.1	0.85	6.0			
1.0	6.1	0.75	8.1	4.5	1.1	4.1	6.2	0.85	7.3	4.8	1.0	4.8
Na_2SO_4 (M)												
0.05	5.1	0.75	6.8	3.9	1.2	3.3						
0.1	4.3	0.90	4.8	3.6	1.2	3.0	5.0	0.90	5.6	3.4	1.2	2.8
0.25	4.8	0.85	5.6	4.2	1.0	4.2						
0.35	5.9	0.75	7.9				6.4	0.85	7.5	4.3	0.9	4.8
0.5	6.2	0.80	7.8	4.2	0.95	4.4						
Sucrose (M)												
0.15	5.8	0.74	7.8	4.1	1.0	4.1						
0.5	5.9	0.73	8.1	4.3	1.0	4.3				4.4	0.9	4.9

*C_m, ΔG_D, and m_g are reported as M, kcal mol^{-1}, and kcal mol^{-1} M^{-1}.The uncertainty of C_m, ΔG_D, and m_g values reported here are ±0.1 M, ±0.2 kcal mol^{-1}, and 0.02 kcal mol^{-1} M^{-1}.

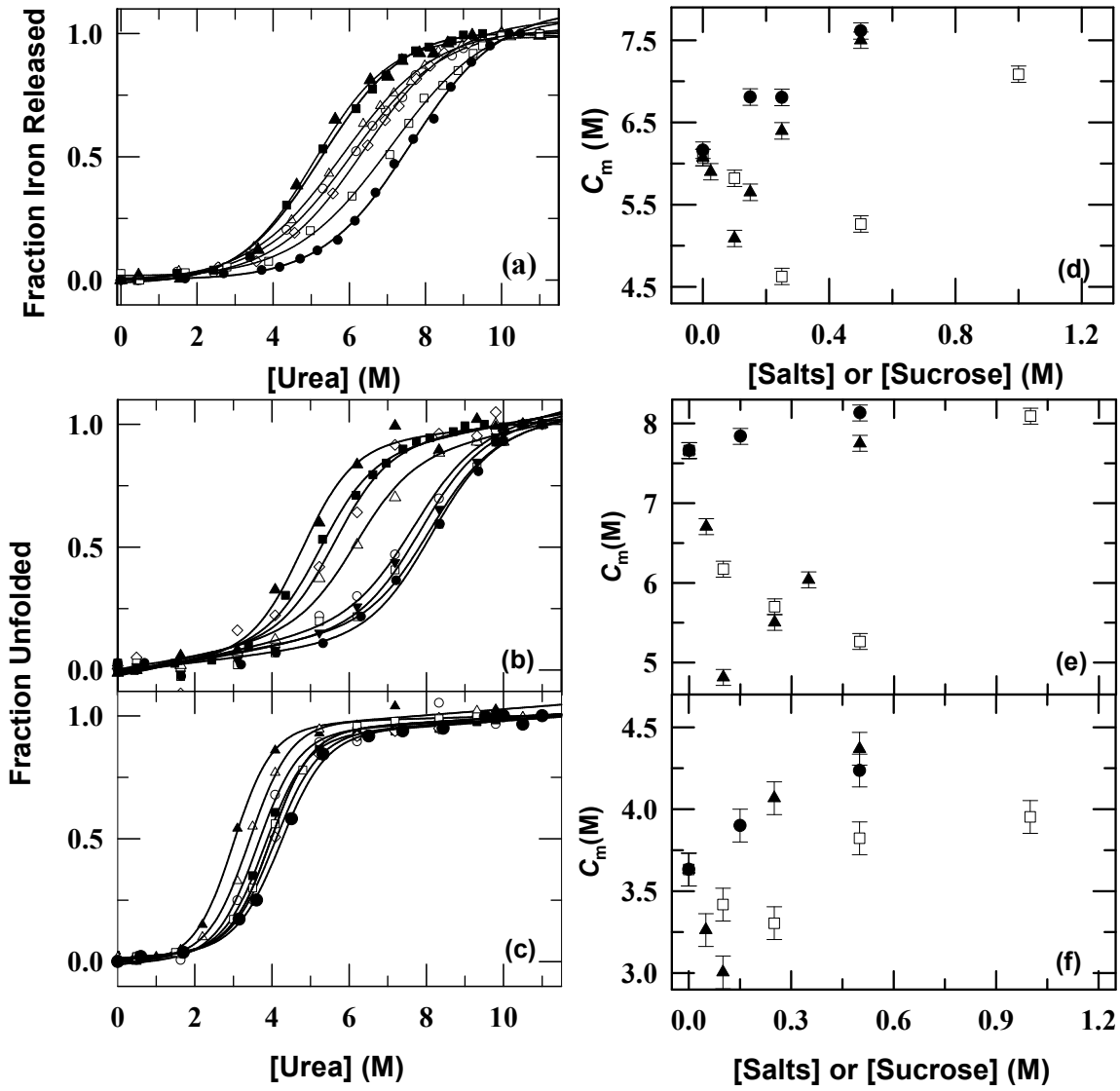

Fig. 6.5. Panel (a) shows the fluorescence-monitored (ex: 280, em: 340) urea dependence of iron release from Fe_2oTf at pH 7.4, in the absence (○), and presence of ~0.1 (Δ), 0.5 (■), and 1.0 M NaCl (□); ~0.1 (▲), and 0.25 M Na_2SO_4 (◊); and ~0.5 M sucrose (●). Panels (b) and (c) show the far- UV CD monitored (222 nm) unfolding of Fe_2oTf and apo-oTf, respectively at pH 7.4 in the absence (○), and presence of ~0.1 (Δ), 0.5 (■), and 1.0 M NaCl (□); ~0.1 (▲), 0.25 (◊), and 0.35 M Na_2SO_4 (▼); and ~0.5 M sucrose (●). The solid lines in panels (a), (b), and (c) represent a non-linear least squares fit of the data to equation 1 (chapter 2). The urea-induced iron release and unfolding midpoint, C_m (=$\Delta G_D/m_g$) was calculated as a function of pH, salts (NaCl, and Na_2SO_4) and sucrose concentrations. Panels (d), (e) and (f) show salts (NaCl (□), and Na_2SO_4 (▲)) and sucrose (●) dependence of C_m of Fe_2oTf and apo-oTf, respectively at pH 7.4.

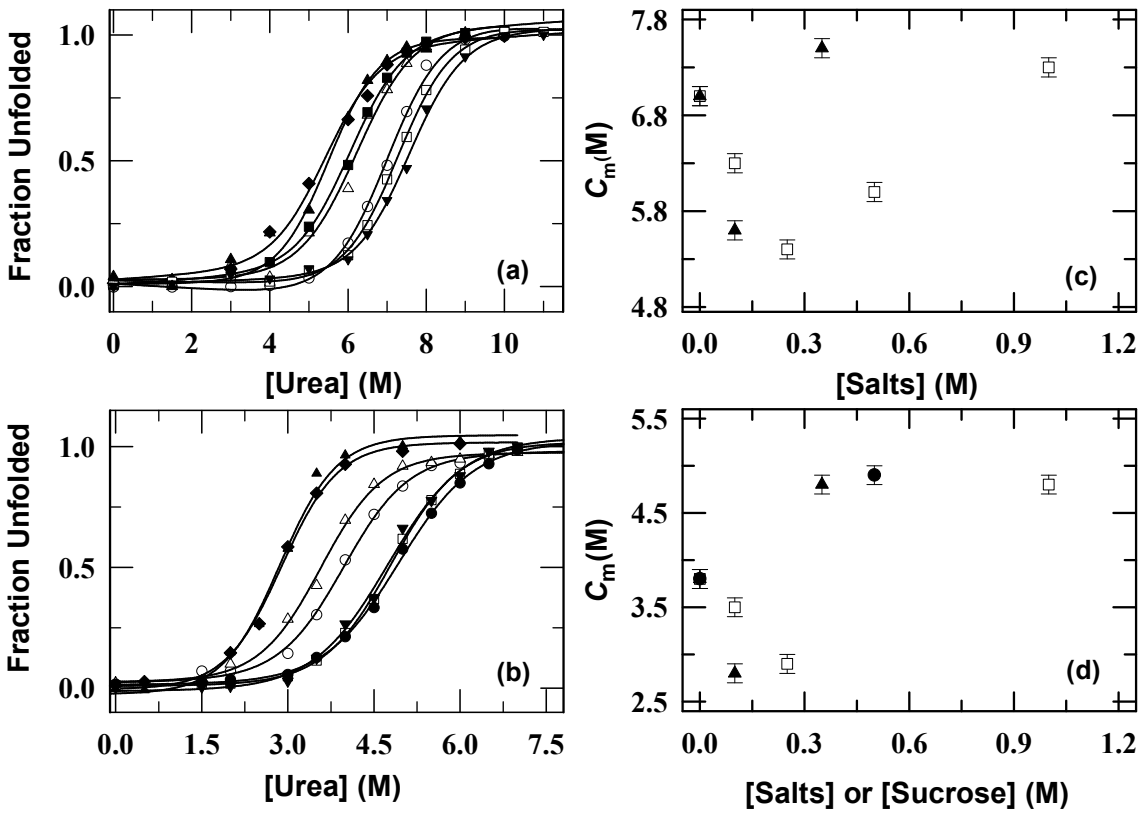

Fig. 6.6. Panel (a) shows the near-UV CD monitored (282 nm) unfolding curves of Fe_2oTf measured at pH 7.4 in the absence (○), and presence of ~0.1 (Δ), 0.25 (♦), 0.5 (■), and 1.0 M NaCl (□); ~0.1 (▲), and 0.35 M Na_2SO_4 (▼). The near-UV CD monitored (282 nm) unfolding curves of apo-oTf measured at pH 7.4 in the absence (○), and presence of ~0.1 (Δ), 0.25 (♦), 0.5 (■), and 1.0 M NaCl (□); ~0.1 (▲), 0.35 M Na_2SO_4 (▼) and ~0.5 M sucrose (●) are shown in panel (b). The solid lines in panel (a) and panel (b) represent a non-linear least squares fit of the data to equation 1 (chapter 2). The urea-induced unfolding midpoint, C_m ($=\Delta G_D/m_g$) was calculated as a function of salts (NaCl, and Na_2SO_4) and sucrose concentrations. Panel (c) shows the salts (NaCl (□), and Na_2SO_4 (▲)) dependence of C_m of Fe_2oTf at pH 7.4. The salts (NaCl (□), and Na_2SO_4 (▲)) and sucrose (●) dependence of C_m of apo-oTf at pH 7.4 is shown in panel (d).

The plots of C_m for unfolding of tertiary structures of Fe_2oTf and apo-Tf as function of salts or sucrose concentration are shown in Figs. 6.6c and 6.6d, respectively. As salt concentration is increased from 0.0 to 1.0 M NaCl or 0.5 M Na_2SO_4, the C_m values for iron release from Fe_2oTf and unfolding of Fe_2oTf and apo-oTf initially decrease at low salt concentration (≤0.1(±0.02) M Na_2SO_4 or ≤0.35 (±0.15) M NaCl) but increase at relatively higher salt concentration (Figs. 6.5d, 6.5e, 6.5f, 6.6c and 6.6d). At higher salt concentrations, Na_2SO_4 has a greater effect than does NaCl in increasing the C_m for both iron release and unfolding (Figs. 6.5d, 6.5e, 6.5f, 6.6c and 6.6d), which indicates that at higher salt concentrations, salt ions

increase the stabilities of the oTf-Fe^{3+} complex and secondary and tertiary structures of the protein according to Hofmeister series [11-15].

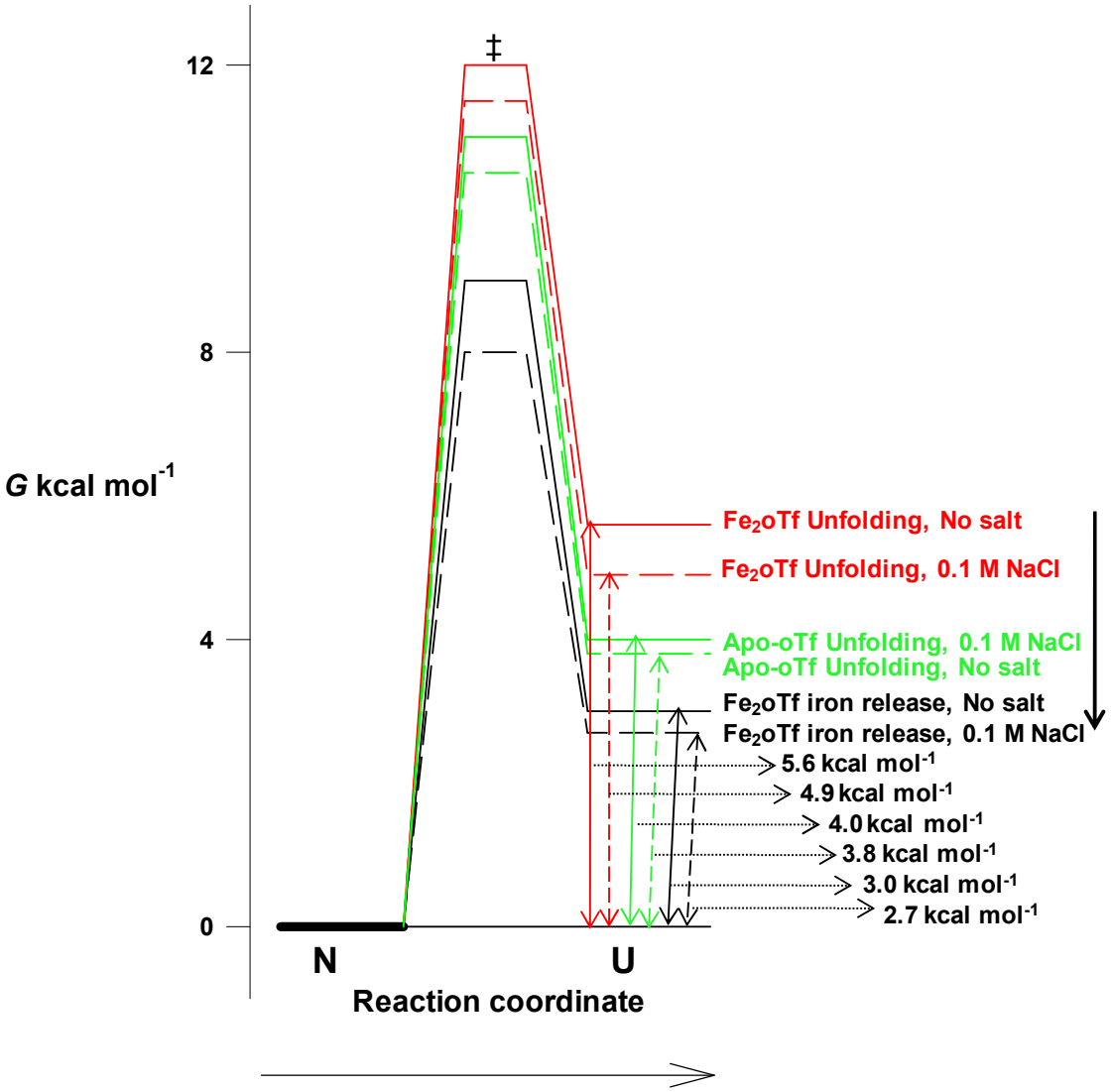

Fig. 6.7 Diagram illustrating the effect of low concentration of salt on the relative free energies of native and unfolded states measured for the unfolding and iron release from Fe_2oTf. The thermodynamic parameters derived from equilibrium unfolding experiments (Tables 2 and 3). The free energy of the native state of protein is arbitrarily set to zero. The energy levels of transition states may not appear scaled exactly.

6.2.7 Effects of salts and sucrose on the pH-linked kinetics of urea-denaturation induced iron release from the Fe_NoTf complex.

To gain insight into the linkage of protein and active site stability to the dynamics of Fe^{3+} release, the kinetics of urea-denaturation-induced Fe^{3+} release from the Fe_NoTf has been studied

as a function of salts (NaCl and Na_2SO_4) and sucrose concentration at pH 7.4 (Figs. 6.8a and 6.8c) and 5.6 (Figs. 6.8b and 6.8d). Figs. 6.8a and 6.8b show the representative urea-denaturation induced iron release kinetic traces of Fe_NoTf measured at pH 7.4 and 5.6, respectively, in the absence of salt at 37 °C. Both kinetic traces were fitted well in a mono-exponential decay function with rate constant, k_{obs}, of ~3.8×10^{-3} and 5.8×10^{-1} sec^{-1} at pH 7.4 and 5.6, respectively. Clearly by decreasing the pH from 7.4 to 5.6, the k_{obs} is increased ~150-fold (Table 6.1) (appendix). At pH ~7.4, with raising the concentration of NaCl from 0.0 to 0.25 M, the value of k_{obs} is increased ~1.5 fold (Fig. 6.8c and Table 6.1) (appendix). On the other hand, with increasing the concentration of sucrose from 0.0 to 0.5 M, the value of k_{obs} is decreased ~1.3 fold (Fig. 6.8c and Table 6.1) (appendix). Figs. 6.8c and 6.8d show the k_{obs} *vs* [salts] or [sucrose] plots for the Fe^{3+} release from the Fe_NoTf complex at pH 7.4 and 5.6, respectively. At pH 7.4, as salt concentration is increased from 0.0 to 1.0 M NaCl or 0.5 M Na_2SO_4, the k_{obs} value initially increases at low salt concentration (≤0.12(±0.03) M NaCl or Na_2SO_4) but decreases at relatively higher salt concentration (Fig. 6.8c and Table 6.1) (appendix). This result is consistent with an earlier report that showed that the rate constant for iron release from an isolated N-lobe of human serum transferrin by EDTA in the absence of urea increases at low salt concentration (≤ 0.3M KCl) but decreases at higher salt concentration [16]. Fig. 6.8c also indicates that at higher salt concentrations, the extent of decrease in the k_{obs} value is found to be more for Na_2SO_4 than that of NaCl. This result suggests that at higher salt concentrations (pH 7.4), the salts ions behave according to Hofmeister series [11-15]. At pH 5.6, as salt concentration is increased, the k_{obs} increases mono-exponentially and plateau at ~0.4(±0.1) M NaCl or ~0.2(±0.05) M Na_2SO_4 (Fig. 6.8d and Table 6.1) (appendix).

This result is consistent with an earlier report that showed that the rate constants for iron release from the N-lobe of human serum transferrin at pH 5.6 increase mono-exponentially with salt concentrations [17]. Fig. 6.8d also indicates that at pH 5.6, the extent of increase in k_{obs} is found to be higher for Na_2SO_4 than that of NaCl. This suggests that Na_2SO_4 as compared to NaCl is more effective in accelerating iron release from the Fe_NoTf.

We have recently shown that at low to intermediate concentrations of salt (≤0.35 M), an extended Debye-Hückel model can be used to explain the effect of ionic strength (I) on the rate of iron release reaction of Tfs [6]. The inset of Fig. 6.8d shows the log k_{obs} *vs* $I^{1/2}/(1+I^{1/2})$ plot for the Fe_NoTf at pH 5.6. Clearly, the log k_{obs} increase linearly with $I^{1/2}/(1+I^{1/2})$, which indicates that

at low to intermediate concentration of salt, the Debye-Hückel screening of diffusive counterions accelerates Fe^{3+} release from the Fe_NoTf at pH 5.6.

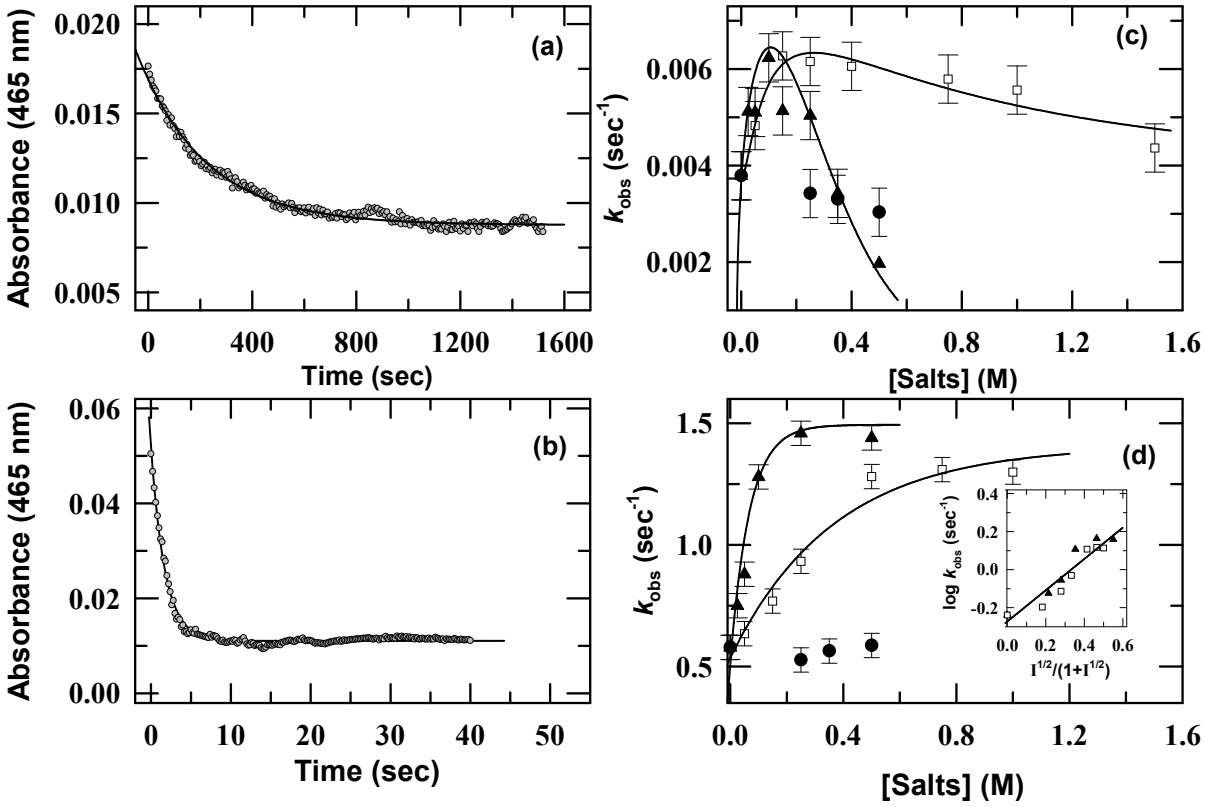

Fig. 6.8. Kinetics of urea-induced iron release from Fe_NoTf at ~37 °C as monitored by the change in absorbance at 465 nm. Panels (a) and (b) present single-phase iron release kinetic traces of Fe_NoTf in the absence of salt at pH 7.4 and 5.6, respectively. The solid lines in panels (a), and (b) show least-squares fits of the data to a single exponential function. The resulting rate constants for iron release, k_{obs}, are plotted as a function of salt (□, NaCl and ▲, Na_2SO_4) and sucrose (●) concentration in panels (c) and (d), respectively. The solid lines in panel (c) through data have been drawn to guide the eye only. The solid lines in panel (d) represent non-linear least squares fits of the data to a single-exponential function. The dependences of log k_{obs} on $I^{1/2}/(1+I^{1/2})$ at pH 5.6 is also shown in the inset of panel (d) (□, NaCl and ▲, Na_2SO_4); the solid line in the inset of panel (d) represent linear least squares fits to the data.

6.2.8 Salt dependence of the apparent activation enthalpy ($\Delta H^{\ddagger}$) of Fe^{3+} release reaction of Fe_NoTf

The effects of salts on the kinetics of Fe^{3+} release are further evaluated by studying the effect of temperature on the urea-denaturation induced iron release rate constant, k_{obs} of Fe_NoTf both in the absence and presence of salts (NaCl and Na_2SO_4). Figs. 6.9a and 6.9b show the Arrhenius plots (ln k_{obs} *vs* 1000/T) for the Fe^{3+} release at pH 7.4 and 5.6, respectively, in the

absence of additive and in the presence of ~0.25 M NaCl and 0.1 M Na_2SO_4. To determine the salt dependence on the apparent activation energy or activation enthalpy, $\Delta H^{\ddagger}$ ($E_a \approx \Delta H^{\ddagger}$) for the Fe^{3+} release, the Arrhenius plots in Figs. 6.9a and 6.9b were fitted linearly to Arrhenius equation [6,18].

The resulting $\Delta H^{\ddagger}$ for iron release are provided in Table 4. At both pH 7.4 and 5.6, as salt concentration is increased from 0.0 to 0.25 M NaCl or 0.1 M Na_2SO_4, the values of $\Delta H^{\ddagger}$ for iron release decrease significantly (Table 4). This indicates that at low to intermediate concentrations of salt, the salt-induced acceleration of Fe^{3+} release is accompanied by substantial decrease in $\Delta H^{\ddagger}$.

Table 4. Salt dependence of the activation enthalpy $\Delta H^{\ddagger}$ ($E_a = \Delta H^{\ddagger}$) of Fe^{3+} release reaction of Fe_NoTf.*

	pH ~7.4	pH ~5.6
	$\Delta H^{\ddagger}$	$\Delta H^{\ddagger}$
Control	18.0	12.0
0.25 M NaCl	14.5	9.3
0.1 M Na_2SO_4	15.5	8.3

*The uncertainty of $\Delta H^{\ddagger}$ values reported here is ±0.5 kcal mol^{-1}

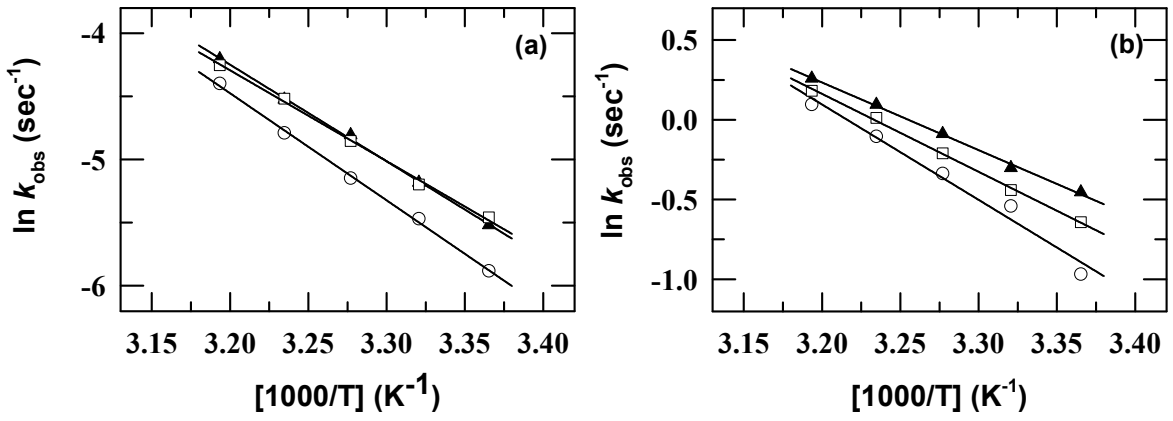

Fig. 6.9. Arrhenius plots derived from the temperature dependence of rate constant of urea-induced iron release from Fe_NoTf at pH 7.4 and 5.6 are shown in panels (a) and (b), respectively ((○), no addition; (□), 0.25 M NaCl; and (▲) 0.1 M Na_2SO_4).

6.2.9 Effects of salts on the pH-linked kinetics of reductive release of iron from the Fe_NoTf complex by sodium dithionite using BPS

To understand how electrostatic interactions influence the dynamics of reductive release of iron (*i.e.,* Fe^{2+} release) from the Fe_NoTf complex, the kinetics of reductive release of iron from the Fe_NoTf complex by sodium dithionite in the presence of BPS has been studied as a function of salts ($NaNO_3$ and Na_2SO_4) and sucrose concentration at pH 7.4 and 5.6. Figs. 6.10a and 6.10b show the representative reductive iron release kinetic traces of Fe_NoTf measured at pH 7.4 and 5.6, respectively, in the absence of salt at 25 °C. Upon reductive iron release from Tf-Fe^{3+} complex, the formation of Fe^{2+}-BPS complex exhibits a visible band at 538 nm so with the release of iron the aborbance of iron-BPS complex at 538 nm increases. The kinetics results of reductive iron release are well fitted to a mono-exponential rise function with rate constants, k_{obs}, of ~1.1×10^{-2} and 9.0×10^{-2} sec^{-1} at pH 7.4 and 5.6, respectively. Clearly, when the pH is decreased from 7.4 to 5.6, the k_{obs} value increases ~8.2-fold (Table 6.2) (appendix). At pH 7.4, with increasing the concentration of salt from 0.0 to 0.1 M $NaNO_3$ or Na_2SO_4, the value of k_{obs} is increased ~1.3 fold (Figs. 6.10c and Table 6.2) (appendix).

Figs. 6.10c and 6.10d show the k_{obs} *vs* [salts] plots for the Fe^{2+} release from the Fe_NoTf complex at pH 7.4, and 5.6, respectively. At pH 7.4, when the salt concentration is increased from 0.0 to 1.0 M $NaNO_3$ or 0.5 M Na_2SO_4, the value of k_{obs} initially increases at low salt concentration (≤0.1(±0.03) M $NaNO_3$ or Na_2SO_4) but decreases at relatively higher salt concentration (Fig. 6.10c and Table 6.2) (appendix). The extent of decrease in the k_{obs} value at higher salts concentrations is found to be more for Na_2SO_4 than that of $NaNO_3$. This finding suggests that at higher salt concentrations (pH 7.4), the salts ions behave according to Hofmeister series [11-15].

At pH 5.6, when [salt] is increased from 0.0 to 0.6 M $NaNO_3$ or Na_2SO_4, the k_{obs} increases mono-exponentially and it level off at ~0.4(±0.1) M $NaNO_3$ or ~0.2(±0.05) M Na_2SO_4 (Fig. 6.10d and Table 6.2) (appendix). Fig. 6.10d also shows that at low to intermediate concentrations of salt (≤ 0.2 M $NaNO_3$or Na_2SO_4), Na_2SO_4 as compared to $NaNO_3$ is more effective in accelerating Fe^{2+} release from the Fe_NoTf. The inset of Fig. 6.10d represents the log k_{obs} *vs* $I^{1/2}/(1+I^{1/2})$ plot for the Fe_NoTf at pH 5.6. The logarithm of k_{obs} increases linearly with $I^{1/2}/(1+I^{1/2})$, indicating that at low to intermediate concentrations of salts, the Debye-Hückel

screening of diffusive counterions also promotes the reductive iron release from the Fe_NoTf at pH 5.6.

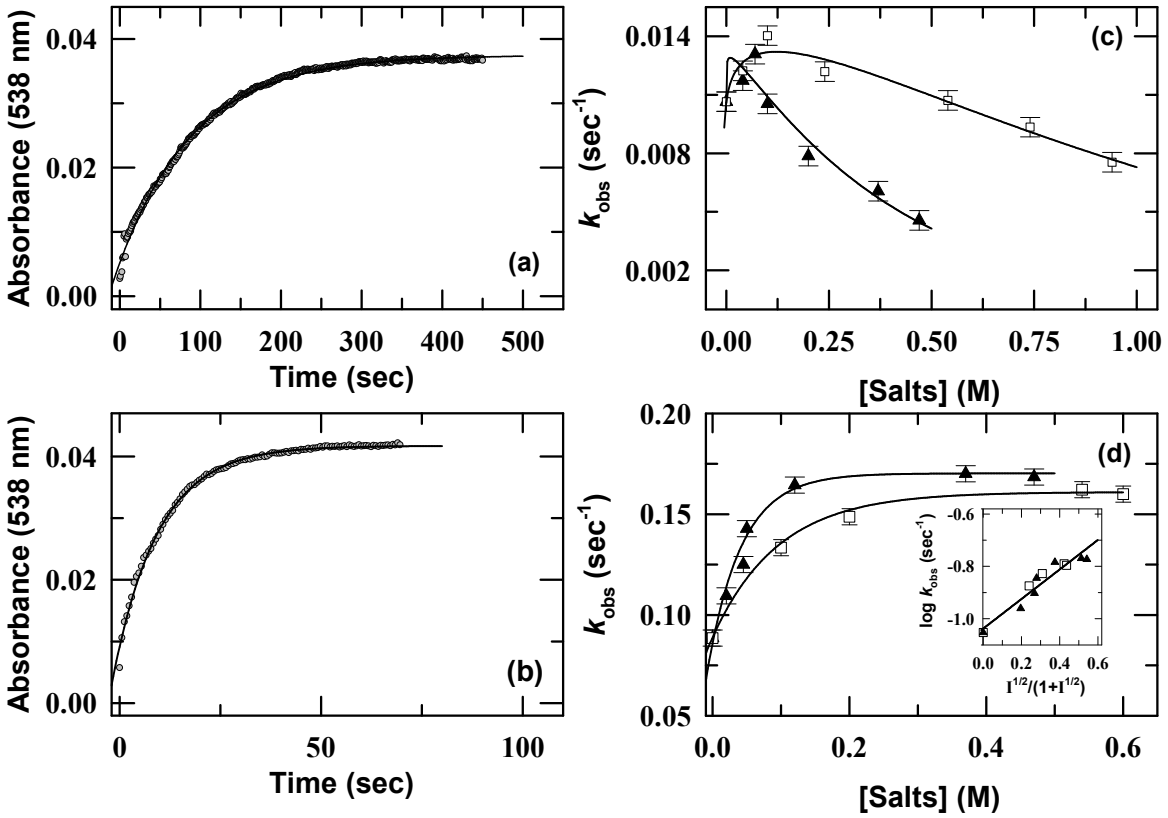

Fig. 6.10. Kinetics of reductive release of iron from the Fe_NoTf complex by sodium dithionite using BPS as monitored by the change in absorbance at 538 nm. Panels (a) and (b) present single-phase reductive iron release kinetic traces of Fe_NoTf in the absence of salt at pH 7.4 and 5.6, respectively. The solid lines in panels (a), and (b) show least-squares fits of the data to a single exponential function. The resulting rate constants for reductive iron release, k_{obs}, are plotted as a function of salt (□, $NaNO_3$ and ▲, Na_2SO_4) concentration in panels (c) and (d), respectively. The solid lines in panel (c) through data have been drawn to guide the eye only. The solid lines in panel (d) represent non-linear least squares fits of the data to a single-exponential function. The dependences of log k_{obs} on $I^{1/2}/(1+I^{1/2})$ at pH 5.6 is also shown in the inset of panel (d) (□, $NaNO_3$ and ■, Na_2SO_4); the solid line in the inset of panel (d) represents linear least squares fits to the data.

6.3 Discussion

6.3.1 How could low concentrations of salts destabilize the Fe_2oTf and apo-oTf?

Salt ions could affect the stability of natively folded proteins in a complex way. The Hofmeister series is often used to define the effectiveness of salt ions in stabilizing proteins at high salt concentrations (>0.5 M) [19]. However, at low salt concentration (<0.3 M), a given salt ions can

exhibit either stabilizing or destabilizing effect which varies with different proteins. For example, SO_4^{2-} has been shown to stabilize native RibonucleaseA [20], but destabilize human serum transferrin [6]. There is growing experimental evidence that the specific interactions between anions and the protein surface affect protein stability [6,21-22]. The current study presents direct experimental evidence that at low salt concentrations (≤0.1(±0.02) M Na_2SO_4 or ≤0.35(±0.15) M NaCl), both NaCl and Na_2SO_4 decrease the stabilities of the oTf-Fe^{3+} complex and secondary and tertiary structures of Fe_2oTf and apo-oTf (Figs. 6.5d, 6.5e, 6.5f, 6.6c and 6d). Since Na_2SO_4 is a kosmotropic salt which generally found to have a stabilizing effect on proteins [20,22-23], therefore, the decrease in the stabilities of the Fe_2oTf complex and secondary and tertiary structures of Fe_2oTf and apo-oTf by Na_2SO_4 is highly unusual. Few other examples are also available which showed that at low to intermediate concentrations of Na_2SO_4 (<0.15 M), the ionic screening of electrostatic interactions can destabilize human serum transferrin [6], human plasma lipoproteins [24-25], human prion protein [26], and an archaebacterial carboxypeptidase [18]. At higher salt concentrations (≥0.1(±0.02) M Na_2SO_4 or 0.35(±0.15) M NaCl), the destabilizing effect was progressively reversed and salts acted as according to their ranking in the Hofmeister series (Figs. 6.5d, 6.5e, 6.5f, 6.6c and 6.6d).

At low salt concentrations (≤0.1(±0.02) M Na_2SO_4 or 0.25(±0.05) M NaCl), the decrease in the structural stability of apo-oTf (Figs. 6.5f and 6.6d and Table 3) by salts suggests that the destabilization of Fe_2oTf complex by salt is attributed to the salt-induced destabilization of the oTf-Fe^{3+} complex and weaken of Coulombic interactions at the protein surface. The current study provides several experimental supports that the salt-induced destabilization of Fe_2oTf complex and apo-oTf are due to the ionic screening of electrostatic interactions. First, at the salt concentrations range (0.01-0.35 M) that destabilize the Fe_2oTf complex and apo-oTf (Figs. 6.5d, 6.5e, 6.5f, 6.6c and 6.6d), the effects of salt on macromolecular stability are governed by ionic screening. The single exponential character of salt effect on oTf-Fe^{3+} complex stability (Fig. 6.1d) is typical of the electrostatic screening by diffusive counterions (e.g., co-solute screening) [6,24,27]. Finally, the opposite effects of salts (destabilizing) and sucrose (stabilizing) on the stability of the oTf-Fe^{3+} complex and secondary and tertiary structures of the protein confirm that the hydrophobic effect is not the factor for the salt-induced destabilization of Fe_2Tf complex and apoTf (Figs. 6.5d, 6.5e, 6.5f, 6.6d and Tables 2 and 3).

6.3.2 pH and anion-binding induced conformational changes play vital roles in promoting iron release from Fe_2oTf complex

During the last few decades, several investigators have spurred great interest in understanding the role of the pH- and anion binding-induced conformational changes that prompt iron release from the monoferric- and diferric-Tfs [3,6,16-17,28-44]. Dewan et al suggested that the charge repulsion and a conformational change resulting from the protonation of the dilysine pair (Lys209-Lys301 located on the opposite domains of N-lobe) appears to be the main driving force to trigger cleft opening of N-lobe at low pH [30]. A recent hydrogen/deuterium exchange study of N-terminal lobe of human serum transferrin in combination with mass spectrometry suggested that at slightly acidic pH conditions, holoprotein exists in the open conformation [32]. Few earlier site-directed mutagenesis studies of human serum transferrin with iron bound only to the N-lobe indicate that charge repulsion and a conformational change resulting from the protonation of the so-called dilysine pair (Lys206-Lys296) are the main driving forces for anion-induced iron release acceleration as pH is decreased [17,34,44].

Kretchmar et al reported that anions requirement is a prerequisite for iron release from the monoferric-Tf [43]. The anion requirement is also necessary for iron release from Fe^{3+}-Tf-receptor complex [45], signifying the implications of some anion for the cellular iron release. Few earlier kinetic and spectroscopic studies revealed that the conformational changes induced by binding of anions to the protein are involved in salt-induced release of iron from the monoferric- and differic-Tfs [3,6,34,46]. Recent anion dependent fluorescence studies of diferric human serum transferrin at low pH also provided direct evidence that the anion binding to the protein induces a structural or conformational change around one or more Trp residues near the iron binding site [6]. In an earlier study, Baldwin et al have argued that both conformational changes and electrostatic interactions induced by binding of ions prompts iron release from the monoferric-Tfs [3]. The current study showed that in the presence of salt, there is a considerable change in the slope of the Arrhenius plot (Figs. 6.9a and 6.9b), insofar this is due to anion-induced conformational change in the protein. Furthermore, the single exponential saturation effect of salt on the iron release rate constant at pH 5.6 (Figs. 6.8d and 6.10d) confirms that anion-binding induced conformational change promotes Fe^{2+} and Fe^{3+} release from the Fe_NoTf.

6.3.3 Electrostatic screening effect of electrolytes controls the kinetics of iron release from Fe_NoTf

While the kinetics of iron release from the monoferric- and diferric-Tfs have been studied as a function of salts concentration [1,3,6,16-17,34,42-45,47-55], few have been studied in sufficient details to provide the mechanism by which the salt ions influence the kinetics of iron release [6,18]. Especially, the roles played by electrostatic interactions in controlling the kinetics of Fe^{2+} and Fe^{3+} release are not clearly known. The current study provides several experimental evidences which show that salt ions prompt Fe^{2+} and Fe^{3+} release from Fe_NoTf complex through the ionic screening effects (Figs. 6.8c, 6.8d, 6.10c and 6.10d). If salt-induced Fe^{2+} and Fe^{3+} release from Fe_NoTf are due to the interference with hydrophobic interactions, then kosmotropic salt (*i.e.* increase the macromolecular stability by strengthening the hydrophobic interactions [12-13,15]) such as Na_2SO_4 should slow down the Fe^{2+} and Fe^{3+} release from Fe_NoTf via strengthening the intramolecular hydrophobic interactions. But, within the pH range of 7.4-5.6, the current results reveal that at lower salt concentrations (≤0.12(±0.05) M NaCl/$NaNO_3$ or Na_2SO_4 (pH 7.4); ≤0.4(±0.1) M $NaNO_3$/NaCl or 0.2(±0.05) M Na_2SO_4 (pH 5.6)), all the salts tested (NaCl, $NaNO_3$, and Na_2SO_4) here promote Fe^{2+} and Fe^{3+} release from Fe_NoTf. The current results also reveal that at higher salt concentrations (≥0.12(±0.05) M NaCl/$NaNO_3$ or Na_2SO_4), the salts retard the Fe^{2+} and Fe^{3+} release from Fe_NoTf at pH 7.4 (Figs. 6.8c and 6.10c), while they accelerate the Fe^{2+} and Fe^{3+} release at pH 5.6 (Figs. 6.8d and 6.10d). At low to intermediate concentrations of salt (0.01-0.35 M), the effects of salts on protein stability are generally attributed to ionic screening effect [6,27,56]. On the other hand, the specific ion binding effect of salt generally apparent at milllimolar concentrations [57] while hydrophobic effect of salt occurs at molar concentrations (>0.5 M) [6,24,27,56,58]. In dilute to moderately concentrated ionic solution, an extended Debye-Hückel model can easily interpret the effect of ionic strength on the rate of iron release reaction of Tfs [12]. At pH 5.6, the values of log k_{obs} for the Fe^{2+} and Fe^{3+} release increase linearly with $I^{1/2}/(1+I^{1/2})$ (Insets of Figs. 6.8d and 6.10d). This finding clearly indicates that the Debye-Hückel screening of diffusive counterions accelerate the Fe^{2+} and Fe^{3+} release from the Fe_NoTf at endosomal pH conditions. Finally, the opposite effect of salts and sucrose (*i.e.,* salt prompts iron release while sucrose inhibits it) confirms that the acceleration of the iron release by salt is not due to the hydrophobic effect.

6.3.4 Both anion binding to KISAB sites and electrostatic screening effect of electrolytes control the kinetics of iron release from Fe_NoTf

To emphasize the allosteric effect on iron release, Egan et al [43,48,50,53] proposed naming the sites to which nonsynergistic anions bind as "kinetically significant anion binding" or KISAB sites. It is widely accepted that the anion binding to KISAB site influences the rate of iron release from Tfs [59, and references therein]. However, the KISAB site has not been well characterized [109]. Few earlier studies have been shown that there are multiple KISAB sites exist for each lobe of Tf [17,32,34,38,42,44,59]. A recent report shows that Arg-143 serves as an authentic KISAB site in the N-lobe of human transferrin [42]. While both electrostatic effect (Debye-Hückel screening of diffusive counterions) and anion binding to the KISAB sites influence the rates of iron release from the Fe_NoTf, the extent of these two effects on rates of iron release will depend on the pH of reaction medium and the concentration of anions. The N-lobe is the first lobe to release iron [60], so it is to be noted that the concentration of anion has the greatest effect on iron release from the N-lobe [42]. At low salt concentrations and at pH ~7.4, Debye-Hückel screening of diffusive counterions facilitate the iron release from Fe_NoTf but under these conditions of pH and salt, anion binding to KISAB site may has little effect on iron release because at neutral pH there are only weak interactions exist between the anions and KISAB sites [17]. At mildly acidic pH (~5.6), the anion binding strength to KISAB sites increases [17], which in results accelerate the iron release from N-lobe of Tfs [17]. The previous section has presented several lines of evidence which suggests that at pH 5.6, Debye-Hückel screening of diffusive counterions facilitates iron release from Fe_NoTf. So, at pH ~5.6, it is likely that both anions binding to the KISAB site and ionic screening of electrostatic interactions together facilitate iron release from Fe_NoTf.

6.4 Conclusions

To assess the effects of salts and sucrose on the stability of the oTf-Fe^{3+} complex and secondary and tertiary structures of protein, Fe_2oTf has been studied as a function of pH and urea in the presence salts (NaCl, Na_2SO_4, NaBr, and $NaNO_3$) and sucrose. Interestingly, the low concentrations of these salts were found to reduce the stability of the oTf-Fe^{3+} complex and secondary and tertiary structures of protein. At relatively higher salt concentrations (≥0.1(±0.02) M Na_2SO_4 or ≥0.35(±0.15) M NaCl), these salts were found to increase the structural stability of

protein. The current study revealed that the destabilization of Fe_2oTf by salts results from both destabilization of oTf-Fe^{3+} complex and ionic screening of electrostatic interactions. At pH 7.4, the low concentrations of Na_2SO_4 and NaCl/$NaNO_3$ were found to promote Fe^{2+} and Fe^{3+} release from Fe_NoTf. At relatively higher salt concentrations (≥0.15(±0.04) M), these salt were found to inhibit iron release and salt ions behave according to Hofmeister series. At pH 5.6, these salts were also found to accelerate the Fe^{2+} and Fe^{3+} release from Fe_NoTf. However, at pH 5.6, the salt-induced Fe^{2+} and Fe^{3+} release accelerating effects are particularly pronounced at low salt concentrations but are saturated at ~0.2(±0.05) M Na_2SO_4 or ~0.4(±0.1) M $NaNO_3$/NaCl, which suggests that the Coulombic interactions play crucial role in the accelerating of Fe^{2+} and Fe^{3+} release from Fe_NoTf at endosomal pH conditions. The current results suggest that there is a general effect from Debeye-Huckel screening that operates in addition to the anion binding to KISAB or any unrecognized sites in regulating the kinetics of iron release from Fe_NoTf at pH ~5.6.

6.5 Reference

[1] Williams J, Chasteen ND, Moreton K, Biochem J 201:527-532 (1982)
[2] Mazurier J, Spik G, Biochim Biophys Acta 629:399–408 (1980)
[3] Baldwin DA, Egan TJ, Marques HM, Biochim Biophys Acta 1038:1-9 (1990)
[4] Harris WR, J Inorg Biochem 27:41-52 (1986)
[5] Kojima N, Bates GW, J Biol Chem 254:8847-8854 (1979)
[6] Kumar R, Mauk AG, J Phys Chem B 113:12400–12409 (2009)
[7] Nakazato K, Yamamura T, Satake K, J Biochem 103:823-828 (1988)
[8] Zhang M, Gumerov DR, Kaltashov IA, Mason AB, J Am Soc Mass Spectrom 15:1658-1664 (2004)
[9] Santoro MM, Bolen DW, Biochemistry 27:8063-8068 (1988)
[10] Tanford C, Advan Protein Chem 23:121-282 (1968)
[11] Baldwin RL, Biophys J 71:2056-2063 (1996)
[12] Cacace MG, Landau EM, Ramsden JJ, Q ReV Biophys 30:241-277 (1997)
[13] Von Hippel PH, Wong KY, Science 145:577-580 (1964)
[14] Pegram LM, Record MT Jr, J Phys Chem B 112:9428-9436 (2008)
[15] Record MT Jr, Anderson CF, Lohman TM, Q ReV Biophys 11:103-178 (1978)
[16] Byrne SL, Chasteen ND, Steere AN, Mason AB, J Mol Biol 396:130-140 (2010)
[17] He QY, Mason AB, Nguyen V, MacGillivray RT, Woodworth RC, Biochem J 350:909-915 (2000)
[18] Villa A, Zecca L, Fusi P, Colombo S, Tedeschi G, Tortora P, Biochem J 295:827-831 (1993)
[19] Curtis RA, Lue L, Chem Eng Sci 61:907−923 (2006)
[20] Ramos CHI, Baldwin RL, Protein Science 11:1771−1778 (2002)
[21] Zhang Y, Cremer PS, Curr Opin Chem Biol 10:658−663 (2006)

[22] Timasheff SN, Annu ReV Biophys Biomol Struct 22:67-97 (1993)
[23] Nishimura C, Uversky VN, Fink AL, Biochemistry 40:2113-2128 (2001)
[24] Jayaraman S, Gantz DL, Gursky O, Biochemistry 45:4620-4628 (2006)
[25] Benjwal S, Jayaraman S, Gursky O, Biochemistry 44:10218-10226 (2005)
[26] Apetri AC, Surewicz WK, J Biol Chem 278:22187-22192 (2003)
[27] Perez-Jimenez R, Godoy-Ruiz R, Ibarra-Molero B, Sanchez-Ruiz JM, Biophys J 86:2414-2429 (2004)
[28] Lee DA, Goodfellow JM, Biophysical J 85:2747-2759 (1998)
[29] Rinaldo D, Field MJ, Biophysical J 85:3485-3501 (2003)
[30] Bobst CE, Zhang M, Kaltashov IA, J Mol Biol 388:954-967 (2009)
[31] Aisen P, Listowsky I, Annu Rev Biochem 49:357-393 (1980)
[32] Dewan JC, Mikami B, Hirose M, Sacchettini JC, Biochemistry 32:11963–11968 (1993)
[33] MacGillivray RT, Moore SA, Chen J, Anderson BF, Baker H, Luo Y, Bewley M, Smith CA, Murphy ME, Wang Y, Mason AB, Woodworth RC, Brayer GD, Baker EN, Biochemistry 37:7919–7928 (1998)
[34] He QY, Mason AB, Tam BM, MacGillivray RT, Woodworth RC, Biochemistry 38:9704-9711 (1999)
[35] Steere AN, Byrne SL, Chasteen ND, Smith VC, MacGillivray RT, Mason AB, J Biol Inorg Chem 15:1341-1352 (2010)
[36] James NG, Byrne SL, Steere AN, Smith VC, MacGillivray RT, Mason AB, Biochemistry 48:2858-2867 (2009)
[37] James NG, Berger CL, Byrne SL, Smith VC, MacGillivray RT, Mason AB, Biochemistry 46:10603-10611 (2007)
[38] Halbrooks PJ, Giannetti AM, Klein JS, Björkman PJ, Larouche JR, Smith VC, MacGillivray RT, Everse SJ, Mason AB, Biochemistry 44:15451-15460 (2005)
[39] Nurizzo D, Baker HM, He QY, MacGillivray RT, Mason AB, Woodworth RC, Baker EN, Biochemistry 40:1616-1623 (2001)
[40] He QY, Mason AB, Tam BM, MacGillivray RT, Woodworth RC, Biochem J 344:881-887 (1999)
[41] Byrne SL, Mason AB, J Biol Inorg Chem 14:771–781 (2009)
[42] Byrne SL, Steere AN, Chasteen ND, Mason AB, Biochemistry 49:4200-4207 (2010)
[43] Kretchmar SA, Raymond KN, Inorg Chem 27:1436–1441 (1988)
[44] Zak O, Tam B, MacGillivray RT, Aisen P, Biochemistry 36:11036-11043 (1997)
[45] Egan TJ, Zak O, Aisen P, Biochemistry 32:8162-8167 (1993)
[46] Folajtar DA, Chasteen ND, J Am Chem Soc 104:5775-5780 (1982)
[47] Egan TJ, Ross DC, Purves LR, Adams PA, Inorg Chem 31:1994-1998 (1992)
[48] Marques HM, Watson DL, Egan TJ, Inorg Chem 30:3758–3762 (1991)
[49] Harris WR, Bali PK, Inorg Chem 27:2687–2691 (1988)
[50] Marques HM, Walton T, Egan TJ, J Inorg Biochem 57:11-21 (1995)
[51] Li Y, Harris WR, Biochim Biophys Acta 1387:89-102 (1998)
[52] Marques HM, Egan TJ, Pattrick G, S Afr J Sci 86:21–24 (1990)
[53] Muralidhara BK, Hirose M, J Biol Chem 275:12463-12469 (2000)
[54] Mizutani K, Muralidhara BK, Yamashita H, Tabata S, Mikami B, Hirose M, J Biol Chem 276:35940-35946 (2001)
[55] Hamilton DH, Turcot I, Stintzi A, Raymond KN, J Biol Inorg Chem 9:936–944 (2004)
[56] Elcock AH, McCammon JA, J Mol Biol 280:731-748 (1998)

[57] van Asselt EJ, Dijkstra BW, FEBS Lett 458:429-435 (1999)
[58] Perl D, Holtermann G, Schmid FX, Biochemistry 40:15501-15511 (2001)
[59] Harris WR, Biochim Biophys Acta 1820:348–361 (2012)
[60] Hemadi M, Ha-Duong NT, El HageChahine JM, J Mol Biol 358:1125-1136 (2006)

Chapter 7
Role of Macromolecular Crowding on Stability and Iron Release Kinetics of Serum Transferrin

7.1 Introduction

To understand how sTf executes its biological function in a highly crowded cellular environment, this chapter evaluated the effects of crowding agents (dextran 70, dextran 40 and ficoll 70) on the sTf-Fe^{3+} complex and structural stability of Fe_2sTf. To determine the effect of crowding agents on the sTf-Fe^{3+} complex stability, the pH- and urea (at pH 7.4 and pH 5.7) denaturations-induced iron release profiles of Fe_2sTf were obtained in the absence and presence of different concentrations of crowding agent (ficoll 70, dextran 40, and dextran 70). To evaluate the effect of crowding agents on the structural stability of Fe_2sTf, the urea-induced unfolding profiles of Fe_2sTf were obtained at pH 7.4 and pH 5.5 in the absence and presence of different concentrations of crowding agent (ficoll 70, dextran 40, and dextran 70). Previous studies revealed that anions (SO_4^{2-}, Cl^-, NO_3^-, ClO_4^-, etc.) play an important role in the stability and iron release dynamics of the Tfs-Fe^{3+} complex [1-37]. However, the effect of crowding agents on the salt dependence of iron release and structural stability of sTf-Fe^{3+} complex are not explored so far. This chapter also evaluated the effects of crowding agent (dextran 40) on the salt (NaCl) dependence of the sTf-Fe^{3+} complex and structural stability of Fe_2sTf. The effect of crowding agents (dextran 70, dextran 40, and ficoll 70) on the reductive iron release (Fe^{2+} release) and urea denaturation induced iron release (Fe^{3+} release) from the N-lobe of sTf (Fe_NsTf) was evaluated at pH 7.4 and pH 5.5. The effects of crowding agent (dextran 40) on the salt dependence reductive iron release (Fe^{2+} release) and urea denaturation induced iron release (Fe^{3+} release) from the N-lobe of sTf (Fe_NsTf) was also evaluated at pH 7.4 and pH 5.5.

7.2 Results

7.2.1 Effects of crowding agents and salt on the pH- and urea dependence of the absorbance spectra of Fe_2sTf

At pH 7.4, the absorption spectrum of Fe_2sTf shows a maximum at ~465 nm (Figs. 7.1a and 7.1b), indicating iron is fully associated with the protein. At pH 7.4, in the presence of 200 mg ml^{-1} dextran 40 or 1.0 M NaCl, the absorbance maximum at 465 nm is not changed greatly (Fig. 7.1a). When pH is lowered from 7.4 to 4.0, the absorbance at 465 nm is completely

diminished, which suggests that a decrease in pH from physiological to mildly acidic induces the release of iron from Fe_2sTf (Fig. 7.1a). When urea concentration is increased from 0.0 to 10.0 M at pH 7.4 (Fig. 7.1b) or 8.5 M at pH 5.7 (Fig. 7.1c), the absorbance at 465 nm is completely diminished (Figs. 7.1b and 7.1c), indicating that the iron is fully released from the Fe_2sTf. At pH 5.0 (Fig. 7.1a) or at pH 7.4 with 5 M urea (Fig. 7.1b) or at pH 5.7 with 3.5 M urea (Fig. 7.1c), the absorbance at 465 nm is diminished by around half (Figs. 7.1a, 7.1b and 7.1c). Interestingly, when 200 mg ml^{-1} dextran 40 is included, the absorbance maximum at 465 nm does not decrease significantly at pH 5.0 (Fig. 7.1a) or at pH 7.4 with 5 M urea (Fig. 7.1b) or at pH 5.7 with 3.5 M urea (Fig. 7.1c), indicating that the crowding agent counteracts on the pH- and urea-denaturation induced decrease in the sTf-Fe^{3+} complex stability. However, the inclusion of 0.3 M NaCl both in the absence and presence of 200 mg ml^{-1} dextran 40 at pH 5.0 (Fig. 7.1a), at pH 7.4 with 5 M urea (Fig. 7.1b) or at pH 5.7 with 3.5 M urea (Fig. 7.1c) decrease the absorbance maximum at 465, indicating that salt exhibits additive effect on the pH- and urea-denaturation induced decreased in the sTf-Fe^{3+} complex stability. Based on these observations, the pH and urea-denaturation equilibrium titrations of Fe_2sTf were performed under (i) different concentrations of crowding agents, and (ii) different concentrations of salt both in the absence and presence of 200 mg ml^{-1} dextran 40.

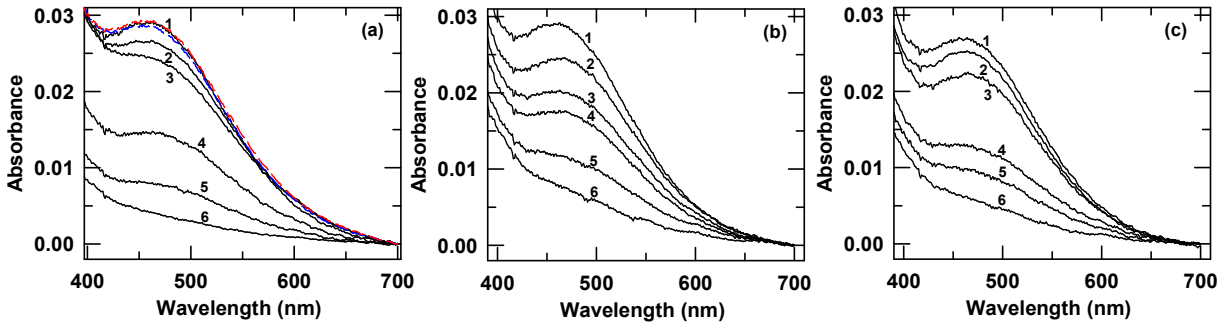

Fig. 7.1. Effect of crowding agent and salt on pH- and urea dependence of the absorbance spectra of Fe_2sTf at 25 °C. (a) Absorbance spectra of Fe_2sTf: (1) pH 7.4, no additive; (2) pH 5.0, 200 mg ml^{-1} dextran 40; (3) pH 5.0, 200 mg ml^{-1} dextran 40 with 0.3 M NaCl; (4) pH 5.0, no additive; (5) pH 5.0, 0.3 M NaCl; (6) pH 4.0, no additive. Red and blue short dash line spectra correspond to Fe_2sTf (pH 7.4) in the presence of 1.0 M NaCl and 200 mg ml^{-1} dextran 40, respectively. Panel (b) shows the absorbance spectra of Fe_2sTf at pH 7.4. Curve labels 1 to 6 correspond to 0.0 M urea; 200 mg ml^{-1} dextran 40 with 5.0 M urea; 5.0 M urea with 0.3 M NaCl and 200 mg ml^{-1} dextran 40; 5.0 M urea; 5.0 M urea with 0.3 M NaCl; and 10.0 M urea, respectively. Panel (c) shows the absorbance spectra of Fe_2sTf at pH 5.7. Curve labels 1 to 6 correspond to 0.0 M urea; 200 mg ml^{-1} dextran 40 with 3.5 M urea; 3.5 M urea with 0.3 M NaCl and 200 mg ml^{-1} dextran 40; 3.5 M urea; 3.5 M urea with 0.3 M NaCl; and 8.5 M urea, respectively.

7.2.2 Effects of crowding agents on the pH- and urea-denaturation induced iron release from Fe_2sTf

To determine the effects of crowding agents on the pH- and urea-denaturation induced iron release from Fe_2sTf, the pH- and urea-denaturation (at pH 7.4 and pH 5.7) induced iron release equilibrium profiles for Fe_2sTf were obtained by monitoring the absorbance at 465 nm in the absence and presence of different concentrations of crowding agent (ficoll 70, dextran 40, and dextran 70). Fig. 7.2a presents the representative absorbance monitored pH-induced iron release profiles of Fe_2sTf in the absence and presence of 200 mg ml^{-1} crowding agent (ficoll 70, dextran 40 and dextran 70) at 25 °C. Figs. 7.2b and 7.2c present the representative absorbance monitored urea-denaturation induced iron release profiles of Fe_2sTf in the absence and presence of 200 mg ml^{-1} crowding agent (dextran 40, dextran 70 and ficoll 70) at pH 7.4 and pH 5.7, respectively. Clearly, in the presence of crowding agent (ficoll 70, dextran 40, and dextran 70), the pH-induced iron release profile shifts toward the lower pH (Fig. 7.2a) while the urea-denaturation induced iron release profile shifts toward the higher concentration of urea (Figs. 7.2b and 7.2c). Furthermore, the crowding agent-induced shifts in the pH profile (toward the lower pH) and urea profile (toward the higher urea concentrations) are more pronounced for dextran 70 and least for ficoll 70 (dextran 70 > dextran 40 > ficoll 70). The pH and urea equilibrium titrations were fitted according to equations (5) and (1) (chapter 2), respectively. The estimated pH-midpoint for iron release (C_m^*) is plotted as a function of [crowding agent] in Fig 7.2d. Fig. 7.2d shows that the C_m^* for iron release decreases in the presence of crowding agents, and typically follows the order, dextran 70 > dextran 40 > ficoll 70, which suggest that dextran 70 is most and ficoll 70 is least effective in decreasing the rate of iron release. The estimated urea denaturation free energy (ΔG_D), surface area exposed by solvent (m_g), and urea-denaturation midpoint for iron release ($C_m = \Delta G_D/m_g$) are summarized in (Table 7.1) (appendix). Figs. 7.2e and 7.2f present C_m *vs* [Crowding agent] plots at pH 7.4 and pH 5.7, respectively. The inset of Figs. 7.2e and 7.2f present ΔG_D *vs* [Crowding agent] plots at pH 7.4 and pH 5.7, respectively. The C_m (Figs. 7.2e and 7.2f) and ΔG_D (Inset of Figs. 7.2e and 7.2f) for iron release increase in the presence of crowding agents and which are more increased for dextran 70 and least for ficoll 70 (dextran 70 > dextran 40 > ficoll 70). These finding indicate that the crowding agent counteracts the pH- and urea-denaturation induced decrease in sTf-Fe^{3+} complex stability and

this effect is more pronounced for dextran 70 and least for ficoll 70 (dextran 70 > dextran 40 > ficoll 70).

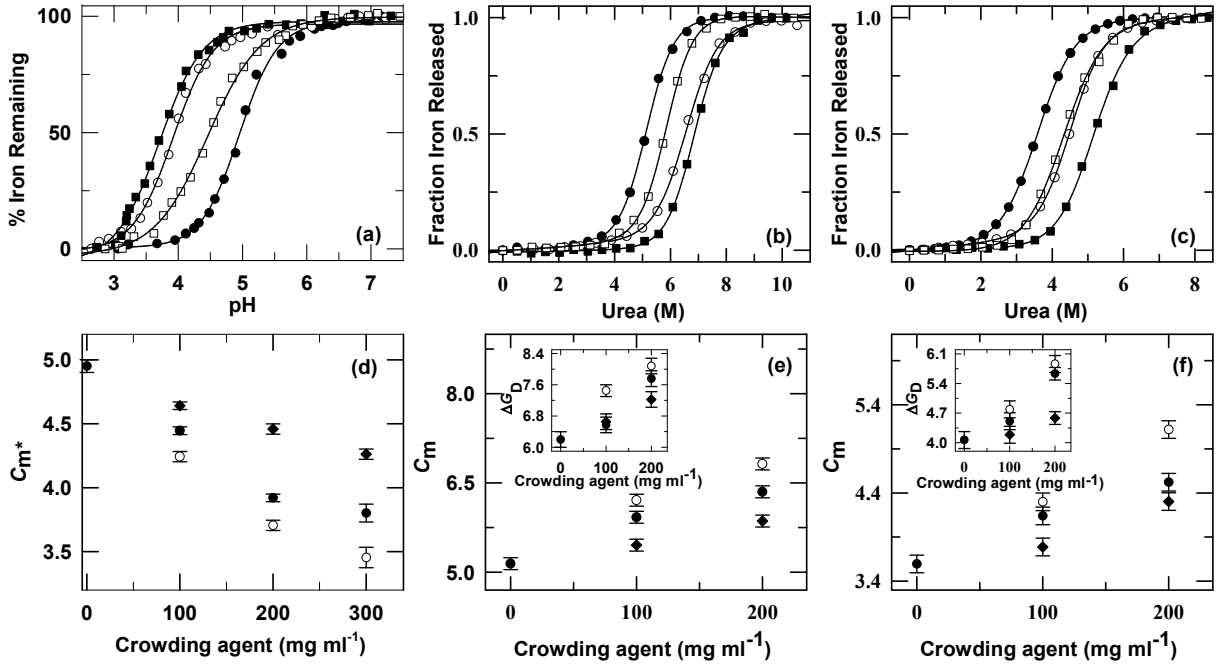

Fig. 7.2 Effect of crowding agents on the pH- and urea-denaturation induced iron release from Fe_2sTf. Panel (a) shows the pH-induced iron release profiles (monitored by absorbance at 465 nm) of Fe_2sTf in the absence (●) and presence of 200 mg ml^{-1} crowding agent (dextran 40 (○), dextran 70 (■) or ficoll 70 (□)). These pH-equilibrium titrations were fitted according to equation (5) (chapter 2). Panels (b) and (c) show the urea-denaturation induced iron release profiles (monitored by absorbance at 465 nm) of Fe_2sTf in the absence (●) and presence of 200 mg ml^{-1} crowding agent (dextran 40 (○), dextran 70 (■) or ficoll 70 (□)) at pH 7.4 and pH 5.7, respectively. The solid lines in panels (b) and (c) represent a non-linear least squares fit of the data to equation (1) (chapter 2). Panel (d) shows the dependence of pH-midpoint (C_m^*) for iron release from Fe_2sTf on [Crowding agent] ((●) dextran 40, (○) dextran 70 and (♦) ficoll 70). Panels (e) and (f) show the dependence of urea-midpoint C_m (=$\Delta G_D/m_g$) for iron release from Fe_2sTf on [Crowding agent] ((●) dextran 40, (○) dextran 70 and (♦) ficoll 70) at pH 7.4 and pH 5.7, respectively. Insets of panels (e) and (f) show the dependence of ΔG_D on [Crowding agent] ((●) dextran 40, (○) dextran 70 and (♦) ficoll 70) at pH 7.4 and pH 5.7, respectively.

7.2.3 Effects of crowding agent on the salt-dependence of pH- and urea-denaturations induced iron release from Fe_2sTf

To determine the effects of crowding agent on the salt dependence of pH- and urea-denaturation induced iron release from Fe_2sTf, the pH and urea (at pH 7.4 and pH 5.7) denaturations-induced iron release profiles of Fe_2sTf were obtained by monitoring the absorbance at 465 nm as a function of [NaCl] both in the absence and presence of 200 mg ml^{-1}

dextran 40. Fig. 7.3a presents the representative absorbance monitored pH-induced iron release profiles of Fe_2sTf measured in the absence and presence of 0.15 M NaCl, 200 mg ml^{-1} dextran 40, 0.15 M NaCl with 200 mg ml^{-1} dextran 40. Figs. 7.3b and 7.3c present the representative urea denaturation-induced iron release profiles of Fe_2sTf in the absence and presence of 0.3 M NaCl, 200 mg ml^{-1} dextran 40, and 0.3 M NaCl with 200 mg ml^{-1} dextran 40 at pH 7.4 and pH 5.7, respectively. Data in Figs. 7.3a, 7.3b and 7.3c clearly show that the salt presence in reaction medium shifts the pH- and urea-denaturations induced iron release profiles of Fe_2sTf toward the higher pH (Fig. 7.3a) and lower urea concentrations (Figs. 7.3b and 7.3c). However, in the presence of 200 mg ml^{-1} dextran 40, the salt-induced shifts in the pH- and urea-denaturations-induced iron release profiles toward the higher pH (Fig. 7.3a) and lower urea concentrations (Figs. 7.3b and 7.3c) are less pronounced than in its absence.

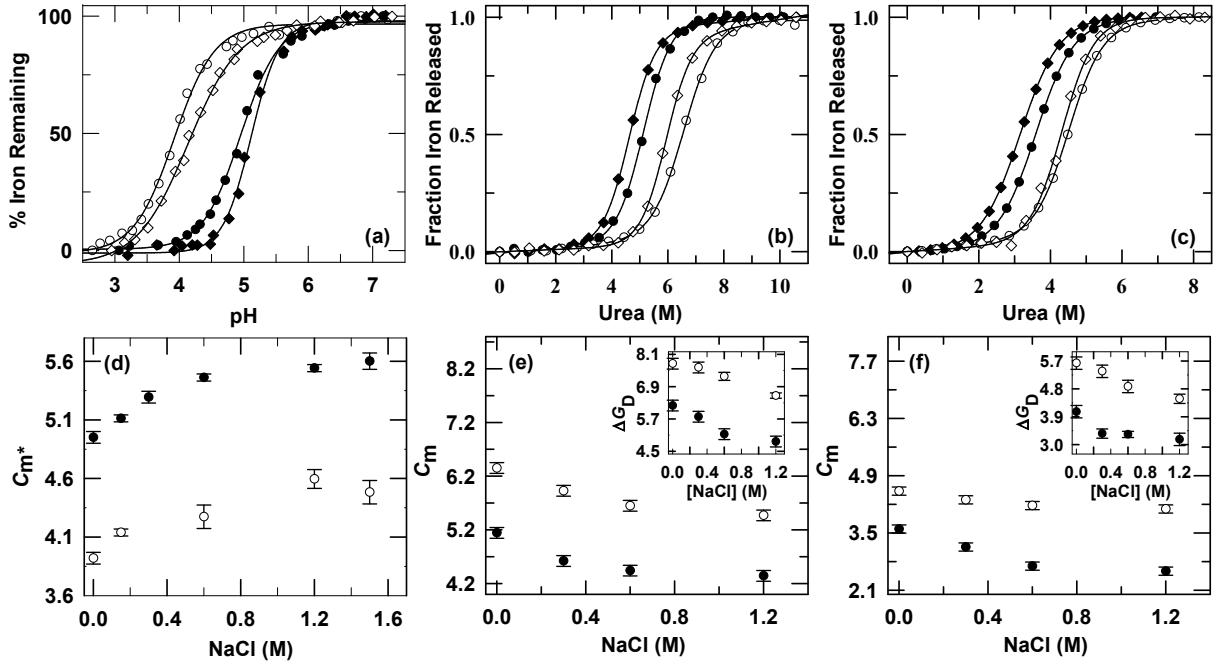

Fig. 7.3 Effect of crowding agent on the salt dependence of pH- and urea-denaturation induced iron release from Fe_2sTf. Panel (a) shows the pH-induced iron release profiles (monitored by absorbance at 465 nm) of Fe_2sTf in the absence (●) and presence of 200 mg ml^{-1} dextran 40 (○), 0.15 M NaCl (♦), 0.15 M NaCl with 200 mg ml^{-1} dextran (◊). These pH-equilibrium titrations were fitted according to equation (5) (chapter 2). Panels (b) and (c) present the urea-denaturation induced iron release profiles (monitored by absorbance at 465 nm) of Fe_2sTf in the absence (●) and presence of 0.3 M NaCl (♦), 200 mg ml^{-1} dextran 40 (○), and 0.3 M NaCl with 200 mg ml^{-1} dextran 40 (◊) at pH 7.4 and pH 5.7, respectively. The solid lines in panels (b) and (c) represent a non-linear least squares fit of the data to equation (1) (chapter 2). (d) The dependence of the pH-midpoint (C_m^*) for the iron release from Fe_2sTf on [NaCl] (in the absence (●) and presence of 200 mg ml^{-1} dextran 40 (○)). Panels (e) and (f) show the dependence of urea-midpoint C_m (=$\Delta G_D/m_g$) for the iron release from Fe_2sTf on [NaCl] (in the absence (●) and presence of

200 mg ml^{-1} dextran 40 (○)) at pH 7.4 and pH 5.7, respectively. Insets of panels (e) and (f) show the dependence of ΔG_D on [NaCl] (in the absence (●) and presence of 200 mg ml^{-1} dextran 40 (○)) at pH 7.4 and pH 5.7, respectively.

This finding indicates that the crowding agent counteracts the salt-induced decrease in the sTf-Fe^{3+} complex stability. The pH and urea titrations were fitted according to equations (5) and (1) (chapter 2), respectively. The estimated pH-midpoint for iron release (C_m^*) in the absence and presence of 200 mg ml^{-1} dextran 40 is plotted as a function of [NaCl] in Fig 7.3d.

As [NaCl] is increased, the C_m^* for iron release increase (Fig. 7.3d), which suggests that the salt presence in reaction medium decreased the sTf-Fe^{3+} complex stability. However, in the presence of crowding agent, the C_m^* for iron release also increases with [NaCl] (Fig. 7.3d). This finding suggests that the presence of crowding agent does not alter the salt effect on sTf-Fe^{3+} complex stability (*i.e.,* salt-induced destabilization of sTf-Fe^{3+} complex stability). The estimated urea denaturation free energy (ΔG_D), surface area exposed by solvent (m_g), and urea-denaturation midpoint for iron release ($C_m=\Delta G_D/m_g$) are summarized in (Table 7.2) (appendix). Figs. 7.3e and 7.3f present C_m *vs* [NaCl] plots in the absence and presence of 200 mg ml^{-1} dextran 40 at pH 7.4 and pH 5.7, respectively. The inset of Figs. 7.3e and 7.3f present the ΔG_D *vs* [NaCl] plots in the absence and presence of 200 mg ml^{-1} dextran 40 at pH 7.4 and pH 5.7, respectively. As [NaCl] is increased, the ΔG_D for iron release decreases (Inset of Figs. 7.3e and 7.3f), indicating that the salt presence decreases the stability sTf-Fe^{3+} complex. However, in the presence of crowding agent, the ΔG_D for iron release also decreases with [NaCl] (Inset of Figs. 7.3e and 7.3f). This finding suggests that the crowding agent presence in reaction medium does not alter the salt effect on the stability of sTf-Fe^{3+} complex (*i.e.,* salt-induced decrease in the stability of sTf-Fe^{3+} complex)

7.2.4 Effects of crowding agents and salt on the far-UV CD spectra of Fe_2sTf

The far-UV CD spectrum of native Fe_2sTf shows negative extrema at ~208 nm and shoulder around 215-225 nm, which reflects the secondary structure of the Fe_2sTf. Figs. 7.4a, 7.4b and 7.4c show the far-UV CD spectra of Fe_2sTf collected at pH 7.4 in the absence and presence of different concentrations of ficoll 70, dextran 40 and dextran 70, respectively. Figs. 7.4d, 7.4e and 7.4f show the far-UV CD spectra of Fe_2sTf collected at pH 5.5 in the absence and presence different concentrations of ficoll 70, dextran 40 and dextran 70, respectively. Figs. 7.4a and 7.4d also show the far-UV CD spectra of Fe_2sTf collected in the presence of 1.0 M NaCl at

pH 7.4 and pH 5.5, respectively. Fig. 7.4 suggests that in the presence of crowding agent or NaCl, the far-UV CD spectrum of native Fe_2sTf is not changed greatly.

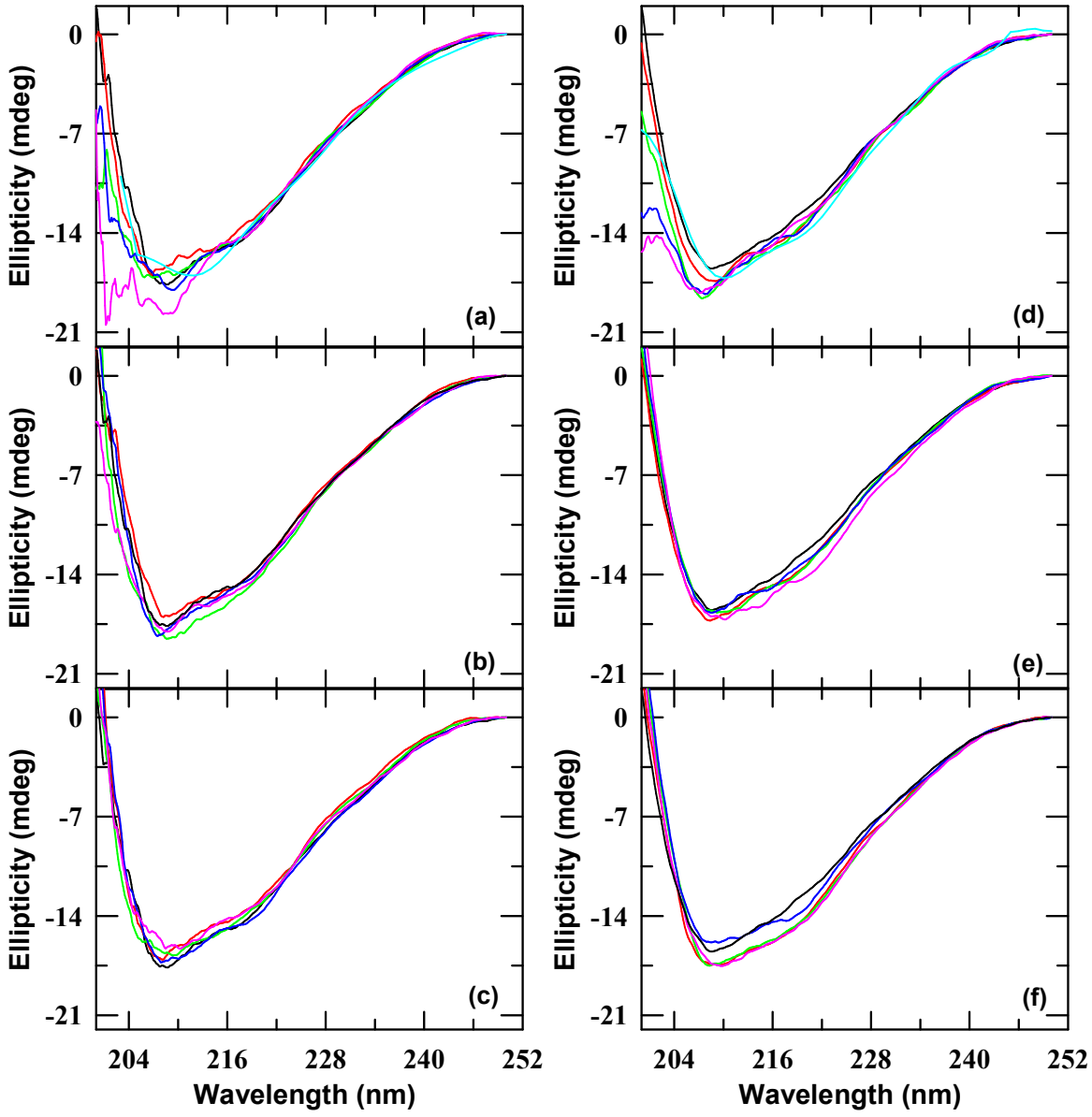

Fig. 7.4. Crowding agents and salt dependence of the far-UV CD spectra of Fe_2sTf. Panels (a), (b) and (c) present the far-UV CD spectra of Fe_2sTf measured at pH 7.4 in the presence of different concentrations of ficoll 70, dextran 40 and dextran 70, respectively. Panel (d), (e) and (f) present the far-UV CD spectra of Fe_2sTf measured at pH 5.5 in the presence of different concentrations of ficoll 70, dextran 40 and dextran 70, respectively. Panel (a) and panel (d) also shows the far-UV CD spectra of Fe_2sTf in the presence of 1.0 M NaCl at pH 7.4 and pH 5.5, respectively. The black, red, green, blue and pink lines are correspond to 50 mg ml^{-1}, 100 mg ml^{-1}, 200 mg ml^{-1}, and 300 mg ml^{-1} concentration of crowding agent, respectively. Cyan line corresponds to 1.0 M NaCl.

7.2.5 Effects of crowding agent and salt on the urea dependence of the far-UV CD spectra of Fe_2sTf

Fig. 5a presents the far-UV CD spectra of Fe_2sTf measured in the absence and presence of 10.8 M urea at pH 7.4, 25 °C. Fig. 7.5b presents the far-UV CD spectra of Fe_2sTf measured in the absence and presence of 8.5 M urea at pH 5.5, 25 °C. Clearly, the negative extrema at 208 nm and shoulder around 215-225 nm at 10.8 M urea, pH 7.4 and 8.5 M urea, pH 5.5 are substantially disrupted (Figs. 7.5a and 7.5b), indicating that the secondary structure of protein is significantly lost. Figs. 7.5a and 7.5b also present the far-UV CD spectra of Fe_2sTf measured at 25 °C in the presence of 8.0 M urea at pH 7.4 (Fig. 7.5a) and 4.5 M urea at pH 5.5 (Fig. 7.5b), 200 mg ml^{-1}dextran 40 with 8.0 M urea at pH 7.4 (Fig. 7.5a) and 4.5 M urea at pH 5.5 (Fig. 7.5b), 1.0 M NaCl with 8.0 M urea at pH 7.4 (Fig. 7.5a) and 4.5 M urea at pH 5.5 (Fig. 7.5b), and 200 mg ml^{-1}dextran and 1.0 M NaCl with 8.0 M urea at pH 7.4 (Fig. 7.5a) and 4.5 M urea at pH 5.5 (Fig. 7.5b). In the presence of 8.0 M urea at pH 7.4 and 4.5 M urea at pH 5.5, the negative extrema at 208 nm and shoulder around 215-225 nm are partially disrupted (Figs. 7.5a and 7.5b). When 200 mg ml^{-1} dextran 40 is included in the presence of 8.0 M urea at pH 7.4 and 4.5 M urea at pH 5.5, the negative extrema at 208 nm and shoulder around 215-225 nm are not greatly changed (Figs. 7.5a and 7.5b), indicating that the crowding agent counteracts on the urea-induced destabilization of secondary structure of Fe_2sTf. When 1.0 M NaCl is included in the presence of 8.0 M urea at pH 7.4 and 4.5 M urea at pH 5.5, the negative extrema at 208 nm and shoulder around 215-225 nm are significantly disrupted (Figs. 7.5a and 7.5b), indicating that the salt exhibits the additive effect on the urea-induced destabilization of secondary structure of Fe_2sTf. However, inclusion of 200 mg ml^{-1}dextran 40 in the presence of 8.0 M urea with 1.0 M NaCl at pH 7.4 and 4.5 M urea with 1.0 M NaCl at pH 5.5, the negative extrema at 208 nm and shoulder around 215-225 nm are not greatly changed (Figs. 7.5a and 7.5b), indicating that the crowding agent counteracts on the salt- induced destabilization of secondary structure of Fe_2sTf.

7.2.6 Effects of crowding agents on the urea-induced unfolding of Fe_2sTf

To determine the effects of crowding agents on the structural stability of Fe_2sTf, the urea-denaturation induced unfolding curves (based on ellipticity at 222 nm) were collected in the absence and presence of 100, 200 and 300 mg ml^{-1} crowding agents (dextran 40, dextran 70 and ficoll 70) at pH 7.4 and pH 5.5, 25 °C. Figs. 7.6a and 7.6b present the representative urea-

denaturation induced unfolding curves of Fe_2sTf measured in the absence and presence of 200 mg ml^{-1} crowding agent (dextran 40, dextran 70 and ficoll 70) at pH 7.4 and pH 5.5, respectively.

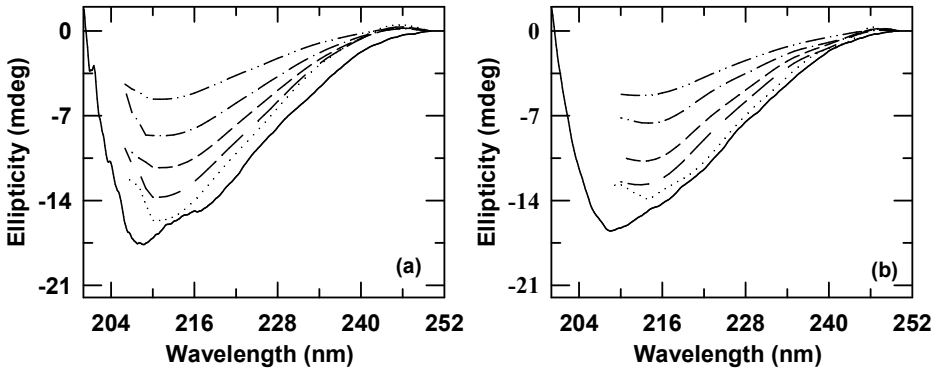

Fig. 7.5. Effects of crowding agents and salt on the urea dependence far-UV CD spectra of Fe_2sTf at 25 °C. (a) presents the far-UV spectra of Fe_2sTf measured in the absence (solid line) and presence of 10.8 M urea (dash dot dot line) at pH 7.4. Panel (a) also presents the far-UV spectra of Fe_2sTf measured at pH 7.4 in the presence of 8.0 M urea (short dash line); 8.0 M urea with 1.0 M NaCl (dash dot line); 8.0 M urea with 200 mg ml^{-1}dextran 40 (dotted line); 8.0 M urea with 200 mg ml^{-1}dextran 40 and 1.0 M NaCl (medium medium dash line) at pH 7.4. Panel (b) presents the far-UV spectra of Fe_2sTf measured in the absence (solid line) and presence of 8.5 M urea (dash dot dot line) at pH 5.5. Panel (b) also presents the far-UV spectra of Fe_2sTf measured at pH 5.5 in the presence of 4.5 M urea (short dash line); 4.5 M urea with 200 mg ml^{-1}dextran 40 (dotted line); 4.5 M urea with 200 mg ml^{-1}dextran 40 and 1.0 M NaCl (medium medium dash line); 4.5 M urea with 1.0 M NaCl (dash dot line).

Figs. 7.6a and 7.6b clearly show that in the presence of crowding agents (dextran 40, dextran 70 and ficoll 70), the urea-denaturation induced unfolding curve shifts toward the higher concentrations of urea. Furthermore, the crowding-induced shift in the urea-denaturation induced unfolding curve at pH 7.4 and 5.5 is more pronounced for dextran 70 and least for ficoll 70 (dextran 70 > dextran 40 > ficoll 70). The urea-denaturation induced unfolding curves were analyzed using equation (1) (chapter 2). The resulting urea unfolding free energy (ΔG_D), surface area exposed by solvent (m_g), and urea unfolding midpoint (C_m=$\Delta G_D/m_g$) are summarized in (Table 7.3) (appendix). Figs. 7.6c and 7.6d show the variation of C_m as a function of [Crowding agents] at pH 7.4 and pH 5.5, respectively. Insets of Figs. 7.6c and 7.6d show the ΔG_D *vs* [Crowding agents] plots at pH 7.4 and pH 5.5, respectively. As [Crowding agent] is increased, the C_m and ΔG_D for unfolding of Fe_2sTf increase, and which are more increased for dextran 70 and least for ficoll 70 (dextran 70 > dextran 40 > ficoll 70) (Figs. 7.6c and 7.6d). This finding indicates that the crowding agents increase the thermodynamic stability of Fe_2sTf and this effect is more pronounced for dextran 70 and least for ficoll 70 (dextran 70 > dextran 40 > ficoll 70).

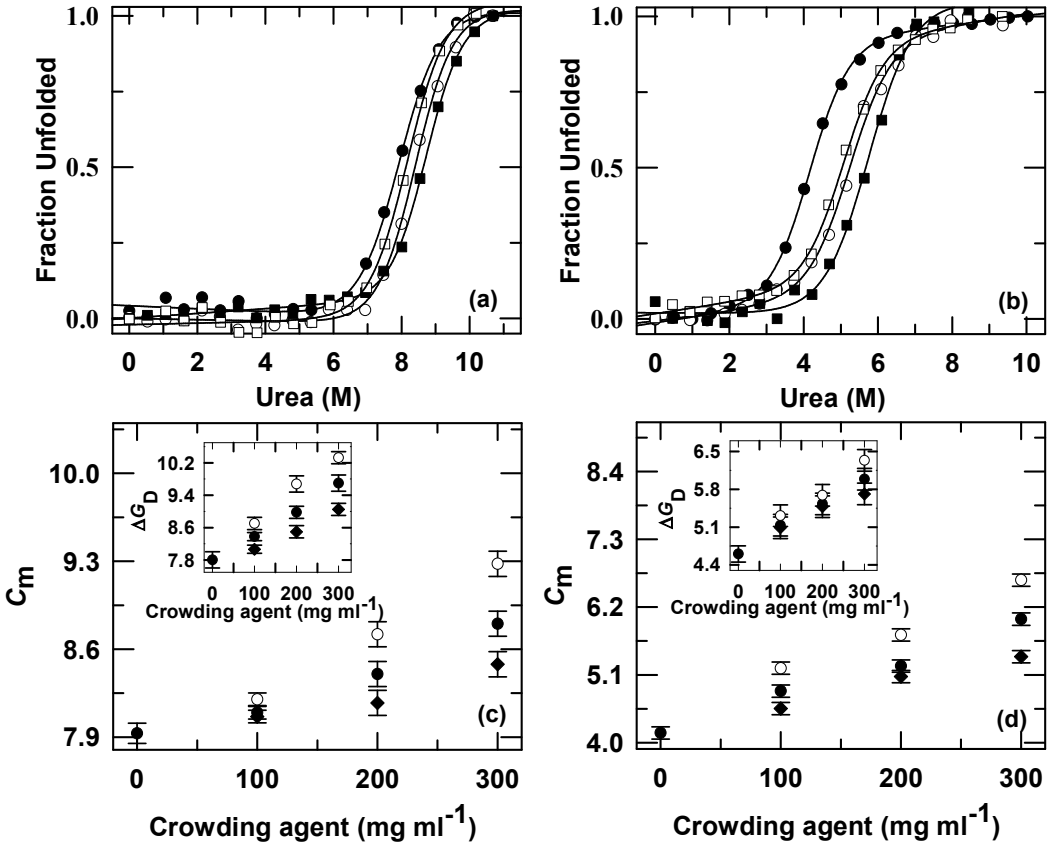

Fig. 7.6 Effect of crowding agents on the urea-induced unfolding of Fe_2sTf. Panels (a) and (b) show the far-UV CD (222 nm) monitored unfolding curves of Fe_2sTf at pH 7.4 and pH 5.5, respectively, in the absence (●) and presence of 200 mg ml^{-1} crowding agent (dextran 40 (○),dextran 70 (■) and ficoll 70 (□). The solid lines in panels (a) and (b) represent a non-linear least squares fit of the data to equation (1) (chapter 2). Panels (c) and (d) show the dependence of urea-midpoint C_m (=$\Delta G_D/m_g$) for the unfolding of Fe_2sTf on [Crowding agent] ((●) dextran 40, (○) dextran 70 and (♦) ficoll 70) at pH 7.4 and pH 5.7, respectively. Insets of panels (c) and (d) show the dependence of ΔG_D on [Crowding agent] ((●) dextran 40, (○) dextran 70 and (♦) ficoll 70) at pH 7.4 and pH 5.5, respectively.

7.2.7 Effects of crowding agent on the salt dependence of the urea-induced unfolding of Fe_2sTf

To determine the effects of crowding agents on the salt dependence of the urea-induced unfolding of Fe_2sTf, the urea-denaturation induced unfolding curves (based on ellipticity at 222 nm) of Fe_2sTf were collected at various concentration of NaCl both in the absence and presence of 200 mg ml^{-1} dextran 40. Figs. 7.7a and 7.7b present the representative urea-denaturation induced unfolding curves of Fe_2sTf measured in the absence and presence 0.3 M NaCl, 200 mg ml^{-1} dextran 40, 0.3 M NaCl with 200 mg ml^{-1} dextran 40 at pH 7.4 and pH 5.5, respectively.

Data in Figs. 7.7a and 7.7b clearly show that the salt presence in reaction medium shifts the urea-denaturation induced unfolding curves of Fe_2sTf towards the lower urea concentrations. However, in the presence of 200 mg ml^{-1} dextran 40, the salt-induced shift in the urea-denaturation-induced unfolding curves towards the lower urea concentrations is less pronounced than in its absence.

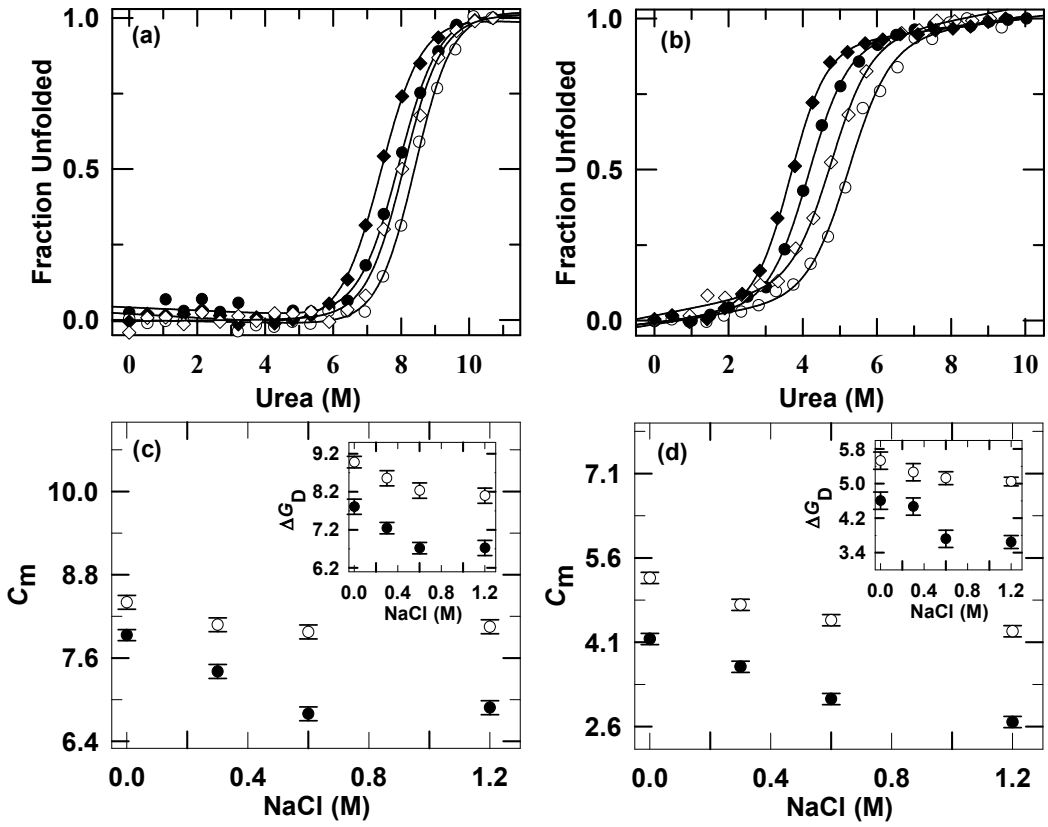

Fig. 7.7. Effect of crowding agents on the salt dependence of the urea-induced unfolding of Fe_2sTf. Panels (a) and (b) show the far-UV CD (222 nm) monitored unfolding curves of Fe_2sTf at pH 7.4 and pH 5.5, respectively, in the absence (●) and presence of 0.3 M NaCl (♦), 200 mg ml^{-1} dextran 40 (○), and 0.3 M NaCl with 200 mg ml^{-1} dextran 40 (◊). The solid lines in panels (a) and (b) represent a non-linear least squares fit of the data to equation (1) (chapter 2). Panels (c) and (d) show the dependence of urea-midpoint C_m (=$\Delta G_D/m_g$) for the unfolding of Fe_2sTf on [NaCl] (in the absence (●) and presence of 200 mg ml^{-1} dextran 40 (○)) at pH 7.4 and pH 5.7, respectively. Insets of panels (c) and (d) show the dependence of ΔG_D on [NaCl] (in the absence (●) and presence of 200 mg ml^{-1} dextran 40 (○)) at pH 7.4 and pH 5.5, respectively.

The urea-denaturation induced unfolding curves were analyzed using equation (1) (chapter 2). The resulting urea unfolding free energy (ΔG_D), surface area exposed by solvent (m_g), and urea unfolding midpoint (C_m=$\Delta G_D/m_g$) are summarized in Table 7.4 (appendix). Figs. 7.7c and 7.7d show the variation of C_m as a function of [NaCl] in the absence and presence of

200 mg ml^{-1} dextran 40 at pH 7.4 and pH 5.5, respectively. Insets of Figs. 7.7c and 7.7d show the ΔG_D *vs* [NaCl] plots in the absence and presence of 200 mg ml^{-1} dextran 40 at pH 7.4 and pH 5.5, respectively. As [NaCl] is increased, the ΔG_D for unfolding decreases (Inset of Figs. 7.7c and 7.7d), indicating that the salt presence decreases the thermodynamic stability of Fe_2sTf. However, in the presence of crowding agent, the ΔG_D for unfolding also decreases with [NaCl] (Inset of Figs. 7.7c and 7.7d). This finding suggests that the crowding agent presence in reaction medium does not alter the salt effect on the thermodynamic stability of Fe_2sTf (*i.e.,* salt-induced decrease in the thermodynamic stability of Fe_2sTf).

7.2.8 Effects of crowding agents on the reduction and urea-denaturation induced iron release from Fe_NsTf

To understand the effects of crowding agents on the reduction and urea-denaturation induced iron release from Fe_NsTf, the kinetics of reduction (Fe^{2+}) and urea-denaturation (Fe^{3+}) iron release from the Fe_NsTf have been studied as a function of crowding agent (dextran 40, dextran 70 and ficoll 70) concentration at pH 7.4 and 5.5. Figs. 7.8a and 7.8b present the representative reduction induced Fe^{2+} release kinetic traces of Fe_NsTf measured in the absence and presence of 200 mg ml^{-1} dextran 40 at pH 7.4 and pH 5.5 (25 °C), respectively. Figs. 7.9a and 7.9b show the representative urea denaturation-induced iron release kinetic traces of Fe_NTf measured in the absence and presence of 200 mg ml^{-1} dextran 40 at pH 7.4 and pH 5.5 (37 °C), respectively. Fe^{2+} and Fe^{3+} release kinetic data in the absence and presence of crowding agent at pH 7.4 and 5.5 are best described by a single exponential rate expression. The observed rate constant, k_{obs} for Fe^{2+} and Fe^{3+} release at different concentrations of crowding agents are summarized in Tables 7.5 and 7.6 (appendix), respectively. The variation of k_{obs} for Fe^{2+} release with [Crowding agent] at pH 7.4 and 5.5 is shown in Figs. 7.8c and 7.8d, respectively. Figs. 7.9c and 7.9d show the variation of k_{obs} for Fe^{3+} release with [Crowding agent] at pH 7.4 and 5.5, respectively. As [Crowding agent] is increased, the rate constants for Fe^{2+} and Fe^{3+} release decrease at pH 7.4 (Figs. 7.8c and 7.9c) and pH 5.5 (Figs. 7.8d and 7.9d), and typically follws the order, dextran 70 > dextran 40 > ficoll 70 (Figs. 7.8c, 7.9c, 7.8d and 7.9d), which suggest that dextran 70 is most and ficoll 70 is least effective in decrasing the rate of iron release. This finding indicates that the crowding agent presence in the reaction medium retards the Fe^{2+} and

Fe^{3+} release at physiological and endosomal pH and this effect is more pronounced for dextran 70 and least for ficoll 70 (dextran 70 > dextran 40 > ficoll 70).

To test whether the presence of crowding agent affects the thermodynamic activation parameter for reductive iron release, the activation enthalpy ($\Delta H^{\ddagger}$), activation entropy ($\Delta S^{\ddagger}$) and activation free energy ($\Delta G^{\ddagger}$) for Fe^{2+} release from Fe_NsTf were determined in the absence and presence of 200 mg ml^{-1} crowding agent (dextran 40, dextran 70 and ficoll 70) at pH 7.0 and pH 5.5. Figs. 7.10a and 7.10b present the Eyring plots for Fe^{2+} release reaction of Fe_NsTf obtained from temperature-dependent data in the absence and presence of 200 mg ml^{-1} crowding agent (dextran 40, dextran 70 and ficoll 70) at pH 7.4 and pH 5.5, respectively. The Eyring plots in Figs. 7.10a and 7.10b were analyzed by using the equation (1):

$$\ln(k_{obs}h/k_B T) = (\Delta S^{\ddagger}/R) - (\Delta H^{\ddagger}/RT) \qquad (1)$$

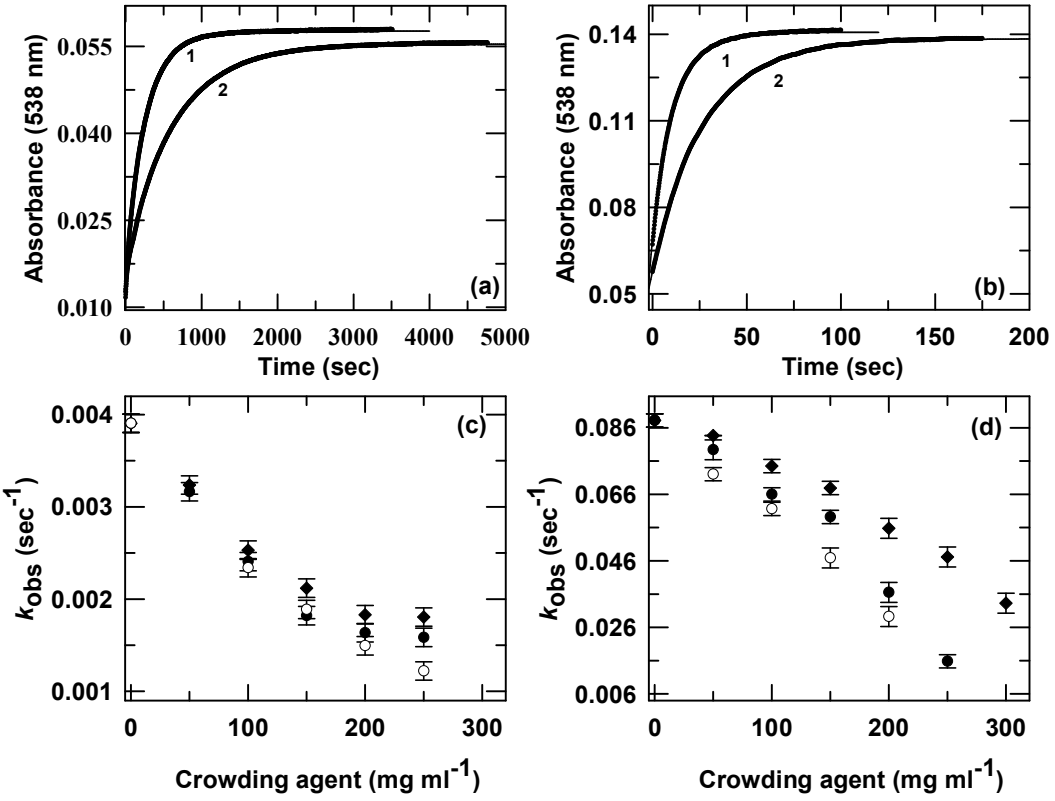

Fig. 7.8. Effects of crowding agents on the reduction induced iron (Fe^{2+}) release from Fe_NsTf. Panel (a) and (b) present the single-phase reductive iron release kinetic traces of Fe_NsTf in the absence (trace 1) and in the presence of 200 mg ml^{-1} dextran 40 (trace 2) at pH 7.4 and pH 5.5 (25 °C), respectively. The solid line in panels (a) and (b) show least-squares fits of the data to a single exponential function. Panels (c)

and (d) show the resulting rate constants for reductive iron release, k_{obs}, as a function of crowding agent (dextran 40 (●), dextran 70 (○) and ficoll 70 (♦)) at pH 7.4 and pH 5.5 (25 °C), respectively.

The estimated values of $\Delta H^{\ddagger}$ and $\Delta S^{\ddagger}$ are summarized in Table 1. By using the $\Delta H^{\ddagger}$ and $\Delta S^{\ddagger}$ values, the corresponding ($\Delta G^{\ddagger}$) is also calculated at 25 °C using Gibbs free energy equation ($\Delta G^{\ddagger} = \Delta H^{\ddagger} - T\Delta S^{\ddagger}$) (Table 1). The data in Table 1 clearly show that (i) the presence of crowding agent in the reaction medium increases the enthalpic barrier ($\Delta H^{\ddagger}$) for Fe^{2+} release reaction at pH 7.4 and 5.5, and which is more increased for dextran 70 and least for ficoll 70 (dextran 70 > dextran 40 > ficoll 70) and (ii) the increase in $\Delta H^{\ddagger}$ in the presence of crowding agent is accompanied by the decrease in the entropy change, $-T\Delta S^{\ddagger}$.

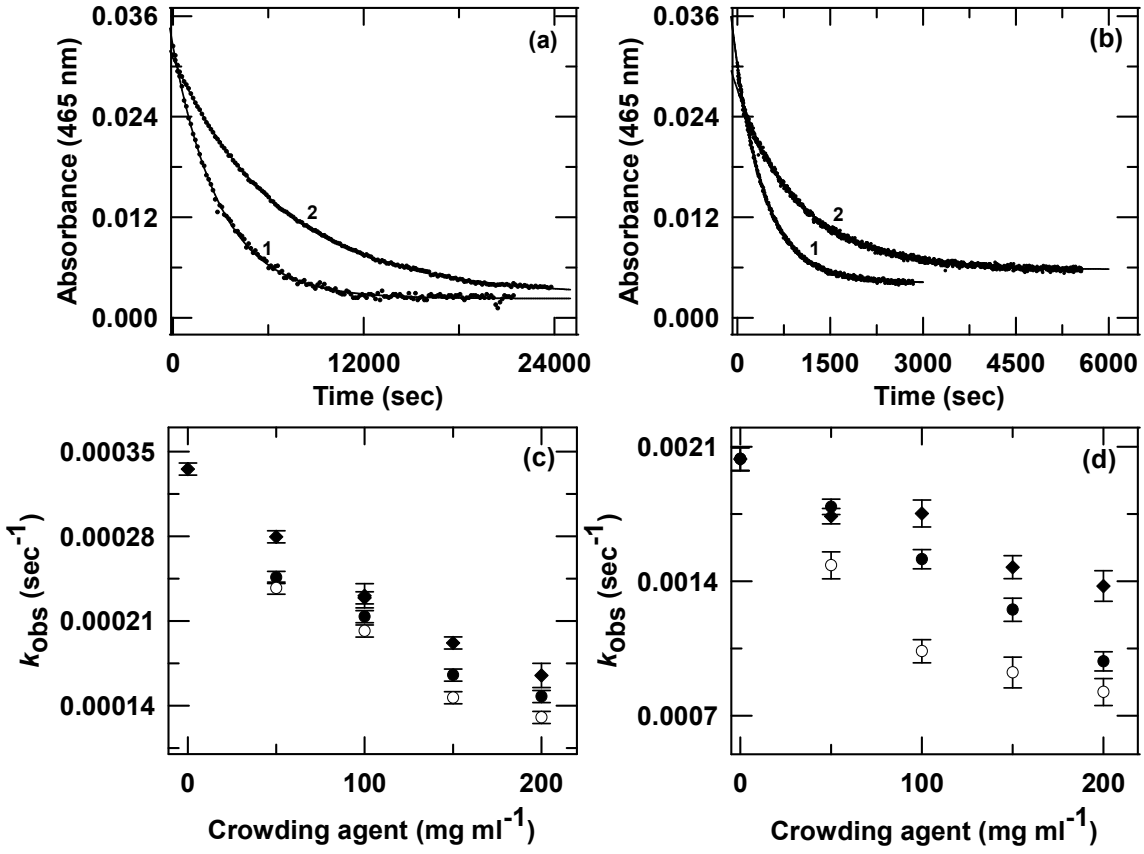

Fig. 7.9. Effects of crowding agents on the urea-induced iron (Fe^{3+}) release from Fe_NsTf. Panels (a) and (b) present the single-phase urea denaturation induced iron release kinetic traces of Fe_NsTf in the absence (trace 1) and in the presence of 200 mg ml^{-1} dextran 40 (trace 2) at pH 7.4 and pH 5.5 (37 °C), respectively. The solid line in panels (a) and (b) show least-squares fits of the data to a single exponential function. Panels (c) and (d) show the resulting rate constants for urea denaturation induced iron release, k_{obs}, as a function of crowding agent (dextran 40 (●), dextran 70 (○) and ficoll 70 (♦)) at pH 7.4 and pH 5.5 (37 °C), respectively.

Table 1. Effects of crowding agents on the activation parameters for Fe^{2+} release reaction of Fe_NsTf.*

	$\Delta G^{\ddagger a}$ (kcal mol^{-1})	$\Delta H^{\ddagger}$ (kcal mol^{-1})	$\Delta S^{\ddagger}$ (cal mol^{-1} K^{-1})	$-T\Delta S^{\ddagger a}$ (kcal mol^{-1})
pH 7.4				
Control	20.9(0.1)	8.9(0.3)	-40.2(1.2)	12.0(0.3)
200 mg ml^{-1} dextran 40	21.4(0.1)	11.5(0.5)	-33.2(1.8)	9.9(0.5)
200 mg ml^{-1} dextran 70	21.2(0.1)	12.2(0.2)	-31.2(0.7)	9.0(0.2)
200 mg ml^{-1} ficoll 70	21.3(0.1)	11.0(0.4)	-34.7(1.3)	10.3(0.4)
pH 5.5				
Control	19.0(0.1)	3.2(0.2)	-52.9(0.6)	15.8(0.2)
200 mg ml^{-1} dextran 40	19.6(0.1)	5.5(0.2)	-47.2(0.7)	14.1(0.2)
200 mg ml^{-1} dextran 70	19.7(0.1)	6.6(0.3)	-43.8(0.9)	13.1(0.3)
200 mg ml^{-1} ficoll 70	19.3(0.1)	4.8(0.2)	-48.7(0.7)	14.5(0.2)

[a] Activation free energy ($\Delta G^{\ddagger}$) and entropy changes ($-T\Delta S^{\ddagger}$) are given at 25 ºC.
*The uncertainties (standard error) in $\Delta H^{\ddagger}$, $-T\Delta S^{\ddagger}$ and $\Delta S^{\ddagger}$ are indicated in parenthesis.

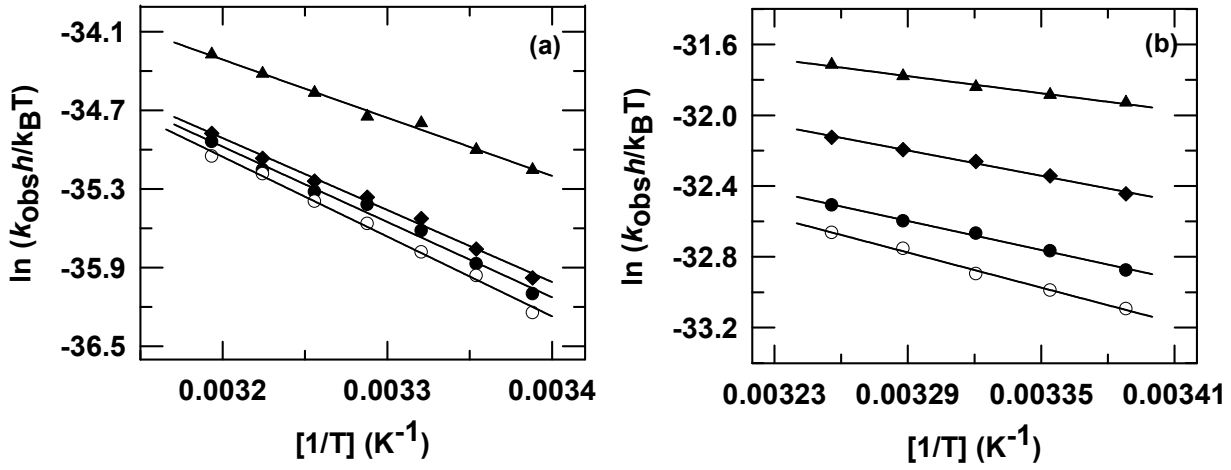

Fig. 7.10. Effects of crowding agents on the thermodynamic activation parameter for reductive iron release at pH 7.4 and 5.5. The Panels (a) and (b) show Erying plots for the reduction-induced iron release from Fe_NsTf at pH 7.4 and pH 5.5, respectively (no addition (▲), 200 mg ml^{-1} crowding agent (dextran 40 (●), dextran 70 (○) and ficoll 70 (♦)).

As described earlier [38-39], the enthalpy-entropy plot could be used to determine enthalpic and entropic contributions toward the stability, folding and dynamics of proteins. The enthalpy-entropy plot has four sectors (Figs. 7.11a and 7.11b). Sectors 1 and 2 correspond to stabilizing cosolutes while sectors 3 and 4 correspond to destabilizing cosolutes. Furthermore,

sectors 1 and 3 represent the enthalpically dominated effect while sectors 2 and 4 represent entropically dominated effect [38]. Figs. 7.11a and 7.11b present the $T\Delta\Delta S$ vs $\Delta\Delta H$ plots for 200 mg ml^{-1} of dextran 40, dextran 70 and ficoll 70. Clearly, the data points for crowding agent lie in sector 1 (Figs. 7.11a and 11b), which is in general agreement with the models that describe enthalpically dominated stabilization [38-40].

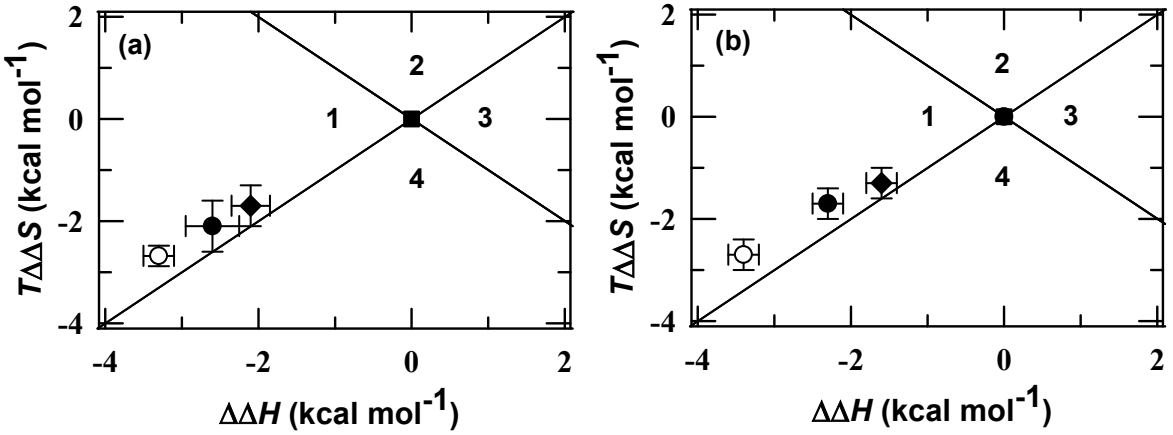

Fig. 7.11. Panels (a) and (b) show the $T\Delta\Delta S$ and $\Delta\Delta H$ plot at pH 7.4 and pH 5.5, respectively. Data points correspond to in the absence (■) and presence of 200 mg ml^{-1} of crowding agent (dextran 40 (●), dextran 70 (○) and ficoll 70 (♦)).

7.2.9 Effects of crowding agent on the salt-dependence of reduction and urea-denaturation induced iron release from Fe_NsTf

To determine the effects of crowding agent on the salt-dependence of reduction and urea denaturation-induced iron release from Fe_NsTf, the kinetics of reduction (Fe^{2+}) and urea-denaturation (Fe^{3+}) iron release from the Fe_NsTf have been measured at different [NaCl] in the absence and presence of 200 mg ml^{-1} dextran 40 at pH 7.4 and 5.5. Figs. 7.12a and 7.12b present the representative kinetic traces of Fe^{2+} release from Fe_NsTf in the absence and presence of 0.5 M NaCl, 200 mg ml^{-1} dextran 40, 0.5 M NaCl with 200 mg ml^{-1} dextran 40 at pH 7.4 and pH 5.5 (25 °C), respectively. Figs. 7.13a and 7.13b present the representative urea denaturation-induced Fe^{3+} release kinetic traces of Fe_NsTf measured in the absence and presence of 0.6 M NaCl, 200 mg ml^{-1} dextran 40, 0.6 M NaCl with 200 mg ml^{-1} dextran 40 at pH 7.4 and pH 5.5 (37 °C), respectively. Fe^{2+} and Fe^{3+} release kinetic data measured at different [NaCl] in the absence and presence of 200 mg ml^{-1} dextran 40 at pH 7.4 and 5.5 are best described by a single exponential rate expression. The observed rate constants, for Fe^{2+} and Fe^{3+} release measured at different

[NaCl] in the absence and presence of 200 mg ml^{-1} dextran 40 at pH 7.4 and 5.5, are summarized in Tables 7.7 and 7.8 (appendix).

As [NaCl] is increased, the rate constants for Fe^{2+} and Fe^{3+} release increase monoexponentially at pH 7.4 (Figs. 7.12c and 7.13c) and pH 5.5 (Figs. 7.12d and 7.13d), which suggests that anion-binding-induced conformational change promote the reduction induced Fe^{2+} release from Fe_NsTf. However, the rate constants for Fe^{2+} and Fe^{3+} also increase with [NaCl] in the presence of crowding agent at pH 7.4 (Figs. 7.12c and 7.13c) and pH 5.5 (Figs. 7.12d and 7.13d). This finding suggests that the presence of crowding agent does not alter the salt effect on reductive iron release from Fe_NsTf.

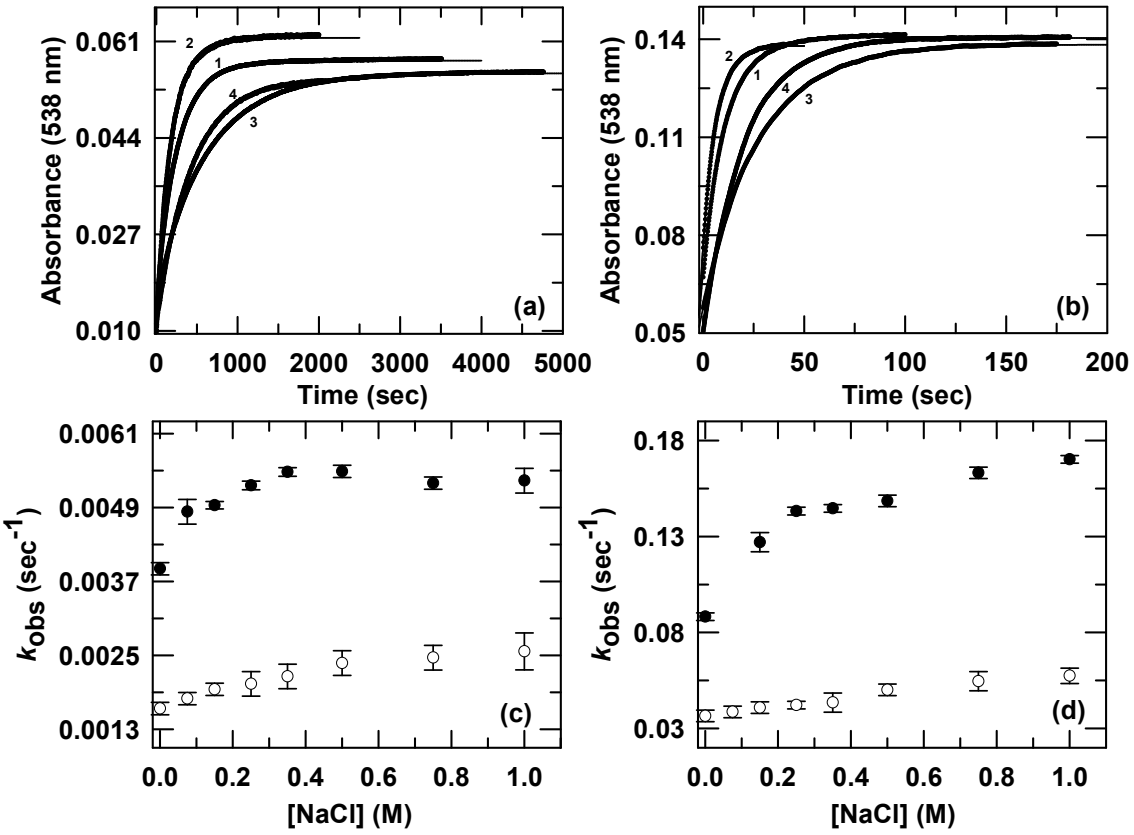

Fig. 7.12. Effects of crowding agent on salt-dependence of the reduction induced iron (Fe^{2+}) release from Fe_NsTf. Panels (a) and (b) present the single-phase reductive iron release kinetic traces of Fe_NsTf in the absence (trace 1) and in the presence of different additives (0.5 M NaCl (trace 2), 200 mg ml^{-1} dextran 40 (trace 3) and 200 mg ml^{-1} dextran 40 with 0.5 M NaCl (trace 4)) at pH 7.4 and pH 5.5 (25 °C) , respectively. The solid line in panels (a) and (b) show least-squares fits of the data to a single exponential function. Panels (c) and (d) show rate constants for reductive iron release, k_{obs}, as a function of NaCl in the absence (●) and presence of 200 mg ml^{-1} dextran 40 (○) at pH 7.4 and pH 5.5 (25 °C), respectively.

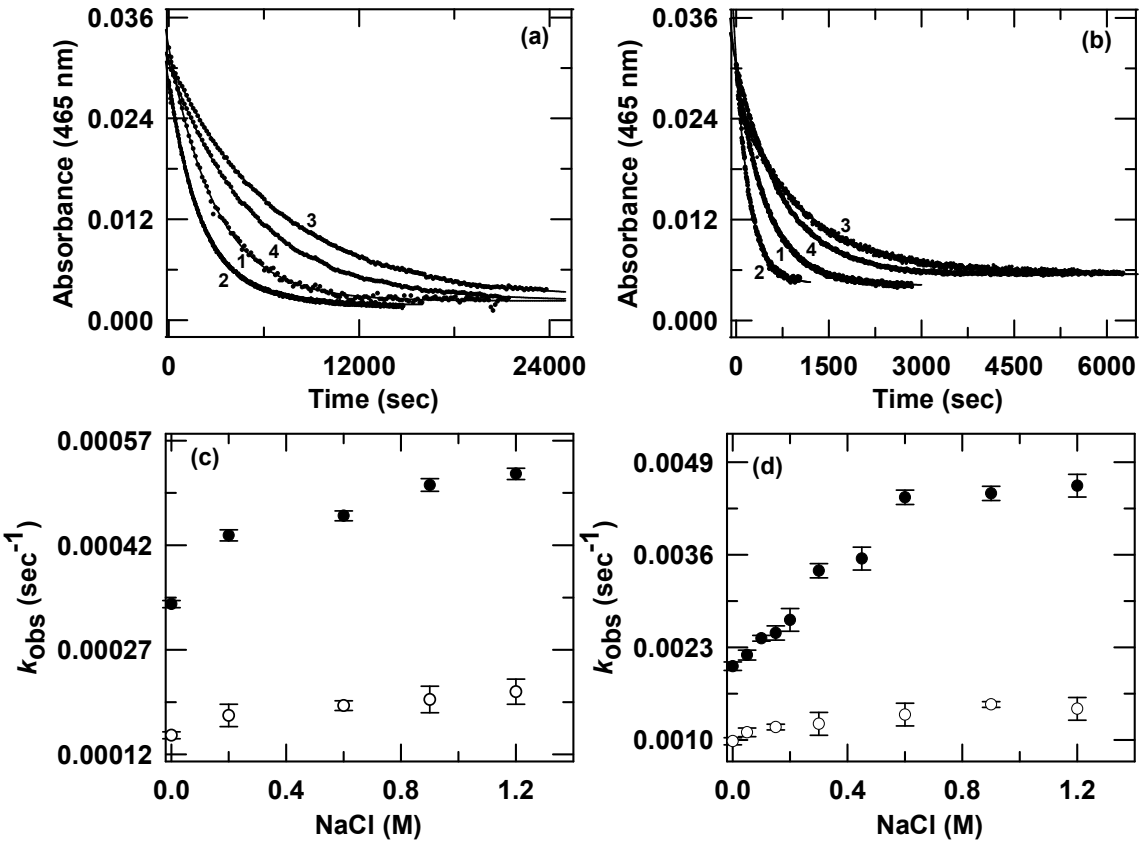

Fig. 7.13. Effects of crowding agent on salt-dependence of the urea-induced iron (Fe^{3+}) release from Fe_NsTf. Panels (a) and (b) present the single-phase urea denaturation induced iron release kinetic traces of Fe_NsTf in the absence (trace 1) and in the presence of different additives (0.6 M NaCl (trace 2), 200 mg ml^{-1} dextran 40 (trace 3) and 200 mg ml^{-1} dextran 40 with 0.6 M NaCl (trace 4)) at pH 7.4 and pH 5.5 (37 °C), respectively. The solid line in panels (a) and (b) show least-squares fits of the data to a single exponential function. Panels (c) and (d) show rate constants for urea denaturation induced iron release, k_{obs}, as a function of NaCl in the absence (●) and presence of 200 mg ml^{-1} dextran 40 (○) at 7.4 and pH 5.5 (37 °C), respectively.

To test whether the presence of crowding agent affects the salt-dependence of thermodynamic activation parameter for reductive iron release, the activation enthalpy ($\Delta H^{\ddagger}$), activation entropy ($\Delta S^{\ddagger}$) and activation free energy ($\Delta G^{\ddagger}$) for Fe^{2+} release from Fe_NsTf were determined in the absence and presence of 0.15 M NaCl, 200 mg ml^{-1} dextran 40, and 0.5 M NaCl with 200 mg ml^{-1} dextran 40 at pH 7.0 and pH 5.5. Figs. 7.14a and 7.14b present the Eyring plots for Fe^{2+} release reaction of Fe_NsTf obtained from temperature-dependent data in the absence and presence of 0.15 M NaCl, 200 mg ml^{-1} dextran 40, and 0.5 M NaCl with 200 mg ml^{-1} dextran 40 at pH 7.0 and pH 5.5. The Eyring plots in Figs. 7.14a and 7.14b were analyzed by

using the equation (1). The estimated values of $\Delta H^{\ddagger}$ and $\Delta S^{\ddagger}$ are summarized in Table 2. By using the $\Delta H^{\ddagger}$ and $\Delta S^{\ddagger}$ values, the corresponding ($\Delta G^{\ddagger}$) is also calculated at 25 °C using Gibbs free energy equation ($\Delta G^{\ddagger} = \Delta H^{\ddagger} - T\Delta S^{\ddagger}$) (Table 2).

Table 2. Effect of crowding agent on the salt dependence of the activation thermodynamic parameters for Fe^{2+} release reaction of Fe_NsTf.*

	$\Delta G^{\ddagger a}$ (kcal mol^{-1})	$\Delta H^{\ddagger}$ (kcal mol^{-1})	$\Delta S^{\ddagger}$ (cal mol^{-1} K^{-1})	$-T\Delta S^{\ddagger a}$ (kcal mol^{-1})
pH 7.4				
Control	20.9(0.1)	8.9(0.3)	-40.2(1.2)	12.0(0.3)
200 mg ml^{-1} dextran 40	21.4(0.1)	11.5(0.5)	-33.2(1.8)	9.9(0.5)
0.5 M NaCl with 200 mg ml^{-1} dextran 40	21.1(0.1)	10.1 (0.2)	-37.1(0.6)	11.0(0.2)
0.15 M NaCl	20.7(0.1)	6.6 (0.3)	-47.3(1.0)	14.1(0.3)
pH 5.5				
Control	19.0(0.1)	3.2(0.2)	-52.9(0.6)	15.8(0.2)
200 mg ml^{-1} dextran 40	19.6(0.1)	5.5(0.2)	-47.2(0.7)	14.1(0.2)
0.15 M NaCl	18.7(0.1)	1.9(0.1)	-56.6(0.2)	16.8(0.1)
0.5 M NaCl with 200 mg ml^{-1} dextran 40	19.3(0.1)	5.1(0.2)	-47.7(0.7)	14.2(0.2)

[a] Activation free energy ($\Delta G^{\ddagger}$) and entropy changes ($-T\Delta S^{\ddagger}$) are given at 25 ºC.
*The uncertainties (standard error) in $\Delta H^{\ddagger}$, $-T\Delta S^{\ddagger}$ and $\Delta S^{\ddagger}$ are indicated in parenthesis.

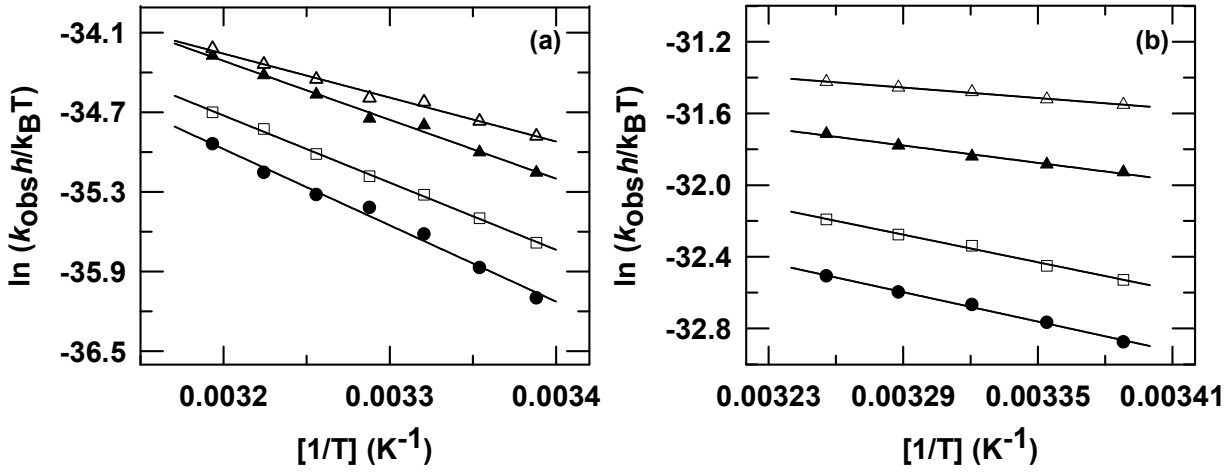

Fig. 7.14. Effects of crowding agent on the salt dependence of thermodynamic activation parameter for reductive iron release at pH 7.4 and 5.5. Panels (a) and (b) show Erying plots for the reduction-induced iron release from Fe_NsTf at pH 7.4 and pH 5.5, respectively (no addition (▲), 200 mg ml^{-1} dextran 40 (●), 0.15 M NaCl (Δ) and 0.5 M NaCl with 200 mg ml^{-1} dextran 40 (□)).

The data in Table 2 clearly show that (i) the presence of salt in the reaction medium decreases the enthalpic barrier ($\Delta H^{\ddagger}$) for Fe^{2+} reaction at pH 7.4 and 5.5, and which is less decreased in the presence of crowding agent than in its absence, which indicates that crowding agent counteracts on the salt-induced decrease in the enthalpic barrier for reductive iron release at both physiological and endosmal pH, and (ii) both in the absence and presence of crowding agent, the salt mediated decrease in $\Delta H^{\ddagger}$ is accompanied by the increase in the entropy change, $-T\Delta S^{\ddagger}$.

7.3 Discussion

This is the first assessment of the effect of crowding agents (dextran 40, dextran 70 and ficoll) on the stability and iron release kinetics of sTf at physiological and endosomal pH. Analysis of the pH and urea-denaturation profiles for iron release of Fe_2sTf, collected in the absence and presence of different concentrations of dextran 40, dextran 70 and ficoll 70 revealed that (i) crowding agents increase the stability of Tf-Fe^{3+} complex under physiological and endosomal pH conditions (Figs. 7.2d, 7.2e and 7.2f) (ii) the stability of Tf-Fe^{3+} complex is found to be increased more for dextran 70 and least for ficoll 70 (dextran 70 > dextran 40 > ficoll 70) (Figs. 7.2d, 7.2e and 7.2f). Fig. 7.15 shows the effects of crowding agents (dextran 40, dextran 70 and ficoll 70) on the relative free energies of native and unfolded states measured for the iron release from Fe_2sTf (pH 7.4). Under solution conditions, the dextran is regarded as a rod-shaped crowding agent while the ficoll is considered as a spherical crowding agent [41]. The more increased of the Tf-Fe^{3+} complex stability for dextran 70 than ficoll 70 (Figs. 7.2d, 7.2e and 7.2f) suggesting that the shape of crowding agent play an important on the stability of iron centers of Fe_2sTf. Dextran 70 has the larger size than that of the dextran 40 [41], so the greater increase of Tf-Fe^{3+} complex stability for dextran 70 (Figs. 7.2d, 7.2e and 7.2f) suggests that the size of crowding agent also plays a vital role in the stability of iron centers of Fe_2sTf.

The secondary structural content in natively folded Fe_2sTf is not greatly changed in the presence of crowding agents (dextran 40, dextran 70 and ficoll) (Fig. 7.4). This result is consistent with the earlier findings with Cyt *c*, Lyz and Cellular retinoic acid-binding protein I in which the secondary structural content was not greatly changed on addition of crowding agent [41-44]. However, crowding agents induces the secondary structure in the natively folded apo and holo-flavodoxin, VlsE, RNase-A and a-LA. [41-47]. Analysis of the urea-denaturation

induced unfolding curves of Fe_2sTf at pH 7.4 and 5.5, collected in the absence and presence of different concentrations of dextran 40, dextran 70 and ficoll 70 revealed that (i) crowding agents increase the structural stability of Fe_2sTf under physiological and endosomal pH conditions (Figs. 7.6c and 7.6d), (ii) the structural stability of Fe_2sTf is found to be increased more for dextran 70 and least for ficoll 70 (dextran 70 > dextran 40 > ficoll 70) (Figs. 7.6c and 7.6d). Fig. 7.15 shows the effects of crowding agents (dextran 40, dextran 70 and ficoll 70) on the relative free energies of native and unfolded states measured for the unfolding of Fe_2sTf (pH 7.4). These finding reveals that the size, shape and concentration of crowding agent control the structural stability of Fe_2Tf under physiological and endosomal pH conditions.

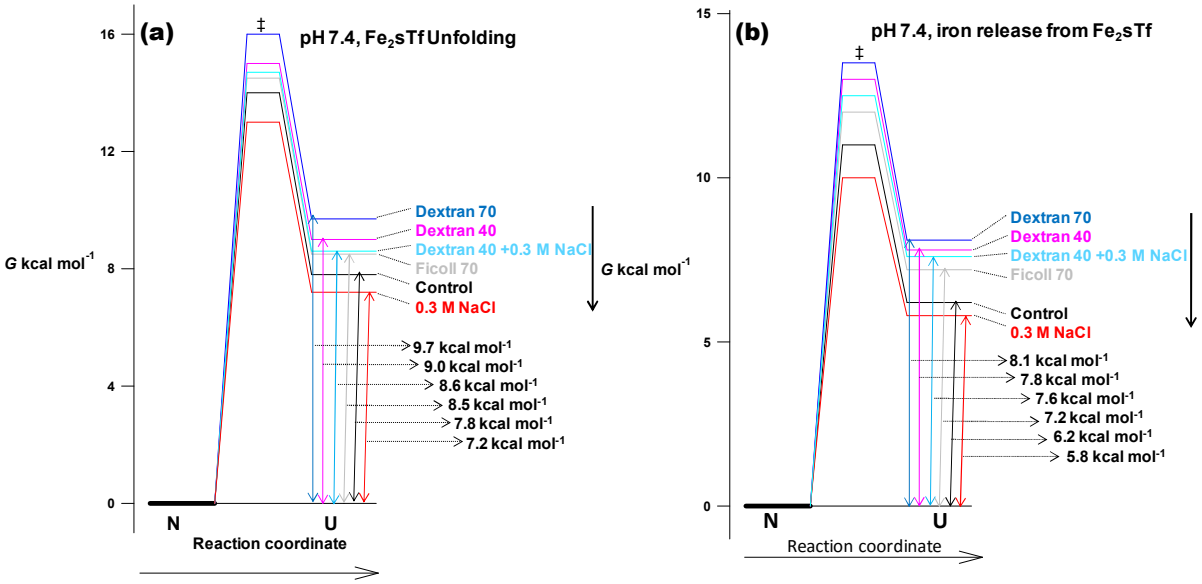

Fig. 7.15 Diagram illustrating the effects of crowding agent and salt on the relative free energies of native and unfolded states measured for the unfolding (a) and iron release (b) from Fe_2sTf. The thermodynamic parameters derived from equilibrium unfolding experiments (Tables 7.1 to 7.4) (appendix). The free energy of the native state of protein is arbitrarily set to zero. The energy levels of transition states may not appear scaled exactly.

Previous reports revealed that presence of crowding agents increase the thermal and structural stability of proteins [41-47]. The GdnHCl-induced equilibrium unfolding of native apoazurin revealed that the stabilizing effect of ficoll 70 is less than any of the dextrans (dextran 20, dextran 40 and dextran 70) and among the dextrans no size dependent effect was observed [44]. However, GdnHCl-induced equilibrium unfolding transitions of native Ferrocyt *c* at pH 7 showed that the smaller sized crowder (dextran 40) has a greater impact on the thermodynamic stability of Ferrocyt *c* (dextran 40 > dextran 70 > ficoll 70) [48]. The thermal stability of

flavodoxin is increased more in the presence of dextran 70 than ficoll 70 [46]. These results suggest that crowding agents of different sizes (dextran 70, dextran 40), shapes (dextran 70 (rod shaped), ficoll 70 (spherical shaped)) have different stabilizing effects on the different proteins.

Previous reports revealed that the crowding agent presence in reaction medium enhances the enzymes activity [49-52], whereas the rates of other are decreased [53-55] or unaltered [56]. Crowding agent can either decrease or increase the reaction rate depending on the concentration of it used [57]. These results suggest the more complicated trends of the effect of macromolecular crowding on the enzyme kinetics. In the present study, the kinetic and thermodynamic analysis of the reduction and urea-denaturation induced iron release at pH 7.4 and 5.5 in the absence and presence of different concentration of dextran 40, dextran 70 and ficoll 70 revealed that (i) crowding agent presence in the reaction medium retards the Fe^{2+} and Fe^{3+} release at physiological and endosomal pH (Fig. 7.8c, 7.8d, 7.9c and 7.9d) (ii) the crowding agent mediated retardation in Fe^{2+} and Fe^{3+} release is more pronounced for dextran 70 and least for ficoll 70 (dextran 70 > dextran 40 > ficoll 70) (Fig. 7.8c, 7.8d, 7.9c and 7.9d), which indicates that size, shape and viscosity of crowding agents control the iron release process of Fe_NsTf because dextran 70 has higher size and viscosity than dextran 40 [58] and different shape than ficoll 70 [41], (iii) the presence of crowding agent in the reaction medium increases the enthalpic barrier ($\Delta H^{\ddagger}$) for Fe^{2+} release reaction at pH 7.4 and pH 5.5, and which is more increased for dextran 70 and least for ficoll 70 (dextran 70 > dextran 40 > ficoll 70) (Table 1), and (iv) the increase in $\Delta H^{\ddagger}$ in the presence of crowding agent is accompanied by the decrease in the entropy change, $-T\Delta S^{\ddagger}$ (Table 1). The increase in $\Delta H^{\ddagger}$ by crowding agents suggests that some crowding agents form attractive interactions with Fe_NsTf and thus block the Fe^{2+} release from Fe_NsTf under physiological and endosomal pH conditions. Some earlier reports revealed that the crowding agent forms the attractive interaction with Cyt *c* and ubiquitin [59-60]. The attractive interactions between crowding agent and proteins can also decrease the entropy of crowding agent in the reaction medium.

Current study provides fundamentally improved system to explain the anion effect on the stability and iron release kinetics of sTf, because the synthetic crowding agents mimic the in vivo macromolecular crowding. Analysis of the pH-induced iron release profiles and urea-denaturation-induced unfolding and iron release profiles of Fe_2sTf, collected at different [NaCl] both in the absence and presence of 200 mg ml^{-1} dextran 40 revealed that (i) the salt presence in

reaction medium decrease the sTf-Fe^{3+} complex (Fig. 7.3d, 7.3e and 7.3f) and structural stability of Fe_2sTf (Fig. 7.7c and 7.7d) while the crowding agent presence increase the sTf-Fe^{3+} complex (Fig. 7.3d, 7.3e and 7.3f) and structural stability of Fe_2sTf (Fig. 7.7c and 7.7d) (ii) salt also decrease the sTf-Fe^{3+} complex (Fig. 7.3d, 7.3e and 7.3f) and structural stability of Fe_2sTf (Fig. 7.7c and 7.7d) in the presence of crowding agent, which indicates that the crowding agent presence in reaction medium does not alter the salt effect on the destabilization of sTf-Fe^{3+} complex and structural stability of Fe_2sTf. Fig. 7.15 shows that the relative free energies of native and unfolded states measured for the iron release and unfolding of Fe_2sTf (pH 7.4).

Kinetics and thermodynamic analysis of reduction and urea-denaturation induced iron release from the Fe_NsTf at different [NaCl] in the absence and presence of 200 mg ml^{-1} dextran 40 at pH 7.4 and 5.5 revealed that (i) both in the absence and presence crowding agent, the anion-binding-induced conformational change promotes the iron release from Fe_NsTf at physiological and endosomal pH (Fig. 7.12c, 7.12d, 7.13c and 7.13d) and (ii) the presence of salt in the reaction medium decreases the enthalpic barrier ($\Delta H^{\ddagger}$) for iron release at pH 7.4 and 5.5 (Table 2), and which is less decreased in the presence of crowding agent than in its absence (Table 2) which indicates that crowding agent counteracts on the salt-induced decrease in the enthalpic barrier for iron release at both physiological and endosmal pH, (ii) both in the absence and presence of crowding agent, the salt mediated decrease in $\Delta H^{\ddagger}$ is accompanied by the increase in the entropy change, $-T\Delta S^{\ddagger}$ (Table 2).

In the present study, the $T\Delta\Delta S$ vs $\Delta\Delta H$ plots for reductive iron release from Fe_NsTf in the absence and presence of 200 mg ml^{-1} of dextran 40, dextran 70 and ficoll 70 at pH 7.4 and 5.5 reveals that in controlling the iron release from Fe_NsTf in the presence of crowding agent under physiological and endosomal pH conditions, the enthalpic effect is more dominated than the entropic effect (Figs. 7.11a and 7.11b). Previously it was established that crowders induced protein stabilization through purely steric excluded volume effect is entropic [61-64]. However, recent studies showed that the observed effect of crowders on protein stability and folding have a significant enthalpic contributions [48,62,64-65], moreover enthalpic effect even dominates the entropic contributions [48,66-73]. To account for enthalpic as well as entropic effects of crowders, some recent reports suggest that it is necessary to augment the steric excluded volume effects with other nonspecific interactions [48,62,64-65]. Current results also suggest that both

hard-core repulsions and nonspecific chemical (soft) interactions must be considered to understand the effects of crowding agent on the reduction induced Fe^{2+} release from Fe_NsTf.

7.4 Conclusions

As the [crowding agent] is increased, the pH-midpoint for iron release of Fe_2sTf shifts toward the lower pH values while the urea-denaturation midpoints for iron release and unfolding of Fe_2sTf at pH 7.4 and 5.7 shift towards the higher urea concentrations, which suggest that the crowding agent presence in the reaction medium increase the sTf-Fe^{3+} complex and structural stability of Fe_2sTf. Furthermore, the crowding agent mediated increase in Tf-Fe^{3+} complex and structural stability of Fe_2sTf typically follows the order: dextran 70 > dextran 40 > ficoll 70, which suggests that size, shape and viscosity of crowding agents control the Tf-Fe^{3+} complex and structural stability of Fe_2sTf. However, as the [NaCl] is increased both in the absence and presence of crowding agent, the pH-midpoint for iron release from Fe_2sTf shifts toward the higher pH values while the urea-denaturation midpoints for iron release and unfolding of Fe_2sTf at pH 7.4 and 5.7 shift toward the lower urea concentrations, which suggest that the salt presence both in the absence and presence of crowding agent decrease the Tf-Fe^{3+} complex and structural stability of Fe_2sTf. At pH 7.4 and pH 5.5, as [crowding agent] is increased, the rate constants for reductive and urea-denaturation induced iron release from Fe_NsTf decrease, which suggest that the crowding agent presence in the reaction medium retards the iron release from Fe_NsTf. Furthermore, the crowding agent-mediated retardation in iron release typically follows the order: dextran 70 > dextran 40 > ficoll 70, which suggest that the size, shape and viscosity of crowding agents control the iron release from Fe_NsTf. The anion mediated acceleration of reduction and urea denaturation induced iron release from Fe_NsTf is also observed both in the absence and presence of crowding agent. The biological significance of the present study is evidenced by the salt induced modulation of iron release from sTf in the presence of crowding agent. On the basis of the current findings the effect of macromolecular crowding can be taken into account in future studies to describe the mechanism of iron release from sTf.

7.5 References

[1] Dewan JC, Mikami B, Hirose M, Sacchettini JC, Biochemistry 32:11963–11968 (1993)

[2] Halbrooks PJ, He QY, Briggs SK, Everse SJ, Smith VC, MacGillivray RT, Mason AB, Biochemistry 42:3701–3707 (2003)
[3] Halbrooks PJ, Giannetti AM, Klein JS, Björkman PJ, Larouche JR, Smith VC, MacGillivray RT, Everse SJ, Mason AB, Biochemistry 44:15451–15460 (2005)
[4] Egan TJ, Zak O, Aisen P, Biochemistry 32:8162–8167 (1993)
[5] Kretchmar SA, Raymond KN, Inorg Chem 27:1436–1441 (1988)
[6] Kumar R, Mauk AG, J Phys Chem B 113:12400–12409 (2009)
[7] Kumar S, Sharma D, Kumar R, Kumar R, J Biol Inorg Chem 6:1009–1024 (2014)
[8] [Lee DA, Goodfellow JM, Biophysical J 85:2747–2759 (1998)
[9] Rinaldo D, Field MJ, Biophysical J 85:3485–3501 (2003)
[10] Bobst CE, Zhang M, Kaltashov IA, J Mol Biol 388:954–967 (2009)
[11] Aisen P, Listowsky I, Annu Rev Biochem 49:357–393 (1980)
[12] MacGillivray RT, Moore SA, Chen J, Anderson BF, Baker H, Luo Y, Bewley M, Smith CA, Murphy ME, Wang Y, Mason AB, Woodworth RC, Brayer GD, Baker EN, Biochemistry 37:7919–7928 (1998)
[13] He QY, Mason AB, Tam BM, MacGillivray RT, Woodworth RC, Biochemistry 38:9704–9711 (1999)
[14] Byrne SL, Chasteen ND, Steere AN, Mason AB, J Mol Biol 396:130–140 (2010)
[15] James NG, Byrne SL, Steere AN, Smith VC, MacGillivray RT, Mason AB, Biochemistry 48:2858–2867 (2009)
[16] James NG, Berger CL, Byrne SL, Smith VC, MacGillivray RT, Mason AB, Biochemistry 46:10603–10611 (2007)
[17] Nurizzo D, Baker HM, He QY, MacGillivray RT, Mason AB, Woodworth RC, Baker EN, Biochemistry 40:1616–1623 (2001)
[18] He QY, Mason AB, Tam BM, MacGillivray RT, Woodworth RC, Biochem J 344:881–887 (1999)
[19] Byrne SL, Mason AB, J Biol Inorg Chem 14:771–781 (2009)
[20] Bali PK, Zak O, Aisen P, Biochemistry 30:324–328 (1991)
[21] Bali PK, Aisen P, Biochemistry 31:3963–3967 (1992)
[22] Jeffrey PD, Bewley MC, MacGillivray RT, Mason AB, Woodworth RC, Baker EN, Biochemistry 37:13978–13986 (1998)
[23] Steere AN, Byrne SL, Chasteen ND, Smith VC, MacGillivray RT, Mason AB, J Biol Inorg Chem 15:1341–1352 (2010)
[24] He QY, Mason AB, Nguyen V, MacGillivray RT, Woodworth RC, Biochem J 350:909–915 (2000)
[25] Byrne SL, Steere AN, Chasteen ND, Mason AB, Biochemistry 49:4200–4207 (2010)
[26] Egan TJ, Ross DC, Purves LR, Adams PA, Inorg Chem 31:1994–1998 (1992)
[27] Marques HM, Watson DL, Egan TJ, Inorg Chem 30:3758–3762 (1991)
[28] Williams J, Chasteen ND, Moreton K, Biochem J 201:527–532 (1982)
[29] Harris WR, Bali PK, Inorg Chem 27:2687–2691 (1988)
[30] Baldwin DA, Egan TJ, Marques HM, Biochim Biophys Acta 1038:1–9 (1990)
[31] Marques HM, Walton T, Egan TJ, J Inorg Biochem 57:11–21 (1995)
[32] Zak O, Tam B, MacGillivray RT, Aisen P, Biochemistry 36:11036–11043 (1997)
[33] Li Y, Harris WR, Biochim Biophys Acta 1387:89–102 (1998)

[34] Marques HM, Egan TJ, Pattrick G, S Afr J Sci 86:21–24 (1990)
[35] Muralidhara BK, Hirose M, J Biol Chem 275:12463–12469 (2000)
[36] Mizutani K, Muralidhara BK, Yamashita H, Tabata S, Mikami B, Hirose M, J Biol Chem 276:35940–35946 (2001)
[37] Hamilton DH, Turcot I, Stintzi A, Raymond KN, J Biol Inorg Chem 9:936–944 (2004)
[38] Sukenik S, Sapir L, Harries D, Curr Opin Colloid Interface Sci 18:495–501 (2013)
[39] Kumar R, Sharma D, Jain R, Kumar S, Kumar R, Biophys Chem 207:61–73 (2015)
[40] Sapir L, Harries D, Curr Opin Colloid Interface Sci 20:3–10 (2015)
[41] Christiansen A, Wang Q, Samiotakis A, Cheung MS, Wittung-Stafshede P, Biochemistry 49:6519–6530 (2010)
[42] Mittal S, Singh LR, PLoS One 8:e78936 (2013)
[43] Hong J, Gierasch LM, J Am Chem Soc 132:10445–10452 (2010)
[44] Christiansen A, Wittung-Stafshede P, Biophys J 105:1689–1699 (2013)
[45] Homouz D, Perham M, Samiotakis A, Cheung MS, Wittung-Stafshede P, Proc Natl Acad Sci USA 105:11754–11759 (2008)
[46] Perham M, Stagg L, Wittung-Stafshede P, FEBS Lett 581:5065–5069 (2007)
[47] Stagg L, Zhang SQ, Cheung MS, Wittung-Stafshede P, Proc Natl Acad Sci USA 104:18976–18981 (2007)
[48] Kumar R, Sharma D, Jain R, Kumar S, Kumar R, Biophys Chem 207:61–73 (2015)
[49] Totani K, Ihara Y, Matsuo I, Ito Y, J Am Chem Soc 130:2101–2107 (2008)
[50] Norris MG, Malys N, Biochem Biophys Res Commun 405:388–392 (2011)
[51] Moran-Zorzano, MT, Viale AM, Munoz FJ, Alonso-Casajus N, Eydallin GG, Zugasti B, Baroja-Fernandez E, Pozueta-Romero J, FEBS Lett 581:1035–1040 (2007)
[52] Dhar A, Samiotakis A, Ebbinghaus S, Nienhaus L, Homouz D, Gruebele M, Cheung MS, Proc Natl Acad Sci USA 107:17586–17591 (2010)
[53] Laurent TC, Eur J Biochem 21:498–506 (1971)
[54] Homchaudhuri L, Sarma N, Swaminathan R, Biopolymers 83:477–486 (2006)
[55] Pastor I, Vilaseca E, Madurga S, Garces JL, Cascante M, Mas F, J Phys Chem B 115:1115–1121 (2011)
[56] Vopel T, Makhatadze GI, PLoS One 7:e39418 (2012)
[57] Pozdnyakova I, Wittung-Stafshede P, Biochim Biophys Acta Proteins Proteomics 1804:740–744 (2010)
[58] Goins AB, Sanabria H, Waxham MN, Biophys J 95:5362–5373 (2008)
[59] Crowley PB, Brett K, Muldoon J, ChemBioChem 9:685–688 (2008)
[60] Kim YC, Mittal J, Phys Rev Lett 110:208102–208105 (2013)
[61] Minton AP, Biopolymers 99:239–244 (2013)
[62] Wang Y, Sarkar M, Smith AE, Krois AS, Pielak GJ, J Am Chem Soc 134:16614-16618 (2012)
[63] Zhou HX, FEBS Lett 587:394−397 (2013)
[64] Senske M, Törk L, Born B, Havenith M, Herrmann C, Ebbinghaus S, J Am Chem Soc 2014 136:9036-9041 (2014)

[65] Benton LA, Smith AE, Young GB, Pielak GJ, Biochemistry 51:9773−9775 (2012)
[66] Mika JT, Poolman B, Curr Opin Biotechnol 22:117-126 (2011)
[67] Knowles DB, LaCroix AS, Deines NF, Shkel I, Record MT Jr, Proc Natl Acad Sci USA 108:12699–12704 (2011)
[68] Fodeke AA, Minton AP, J Phys Chem B 115:11261–11268 (2011)
[69] Miklos AC, Sarkar M, Wang Y, Pielak GJ, J Am Chem Soc 133:7116–7120 (2011)
[70] Asakura S, Oosawa F, J Polym Sci B 33:183-192 (1958)
[71] Groen J, Foschepoth D, te Brinke E, Boersma AJ, Imamura H, Rivas G, Heus HA, Huck WT, J Am Chem Soc 137:13041-13048 (2015)
[72] Crowley PB, Chow E, Papkovskaia T, Chem Bio Chem 12:1043–1048 (2011)
[73] Wang Q, Zhuravleva A, Gierasch LM, Biochemistry 50:9225–9236 (2011)

Chapter 8
Transferrins: The Mechanism of Iron Release from Diferric Ovotransferrin at Mildly Acidic pH in the Presence of Nonsynergistic Anions

8.1 Introduction

Nonsynergistic anions (ATP, citrate and chloride) that occur in the cytosol in millimolar concentrations [1] and other nonsynergistic anions (SO_4^{2-}, NO_3^-, ClO_4^- *etc.*) play a vital role in the uptake and release of iron from sTf [2]. The release of iron from the N-lobes of sTf and oTf are more facile as compared with their C-lobes, either in the independent half or full-length molecule [3-5]. However, the detailed molecular origins of these differences are not clearly understood. The differences in the mechanism of iron release from N- and C-lobes appear to arise from differences in the "second-shell" residues [6-8]. These residues do not bind directly to iron but form an intricate hydrogen bonding network with the iron coordinating ligands. Dewan et al have suggested that charge repulsion and a conformational change resulting from protonation of the dilysine pair (second shell lysine residues, Lys209-Lys301 located on opposite domains of the N-lobe) appears to be the main driving force to trigger cleft opening of the N-lobe of oTf at low pH [9]. A similar dilysine pair (Lys206-Lys296) also exists in the N-lobe of sTf, but are absent in the C-lobes of oTf and sTf and in both the lobes of Lf [7,9-12]. The dilysine pair is mainly responsible for release of iron from the N-lobes of oTf and sTf at relatively higher pH [10,13]. Due to lack of dilysine pair the C-lobes of oTf and sTf release iron at relatively lower pH [11,14]. Similarly, both the lobes of Lf retain iron at much lower pH as compared to that of sTf and oTf [15-17]. Nonsynergistic anions interact with the Tfs through specific anion binding sites [9,14,18-24]. Egan et al proposed naming the sites to which nonsynergistic anions bind as "kinetically significant anion binding" or KISAB sites [19,21-23]. The binding of nonsynergistic anion to protein influences the rate of iron release from both the lobes of oTf and sTf [9,14,18-24]. However, the extent of these two effects, *i.e.*, dilysine pair and nonsynergistic anion binding on iron release from oTf depends on the pH of the reaction medium and the concentration of anions [25 and references their in]. The N-lobe is the first lobe to release iron [26], so it is to be noted that the concentration of nonsynergistic anion has the greatest effect on iron release from the N-lobe [20]. The mechanism by which nonsynergistic anions control the iron release from both the lobes of oTf is not clearly understood. The kinetic inequivalence

between the N and C-lobes in addition to prerequisite of nonsynergistic anion and inter-lobe interaction makes the process much more complex in diferric Tfs.

In vitro the mechanism of iron release from Tfs has been explored using small molecular weight iron removing chelators [4-5,14, 18-19,24-25,27-29], combined with pH-jump techniques [3,26,30-33] in the absence or presence of Tf receptor [23,26,31,34-35]. Previous reports revealed that protonation and nonsynergistic anion binding control the iron release from Fe_2sTf and Fe_2Lf [26, 31-33,36-37] and differences have been observed in the rates and number of proton transfer reactions [32-33,37]. To explore the mechanism of iron release from Fe_2oTf at mildly acidic pH conditions (3.9-4.3) which is the characteristic of the endosome, the effect of nonsynergistic anions (Cl^- and SO_4^{2-}, using their Na^+ salts) on the iron release kinetics of Fe_2oTf have been studied in the absence of receptor without using chelator. The kinetic data were analyzed by means of the techniques and methods of chemical relaxation. Analysis of kinetic data suggests that the protonation and nonsynergistic anion binding to protein control the iron release kinetics from both the lobes of Fe_2oTf.

8.2 Results

8.2.1 Kinetics of iron release from Fe_2oTf at mildly acidic pH in the presence of nonsynergistic anion

Nonsynergistic anions induce the iron release from Fe_2oTf under acidic pH conditions and the effect of SO_4^{2-} is greater than the Cl^- in the acceleration of iron release from Fe_2oTf [38]. To further explore the effect of nonsynergistic anions (Cl^- and SO_4^{2-}) on the pH-dependent iron release kinetic profiles of Fe_2oTf, the iron release kinetics were recorded in the absence and presence of different concentrations of Cl^- and SO_4^{2-} over the pH range of 3.9-4.3.

When a solution of Fe_2oTf is submitted to a fast pH jump from neutral to acidic conditions in the presence of Cl^- and SO_4^{2-}, the release of iron from Fe_2oTf exhibits biphasic kinetics (monitored at 465 nm) (Fig. 8.1a). Fig. 8.1a shows that after a burst phase that occurs within the mixing time of the spectrophotometer (~1 s), the absorbance decreases up to ~10^4 s when Fe_2oTf of pH 7.4 was submitted to pH 4.2 in acetate buffer (~8 mM) containing 0.04 M Cl^-. The experimental relaxation times that fall in mixing time (~ 1 s) cannot be analyzed precisely. Earlier reports revealed that the proton-assisted release of the synergistic carbonate

anion in acidic media is a prerequisite for iron release and it occurs in ≤ 5 ms of burst phase [3,32-33],

$$Fe_2oTf + nH \rightleftharpoons Fe_2oTf^* \text{ or } Fe_{NC}oTf^* + H_2CO_3 \qquad R1$$

where, Fe_2oTf is the iron loaded protein with carbonate bound and $Fe_{NC}oTf^*$ is same protein without carbonate bound. Both forms of the Fe_2oTf are in an unknown state of protonation. Because the fast step (R1) cannot be determined accurately, so arbitrarily *n* protons written in equation R1 [3,37].

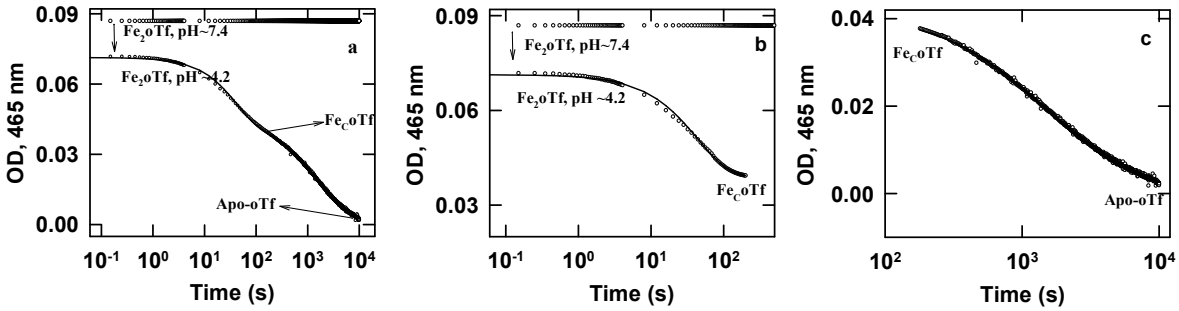

Fig. 8.1 Kinetics of iron release from Fe_2oTf (~8 μM) monitored at 465 nm on decreasing the pH from 7.4 to 4.2 in the presence of acetate buffer (8 mM) containing 0.04 M chloride (25 °C). (a) Fe_2oTf exhibits biphasic kinetics following a burst phase that occurs within the mixing time of the spectrophotometer (~1 s). (b) A representative kinetic trace of the rapid phase (up to 150 s) of iron release. The kinetics is best described by two relaxation processes with time constants of ~7.3 and ~49 s. The absorbance of Fe_2oTf pH 7.4 without pH-jump is also shown in Panel (a) and (b). (c) A representative trace of the slow phase (150-10^4 s) of iron release under identical conditions. The kinetics of this phase is best described by two relaxation processes with time constants of ~0.28 hrs and ~1.3 hrs.

The kinetic process (in the range of 5 ms to 200 ms) which occurs immediately after the proton assisted release of the synergistic carbonate anion in acidic media is the involvement of single proton transfer for $Fe_{NC}oTf^*$ [3]. This very fast phenomenon occurs within the limits of the mixing time of the protein solution (pH 7.4) with acidic buffer (pH 3.9-4.3) containing a desired salt concentration.

Nevertheless, for processes occurring up to 150 s after mixing, the kinetics data are best described by a two-exponential fit with the time constants τ_{1N} ~7.3 s and τ_{2N} ~49 s. The chemical processes accountable for these kinetic phases are linked to release of iron from the N-site of $Fe_{NC}oTf^*$ because under acidic conditions, iron release from $Fe_{NC}oTf^*$ occurs first from the N-site and after that from the C-site [3]. After ~150 s, absorbance at 465 nm continues to decrease

in a way consistent with another two-exponential decay process with time constants τ_{3C} ~1010 s and τ_{4C} ~4700 s (Fig. 8.1c) and these processes are linked to iron release from the C-site.

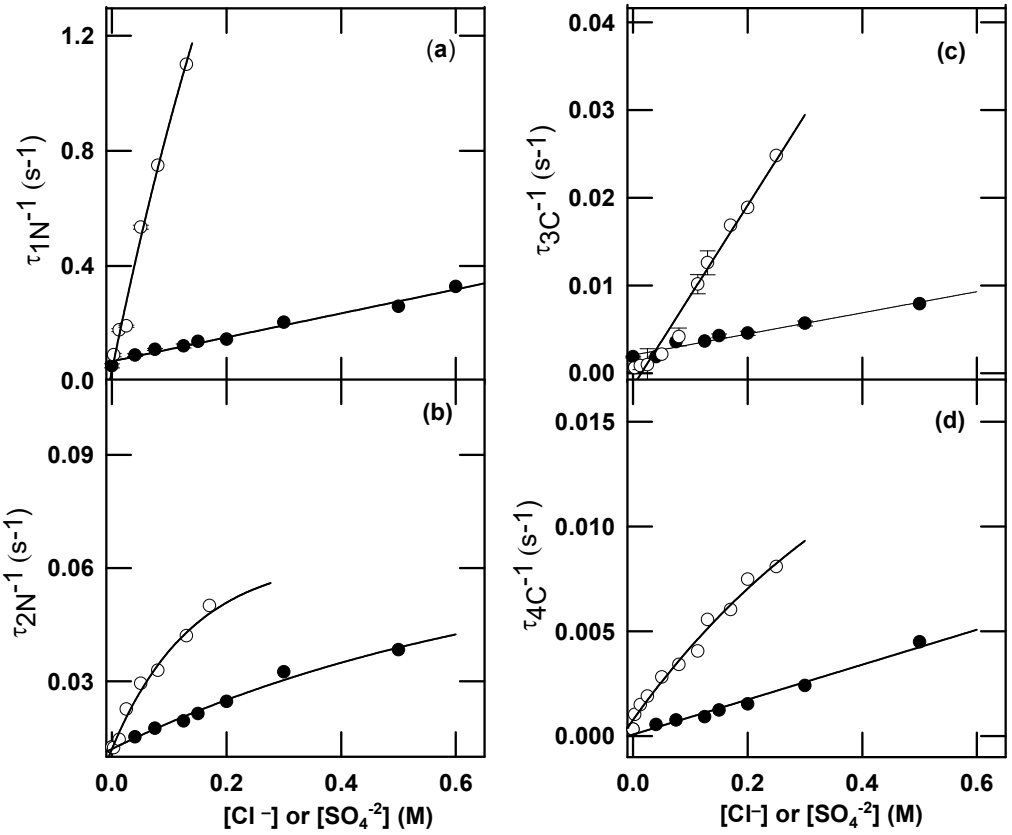

Fig. 8.2. Panels (a) and (b) show the reciprocal time constants, τ_{1N}^{-1} and τ_{2N}^{-1} for rapid phase of iron release are plotted as a function of Cl^- (•) or SO_4^{2-} (○) concentration. The solid line in panel (a) is linear least squares fits to the data and solid line in panel (b) is non-linear least squares fits to the data. Panels (c) and (d) show the reciprocal time constants, τ_{3C}^{-1} and τ_{4C}^{-1} for slow phase of iron release are plotted as a function of Cl^- (•) or SO_4^{2-} (○) concentration. The solid line in panel (c) is linear least squares fits to the data and solid line in panel (d) is non-linear least squares fits to the data.

The inverse of the time constants, τ_{1N}^{-1} and τ_{3C}^{-1} increased almost linearly with increase in Cl^- or SO_4^{2-} concentration (Figs. 8.2a and 8.2c) while the $\tau_{2N}^{-1}$and τ_{4C}^{-1} exhibited a simple mono-exponential variation with increase in Cl^- or SO_4^{2-} concentration (Figs. 8.2b and 8.2d). Ultimately, these results suggests that SO_4^{2-} has a greater effect in accelerating the rate of iron release from Fe_{NC}oTf* than does Cl^- (Figs. 8.2a, 8.2b, 8.2c and 8.2d). Over the pH range of 3.9-4.3, τ_{1N}^{-1} and τ_{3C}^{-1} increase linearly with the increment of Cl^- and SO_4^{2-} concentration whereas τ_{2N}^{-1} and τ_{4C}^{-1} increase mono-exponentially with the increment of Cl^- and SO_4^{2-} concentration. These interpretation needed a chemical relaxation analysis of the kinetic processes that are

responsible for the acid-induced iron release from Fe_2oTf (pH 3.9-4.3) as a function of Cl^- or SO_4^{2-} concentration.

8.2.2 Chemical relaxation analysis of proton-linked iron release from Fe_2oTf as a function of Cl^- and SO_4^{2-} concentration (pH 3.9-4.3)

By using the methods and techniques of chemical relaxation, the mechanism of iron release from Fe_2oTf was investigated with the help of experimentally measured iron release relaxation times of Fe_2oTf at the mildly acidic pH (pH 3.9-4.3) in the presence of different concentrations of Cl^- or SO_4^{2-}.

When a solution of Fe_2oTf is submitted to a fast pH jump from neutral to acidic conditions in the presence of Cl^- or SO_4^{2-}, five kinetic processes can be observed up to 10^4 s (Fig. 8.1). The experimental relaxation times that fall in mixing time of ≤1 s cannot be analyzed accurately. However, the proton-assisted release of the synergistic carbonate anion (Fig. 8.1a and equation (R1)) in acidic media is a prerequisite for iron release and this phenomenon typically occurs in the range of ~3 to 5 ms [3,32]. Immediately, after the proton assisted release of the synergistic carbonate anion in acidic media is the involvement of single proton transfer for Fe_2oTf (in the range of 5 ms to 200 ms) [3].

$$Fe_{NC}oTf^* + H^+ \underset{k_{-1}}{\overset{k_1}{\rightleftharpoons}} Fe_{NC}oTf^*H \qquad R2$$

The protonated carbonate-free protein, Fe_{NC}oTf*H, subsequently begins to release iron in two kinetically detectable steps: a fast step and a slow step (Fig. 8.1a). The fast step can be treated as a relaxation process [39-40]. By assuming that in this step the protein undergoes interaction with the nonsynergistic anions of the solution and binds a proton at the rate of diffusion [39-40], two mechanisms are possible. The first mechanism involves nonsynergistic anions binding to Fe_{NC}oTf*H followed by protonation (equation (R3) and (R4)), where S represents anion).

$$Fe_{NC}oTf^*H + nS \underset{k'_{-1N}}{\overset{k'_{1N}}{\rightleftharpoons}} Fe_{NC}oTf^*HS_n \qquad R3$$

$$Fe_{NC}oTf^*HS_n + H^+ \rightleftharpoons Fe_{NC}oTf^*H_2S_n \qquad R4$$

The second mechanism involves protonation of Fe_{NC}oTf*H followed by nonsynergistic anion binding (equation (R5) and (R6)).

$$Fe_{NC}oTf^*H + H^+ \rightleftharpoons Fe_{NC}oTf^*H_2 \qquad R5$$

$$Fe_{NC}oTf^*H_2 + nS \underset{k_{-1N}}{\overset{k_{1N}}{\rightleftharpoons}} Fe_{NC}oTf^*S_nH_2 \qquad R6$$

Here, K_{1H} = $[Fe_{NC}oTf^*H][H^+]/[Fe_{NC}oTf^*H_2]$, and K_{1S} = $[Fe_{NC}oTf^*H_2][S]^n/[Fe_{NC}oTf^*S_nH_2]$. When equation (R6) is considered rate limiting, then the reciprocal relaxation time associated with equation (R6) can be expressed as equation (7).

$$\tau_{1N}^{-1} = k_{-1N} + \{k_{1N}\left([H^+]\,[S]^n\right)/K_{1H}\} \qquad 7$$

The relaxation times determined in this study provide evidence that nonsynergistic anion binding is rate limiting (Fig. legend 8.3a), thus $Fe_{NC}oTf^*H$ is protonated prior to anion binding as described by the second mechanism (equations (R5) and (R6)). Only rate-limiting equation (7) with n = 2 for Cl^- and n = 1 for SO_4^{2-} (as shown in Fig. 8.3a) permits the interpretation of the experimental data.

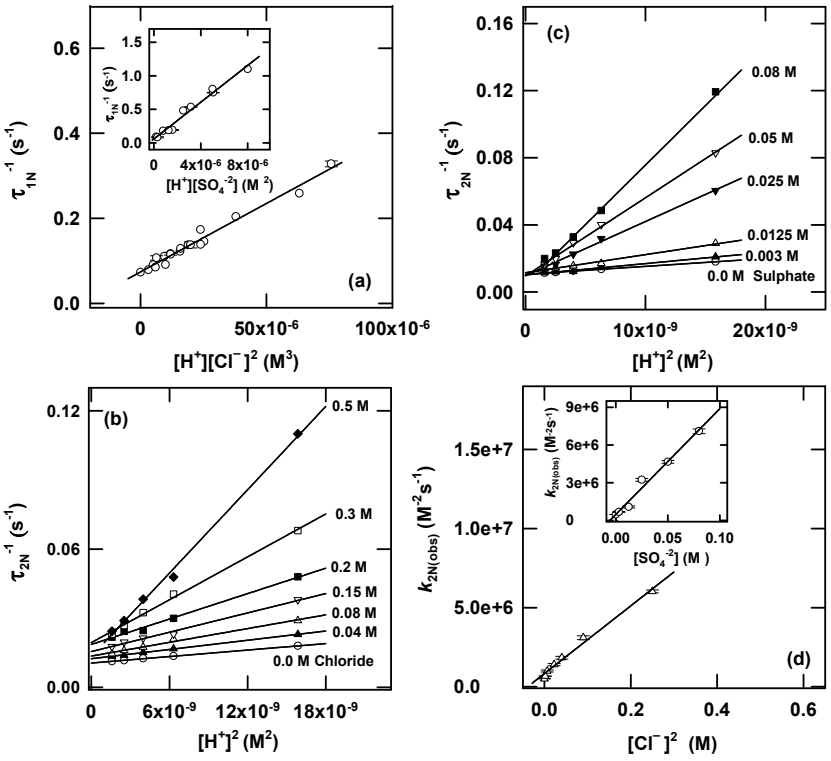

Fig. 8.3. Panel (a) presents plot of τ_{1N}^{-1} against $[H^+][Cl^-]^2$ at 25°C for 3.9 ≤ pH ≤ 4.3, with 0.0 M ≤ $[Cl^-]$ ≤ 0.6 M. The linear least-squares fitting of the data in panel (a) (solid line) yields, intercept ~0.074 (±0.003) s^{-1} and slope ~3.2 (±0.01) × 10^3 $M^{-3}s^{-1}$. Inset of panel (a) presents plot of τ_{1N}^{-1} against $[H^+][SO_4^{2-}]$ at 25 °C for 3.9 ≤ pH ≤ 4.3, with 0.0 M ≤ $[SO_4^{2-}]$ ≤ 0.13 M. The linear least-squares fitting of the data in inset of panel (a) (solid line) yields, intercept ~0.058 (±0.01) s^{-1} and slope ~1.4 (±0.07) × 10^5 $M^{-2}s^{-1}$. Panel (b) presents plots of τ_{2N}^{-1} against $[H^+]^2$ at fixed concentration of Cl^- at 25°C, 3.9 ≤ pH ≤ 4.3. The slopes of the regression lines (equation (11)) at fixed concentration of Cl^- (panel b) are plotted as a function of $[Cl^-]^2$ in panel (d). The linear least-squares fitting of the data in panel (d) (solid line) yields, intercept ~8.1 (±0.1) × 10^5 $M^{-2}s^{-1}$ and slope ~2.1 (±0.1) × 10^7 $M^{-4}s^{-1}$. Panel (c) present plots of τ_{2N}^{-1} against $[H^+]^2$ at fixed $[SO_4^{2-}]$ at 25°C, 3.9 ≤ pH ≤ 4.3. The slopes of the regression lines (equation (11)) at fixed concentration of $[SO_4^{2-}]$ (panel (c)) are plotted as a function of $[SO_4^{2-}]$ in inset of panel (d). The

linear least-squares fitting of the data in inset of panel (d) (solid line) yields, intercept ~4.75 (±1) × 10^5 $M^{-2}s^{-1}$ and slope ~8.4 (±0.06) × 10^7 $M^{-3}s^{-1}$. Specifically, in these analyses only those values of τ_{1N}^{-1} and τ_{2N}^{-1} are used where at a given pH and anion concentration the N-site of $Fe_{NC}oTf^*H$ is fully released its metal ion.

In the next step iron is released from the $Fe_{NC}oTf^*S_nH_2$ intermediate (Step 3). To understand the release of iron from $Fe_{NC}oTf^*S_nH_2$ intermediate, it is will be useful to discuss all the mechanisms by which $Fe_{NC}oTf^*S_nH_2$ can protonate, interact with nonsynergistic anions and release iron. Based on the experimental observations the following processes are possible:

$$Fe_{NC}oTf^*S_nH_2 \underset{k'_{-2N}}{\overset{k'_{2N}}{\rightleftharpoons}} Fe_{C}oTf^*S_nH_2 + Fe \qquad R8$$

$$Fe_{C}oTf^*S_nH_2 + 2H^+ \underset{k_{-2N}}{\overset{k_{2N}}{\rightleftharpoons}} Fe_{C}oTf^*S_nH_4 \qquad R9$$

$$Fe_{C}oTf^*S_nH_4 \underset{k''_{-2N}}{\overset{k''_{2N}}{\rightleftharpoons}} Fe_{C}oTf^*H_4 + nS \qquad R10$$

where, $K_{2Fe} = [Fe_{C}oTf^*S_nH_2][Fe^{+3}]/[Fe_{NC}oTf^*S_nH_2]$, $K_{2H} = [Fe_{C}oTf^*S_nH_2][H^+]^2/[Fe_{C}oTf^*S_nH_4]$, and $K_{2S} = [Fe_{C}oTf^*H_4][S]^n/[Fe_{C}oTf^*S_nH_4]$. To conclude which of these steps is rate limiting, the data was analyzed with the assumption that one of these rate step could contribute to rate limitation and conclude that only by assuming that equation (R9) is rate-limiting could the data be fitted successfully (Fig. 8.3). If equation (R9) is rate-limiting, then the equation that illustrates the reciprocal relaxation time for step can be expressed as equation (11),

$$\tau_{2N}^{-1} = k_{-2N}([S]^n/K_{2S}) + k_{2N(obs)}[H^+]^2 \qquad 11$$

and under current experimental conditions ($3.9 \leq pH \leq 4.3$):

$$k_{2N(obs)} = k_{2N} + k_{2N}[S]^n/K_{2S} \qquad 12$$

At fixed concentration of S (when S is Cl^- or SO_4^{2-}), the reciprocal relaxation times associated with equation (11) observed in current experiments are linearly dependent on $[H^+]^2$ (Figs. 8.3b and 8.3c). The slopes determined for each [S] from linear regression to equation (11) provide $k_{2N(obs)}$ (Figs. 8.3b and 8.3c), and k_{2N} and K_{2S} are determined from the slopes and intercepts of regression line (equation (12)) (Fig. 8.3d and inset of Fig. 8.3d). These cotcome suggest that iron release from $Fe_{C}oTf^*S_nH_2$ is controlled by a slow gain of two protons as illustrated by equation (R8) to (R10).

After release of the iron from N-lobe, an intermediate $Fe_{C}oTf^*H_4$ forms in which iron is linked to the C-lobe but without synergistic carbonate anion. Iron release from C-lobe also requires a sequence of processes that finally results in apo-ovotransferrin. Iron release from

$Fe_COTf^*H_4$ take place in two kinetically detectable steps (Figs. 8.1a and 8.1c). The faster step can be treated as a relaxation process [39-40]. If the data was analyzed with the assumption that in this step protein molecule may undergoes an interaction with the nonsynergistic anions and then binds a proton at the rate of diffusion [39-40], two mechanisms can be possible. The first mechanism involves nonsynergistic anions binding to $Fe_COTf^*H_4$ followed by protonation (equation (R13) and (R14), where S represents a nonsynergistic anion).

$$Fe_COTf^*H_4 + nS \underset{k'_{-1C}}{\overset{k'_{1C}}{\rightleftharpoons}} Fe_COTf^*S_nH_4 \qquad R13$$

$$Fe_COTf^*S_nH_4 + H^+ \rightleftharpoons Fe_COTf^*S_nH_5 \qquad R14$$

The second mechanism involves protonation of $Fe_COTf^*H_4$ followed by nonsynergistic anion binding (equation (R15) and (R16))

$$Fe_COTf^*H_4 + H^+ \rightleftharpoons Fe_COTf^*H_5 \qquad R15$$

$$Fe_COTf^*H_5 + nS \underset{k_{-1C}}{\overset{k_{1C}}{\rightleftharpoons}} Fe_COTf^*S_nH_5 \qquad R16$$

Here, $K_{1H} = [Fe_COTf^*H_4][H^+]/[Fe_COTf^*H_5]$, and $K_{1S} = [Fe_COTf^*H_5][S]^n/[Fe_COTf^*S_nH_5]$. When equation (R16) is considered rate limiting, then the reciprocal relaxation time equation associated with equation (R16) can be expressed as equation (17).

$$\tau_{3C}^{-1} = k_{-3C} + \{k_{3C}\left([H^+][S]\right)/K_{1H}\} \qquad 17$$

Only the rate equations describing the reciprocal relaxation times derived by assuming that equation (R16) (with n = 2 for Cl^- and n = 1 for SO_4^{2-}) is rate limiting resulted in an acceptable fit to these kinetics data (Fig. 8.4a).

Now the process of iron release starts from the intermediate species, $Fe_COTf^*S_nH_5$. Protonation and nonsynergistic anion binding can control the iron release from $Fe_COTf^*S_nH_5$ in a similar fashion as does occur for the corresponding species, $Fe_{NC}OTf^*S_nH_2$. The following sequence of processes can occur prior to iron release from $Fe_COTf^*S_nH_5$:

$$Fe_COTf^*S_nH_5 \underset{k'_{-2C}}{\overset{k'_{2C}}{\rightleftharpoons}} oTf^*S_nH_5 + Fe \qquad R18$$

$$oTf^*S_nH_5 + 2H^+ \underset{k_{-2C}}{\overset{k_{2C}}{\rightleftharpoons}} oTf^*S_nH_7 \qquad R19$$

$$oTf^*S_nH_7 \underset{k''_{-2C}}{\overset{k''_{2C}}{\rightleftharpoons}} oTf^*H_7 + nS \qquad R20$$

Fitting of the kinetic data to the equations illustrating the reciprocal relaxation times related to equations (R18), (R19), and (R20) when each equation is assumed to be rate-limiting conclude that only by assuming that equation (R19) is rate-limiting could the data be fitted successfully

(Fig. 8.4). If equation (R19) is considered to be rate-limiting, then the equation describing the reciprocal relaxation time related to equation (R19) can be expressed as equation (21),

$$\tau_{2C}^{-1} = k_{-2C}([S]^n / K_{2S}) + k_{2C(obs)}[H^+]^2 \qquad 21$$

and under current experimental conditions ($3.9 \leq$ pH ≤ 4.3):

$$k_{2C(obs)} = k_{2C} + k_{2C}[S]^n / K_{2S} \qquad 22$$

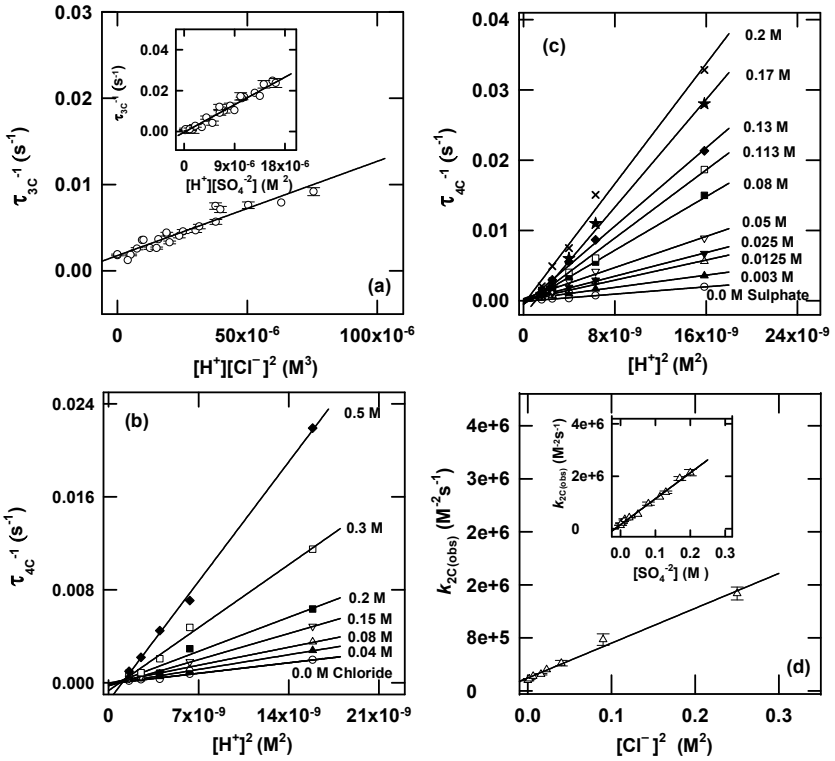

Fig. 8.4. Panel (a) presents plot of τ_{3C}^{-1} against $[H^+][Cl^-]^2$ at 25°C for $3.9 \leq pH \leq 4.3$, with $0.0\ M \leq [Cl^-] \leq 0.6\ M$. The linear least-squares fitting of the data in panel (a) (solid line) yields, intercept ~0.0017 (±0.0001) s^{-1} and slope ~1.1 (±0.03) × 10^2 $M^{-3}s^{-1}$. Inset of panel (a) presents plot of τ_{3C}^{-1} against $[H^+][SO_4^{2-}]$ at 25 °C for $3.9 \leq pH \leq 4.3$, with $0.0\ M \leq [SO_4^{2-}] \leq 0.13$ M. The linear least-squares fitting of the data in inset of panel (a) (solid line) yields intercept ~ -0.0003 (±0.01) s^{-1} and slope ~1.5 (±0.02) × 10^3 $M^{-2}s^{-1}$. Panel (b) present plots of τ_{4C}^{-1} against $[H^+]^2$ at fixed concentration of Cl^- at 25°C, $3.9 \leq pH \leq 4.3$. The slopes of the regression lines (equation (21)) at fixed concentration of Cl^- (panel (b)) are plotted as a function of $[Cl^-]^2$ in panel (d). The linear least-squares fitting of the data in panel (d) (solid line) yields, intercept ~1.9 (±0.2) × 10^5 $M^{-2}s^{-1}$ and slope ~5.3 (±0.2) × 10^6 $M^{-4}s^{-1}$. Panel (c) present plots of τ_{4C}^{-1} against $[H^+]^2$ at fixed concentration of SO_4^{2-} at 25°C, $3.9 \leq pH \leq 4.3$. The slopes of the regression lines (equation (21)) at fixed concentration of SO_4^{2-} (panel (c)) are plotted as a function of $[SO_4^{2-}]$ in inset of panel (d). The linear least-squares fitting of the data in inset of panel (d) (solid line) yields, intercept ~1.6 (±0.3) × 10^5 $M^{-2}s^{-1}$ and slope ~9.9 (±0.3) × 10^6 $M^{-3}s^{-1}$.

At fixed concentration of S (when S is Cl^- or SO_4^{2-}), the experimental reciprocal relaxation times associated with equation (R20) are linear with respect to $[H^+]^2$, as shown for Cl^-

and SO_4^{2-} (Figs. 8.4b and 8.4c). Values for $k_{2C(obs)}$ (equation (21)) were determined for each concentration of S from the slopes of the regression lines for fits of the data to equation (R19) at fixed concentration of S (Figs. 8.4b and 8.4c), and k_{2C}, and values for K_{2S} were determined from the slopes and intercepts of regression lines for fits to equation (22) (Fig. 8.4d and inset). These results suggest that iron release from $Fe_COTf^*S_nH_5$ is controlled by slow binding of two protons (equations (R18-R20)).

8.3 Discussion

The present study provides the analysis of iron release from Fe_2oTf under pH conditions similar to that found in endosome ($3.9 \leq pH \leq 4.3$). Iron release from Fe_2oTf typically follows the sequence of reactions summarized in scheme 1. Previous articles described the mechanisms of iron release from Fe_2sTf (Scheme 2) and Fe_2Lf (Scheme 3) under mildly acidic pH conditions [32,37]. While the net result of the iron release process of Fe_2oTf is very similar to Fe_2sTf. However, it is notable that one more step (Step 2) in this sequence of reactions are kinetically detectable for iron release from Fe_2oTf (Scheme 1) than for iron release from Fe_2sTf (Scheme 2). Furthermore, two monoanions are required for iron release from Fe_2oTf while one monoanion is required for Fe_2sTf. Under similar conditions, as compared to Fe_2Lf (Scheme 3), the iron release from Fe_2oTf and Fe_2sTf occurs in two phases, first iron releases from the N-lobe and then from the C-lobe. However, Fe_2Lf releases iron simultaneously from both the lobes.

Scheme 1. The mechanism of iron release from Fe_2oTf

Step 1 involves pH-linked proton assisted release of carbonate from Fe_2oTf (most rapid, < 5 ms)

$$Fe_2oTf + nH \rightleftharpoons Fe_2oTf^* \text{ or } Fe_{NC}oTf^* + H_2CO_3 \qquad (A)$$

Step 2, the N-site gains one proton (< 200 ms)

$$Fe_{NC}oTf^* + H^+ \rightleftharpoons Fe_{NC}oTf^*H \qquad (B)$$

In Step 3, the N-site gains one proton with kinetic linkage to the binding of two monoanions (S) and one dianion

$$Fe_{NC}oTfH^* + H^+ \rightleftharpoons Fe_{NC}oTf^*H_2 \qquad (C)$$

$$Fe_{NC}oTf^*H_2 + nS \underset{k_{-1N}}{\overset{k_{1N}}{\rightleftharpoons}} Fe_{NC}oTf^*S_nH_2 \qquad (D)$$

In Step 4, iron is released from $Fe_{NC}oTf^*S_nH_2$ according to equations (E) to (G)

$$Fe_{NC}oTf^*S_nH_2 \underset{k'_{-2N}}{\overset{k'_{2N}}{\rightleftharpoons}} Fe_COTf^*S_nH_2 + Fe \qquad (E)$$

$$Fe_{NC}oTf^*S_nH_2 + 2H^+ \underset{k_{-2N}}{\overset{k_{2N}}{\rightleftharpoons}} Fe_COTf^*S_nH_4 \qquad (F)$$

$$Fe_COTf^*S_nH_4 \underset{k''_{-2N}}{\overset{k''_{2N}}{\rightleftharpoons}} Fe_COTf^*H_4 + nS \qquad (G)$$

In Step 5, the C-lobe gains one proton with kinetic linkage to the binding of two mono anions (S) and one dianion

$$Fe_COTf^*H_4 + H^+ \rightleftharpoons Fe_COTf^*H_5 \quad (H)$$

$$Fe_COTf^*H_5 + nS \underset{k_{-1C}}{\overset{k_{1C}}{\rightleftharpoons}} Fe_COTf^*S_nH_5 \quad (I)$$

In Step 6, iron is released from $Fe_cOTf^*S_nH$ according to equations (J) to (L)

$$Fe_COTf^*S_nH_5 \underset{k'_{-2C}}{\overset{k'_{2C}}{\rightleftharpoons}} OTf^*S_nH_5 + Fe \quad (J)$$

$$OTf^*S_nH_5 + 2H^+ \underset{k_{-2C}}{\overset{k_{2C}}{\rightleftharpoons}} OTf^*S_nH_7 \quad (K)$$

$$OTf^*S_nH_7 \underset{k''_{-2C}}{\overset{k''_{2C}}{\rightleftharpoons}} OTf^*H_7 + nS \quad (L)$$

Scheme 2. The mechanism of iron release from Fe_2sTf-

Step 1 involves pH-linked carbonate release from Fe_2sTf (most rapid, < 5 ms)

$$Fe_2sTf + nH \rightleftharpoons Fe_2sTf^* \text{ or } Fe_{NC}sTf^* + H_2CO_3 \quad (A)$$

In Step 2, the N-site gains one proton with kinetic linkage to the binding of one anion (S)

$$Fe_{NC}sTf^* + H^+ \rightleftharpoons Fe_{NC}sTf^*H \quad (B)$$

$$Fe_{NC}sTf^*H + S \underset{k_{-1N}}{\overset{k_{1N}}{\rightleftharpoons}} Fe_{NC}sTf^*SH \quad (C)$$

In Step 3, iron is released from Fe_{NC}sTf*SH according to equations (D) to (F)

$$Fe_{NC}sTf^*SH \underset{k'_{-2N}}{\overset{k'_{2N}}{\rightleftharpoons}} Fe_CsTf^*SH + Fe \quad (D)$$

$$Fe_CsTf^*SH + 2H^+ \underset{k_{-2N}}{\overset{k_{2N}}{\rightleftharpoons}} Fe_CsTf^*SH_3 \quad (E)$$

$$Fe_CsTf^*SH_3 \underset{k''_{-2N}}{\overset{k''_{2N}}{\rightleftharpoons}} Fe_CsTf^*H_3 + S \quad (F)$$

In Step 4, the C-lobe gains one proton with kinetic linkage to the binding of one anion

$$Fe_CsTf^*H_3 + H^+ \rightleftharpoons Fe_CsTf^*H_4 \quad (G)$$

$$Fe_CsTf^*H_4 + S \underset{k_{-1C}}{\overset{k_{1C}}{\rightleftharpoons}} Fe_CsTf^*SH_4 \quad (H)$$

In Step 5, iron is released from Fe_CsTf^*SH according to equations (I) to (K)

$$Fe_CsTf^*SH_4 \underset{k'_{-2C}}{\overset{k'_{2C}}{\rightleftharpoons}} sTf^*SH_4 + Fe \quad (I)$$

$$sTf^*SH_4 + 2H^+ \underset{k_{-2C}}{\overset{k_{2C}}{\rightleftharpoons}} sTf^*SH_6 \quad (J)$$

$$sTf^*SH_6 \underset{k''_{-2C}}{\overset{k''_{2C}}{\rightleftharpoons}} sTf^*H_6 + S \quad (K)$$

Scheme 3. The mechanism of iron release from Fe_2Lf-

Step 1 involves pH-linked carbonate release from Fe_2Lf (most rapid, < 5 ms)

$$Fe_2Lf + nH \rightleftharpoons Fe_2Lf^* \text{ or } Fe_{NC}Lf^* + H_2CO_3 \qquad (A)$$

In Step 2, Fe_2Lf gains two protons with kinetic linkage to the binding of two monoanions (S) and one dianion

$$Fe_2Lf^* + 2H^+ \rightleftharpoons Fe_2Lf^*H_2 \qquad (B)$$

$$Fe_2Lf^*H_2 + nS \underset{k_{-1N}}{\overset{k_{1N}}{\rightleftharpoons}} Fe_2Lf^*S_nH_2 \qquad (C)$$

In Step 3, iron is released from $Fe_2Lf^*S_nH_2$ according to equations (D) to (F)

$$Fe_2Lf^*S_nH_2 \underset{k'_{-2N}}{\overset{k'_{2N}}{\rightleftharpoons}} Lf^*S_nH_2 + 2Fe \qquad (D)$$

$$Lf^*S_nH_2 + 2H^+ \underset{k_{-2N}}{\overset{k_{2N}}{\rightleftharpoons}} Lf^*S_nH_4 \qquad (E)$$

$$Lf^*S_nH_4 \underset{k''_{-2N}}{\overset{k''_{2N}}{\rightleftharpoons}} Lf^*H_4 + nS \qquad (F)$$

The loss of synergistic anion carbonate is prerequisite for iron release from Tfs [3,32-33] and this fast step cannot be analyzed unambiguously. In acidic media the gain of first proton occurs immediately after the release of the synergistic carbonate anion from Fe_2oTf [3]. The Fe_{NC}oTf*H (N-site) then gains one proton (equation (R5)) in a sequential manner followed by binding of two monoanions or one dianion (equation (R6)). Previous reports revealed that protonation of dilysine residues, Lys209 and Lys301 may trigger the opening of the N-lobe of oTf during the iron release [9]. However, the protonation of other unknown sites cannot be excluded. While the intensive studies by site-specific mutation analyses have been carried out, but the nonsynergistic anion binding sites in Tfs remained largely unclear [7,18,25,29,41]. Positively charged (Lys, Arg and His) residues are obvious choices for possible KISAB sites. A previous report revealed that two SO_4^{2-} binding sites exist in the iron-binding cleft of the N-lobe of oTf, one SO_4^{2-} binds to His250 (one of the iron binding site) and the other binds to Arg121 (one of the carbonate binding site) [13]. It is expected that other nonsynergistic anions can also accommodate these and other sites in oTf as well. Nonsynergistic anion binding to these sites may play a significant role in the iron release from N-lobe of oTf because these sites include the protein groups that make functionally essential interactions closely related to the anion-dependent iron release in which a domain opening and CO_3^{2-} release are the prerequisites. The role of nonsynergistic anion binding to dilysine residues is not established for oTf as described for sTf in which anion interacts with Lys296 [29].

Usually, this kind of electrostatic interaction is diffusion controlled. The reciprocal relaxations time τ_{1N}^{-1} dependence on anion concentration (equation (7) and Fig. 8.3a) does not essentially appear from the anion binding, and probably also controlled by the conformational changes that kinetically control the anion binding. After the iron release from N-lobe (equation (R8)), protein first gain two protons followed by anion release (equation (R9- R10)). Usually the diffusion-controlled proton transfers reactions are very fast and occurs in the range of microseconds [39,42]. Here, the conformational change in oTf may also controls the proton access to the protein consistent with the dependence of equations (11) and (21) on $[H^+]^2$. Similar possibility of slow proton transfer has also been suggested for the sTf and Lf [32-33,37]. This result shows that at acidic pH, the iron release from the N-lobe of Fe_2oTf involves binding of two monoanions or one dianion and four protons for the protonation of possible sites, His250 and Arg121 [13] and other unknown sites in protein.

After the iron release from N-lobe (equation R8), an intermediate Fe_CoTf*H_4 is produced with iron coordinated to only at C-lobe. Fe_CoTf*H_4 first gains one proton (equation (R15)) followed by binding of two mono anions or one dianion (equation R16). The possible site of protonation is Lys638 and a previous report also revealed that one SO_4^{2-} binds to His592 (an iron-binding residue) in the C-lobe of oTf [14]. However, nonsynergistic anions binding to other unknown sites cannot be ignored. It is possible that nonsynergistic anion binding to His592 may play significant role in the iron release from the C-lobe of oTf because this site include the protein groups that make functionally essential interactions closely related to the anion-dependent iron release. After binding of anions, the intermediate complex first releases iron (equation (R18)) and then gains two protons (equation (R19)) and finally releases anion (equation (R20)). The anion binding and slow proton transfer probably controlled by the conformational change in protein from close to open occurring upon release. Similar hypothesis has been proposed for the iron release from sTf and Lf [32,37].

During the last few decades, several investigators have spurred great interest in understanding the role of the pH- and nonsynergistic anion binding-induced conformational changes that prompt iron release from the monoferric- and diferric-Tfs [7,9,18,20,25,29,43-57]. The necessity of binding of nonsynergistic anions to Tfs for iron release has been proposed by several research groups [56-57]. Wishnia et al. have proposed that during the course of iron release ~17 Cl^- bind to oTf [58]. EPR spectrum study suggests that nonsynergistic anion binding

induces a conformational change in Fe_2sTf [59]. Kretchmar et al. have also revealed that conformational changes induced by nonsynergistic anion binding to protein are involved in iron release from isolated N- and C-lobes of sTf [56]. The nonsynergistic anion-induced promotion in iron release from Fe_2oTf typically follows an order, $SO_4^{2-} > NO_3^- > Cl^- > Br^-$ [38] and for Fe_2sTf typically follows an order, $SO_4^{2-} > NO_3^- > Cl^- > ClO_4^-$ [60]. These observed trends are different from the usually described lyotropic series, a ranking of salt ions according to their behavior against protein stability [61-62]. However, other report showed that binding of non-synergistic anions to sTf follows the lyotropic series, $SCN^- > ClO_4^-$ > pyrophosphate (pp_i) > ATP > $Cl^- > BF_4^-$ [59]. However, some other reports also revealed that anions effect on the iron release from Tfs does not follows the lyotropic series [22,63-65]. A previous report also proposed that the anion binding ability to protein is closely related to iron release from the isolated N-lobe of sTf [29]. At pH 4.2, SO_4^{2-} has a greater effect than the Cl^- on the iron release (Fig. 8.2). This is possible because SO_4^{2-} binds more avidly to the protein than does Cl^- [29,66]. Interestingly, before the iron release from the N and C-lobes, oTf interacts with two monoanions or one dianion (*i.e.,* two times), which indicates at least two specific sites of electrostatic interaction on each lobe. However, sTf interacts with one monoanion or one dianion before the iron release from N and C-lobes (*i.e.,* two times) (Scheme 2) which indicates at least one specific sites of electrostatic interaction on each lobe. Lf interacts with two monoanions or one dianion before the simultaneous iron release of iron from both the lobes (*i.e.,* one time) (Scheme 3) which indicates at least two specific sites of electrostatic interaction on Lf.

The amino acid sequence of the N and C-lobes of oTf are ~36% identical. The iron coordinated residues are conserved in both the lobes *i.e.*, Asp60, Tyr92, Tyr191 and His250 in N-lobe and Asp395, Tyr431, Tyr524 and His592 in C-lobe [67]. Besides these similarities, the N and C-lobes differ in affinity for iron under acidic pH conditions because first iron releases from the N-lobe and then from the C-lobe. The differences in affinity of iron for N and C-lobes may be originated due to following reasons: (i) the presence of pH-sensitive dilysine (Lys209-Lys301) trigger in the N-lobe, which facilitates the iron release from the N-lobe at relatively higher pH than the C-lobe because the protonation of the dilysine residues in an acidic medium open the inter-domain cleft of the N-lobe [3], (ii) the interdomain disulfide bridge (Cys478-Cys671), found only in the C-lobe, may restrict domain opening at higher pH and can retard iron

release at relatively higher pH, [68], and (iii) differences in the interdomain hydrogen bonding pattern in the N and C-lobes [68].

8.4 Conclusions

Iron release from Fe_2oTf at mildly acidic pH in the presence of nonsynergistic anions occurs in at least six kinetically detectable steps. Step 1 involves the proton-assisted loss of the synergistic carbonate anion. In subsequent steps, iron release is controlled by slow proton transfers and anion binding. In Step 2, the N-lobe gains one proton. In Step 3, the N-lobe gains one proton with kinetic linkage to the binding of two monoanions or one dianion. In step 4, iron is released from the N-lobe with kinetic linkage to the uptake of two protons accompanied by the loss of anions. In Step 5, the C-lobe gains one proton with kinetic linkage to the binding of two mono anions or one dianion. In Step 6, iron release from the C-lobe occurs with the gains of two protons accompanied by the loss of anions.

8.5 Derivation of Equations

The substitution method was employed to derive the equations for reciprocal relaxation times, equations (28), (40), (44), and (47-51) [32-33,39-40,42,69]. In the current experimental conditions, $[H^+]$ and [S] » [oTf], so for each kinetic run, their concentrations are considered as constant ($\Delta[S] \approx \Delta[H^+] \approx 0$).

Derivation of the reciprocal relaxation time when Fe_{NC}oTf*H first binds a proton and then anions (equation (28))

Fe_{NC}oTf*H first binds a proton (equation (R5)) and then an anion (equation (R6)):

$$Fe_{NC}oTf^*H + H^+ \rightleftharpoons Fe_{NC}oTf^*H_2 \qquad R5$$

$$Fe_{NC}oTf^*H_2 + nS \underset{k_{-1N}}{\overset{k_{1N}}{\rightleftharpoons}} Fe_{NC}oTf^*H_2S_n \qquad R6$$

So, $K_{1H} = [Fe_{NC}oTf^*H]\,[H^+]/[Fe_{NC}oTf^*H_2]$, and $K_{1S} = [Fe_{NC}oTf^*H_2]\,[S]^n/[Fe_{NC}oTf^*H_2S_n]$. If the reaction in equation (R6) is rate limiting, the reciprocal relaxation time associated with equation (R6) can be written as:

$$-d\Delta[Fe_{NC}oTf^*H_2S_n]/dt = k_{-1N}\Delta[Fe_{NC}oTf^*H_2S_n] - k_{1N}[S]^n\Delta[Fe_{NC}oTf^*H_2] \qquad (23)$$

Conservation of mass permits to write:

$$\Delta[[Fe_{NC}oTf^{*}H_2S_n] + \Delta[Fe_{NC}oTf^{*}H_2] + \Delta[Fe_{NC}oTf^{*}H] = 0 \quad (24)$$

If the reaction in equation (R5) is at steady-state, then

$$\Delta[Fe_{NC}oTf^{*}H_2] = [H^+]\Delta[Fe_{NC}oTf^{*}H]/K_{1H} \quad (25)$$

From equations (24) and (25)

$$\Delta[Fe_{NC}oTf^{*}H_2] = \frac{-[H^+]\Delta[Fe_{NC}oTf^{*}H_2S_n]}{([H^+] + K_{1H})} \quad (26)$$

From equations (23) and (26)

$$-d\Delta[Fe_{NC}oTf^{*}H_2S_n]/dt = k_{-1N}\Delta[Fe_{NC}oTf^{*}H_2S_n] + k_{1N}[S]^n[H^+]\Delta[Fe_{NC}oTf^{*}H_2S_n]/([H^+]+K_{1H}]) \quad (27)$$

The pK_a of carboxylate group of aspartic acid is around 3.9, if this is involved then the value of K_{1H} or K_a would be ~126 μM [37]. In the pH range of $3.9 \leq pH \leq 4.3$, the concentration of range of $[H^+]$ varies between 125 to 501 μM so for these conditions, $K_{1H} >> [H^+]$, this assumption allows to write equation (27) as equation (27a)

$$-d\Delta[Fe_{NC}oTf^{*}H_2S_n]/dt = k_{-1N}\Delta[Fe_{NC}oTf^{*}H_2S_n] + k_{1N}[S]^n[H^+]\Delta[Fe_{NC}oTf^{*}H_2S_n]/K_{1H} \quad (27a)$$

Equation (27a) can be written as equation (27b)

$$-d\Delta[Fe_{NC}oTf^{*}H_2S_n]/\Delta[Fe_{NC}oTf^{*}H_2S_n] = (k_{-1N} + k_{1N}[S]^n[H^+]/K_{1H}])dt \quad (27b)$$

Integration with the correct limits allows to write (27c) [39-40,42,69],

$$\Delta[Fe_{NC}oTf^{*}H_2S_n] = \Delta[Fe_{NC}oTf^{*}H_2S_n]\exp(-t/\tau_{1N}) \quad (27c)$$

with the reciprocal relaxation time (equation (28)) for the reaction

$$\tau_{1N}^{-1} = k_{-1N} + \{k_{1N}\left([H^+]\,[S]\right)/K_{1H}\} \quad (28)$$

where in equation (27c), the term $\Delta[Fe_{NC}oTf^{*}H_2S_n]$ is the equilibrium concentration change.

Derivation of the reciprocal relaxation times when the intermediate $Fe_{NC}oTf^{*}S_nH_2$ releases an iron (equations (40), (44), and (47))

Step 3 (Scheme 1) illustrates the release of iron from the $Fe_{NC}oTf^*S_nH_2$ intermediate complex. Thus every possible mechanism by which $Fe_{NC}oTf^*S_nH_2$ can protonate, bind nonsynergistic anions and lose iron should be considered.

$$Fe_{NC}oTf^*S_nH_2 \underset{k'_{-2N}}{\overset{k'_{2N}}{\rightleftharpoons}} Fe_CoTf^*S_nH_2 + Fe \qquad R8$$

$$Fe_CoTf^*S_nH_2 + 2H^+ \underset{k_{-2N}}{\overset{k_{2N}}{\rightleftharpoons}} Fe_CoTf^*S_nH_4 \qquad R9$$

$$Fe_CoTf^*S_nH_4 \underset{k''_{-2N}}{\overset{k''_{2N}}{\rightleftharpoons}} Fe_CoTf^*H_4 + nS \qquad R10$$

For the equilibria described by equations (R8-R10), K_{2Fe}= $[Fe_CoTf^*S_nH_2][Fe]/[Fe_{NC}Tf^*S_nH_2]$, K_{2H} = $[Fe_CoTf^*S_nH_2][H^+]^2/[Fe_CoTf^*S_nH_4]$, and K_{2S} = $[Fe_CoTf^*H_4][S]^n/[Fe_CoTf^*S_nH_4]$. By assuming each of the reaction (equation (R8-R10)) is rate limiting then the equations related to their individual reciprocal relaxation times could be given by equations (29-31), respectively,

$$-d\Delta[Fe_{NC}oTf^*S_nH_2]/dt = k'_{2N}\Delta[Fe_{NC}oTf^*S_nH_2] - k'_{-2N}([Fe]\Delta[Fe_CoTf^*S_nH_2] + [Fe_CoTf^*S_nH_2]\Delta[Fe]) \qquad (29)$$

$$-d\Delta[Fe_CoTf^*]/dt = k_{-2N}\Delta[Fe_CoTf^*S_nH_4] - k_{2N}[H^+]^2\Delta[Fe_CoTf^*S_nH_2] \qquad (30)$$

$$-d\Delta[Fe_CoTf^*H_4]/dt = k''_{-2N}[S]^n\Delta[Fe_CoTf^*H_4] - k''_{2N}\Delta[Fe_CoTf^*S_nH_4] \qquad (31)$$

Conservation of mass allows to write:

$$\Delta[Fe_{NC}oTf^*S_nH_2] + \Delta[Fe_CoTf^*S_nH_2] + \Delta[Fe_CoTf^*S_nH_4] + \Delta[Fe_CoTf^*H_4] = 0 \qquad (32)$$

$$\Delta[Fe_{NC}oTf^*S_nH_2] + \Delta[Fe^{3+}] + \Delta[Fe_CoTf^*S_nH_4] + \Delta[Fe_CoTf^*H_4] = 0 \qquad (33)$$

By assuming the reactions represented by equations (R8-R10) are, one at a time, at steady state, then one can write the equations (34-36), respectively:

$$\Delta[Fe_{NC}oTf^*S_nH_2] = ([Fe_CoTf^*S_nH_2]\Delta[Fe^{3+}]/K_{2Fe}) + ([Fe^{3+}]\Delta[Fe_CoTf^*S_nH_2]/K_{2Fe}) \qquad (34)$$

$$\Delta[Fe_CoTf^*S_nH_4] = [H^+]^2\Delta[Fe_CoTf^*S_nH_2]/K_{2H} \qquad (35)$$

$$\Delta[Fe_CoTf^*S_nH_4] = [S]^n\Delta[Fe_CTf^*H_4]/K_{2S} \qquad (36)$$

From equations (29), (32), and (33)

$$-d\Delta[Fe_{NC}oTf^*S_nH_2]/dt = k'_{2N}\Delta[Fe_{NC}oTf^*S_nH_2] - k'_{-2N}\{\Delta[Fe_CoTf^*S_nH_2]([Fe]+[Fe_CoTf^*S_nH_2])\} \qquad (37)$$

From equations (32), (35), and (36)

$$\Delta[Fe_C oTf^*S_nH_2] = \frac{-K_{2H}[S]^n \Delta[Fe_{NC} oTf^*S_nH_2]}{(K_{2H}[S]^n + [H^+]^2[S]^n + [H^+]^2 K_{2S})} \quad (38)$$

From equations (37) and (38)

$$-d\Delta[Fe_{NC} oTf^*S_nH_2]/dt = k'_{2N}\Delta[Fe_{NC} oTf^*S_nH_2] + \frac{k'_{-2N}K_{2H}[S]\Delta[Fe_{NC} oTf^*S_nH_2])([Fe]+[Fe_C oTf^*S_nH_2])}{K_{2H}[S]^n + [H^+]^2[S]^n + [H^+]^2 K_{2S}} \quad (39)$$

Equation (39) can be represented in a simplified way as equation (39a)

$$-d\Delta[Fe_{NC} oTf^*S_nH_2]/\Delta[Fe_{NC} oTf^*S_nH_2] = \{k'_{2N} + \frac{k'_{-2N}K_{2H}[S]^n([Fe]+[Fe_C oTf^*S_nH_2])}{K_{2H}[S]^n + [H^+]^2[S]^n + [H^+]^2 K_{2S}}\}dt \quad (39a)$$

Integration with the correct limits allows to write (39) [39-40,42,69],

$$\Delta[Fe_{NC} oTf^*S_nH_2] = \Delta[Fe_{NC} oTf^*S_nH_2]\exp(-t/\tau'^{-1}_{2N}) \quad (39b)$$

with the reciprocal relaxation time (equation (40)) for the reaction

$$\tau'^{-1}_{2N} = k'_{2N} + \frac{c_1 k'_{-2N} K_{2H}[S]^n}{K_{2H}[S]^n + [H^+]^2[S]^n + [H^+]^2 K_{2S}} \quad (40)$$

where in equation (39b), the term $\Delta[Fe_{NC} oTf^*S_nH_2]$ is the equilibrium concentration change.

From equations (32), (33), and (34)

$$\Delta[Fe_{NC} oTf^*S_nH_2] = \Delta[Fe_C oTf^*S_nH_2]\{([Fe^{+3}]/K_{2Fe}) + ([Fe_C oTf^*S_nH_2]/K_{2Fe})\} \quad (41)$$

From equations (32), (36), and (41)

$$\Delta[Fe_C oTf^*S_nH_2] = \frac{-K_{2Fe}(1+[S]^n/K_{2S})\Delta[Fe_C oTf^*H_4]}{K_{2Fe}+[Fe^{3+}]+[Fe_C oTf^*S_nH_2]} \quad (42)$$

From equations (30), (36), and (42)

$$-d\Delta[Fe_C oTf^*H_4]/dt = k_{-2N}([S]^n/K_{2S})\Delta[Fe_C oTf^*H_4] + \frac{K_{2Fe}k_{2N}[H^+]^2(1+[S]^n/K_{2S})\Delta[Fe_C oTf^*H_4]}{K_{2Fe}+[Fe^{3+}]+[Fe_C oTf^*S_nH_2]} \quad (43)$$

In the pH range of 3.9-4.3, the affinity of oTf for iron decreased [38]. Under these conditions $K_{2Fe} >> [Fe^{+3}]$ and $[Fe_C oTf^*S_nH_2]$ and equation (43) can be written as equation (43a)

$$-d\Delta[Fe_C oTf^*H_4]/dt = k_{-2N}([S]^n/K_{2S})\Delta[Fe_C oTf^*H_4] + k_{2N}[H^+]^2(1+[S]^n/K_{2S})\Delta[Fe_C oTf^*H_4] \quad (43a)$$

Equation (43a) can be represented in a simplified way as equation (43b)

$$-d\Delta[Fe_CoTf^*H_4]/\Delta[Fe_CoTf^*H_4] = (k_{-2N}([S]^n / K_{2S}) + k_{2N}[H^+]^2(1+[S]^n / K_{2S}))dt \quad (43b)$$

Integration with the-correct limits allows to write (43c) [39-40,42,69]

$$\Delta[Fe_CoTf^*H_4] = \Delta[Fe_CoTf^*H_4] \exp(-t/\tau_{2N}) \quad (43c)$$

with the reciprocal relaxation time (equation (44)) for the reaction

$$\tau_{2N}^{-1} = k_{-2N}([S]^n / K_{2S}) + k_{2N(obs)}[H^+]^2 \quad (44)$$

where in the equation (43c), the term $\Delta[Fe_CoTf^*]$ is the equilibrium concentration change, and in equation (44), $k_{2N(obs)} = k_{2N} + k_{2N}[S]^n / K_{2S}$

From equation (32), (35), and (41),

$$\Delta[Fe_CoTf^*S_nH_4] = \frac{-[H^+]^2 \Delta[Fe_CoTf^*H_4]}{[H^+]^2 + K_{2H} + K_{2H}K_{2Fe}^{-1}([Fe^{3+}] + [Fe_CoTf^*S_nH_2])} \quad (45)$$

From equations (31) and (45)

$$-d\Delta[Fe_CoTf^*H_4]/dt = k''_{-2N}[S]^n \Delta[Fe_CoTf^*H_4] + \frac{(k''_{2N}[H^+]^2 \Delta[Fe_CoTf^*H_4])}{[H^+]^2 + K_{2H} + K_{2H}K_{2Fe}^{-1}([Fe^{3+}] + [Fe_CoTf^*S_nH_2])} \quad (46)$$

Equation (46) can be simplified as equation (46a)

$$-d\Delta[Fe_CoTf^*H_4]/\Delta[Fe_CoTf^*H_4] = \{k''_{-2N}[S]^n + \frac{k''_{2N}[H^+]^2)}{[H^+]^2 + K_{2H} + K_{2H}K_{2Fe}^{-1}([Fe^{3+}] + [Fe_CoTf^*S_nH_2])}\}dt \quad (46a)$$

Integration with the correct limits allows to write (46b) [39-40,42,69],

$$\Delta[Fe_CoTf^*H_4] = \Delta[Fe_CoTf^*H_4] \exp(-t/\tau''_{2N}) \quad (46b)$$

with the reciprocal relaxation time (equation (47)) for the reaction

$$\tau''^{-1}_{2N} = k''_{-2N}[S]^n + \frac{k''_{2N}[H^+]^2}{[H^+]^2 + K_{2H} + c_1 K_{2H}/K_{2Fe}} \quad (47)$$

where in equation (46b), the term $\Delta[Fe_CoTf^*H_4]$ is equilibrium concentration change. The experimental reciprocal relaxation times associated with step 3 (Scheme 1) are independent of

the protein concentration used which discards equation 40. Moreover, equation 42 will not be valid unless $K_{2H} >> [H^+]^2$. Only equation (44) is followed by current experimental data.

Derivation of the reciprocal relaxation time when $Fe_COTf^*H_4$ binds one proton and then anions

Equation (48): $Fe_COTf^*H_4$ first binds a proton and then binds anions,

$$Fe_COTf^*H_4 + H^+ \rightleftharpoons Fe_COTf^*H_5 \qquad \text{R15}$$

$$Fe_COTf^*H_5 + nS \underset{k_{-1C}}{\overset{k_{1C}}{\rightleftharpoons}} Fe_COTf^*S_nH_5 \qquad \text{R16}$$

so $K_{1H} = [Fe_COTf^*H_4][H^+]/[Fe_COTf^*H_5]$, and $K_{1S} = [Fe_COTf^*H_5][S]^n/[Fe_COTf^*S_nH_5]$. The reciprocal relaxation time associated with equation (R16) can be written as equation (48) when it is assumed to be rate-limiting,

$$\tau_{3C}^{-1} = k_{-1C} + \{k_{1C}\left([H^+][S]^n\right)/K_{1H}\} \qquad (48)$$

Here, equation (48) is derived using the similar procedure used to derive equation (28) when $Fe_{NC}OTf^*$ first binds a proton (equation (R5)) and then binds anions (equation (R6)).

Derivation of the reciprocal relaxation time when the intermediate $Fe_COTf^*S_nH_5$ releases an iron (equations (49-51))

Step 5 (Scheme 1) illustrates release of iron from the $Fe_COTf^*S_nH_5$ intermediate. By considering every possible mechanisms by which the intermediate $Fe_COTf^*S_nH_5$ can protonate, bind nonsynergistic anion and release iron, the following equations can be written

$$Fe_COTf^*S_nH_5 \underset{k'_{-2C}}{\overset{k'_{2C}}{\rightleftharpoons}} oTf^*S_nH_5 + Fe \qquad \text{R18}$$

$$oTf^*S_nH_5 + 2H^+ \underset{k_{-2C}}{\overset{k_{2C}}{\rightleftharpoons}} oTf^*S_nH_7 \qquad \text{R19}$$

$$oTf^*S_nH_7 \underset{k''_{-2C}}{\overset{k''_{2C}}{\rightleftharpoons}} oTf^*H_7 + nS \qquad \text{R20}$$

The equilibrium constants for above reactions are $K_{2Fe} = [oTf^*S_nH_5][Fe]/[Fe_COTf^*S_nH_5]$, $K_{2H} = [oTf^*S_nH_5][H^+]^2/[oTf^*S_nH_7]$, and $K_{2S} = [oTf^*H_7][S]^n/[oTf^*S_nH_7]$. By assuming each of the reaction (equation (R18-R20)) is rate limiting then the equations related to their individual reciprocal relaxation times could be given by equations (49-51).

$$\tau'^{-1}_{2C} = k'_{2C} + \frac{c_2 k'_{-2C} K_{2H}[S]^n}{(K_{2H}[S]^n + [H^+]^2[S]^n) + [H^+]^2 K_{2S})} \qquad (49)$$

$$\tau_{2C}^{-1} = k_{-2C}([S]^n / K_{2S}) + k_{2C(obs)}[H^+]^2 \quad (50)$$

where, $k_{2C(obs)} = k_{2C} + k_{2C}[S]^n / K_{2S}$

$$\tau''_{2C}{}^{-1} = k''_{-2C}[S]^n + \frac{k''_{2C}[H^+]^2}{[H^+]^2 + K_{2H} + c_2 K_{2H} / K_{2Fe}} \quad (51)$$

Equations (49-51) are derived using the similar procedure used to derive equations (40), (44), and (47), respectively, when the intermediate $Fe_{NC}oTf^*S_nH_2$ loses an iron according to equations (R8) to (R10).

8.6 References

[1] Ling GN, The Aqueous Cytoplasm, Marcel Dekker: New York, Vol. 1, pp 1−230 (1979)
[2] Chasteen ND, Iron binding proteins without cofactors or sulfur clusters, Elsevier: New York, Vol. 5; pp 201−233 (1983)
[3] Bou-Abdallah, F, El Hage Chahine, JM, Eur J Biochem 263:912−920 (1999)
[4] Kretchmar SA, Raymond KN, J Am Chem Soc 108:6212−6218 (1986)
[5] Bali PK, Harris WR, J Am Chem Soc 111:4457–4461 (1989)
[6] Baker HM, Anderson BF, Brodie AM, Shongwe MS, Smith CA, Baker EN, Biochemistry 35:9007–9013 (1996)
[7] MacGillivray RT, Moore SA, Chen J, Anderson BF, Baker H, Luo Y, Bewley M, Smith CA, Murphy ME, Wang Y, Mason AB, Woodworth RC, Brayer GD, Baker EN, Biochemistry 37:7919–7928 (1998)
[8] Jeffrey PD, Bewley MC, MacGillivray RT, Mason AB, Woodworth RC, Baker EN, Biochemistry 37:13978–13986 (1998)
[9] Dewan JC, Mikami B, Hirose M, Sacchettini JC, Biochemistry 32:11963–11968 (1993)
[10] Nurizzo D, Baker HM, He QY, MacGillivray RT, Mason AB, Woodworth RC, Baker EN, Biochemistry 40:1616−1623 (2001)
[11] Halbrooks PJ, He QY, Briggs SK, Everse SJ, Smith VC, MacGillivray RT, Mason AB, Biochemistry 42:3701–3707 (2003)
[12] Moore SA, Anderson BF, Groom CR, Haridas M, Baker EN, J Mol Biol 274:222-236 (1997)
[13] Mizutani K, Yamashita H, Mikami B, Hirose M, Biochemistry 39:3258–3265 (2000)
[14] Mizutani K, Muralidhara BK, Yamashita H, Tabata S, Mikami B, Hirose M, J Biol Chem 276:35940–35946 (2001)
[15] Baker EN, Baker HM, Kidd RD, Biochem Cell Biol 80:27–34 (2002)
[16] Peterson NA, Anderson BF, Jameson GB, Tweedie JW, Baker EN, Biochemistry 39:6625–6633 (2000)
[17] Sreedhara A, Flengsrud R, Langsrud T, Kaul P, Prakash V, Vegarud GE, Biometals 23:1159–1170 (2010)
[18] Zak O, Tam B, MacGillivray RTA, Aisen P, Biochemistry 36:11036−11043 (1997)
[19] Egan TJ, Ross DC, Purves LR, Adams PA, Inorg Chem 31:1994−1998 (1992)

[20] Byrne SL, Steere AN, Chasteen ND, Mason AB, Biochemistry 49:4200–4207 (2010)
[21] Marques HM, Egan TJ, Pattrick G, S Afr J Sci 86:21–24 (1990)
[22] Marques HM, Watson DL, Egan TJ, Inorg Chem 30:3758–3762 (1991)
[23] Egan TJ, Zak O, Aisen P, Biochemistry 32:8162–8167 (1993)
[24] Muralidhara BK, Hirose M, J Biol Chem 275:12463–12469 (2000)
[25] He QY, Mason AB, Nguyen V, MacGillivray RT, Woodworth RC, Biochem J. 350 Pt 3:909–915 (2000)
[26] Hemadi M, Ha-Duong NT, El HageChahine JM, J Mol Biol 358:1125–1136 (2006)
[27] Marques HM, Walton T, Egan TJ, J Inorg Biochem 57:11−21 (1995)
[28] Zak O, Aisen P, Crawley JB, Joannou CL, Patel KJ, Rafiq M, Evans RW, Biochemistry 34:14428−14434 (1995)
[29] He QY, Mason AB, MacGillivray RTA, Woodworth RC, Biochemistry 38:9704−9711 (1999)
[30] Bou-Abdallah, F, El Hage Chahine JM, Eur J Biochem 258:1022−1031 (1998)
[31] Chikh Z, Hemadi M, Miquel G, Ha-Duong NT, El Hage Chahine JM, J Mol Biol 380:900−916 (2008)
[32] Bou-Abdallah F, El Hage Chahine JM, J Mol Biol 303:255−266 (2000)
[33] El Hage Chahine JM, Pakdaman R, Eur J Biochem 230:1102−1110 (1995)
[34] He QY, Mason AB, Woodworth RC, Tam BM, Wadsworth T, MacGillivray RT, Biochemistry 36:5522−5528 (1997)
[35] Mason A, He QY, Tam B, MacGillivray RA, Woodworth R, Biochem J 330 Pt 1:35−40 (1998)
[36] El Hage Chahine JM, Fain D, Eur J Biochem 223:581−587 (1994)
[37] Kumar R, Mauk AG, J Phys Chem B 116:3795–3807 (2012)
[38] Kumar S, Sharma D, Kumar R, Kumar R, J Biol Inorg Chem 6:1009–1024 (2014)
[39] Eigen M, deMaeyer L, Relaxation Methods. In Techniques of Organic Chemistry, Friess SL, Lewis ES, Weissberger, A, Eds., Interscience: New York, Vol. 8 (pt. 2), pp 895−1029 (1963)
[40] Brouillard RJ, Chem Soc Faraday Trans 76:583−587 (1980)
[41] Cheng Y, Mason AB, Woodworth RC, Biochemistry 34:14879−14884 (1995)
[42] Bernasconi CF, Relaxation Kinetics, Academic Press: New York (1976)
[43] Aisen P, Listowsky I, Annu Rev Biochem 49:357–393 (1980)
[44] Lee DA, Goodfellow JM, Biophysical J 85:2747–2759 (1998)
[45] Rinaldo D, Field MJ, Biophysical J 85:3485–3501 (2003)
[46] Bobst CE, Zhang M, Kaltashov IA, J Mol Biol 388:954–967 (2009)
[47] Byrne SL, Chasteen ND, Steere AN, Mason AB, J Mol Biol 396:130–140 (2010)
[48] Steere AN, Byrne SL, Chasteen ND, Smith VC, MacGillivray RT, Mason AB, J Biol Inorg Chem 15:1341–1352 (2010)
[49] James NG, Byrne SL, Steere AN, Smith VC, MacGillivray RT, Mason AB, Biochemistry 48:2858–2867 (2009)
[50] James NG, Berger CL, Byrne SL, Smith VC, MacGillivray RT, Mason AB, Biochemistry 46:10603–10611 (2007)
[51] Halbrooks PJ, Giannetti AM, Klein JS, Björkman PJ, Larouche JR, Smith VC, MacGillivray RT, Everse SJ, Mason AB, Biochemistry 44:15451–15460 (2005)
[52] Nurizzo D, Baker HM, He QY, MacGillivray RT, Mason AB, Woodworth RC, Baker EN, Biochemistry 40:1616–1623 (2001)

[53] He QY, Mason AB, Tam BM, MacGillivray RT, Woodworth RC, Biochem J 344:881–887 (1999)
[54] Byrne SL, Mason AB, J Biol Inorg Chem 14:771–781 (2009)
[55] Kumar R, Mauk AG, J Phys Chem B 113:12400–12409 (2009)
[56] Kretchmar SA, Raymond KN, Inorg Chem 27:1436–1441 (1988)
[57] Baldwin DA, Egan TJ, Marques HM, Biochim Biophys Acta 1038:1–9 (1990)
[58] Wishnia A, Weber L, Warner RC, J Am Chem Soc 83:2071−2080 (1961)
[59] Folajtar DA, Chasteen ND, J Am Chem Soc 104:5775−5780 (1982)
[60] Foley AA, Bates GW, Biochim Biophys Acta 965:154−162 (1988)
[61] Record MT Jr, Anderson CF, Lohman TM, Q Rev Biophys 11:103−178 (1978)
[62] Cacace MG, Landau EM, Ramsden JJ, Q Rev Biophys 30:241−277 (1997)
[63] Baldwin DA, Biochim Biophys Acta 623:183−198 (1980)
[64] Li Y, Harris WR, Biochim Biophys Acta 1387:89−102 (1998)
[65] Harris WR, Bali PK, Inorg Chem 27:2687−2691 (1988)
[66] Harris WR, Cafferty AM, Abdollahi S, Trankler K, Biochim Biophys Acta 1383:197−210 (1998)
[67] Kurokawa H, Mikami B, Hirose M, J Mol Biol 254:196−207 (1995)
[68] Kurokawa H, Dewan JC, Mikami B, Sacchettini JC, Hirose M, J Biol Chem 274:28445–28452 (1999)
[69] Czerlinski GH, Chemical Relaxation, Marcel Dekker, New York, pp. 314 (1966)

9.0 Appendix

Chapter 5

Table 5.1. Sugar (glycerol, ribose, glucose, maltose, sucrose and trehalose) dependence of thermodynamic parameters for thermal denaturation of Lyz at pH 2.3 as monitored by absorbance at 292 nm.

sugar	concentration (M)	T_m (K)	ΔH_m (kcal mol^{-1})
Control	0.0	329.3	77.9
glycerol	0.5	329.8	83.2
	0.75	330.4	84.4
	1.0	330.9	90.1
	1.5	332.0	90.1
	2.0	333.0	93.5
Ribose	0.25	330.1	81.9
	0.5	330.6	84.8
	0.75	331.6	85.4
	1.0	332.0	95.9
Glucose	0.25	330.8	77.6
	0.5	331.6	85.1
	0.75	332.7	89.0
	1.0	335.4	95.4
	1.25	336.2	99.3
	1.5	338.1	101.3
Maltose	0.25	331.0	83.6
	0.75	334.9	93.0
	1.0	336.6	97.1
	1.25	339.1	99.0
Sucrose	0.25	331.1	85.0
	0.5	332.7	90.3
	0.75	335.0	98.0
trehalose	0.25	331.3	85.0
	0.5	332.9	93.0
	0.75	335.0	95.3
	1.0	337.8	104.4
	1.25	340.4	107.5

The uncertainties of T_m and ΔH_m reported here are ±0.5 °C, and ±5.0 kcal mol^{-1}, respectively.

Table 5.2. Sugar (glycerol, and trehalose) dependence of thermodynamic parameters for thermal denaturation of Lyz at pH 13 as monitored by CD signal at 222 nm.

sugar	concentration (M)	T_m (K)	ΔH_m (kcal mol^{-1})
Control	0.0	322.2	77.6
glycerol	2.5	325.6	100.1
	5.0	330.2	80.3
trehalose	0.5	330.6	107.4
	1.0	337.9	118.5

The uncertainties of T_m and ΔH_m and reported here are ±0.5 °C, and ±5.0 kcal mol^{-1}, respectively.

Table 5.3. GdnHCl dependence of the thermodynamic parameters for thermal unfolding of Lyz (absorbance at 292 nm) in the absence and presence of 0.75 M sugar (glycerol, ribose, glucose, maltose, sucrose and trehalose) at pH 2.3.

sugar	GdnHCl (M)	T_m (K)	ΔH_m (kcal mol^{-1})
Control	0.0	329.3	77.9
	0.15	326.7	74.8
	0.25	325.7	72.8
	0.5	323.4	69.4
	0.75	323.2	67.8
	1.0	320.1	65.0
	1.5	316.4	58.6
	2.0	312.8	52.2
glycerol	0.0	330.4	84.4
	0.25	327.2	77.5
	0.5	326.4	73.5
	1.0	321.8	68.1
	1.25	319.9	65.1
	1.5	317.9	62.8
	2.0	314.1	57.1
Ribose	0.0	331.6	85.4
	0.25	329.0	80.3
	0.5	326.8	75.8
	1.0	323.3	71.9
	1.5	319.6	67.1
	2.0	316.5	62.4
Glucose	0.0	332.7	89.0
	0.1	332.3	80.8
	0.25	331.1	81.0
	0.5	328.4	77.4
	0.75	325.0	70.4
	1.0	324.7	71.1
	1.5	321.2	63.3
	2.0	317.3	61.2
Maltose	0.0	334.9	93.0
	0.1	333.4	86.5
	0.25	331.3	82.5
	0.5	329.3	79.4
	1.0	325.8	74.3
	1.5	321.2	62.0
	2.0	318.0	62.7
Sucrose	0.0	335.0	98.0
	0.25	332.6	86.6
	0.5	330.0	75.0
	1.0	326.0	73.7

	1.5	322.6	57.9
	2.0	318.9	53.2
trehalose	0.0	335.0	95.3
	0.25	332.4	90.9
	0.5	330.0	85.6
	1.0	327.6	73.1
	1.5	323.3	67.2
	2.0	320.2	64.6

The uncertainties of T_m and ΔH_m reported here are ±0.5 °C, and ±5.0 kcal mol^{-1}, respectively.

Table 5.4. Urea dependence of the thermodynamic parameters for thermal unfolding of Lyz (absorbance at 292 nm) in the absence and presence of 0.75 M sugars (glycerol, glucose, maltose, and trehalose) at pH 2.3.

sugar	urea (M)	T_m (K)	ΔH_m (kcal mol^{-1})
Control	0.0	329.3	77.9
	0.5	326.2	72.3
	1.0	323.0	68.7
	1.5	320.9	64.3
	2.0	318.2	62.4
	2.5	316.2	59.4
	3.0	314.0	55.9
	4.0	309.0	50.2
glycerol	0.0	330.4	84.4
	0.5	328.0	75.9
	1.0	324.8	70.9
	2.0	320.4	65.8
	3.0	316.3	62.9
	4.0	313.1	58.5
Glucose	0.0	332.7	89.0
	0.5	329.8	85.0
	1.0	327.2	81.5
	1.5	325.2	77.0
	2.0	322.8	75.5
	2.5	321.0	68.3
	3.0	319.3	62.5
	4.0	316.4	60.4
Maltose	0.0	332.7	89.0
	0.0	334.9	93.0
	0.5	331.3	89.6
	1.5	326.7	81.1
	1.0	328.8	82.8
	2.0	324.2	76.8
	2.5	322.4	75.5
	3.0	320.9	70.6
	4.0	317.7	63.0
trehalose	0.0	335.0	95.3
	1.0	330.3	85.3
	1.5	327.3	83.0
	2.0	325.9	78.3
	3.0	322.7	70.1
	4.0	320.3	63.1

The uncertainties of T_m and ΔH_m reported here are ±0.5 °C, and ±5.0 kcal mol^{-1}, respectively.

Table 5.5. Dependence of the ΔG_D and C_m values for urea denaturation of Lyz on sugar (glycerol, ribose, glucose, maltose, sucrose and trehalose) at pH 2.3 as monitored by fluorescence (ex: 280 nm, em: 360 nm) at pH 2.3.

sugar	concentration (M)	ΔG_D (kcal mol^{-1})	m_g (kcal mol^{-1} M^{-1})	C_m (M)
Control	0.0	3.33	1.13	2.94
Glycerol	0.75	3.66	0.96	3.81
	1.12	4.01	1.00	4.01
	1.5	4.24	0.96	4.41
Ribose	0.75	4.07	0.99	4.11
	1.12	4.57	0.99	4.61
	1.5	4.82	0.99	4.86
Glucose	0.75	4.39	1.00	4.39
	1.12	4.90	0.99	4.94
	1.5	5.25	0.96	5.46
Maltose	0.75	4.63	0.91	5.08
	1.12	5.40	1.00	5.4
	1.5	6.22	1.00	6.22
Sucrose	0.75	5.10	0.95	5.36
	1.12	5.70	1.01	5.64
	1.5	6.80	1.03	6.6
trehalose	0.75	5.23	0.96	5.44
	1.12	6.00	0.98	6.12
	1.5	7.80	1.10	7.09

The uncertainties of m_g and ΔG_D values reported here are ± 0.2 kcal mol^{-1} M^{-1} and ±0.2 kcal mol^{-1}, respectively. The uncertainty of C_m values reported here is ±0.2 M.

Table 5.6. Dependence of the ΔG_D and C_m values for GdnHCl denaturation of Lyz on sugar (glycerol and trehalose) at pH 13 as monitored by as monitored by fluorescence (ex: 280 nm, em: 360 nm) at pH 13.

sugar	concentration (M)	ΔG_D (kcal mol^{-1})	m_g (kcal mol^{-1} M^{-1})	C_m (M)
control	0.0	2.94	1.36	2.16
trehalose	0.5	3.20	1.18	2.71
	1.0	3.40	1.15	2.95
	1.5	3.76	1.03	3.65
glycerol	1.25	3.20	1.39	2.30
	2.5	3.34	1.29	2.58
	5.0	3.66	1.33	2.75

The uncertainties of m_g and ΔG_D values reported here are ±0.1 kcal mol^{-1} M^{-1} and ±0.1 kcal mol^{-1}, respectively. The uncertainty of C_m values reported here is ±0.1 M.

Table 5.7. Dependence of the ΔG_D and C_m values of Lyz on GdnHCl in the absence and presence of 0.75 M sugar (glycerol, ribose, glucose, maltose, sucrose and trehalose) at pH 2.3 as monitored by fluorescence (ex: 280 nm, em: 360 nm).

sugar	GdnHCl (M)	ΔG_D (kcal mol^{-1})	m_g (kcal mol^{-1} M^{-1})	C_m (M)
Control	0.0	3.33	1.13	2.94
	0.5	2.79	1.11	2.51
	1.0	2.27	1.09	2.08
	1.5	1.80	0.97	1.85
glycerol	0.0	3.66	0.96	3.81
	0.5	3.18	0.91	3.49
	1.0	2.89	0.90	3.21
	1.5	2.60	0.86	3.02
Ribose	0.0	4.07	0.99	4.11
	0.5	3.27	0.89	3.67
	1.0	3.15	0.92	3.42
	1.5	2.84	0.90	3.15
Glucose	0.0	4.39	1.00	4.39
	0.5	3.76	0.96	3.91
	1.0	3.24	0.90	3.60
	1.5	3.10	0.95	3.26
Maltose	0.0	4.63	0.91	5.08
	0.5	4.37	0.96	4.55
	1.0	3.91	0.93	4.20
	1.5	3.73	0.99	3.76
Sucrose	0.0	5.10	0.95	5.36
	0.5	4.71	1.02	4.60
	1.0	4.30	0.99	4.34
	1.5	3.94	0.98	4.02
trehalose	0.0	5.23	0.96	5.44
	0.5	5.01	1.03	4.86
	1.0	4.38	0.99	4.42
	1.5	4.39	1.02	4.30

The uncertainties of m_g and ΔG_D values reported here are ±0.2 kcal mol^{-1} M^{-1} and ±0.2 kcal mol^{-1}, respectively. The uncertainty of C_m values reported here is ±0.2 M.

Chapter 6

Table 6.1. Effects of salts and sucrose on the k_{obs} (rate constant) for urea-denaturation induced iron release kinetics of the Fe_NoTf complex at pH ~7.4 and pH ~5.6.*

pH ~7.4		pH ~5.6	
	$k_{obs}(sec^{-1})$		$k_{obs}(sec^{-1})$
Control	3.8×10^{-3}	Control	0.58
[NaCl] (M)		[NaCl] (M)	
0.05	4.8×10^{-3}	0.05	0.63
0.15	6.3×10^{-3}	0.15	0.77
0.25	6.2×10^{-3}	0.25	0.93
0.4	6.1×10^{-3}	0.5	1.28
0.75	5.8×10^{-3}	0.75	1.31
1.0	5.6×10^{-3}	1.0	1.30
1.5	4.4×10^{-3}		
$[Na_2SO_4]$ (M)		$[Na_2SO_4]$ (M)	
0.025	5.1×10^{-3}	0.025	0.75
0.05	5.1×10^{-3}	0.05	0.88
0.1	6.2×10^{-3}	0.1	1.28
0.15	5.1×10^{-3}	0.25	1.46
0.25	5.0×10^{-3}	0.5	1.44
0.35	3.4×10^{-3}	-	-
0.5	2.0×10^{-3}	-	-
[Sucrose] (M)		[Sucrose] (M)	
0.25	3.4×10^{-3}	0.25	0.53
0.35	3.3×10^{-3}	0.35	0.56
0.5	3.0×10^{-3}	0.5	0.59

*The standard error of k_{obs} is ±5% observed by independent set of experiment.

Table 6.2. Effects of salts on the k_{obs} (rate constant) for Fe^{2+} release kinetics of Fe_NoTf complex at pH ~7.4 and pH ~5.6.*

pH ~7.4		pH ~5.6	
	$k_{obs}(sec^{-1})$		$k_{obs}(sec^{-1})$
Control	1.1×10^{-2}	Control	0.09
$[NaNO_3]$ (M)		$[NaNO_3]$ (M)	
0.04	1.2×10^{-2}	0.1	0.13
0.1	1.4×10^{-2}	0.2	0.15
0.25	1.2×10^{-2}	0.5	0.16
0.5	1.1×10^{-2}	0.6	0.16
0.75	9.3×10^{-3}		
0.95	7.5×10^{-3}		
$[Na_2SO_4]$ (M)		$[Na_2SO_4]$ (M)	
0.04	1.17×10^{-2}	0.02	0.11
0.07	1.31×10^{-2}	0.045	0.13
0.1	1.05×10^{-2}	0.050	0.14
0.2	7.8×10^{-3}	0.12	0.16
0.4	6.0×10^{-3}	0.4	0.17
0.5	4.5×10^{-3}	0.5	0.17

*The standard error of k_{obs} is ±5% observed by independent set of experiment.

Chapter 7

Table 7.1. Crowding agent dependence of C_m, ΔG_D, and m_g derived for urea-denaturation induced iron release from Fe_2sTf at pH 7.4 and pH 5.7 as monitored by absorbance at 465 nm.*

	pH 7.4			pH 5.7		
	ΔG_D	m_g	C_m	ΔG_D	m_g	C_m
Control	6.2	1.20	5.2	4.1	1.13	3.6
dextran 40 100 mg ml^{-1}	6.6	1.10	6.0	4.5	1.08	4.2
dextran 40 200 mg ml^{-1}	7.8	1.22	6.4	5.6	1.24	4.5
dextran 70 100 mg ml^{-1}	7.4	1.19	6.2	4.8	1.11	4.3
dextran 70 200 mg ml^{-1}	8.1	1.18	6.9	5.9	1.14	5.2
ficoll 70 100 mg ml^{-1}	6.7	1.22	5.5	4.2	1.10	3.8
ficoll 70 200 mg ml^{-1}	7.2	1.23	5.9	4.6	1.06	4.3

*C_m, ΔG_D, and m_g are reported as M, kcal mol^{-1}, and kcal mol^{-1} M^{-1}. The uncertainty of C_m, ΔG_D, and m_g values reported here is ±0.1 M, ±0.2 kcal mol^{-1}, and 0.05 kcal mol^{-1} M^{-1}.

Table 7.2. Effect of crowding agent on the salt dependence of C_m, ΔG_D, and m_g derived for urea-induced iron release from Fe_2sTf at pH 7.4 and pH 5.7 as monitored by absorbance at 465 nm.*

	pH 7.4			pH 5.7		
	ΔG_D	m_g	C_m	ΔG_D	m_g	C_m
Control	6.2	1.20	5.2	4.1	1.13	3.6
dextran 40 200 mg ml^{-1}	7.8	1.22	6.4	5.6	1.24	4.5
0.3 M NaCl	5.8	1.25	4.6	3.4	1.06	3.2
0.6 M NaCl	5.1	1.15	4.4	3.3	1.23	2.7
1.2 M NaCl	4.9	1.11	4.4	3.2	1.23	2.6
0.3 M NaCl + dextran 40 200 mg ml^{-1}	7.6	1.28	5.9	5.4	1.24	4.4
0.6 M NaCl + dextran 40 200 mg ml^{-1}	7.3	1.28	5.7	4.9	1.16	4.2
1.2 M NaCl + dextran 40 200 mg ml^{-1}	6.6	1.20	5.5	4.5	1.09	4.1

*C_m, ΔG_D, and m_g are reported as M, kcal mol^{-1}, and kcal mol^{-1} M^{-1}. The uncertainty of C_m, ΔG_D, and m_g values reported here is ±0.1 M, ±0.2 kcal mol^{-1}, and 0.05 kcal mol^{-1} M^{-1}.

Table 7.3. Effect of crowding agent on the C_m, ΔG_D, and m_g derived for urea-induced unfolding of Fe_2sTf at pH 7.4 and pH 5.5 as monitored by monitored by CD at 222.*

	pH 7.4			pH 5.5		
	ΔG_D	m_g	C_m	ΔG_D	m_g	C_m
Control	7.8	0.98	8.0	4.6	1.10	4.2
dextran 40 100 mg ml^{-1}	8.4	1.03	8.2	5.1	1.06	4.8
dextran 40 200 mg ml^{-1}	9.0	1.06	8.5	5.5	1.05	5.2
dextran 40 300 mg ml^{-1}	9.7	1.10	8.8	6.0	0.99	6.1
dextran 70 100 mg ml^{-1}	8.7	1.06	8.2	5.3	1.01	5.2
dextran 70 200 mg ml^{-1}	9.7	1.10	8.8	5.7	0.98	5.8
dextran 70 300 mg ml^{-1}	10.3	1.11	9.3	6.3	0.95	6.6
ficoll 70 100 mg ml^{-1}	8.1	1.00	8.1	5.1	1.11	4.6
ficoll 70 200 mg ml^{-1}	8.5	1.03	8.3	5.5	1.07	5.1
ficoll 70 300 mg ml^{-1}	9.1	1.06	8.6	5.7	1.05	5.4

*C_m, ΔG_D, and m_g are reported as M, kcal mol^{-1}, and kcal mol^{-1} M^{-1}. The uncertainty of C_m, ΔG_D, and m_g values reported here is ±0.1 M, ±0.2 kcal mol^{-1}, and 0.05 kcal mol^{-1} M^{-1}.

Table 7.4. Effect of crowding agents on salt dependence of C_m, ΔG_D, and m_g derived for urea-induced unfolding of Fe_2sTf at pH 7.4 and pH 5.5 as monitored by monitored by CD at 222.*

	pH 7.4			pH 5.5		
	ΔG_D	m_g	C_m	ΔG_D	m_g	C_m
Control	7.8	0.98	8.0	4.6	1.10	4.2
dextran 40 200 mg ml^{-1}	9.0	1.06	8.5	5.5	1.05	5.2
0.3 M NaCl	7.2	0.97	7.4	4.5	1.21	3.7
0.6 M NaCl	6.7	0.98	6.8	3.7	1.20	3.1
1.2 M NaCl	6.7	0.97	6.9	3.6	1.35	2.7
0.3 M NaCl + dextran 40 200 mg ml^{-1}	8.6	1.05	8.2	5.3	1.10	4.8
0.6 M NaCl + dextran 40 200 mg ml^{-1}	8.2	1.03	8.0	5.1	1.14	4.5
1.2 M NaCl + dextran 40 200 mg ml^{-1}	8.1	1.00	8.1	5.0	1.17	4.3

*C_m, ΔG_D, and m_g are reported as M, kcal mol^{-1}, and kcal mol^{-1} M^{-1}. The uncertainty of C_m, ΔG_D, and m_g values reported here is ±0.1 M, ±0.2 kcal mol^{-1}, and 0.05 kcal mol^{-1} M^{-1}.

Table 7.5. Effects of crowding agents on the k_{obs} (rate constant) for Fe^{2+} release kinetics of Fe_NsTf complex at pH 7.4 and pH 5.5 (25 °C).*

pH 7.4		pH 5.5	
	k_{obs}(sec^{-1})		k_{obs}(sec^{-1})
Control	3.9×10^{-3}	Control	0.088
[ficoll 70] (mg ml^{-1})		[ficoll 70] (mg ml^{-1})	
50	3.2×10^{-3}	50	0.083
100	2.5×10^{-3}	100	0.074
150	2.1×10^{-3}	150	0.067
200	1.8×10^{-3}	200	0.055
250	1.8×10^{-3}	250	0.047
		300	0.033
[dextran 40] (mg ml^{-1})		[dextran 40] (mg ml^{-1})	
50	3.2×10^{-3}	50	0.079
100	2.4×10^{-3}	100	0.066
150	1.8×10^{-3}	150	0.059
200	1.6×10^{-3}	200	0.036
250	1.6×10^{-3}	250	0.015
[dextran 70] (mg ml^{-1})		[dextran 70] (mg ml^{-1})	
100	2.3×10^{-3}	50	0.072
150	1.9×10^{-3}	100	0.061
200	1.5×10^{-3}	150	0.046
250	1.2×10^{-3}	200	0.029

*The standard error of k_{obs} is ±7% observed by independent set of experiment.

Table 7.6. Effects of crowding agents on the k_{obs} for Fe^{3+} release kinetics of Fe_NsTf at pH 7.4 and pH 5.5, (37 °C).*

pH 7.4		pH 5.5	
	$k_{obs}(sec^{-1})$		$k_{obs}(sec^{-1})$
Control	3.4×10^{-4}	Control	2.0×10^{-3}
[ficoll 70] (mg ml^{-1})		[ficoll 70] (mg ml^{-1})	
50	2.8×10^{-4}	50	1.7×10^{-3}
100	2.3×10^{-4}	100	1.7×10^{-3}
150	1.9×10^{-4}	150	1.5×10^{-3}
200	1.6×10^{-4}	200	1.4×10^{-3}
[dextran 40] (mg ml^{-1})		[dextran 40] (mg ml^{-1})	
50	2.5×10^{-4}	50	1.8×10^{-3}
100	2.1×10^{-4}	100	1.5×10^{-3}
150	1.6×10^{-4}	150	1.3×10^{-3}
200	1.5×10^{-4}	200	9.8×10^{-4}
[dextran 70] (mg ml^{-1})		[dextran 70] (mg ml^{-1})	
50	2.4×10^{-4}	50	1.5×10^{-3}
100	2.0×10^{-4}	100	1.0×10^{-3}
150	1.5×10^{-4}	150	9.2×10^{-4}
200	1.3×10^{-4}	200	8.2×10^{-4}

*The standard error of k_{obs} is ±7% observed by independent set of experiment.

Table 7.7. Effects of crowding agent on the salt dependence of k_{obs} (rate constant) for Fe^{2+} release kinetics of Fe_NsTf complex at pH 7.4 and pH 5.5 (25 °C).*

pH 7.4		pH 5.5	
	$k_{obs}(sec^{-1})$		$k_{obs}(sec^{-1})$
Control	3.9×10^{-3}	Control	0.088
[dextran 40] (mg ml^{-1})		[dextran 40] (mg ml^{-1})	
200	1.6×10^{-3}	200	0.036
[NaCl] (M)		[NaCl] (M)	
0.075	4.8×10^{-3}	0.15	0.127
0.15	4.9×10^{-3}	0.25	0.143
0.25	5.3×10^{-3}	0.35	0.144
0.35	5.5×10^{-3}	0.5	0.148
0.5	5.5×10^{-3}	0.75	0.163
0.75	5.3×10^{-3}	1.0	0.170
1.0	5.3×10^{-3}		
200 mg ml^{-1} dextran 40 + [NaCl] (M)		200 mg ml^{-1} dextran 40 + [NaCl] (M)	
0.075	1.8×10^{-3}	0.075	0.038
0.15	1.9×10^{-3}	0.15	0.040
0.25	2.0×10^{-3}	0.25	0.042
0.35	2.2×10^{-3}	0.35	0.043
0.5	2.4×10^{-3}	0.5	0.050
0.75	2.5×10^{-3}	0.75	0.054
1.0	2.6×10^{-3}	1.0	0.057

*The standard error of k_{obs} is ±7% observed by independent set of experiment.

Table 7.8. Effects of crowding agent on the salt dependence of k_{obs} (rate constant) for Fe^{3+} release kinetics of Fe_NsTf at pH 7.4 and pH 5.5 (37 °C).*

pH 7.4		pH 5.5	
	$k_{obs}(sec^{-1})$		$k_{obs}(sec^{-1})$
Control	3.4×10^{-4}	Control	2.0×10^{-3}
[dextran 40] (mg ml^{-1})		[dextran 40] (mg ml^{-1})	
200	1.5×10^{-4}	200	9.8×10^{-4}
[NaCl] (M)		[NaCl] (M)	
0.2	4.3×10^{-4}	0.05	2.2×10^{-3}
0.6	4.6×10^{-4}	0.1	2.4×10^{-3}
0.9	5.1×10^{-4}	0.15	2.5×10^{-3}
1.2	5.2×10^{-4}	0.2	2.7×10^{-3}
		0.3	3.4×10^{-3}
		0.45	3.5×10^{-3}
		0.6	4.4×10^{-3}
		0.9	4.5×10^{-3}
		1.2	4.6×10^{-3}
		1.5	4.7×10^{-3}
200 mg ml^{-1} dextran 40 + [NaCl] (M)		200 mg ml^{-1} dextran 40 + [NaCl] (M)	
0.2	1.8×10^{-4}	0.05	1.1×10^{-3}
0.6	1.9×10^{-4}	0.15	1.2×10^{-3}
0.9	2.0×10^{-4}	0.3	1.2×10^{-3}
1.2	2.1×10^{-4}	0.6	1.4×10^{-3}
		0.9	1.5×10^{-3}
		1.2	1.4×10^{-3}

*The standard error of k_{obs} is ±7% observed by independent set of experiment.

List of Publications

Papers in SCI/refereed journals

1. **Sandeep Kumar**, Deepak Sharma, Rajesh Kumar and Rajesh Kumar. "Electrostatic effects controls the stability and iron release kinetics of ovotransferrin", *J. Biol. Inorg. Chem.* 19(6) (2014) 1009-1024. (Impact Factor = 2.54)

2. **Sandeep Kumar**, Deepak Sharma and Rajesh Kumar. "Effect of urea and alkylureas on the stability and structural fluctuation of the M80-containing Ω-loop of horse cytochrome *c*", *Biochimica et Biophysica Acta* 1844(3) (2014) 641–655. (Impact Factor = 2.75)

3. Rishu Jain, Deepak Sharma, **Sandeep Kumar** and Rajesh Kumar. "Factor defining the effects of glycine betaine on the thermodynamic stability and internal dynamics of horse cytochrome *c*", *Biochemistry (ACS)* 53(32) (2014) 5221-5235. (Impact Factor = 3.02)

4. Rajesh Kumar, Deepak Sharma, Rishu Jain, **Sandeep Kumar** and Rajesh Kumar. "Role of macromolecular crowding and salt ions on the structural-fluctuation of a highly compact configuration of carbonmonoxycytochrome *c*", *Biophysical Chemistry* 207 (2015) 61-73. (Impact Factor = 2.0)

5. Rishu Jain, Rajesh Kumar, **Sandeep Kumar**, Ritika Chhabra, Mukesh Chand Agarwal and Rajesh Kumar. "Analysis of the pH-dependent stability and millisecond folding kinetics of horse cytochrome *c*", *Archive of Biochemistry and Biophysics* 585 (2015) 52-63. (Impact Factor = 3.1)

Papers/posters in Conferences

1. **Sandeep Kumar**, Rishu Jain and Rajesh Kumar. "Iron release from diferric ovotransferrin in the absence of chelators involves six kinetic steps at acidic pH", *6th National conference on thermodynamics of Chemical and Biological systems 2011*, Maharishi Dayanand University, Rohtak.

2. **Sandeep Kumar** and Rajesh Kumar. "Hydrophobicity of denaturants control the local dynamics of a native-like compact state of horse ferrocytochrome *c*", *NCIMSF 2013*, Thapar University, Patiala

3. **Sandeep Kumar**, Rajesh Kumar and Rajesh Kumar. "Atypical effect of salts on the stability of Fe^{3+}-ovotransferrin-CO_3^{2-} complex", *Material Research Society of India (23rd Annual meeting 2012)* Thapar University, 134.

4. Rajesh Kumar, **Sandeep Kumar**, and Rajesh Kumar. "Effect of neutral salts on the stability of acid-denatured hen egg white lysozyme", *Material Research Society of India (23rd Annual meeting 2012)* Thapar University, 143.

Biochimica et Biophysica Acta 1844 (2014) 641–655

Contents lists available at ScienceDirect

Biochimica et Biophysica Acta

journal homepage: www.elsevier.com/locate/bbapap

Effect of urea and alkylureas on the stability and structural fluctuation of the M80-containing Ω-loop of horse cytochrome *c*

Sandeep Kumar [a], Deepak Sharma [b], Rajesh Kumar [a,*]

[a] School of Chemistry and Biochemistry, Thapar University, Patiala 147004, India
[b] Council of Scientific and Industrial Research – Institute of Microbial Technology, Sector 39A, Chandigarh, India

ARTICLE INFO

Article history:
Received 20 September 2013
Received in revised form 10 January 2014
Accepted 22 January 2014
Available online 28 January 2014

Keywords:
Structural fluctuation
Constrained dynamics
Conformational entropy
Denaturant-mediated
cross-linking interactions
Thermodynamic stability
Water activity

ABSTRACT

The effect of denaturants on the structural fluctuation of M80-containing Ω-loop of ferrocytochrome *c* was determined by measuring the rate coefficient of CO-association with ferrocytochrome *c* under varying concentrations of urea and alkylureas (methylurea (MU), *N*,*N*′-dimethylurea (DMU), ethylurea (EU), tetramethylurea (TMU)) at pH 7.0, 25 °C. As denaturant concentration is increased within the subdenaturing limit, the CO-association reaction is decelerated indicating that subdenaturing concentrations of denaturant reduce the structural fluctuation of the Ω-loop. Structural fluctuation of the Ω-loop is reduced more for urea and least for TMU. Intermolecular docking between horse cytochrome *c* and denaturant molecule (urea, MU, DMU, EU and TMU) reveals that polyfunctional interactions between the denaturant and different groups of Ω-loop and other part of protein decrease with an increase of alkyl group on urea molecule, which suggests that the decrease in the extent of restricted dynamics of Ω-loop with a corresponding increase of alkyl groups on urea molecule is due to the decrease of denaturant-mediated cross-linking interactions. These denaturant-mediated interactions are expected to reduce the conformational entropy of protein. Analysis of rate-temperature data shows a progressive decrease in conformational entropy of protein in the native to subdenaturing region. Thermodynamic analysis of denaturant (urea, MU, DMU, EU, TMU) effects on the thermal unfolding of ferrocytochrome *c* reveals that (i) thermodynamic stability of protein decreases with increasing concentration of denaturant or hydrophobicity of urea derivatives, (ii) water activity plays an important role in stabilization of ferrocytochrome *c*, and (iii) destabilization of ferrocytochrome *c* by denaturant occurs through the disturbance of hydrophobic interactions and hydrogen-bonding.

1. Introduction

The various solvent additives, such as guanidine hydrochloride (GdnHCl) [1,2], urea [1–4], and alcohols [5,6] are commonly known to denature the proteins. However, the mechanisms by which these denaturants unfold proteins in aqueous solution are poorly understood. GdnHCl and urea can denature proteins through directly binding to peptide groups [1,7–9] or indirectly by altering the solvent environment [10–12]. Calorimetric studies with cyclic dipeptides in urea reveal that both mechanisms can contribute significantly in the denaturant-induced unfolding of proteins [13]. Alcohols are known to stabilize helical secondary structure [5,14] but destabilize tertiary structure of folded proteins [15]. Few earlier studies have shown that alkylureas similarly to alcohols induce a formation of α-helical secondary structure in β-lactoglobulin A [16] and α-chymotrypsinogen A [17]. Poklar et al. investigated the effect of alkylureas on the thermodynamic stability of β-lactoglobulin A [18,19], α-chymotrypsinogen A [20,21], and ribonuclease A [22,23]. They reported two important results: (i) the thermodynamic stability of these proteins decrease with increasing hydrophobicity of urea derivatives [18–23], and (ii) depending on the hydrophobicity and concentration of alkylureas, they also destabilize the tertiary structure and can cause rearrangement and distortion of secondary structure of proteins [18–23].

The interrelationships between protein function, stability, and dynamics play significant roles in protein engineering and biological process. In last few years, XRD-technique [24,25] and NMR spectroscopy [25,26] have been vastly used to correlate structure, conformational changes, function, and stability of proteins. Despite a commendable progress has been made in understanding the physics of protein folding, the investigations of protein dynamics are still in its infancy [27]. In particular, internal dynamics that include small amplitude collective motions [28], large amplitude cooperative breathing modes [29], and structural fluctuations at the subglobal level [30] are poorly understood.

The stability and dynamics of proteins in solution are strongly coupled to the dynamics of solvent [27,31–34]. In terms of time scale, protein undergoes structural fluctuations from ultrafast (in the femtoseconds to picoseconds range) to relatively slow (in the range of seconds) [35–39]. Structural fluctuations which occur on the ultrafast time scale eventually facilitate larger scale protein rearrangements that are responsible for modulating the biological functions of proteins [31,40,41]. Although, the fast protein motions

* Corresponding author. Tel.: +91 175 139 3832; fax: +91 175 236 4498.
E-mail address: rajesh.kumar@thapar.edu (R. Kumar).

1570-9639/$ – see front matter © 2014 Elsevier B.V. All rights reserved.
http://dx.doi.org/10.1016/j.bbapap.2014.01.012

J Biol Inorg Chem (2014) 19:1009–1024
DOI 10.1007/s00775-014-1145-2

ORIGINAL PAPER

Electrostatic effects control the stability and iron release kinetics of ovotransferrin

Sandeep Kumar · Deepak Sharma · Rajesh Kumar · Rajesh Kumar

Received: 4 August 2013 / Accepted: 29 April 2014 / Published online: 22 May 2014

Abstract The contribution of electrostatic interactions to the stability of ovotransferrin-Fe^{3+} (oTf-Fe^{3+}) complex has been assessed by equilibrium experiments that measure iron retention level of diferric-ovotransferrin (Fe_2oTf) as a function of pH and urea in the presence of salts (NaCl, Na_2SO_4, NaBr, $NaNO_3$) and sucrose at 25 °C. As [salt] is increased, the pH-midpoint for iron release increases monoexponentially and plateau at $\sim$0.4($\pm$0.05) M NaCl/NaBr/$NaNO_3$ or $\sim$0.15($\pm$0.03) M Na_2SO_4. However, at pH 7.4, the urea-midpoints for iron release (based on fluorescence emission at 340 nm) and for unfolding of Fe_2oTf and apo-ovotransferrin (based on ellipticity values at 222 and 282 nm) decrease at low salt concentrations [$\leq$0.1($\pm$0.02) M Na_2SO_4 or $\leq$0.35($\pm$0.15) M NaCl], but increase at higher salt concentrations. Furthermore, Na_2SO_4 has a greater effect than NaCl in increasing the urea-midpoints for iron release and unfolding. These results indicate that at low salt concentrations, the electrostatic effects destabilize the oTf-Fe^{3+} complex and also decrease the structural stability of the proteins. In contrast, at higher concentrations, salt ions behave according to Hofmeister series. At pH 5.6, as [salt] is increased, the rate constants for reductive iron release (Fe^{2+} release) and urea denaturation-induced iron release (Fe^{3+} release) from the N-lobe of oTf (Fe_NoTf) increase monoexponentially and plateau at $\sim$0.4($\pm$0.1) M $NaNO_3$/NaCl or $\sim$0.2($\pm$0.05) M Na_2SO_4. These results suggest that the anion-binding-induced conformational change as well as the electrostatic screening of surface Coulombic interactions plays important role in accelerating the iron release from Fe_NoTf under endosomal pH conditions.

Keywords Iron release · Electrostatic interactions · Anion-binding · Conformational change · Structural stability

Introduction

The stability of proteins is generally governed by noncovalent interactions such as hydrophobic [1, 2], electrostatic [3–7], and hydrogen bonding [8, 9]. However, the relative contributions of these interactions to protein stability are not fully resolved. In particular, the role of ionic interactions in protein stability is relatively more complex [10]. Buffer conditions such as pH and salt can have dramatic effect on the stability and biological functions of proteins. For example, the low pH triggers a large conformational change in transferrins (Tfs), which is a critical step for iron release in endosome [11–25]. In general, pH modulates the protein stability by altering the charges on ionizable groups in the proteins through protonation or deprotonation [26]. Salt ions also modulate the stability of proteins [27, 28]. At low concentrations, salt ions affect the stability of proteins by altering the electrostatic (Debye-Hückel) screening of Coulombic interactions [9, 29, 30]. At relatively higher concentrations, salt ions follow the Hofmeister effect, which eventually depends on the nature of added ions and modulates the stability of proteins by increasing the surface

Electronic supplementary material The online version of this article (doi:10.1007/s00775-014-1145-2) contains supplementary material, which is available to authorized users.

S. Kumar · R. Kumar · R. Kumar (✉)
School of Chemistry and Biochemistry, Thapar University, Patiala 147004, India
e-mail: rajesh.kumar@thapar.edu

D. Sharma
Institute of Microbial Technology, Council of Scientific and Industrial Research, Sector 39A, Chandigarh, India